CONTINUUM AND STRUCTURAL ASPECTS OF ALUMINIUM ALLOY EXTRUSION

A Thesis Presented for
the Degree of Doctor of Philosophy
of London University

by

ALAN FREDERICK CASTLE

September .1974

John Percy Research Group
Metallurgy Department,
Royal School of Mines,
Imperial College of Science
and Technology,
London S.W.7

ABSTRACT

The extrusion of seven different aluminium alloys through single, multihole and simple shape dies has been studied over a wide range of temperatures and strain rates. Hot torsion and tensile tests were also carried out on two of the alloys.

The flow stress in extrusion was calculated from minimized plane strain solutions and the mean deformation temperature from a modified integral profile model. Hot working theory could be successfully applied to the hot torsion and tensile data, but a correction factor, dependent on the die profile only, had to be applied to the temperature compensated strain rate before the theory could be used to correlate the results from extrusion. A significant discrepancy between the results from the two methods of testing was found. It is suggested that this is due to the assumptions made in the extrusion theory.

The dependence of the peak load and the peak height on the extrusion ratio & ram speed and temperature has been investigated. Also the development of the macrostructure and the microstructure at the start of extrusion were studied and a suggestion for the cause of the peak is made.

Flow patterns for single hole extrusion at different billet lengths showed reasonable agreement with those predicted by a minimised plane strain upper bound solution. The flow patterns developed during multi hole extrusion were also investigated.

The structures of the as extruded rod have been examined using both optical and transmission electron microscopes. The mechanical properties were measured by tensile tests. The structure could be classified into three overlapping types, the occurrence of which depended on the flow stress and the alloy content. The recrystallized structure had superior properties to those found in the fibrous structure. This may be due to the retention of the solute in solid solution in the former and preferential precipitation, during quenching, onto the sub grain boundaries in the latter.

No evidence of dynamic recrystallization was found and it is concluded that the static restoration process must have occurred in the time between leaving the die and entering the quench.

Hot shortness was found above a critical temperature and the defect was studied in the scanning electron microscope. A comparison between a good surface finish and an unacceptable finish has also been made.

Limit diagrams for two of the alloys are presented.

ACKNOWLEDGEMENTS

The author would like to thank Mr T. Sheppard for the initiation of this project and for his assistance in overcoming many of the problems encountered during the research.

Thanks are also due to Mr A. Neve and Mr A.J. Haynes who, along with their fellow technicians, offered very practical help throughout the experimental program and showed great patience and skill in maintaining the extrusion press in a useable condition.

A special mention must also be made to the assistance provided by the members of the John Percy Research Group in complying with the safety regulations of the press.

The help received from the Phot graphy section, the Electron Microscopy group, and the Departmental Workshop was much appreciated.

Some financial assistance was provided by the Science Research Council and the material by Alcan International. The assistance given by the latter, especially Dr, A.J. Bryant , was extremely useful.

I am very grateful to my mother for typing this thesis .

Finally I must thank Helen for her patience and financial support throughout the last three years, particularly during the final months,and for her skill in stencilling all the graphs.

CONTENTS

CHAPTER ONE

LITERATURE SURVEY

1.1	Introduction	9
1.2	General Features of Aluminium Alloy Extrusion	11
1.3	Hot Working	13
1.3.1	Methods of Testing	14
1.3.2	Empirical Approach to Hot Working	15
1.3.3	Structural Aspects Of Hot Working	19
1.3.4	Static Restoration Processes	20
1.3.5	Development of the Hot Worked Structure	22
1.3.6	Theoretical Approach to the Mechanisms Operating During Hot Working	24
1.3.6.1	The Jog Screw Model	25
1.3.6.2	Dislocation Climb Models	26
1.3.6.3	Three Dimensional Network Model	27
1.3.7	The Dependence of the Mechanical Properties on the Structure	28
1.3.8	A Summary of Hot Working	29
1.4	The Analysis of Extrusion	30
1.4.1	The Theoretical Approach to Extrusion Pressures	30
1.4.1.2	Slip Line Field Techniques	31
1.4.1.3	Upper Bound Techniques	32
1.4.1.4	Axisymmetric Solutions	33
1.4.2	Empirical Approaches to Extrusion Pressure Determination	35
1.4.3	Pressure for Multihole and Complex Shape Extrusion	37
1.4.4	Flow Patterns Developed During Extrusion	40
1.4.5	The Effect of Ram Speed on Extrusion Pressure	42
1.4.6	The Influence of Temperature on the Extrusion Pressure	42
1.4.7	The Temperature Rise During Extrusion	43
1.4.8	Strain Rates in Extrusion	45
1.4.9	The Peak Loads Developed In Extrusion	49
1.4.10	Measurement of the Flow Stress in Extrusion	53
1.4.11	Defects in Extrusion	54
1.4.12	Limit Diagrams	55
1.5	Summary	59

CHAPTER TWO

THEORY

2.1	Derivation of Stress Strain Curves from Torsion Tests	60
2.2	Upper Bound Solutions for Extrusion	62
2.2.1	Plane Strain Single Hole Extrusion	63
2.2.2	A Plane Strain Solution for Two Hole Extrusion	66
2.2.3	Plane Strain Solution for Three Hole Extrusion	66
2.2.4	An Upper Bound Axisymmetric Solution	71
2.3	The Prediction of Flow Patterns by Means of an Upper Bound Solution	72
2.4	The Variation in Load with the Billet Length	75
2.5	The Method Used to Calculate the Flow Stress from the Experimental Results	78
2.6	The Integral Profile Model for the Temperature Rise	78
2.6.1	Assumptions Made in the Integral Profile Model	78
2.6.2	The Calculation of the Temperature Rise	79
2.7	An Approximate Method of Allowing for Additional Heat Losses to a Cooler Container	84
2.8	A Summary of the Method Used to Calculate the Temperature Rise	85
2.9	The Temperature Rise at the Peak Load	86
2.10	The Strain Rate	86
2.11	The Calculation of the Constants in the Hot Working Equation	87
2.12	The Method of Measuring the Peak Load	90

CHAPTER THREE

EXPERIMENTAL

3.1	The Press	91
3.1.1	Load Measurement	91
3.1.2	Ram Speed and Displacement	91
3.1.3	Container Heating	93
3.1.4	Billet Preheating	93
3.1.5	Tooling	93
3.2	Water Quench	94
3.3	Materials	99
3.4	Experimental Procedure	99
3.5	Temperature Measurements	101
3.6	Flow Patterns	103
3.7	Torsion Testing	103
3.8	Hot Tensile Tests	104

3.9	Specimen Examination	105
3.9.1	Optical Microscopy	105
3.9.2	Transmission Electron Microscopy	107
3.9.3	Scanning Electron Microscopy	107
3.9.4	Hardness Tests	107
3.9.5	Tensile Tests	107

CHAPTER FOUR

RESULTS

4.1	Hot Working	108
4.11	Hot Torsion and Tensile Tests	109
4.1.2	Extrusion Results	119
4.2	The Load at the Start of Extrusion	130
4.2.1	The Dependence of the Peak Load on the Extrusion Ratio	131
4.2.2	The Effect of the Initial Billet Temperature on the Peak Load	134
4.2.3	The Effect of a Change in the Ram Speed on the Peak Load	134
4.2.4	The Effect of the Billet Length	134
4.2.5	The Application of an Arrhenius Type Energy Term to the Peak Load	139
4.3'	The Height of the Peak at the Start of Extrusion	139
4.3.1	The Variation in the Peak Height with the Ram Speed	144
4.3.2	The Effect of the Initial Billet Temperature on the Peak Height	144
4.3.3	The Dependence of the Peak Height on the Peak Load	144
4.4	The Effect of Removing the Load During Extrusion	144
4.5	The Effect of Section Shape on the Load	155
4.6	The General Nature of the Load Displacement Curve	155
4.7	The Relationship Between the Mechanical Properties and the Flow Stress	155
4.8	The Dependence of the Mechanical Properties on the Grain Size	162
4.9	The Variation in the Properties of the Multihole Extrudes	162
4.10	The Hardness Across the Extrude	162
4.11	The Variation in Hardness Across the Stop Mark in the Load Removal Experiments	170
4.12	Limit diagrams	170

4.13 Flow Patterns and Microstructures 174

CHAPTER FIVE

DISCUSSION

5.1 Possible Sources of Errors in the Experimental Results 175
5.2 The Structure of the Material Before Extrusion 177
5.3 The Results Obtained from the Hot Torsion and Tensile Tests 179
5.3.1 Acomparison Between the Calculated Constants in the Hot Working Equations 179
5.3.2 The Use of $\sigma_{1.5}$ for the Flow Stress in Torsion 181
5.3.3 The Value of the Activation Energy 181
5.3.4 The Application of the General Hot Working Equation 182
5.4 The Importance of the Temperature Rise in Torsion 184
5.5 The Analysis of the Extrusion Results 186
5.5.1 The Mean Flow Stress in Extrusion 186
5.5.2 The Temperature Rise 188
5.5.3 The Strain Rate 190
5.5.4 Extrusion as a Hot Working Process 191
5.5.5 A Summary of the Application of Hot Working Theory 195
5.6 The Peak Load Developed During Extrusion 199
5.7 The Height of the Peak at the Start of Extrusion 201
5.8 The Development of the Flow Pattern at the Start of Extrusion 202
5.9 Structural changes Prior to the Peak Load 204
5.9.1 A Summary of the Microstructures Developed at the Start of Extrusion 215
5.10 The Structure at the Front of the Extrude 216
5.11 The Effect of the Removal and Reapplication of the Load During Extrusion 220
5.12 The Effect of the Billet Length on the Flow Pattern and Load 224
5.13 The Flow Patterns in Multihole Extrusion 228
5.14 The Structures Observed During Extrusion 230
5.15 The Relationship Between the Flow Stress and the as Extruded Structure 238
5.16 The Occurrence of a Recrystallized Structure in Extrusion 239
5.17 The Relationship of the Mechanical Properties with the Structure and the Flow Stress 241

5.18	The Variation in Mechanical Properties Across the Extrude	242
5.19	The Variation in mechanical Properties in the Multihole Extrudes	243
5.20	Surface Defects in Aluminium Alloy Extrusion	244
5.21	The Load Displacement Curves	250
5.22	The Effect of Section Shape on the Extrusion Load	251
5.23	Limit Diagrams	252
5.24	A Criticism of the Present Work	253
5.25	The Industrial Relevance of the Present Work	254
CONCLUSIONS		256
AppendixI	Computer Programs	258
Appendix II	Constants used in the analysis of extrusion	267
Appendix III	Calibration Curves	274
Appendix IV	Die Dimensions	279
Appendix V	The Results	280
Appendix VI	Stress Strain Curves from Torsion	291
Nomenclature		299
References		301

CHAPTER ONE

LITERATURE SURVEY

1.1 Introduction

As an industrial process for metal fabrication, extrusion is a comparative newcomer, but it is now recognised as being the most efficient method of producing complex shapes from a cast billet. Many of the sections extruded today would be impossible to produce by any other method.

The first record of extrusion[1] is in a patent granted to Joseph Bramah in 1797 for 'A press designed to extrude lead pipe'. There is no evidence of the success of his method but by the end of the nineteenth century the lead extrusion industry was well established. Many of the practises in use to-day, such as bridge-dies, fixed and floating mandrels, heated containers, and accumulator drive, were developed on these early presses. At first the process was restricted to lead, because of the difficulty in constructing presses and tooling rigid enough for the harder metals. These problems were overcome by Alexander Dick who, in 1894, designed a horizontal press that could be used to extrude the $(\alpha+\beta)$ brasses. From this press, and later ones designed by Dick, developed the large industrial presses in use today. The only improvements have been in their size and efficiency and it is now possible to extrude almost all metals, from the soft aluminium alloys to the high temperature nickel alloys. Although production was originally limited to lead and some copper alloys, the bulk of extrusion is now carried out in the aluminium and copper industries. The ease with which they can be worked enables almost any shape to be produced, from a simple rod to complex hollow sections.

The extrusion process has been the subject of much research and this can be divided into several distinct categories.

The early work[1] was concerned with empirical relationships between the extrusion parameters of pressure, speed, temperature and material. This has provided a useful background to an understanding of the process but most of the work was limited by the experimental facilities available and the results obtained only apply to a very limited range of conditions. Some of the structural changes that occur during extrusion were also studied and often these are still the only results available.

The next important development in the research was the application of the plasticity theory[2,3]. Using this approach slip-line field and upper-bound solutions have been obtained for a variety of conditions. These methods enable reasonably accurate values for the extrusion pressure to be obtained but they are limited by the assumptions that have to be made. The slip-line field can only be applied to plane-strain conditions and a rigid perfectly plastic material, the upper-bound solution has been applied to axisymmetric solutions but the limitation on the material still applies. More recent work has developed a solution for strain hardening materials,[4,5] but the application is very limited.

Following on from this work the importance of the temperature changes occurring during extrusion was recognized. This has been studied by a variety of methods both theoretical and experimental[6-13]. The results have shown the importance of the temperature rise, especially when working near the melting-point of the alloy being used, or close to a phase change boundary.

The most recent development has been in the application of hot-working theory to extrusion[14-17]. The results have shown the similarity between extrusion and other hot working processes and tests, such as rolling, compression, and torsion. This work has also pointed out the limitations of the basic extrusion theory in predicting a value of the strain-rate, flow-stress, and temperature to be used in any calculations.

Although this research has been quite detailed it must be admitted that extrusion theory lags a long way behind extrusion practise, and it is often argued by many industrialists that the research is of little or no importance. However, there are still many practical problems that have to be solved and here research can assist the industrialist. Examples are;-

1. To attain the optimum operating conditions a knowledge is required of the behaviour of an alloy under different combinations of ram-speed, temperature, reduction ratio.
2. The properties of the extrude can be related to the extrusion conditions and correlation is needed between the results obtained by other testing methods and those by extrusion.
3. There is still no accurate means of predicting the load developed during extrusion. It can be said that, with to-day's presses,

the load is not important when compared with other factors. This ignores the fact that greater reductions can be achieved if the load required is lowered, longer billets can be extruded on a given press, leading to increased production with less scrap, and smaller presses can be installed.

4. The surface finish is of major industrial importance but there is very little quantitative work available on the relationship between the surface finish and the extrusion parameters.
5. Most industrial extrusion is concerned with the production of shapes of differing complexity. There is no way of predicting how the final properties will vary throughout the section or even of how the die should be designed for maximum efficiency.

It can be seen that there are still many fields that can be profitably studied.

1.2. General Features of Aluminium Extrusion

The ease of fabrication of this metal, and its alloys, has led to the development of a very large extrusion industry, producing a variety of shapes in alloys of widely differing properties. A review of the extrusion of these alloys was published by Smith[18] in 1949 and most of this is still relevent.

The nature of the flow in extrusion results in the outer surface of the product being subjected to very heavy shear stresses. This results in a heavily worked outer region and subsequent heat-treatment can cause abnormally large peripheral grains to be formed.[1,18] This appears analogous to the critical strain for recrystallization in cold-worked metals but, as pointed out by Pearson[1], this is not the case in extrusion where the process is characterized by heavy deformation and high temperatures. A suggestion made is that the degree of strain hardening may be the important factor and a critical value may be reached in the outer region. In alloys that are to be heat-treated the possibility of a coarse grained peripheral region is a major problem, because of its reduced mechanical properties and susceptibility to stress-corrosion[18,22]. The addition of zirconium and manganese can retard its occurrence [22]. Where complex shapes are being produced the problem can be intensified[18.23].

Apart from the heavily worked outer region, the structure can be fully recrystallized, fibrous, or a combination of both. The

type of structure found depends on the alloy used, the pre-extrusion heat treatment, the extrusion parameters, and the post-extrusion treatment[29,30]. The fibrous structure has the best mechanical properties and Unckel, as reported by Pearson[1], attributed this to the preferred orientation found in this structure. Hardy[19] agreed with this view and recent work by Althoff[21] has shown how the anisotropic properties can be reduced by the presence of a coarse precipitate of Mg_2 Si. They also noticed long particles of Al(MnFe)Si preferentially orientated in the extrusion direction. Their size was approximately 0.2 m diameter by 1.5 m long. The fibrous structure can be retained at high temperatures, and this is known as the extrusion effect. The presence of manganese helps in its retention[18,22,29]. Comparing mechanical properties obtained for similar alloys, except for the presence of manganese, there can be a difference of up to 25% after heat treatment and this is associated with the beneficial effect of manganese in retaining a fibrous structure[18,19,20,22]. Chromium has a similar but less pronounced effect.

In the case of multi-hole extrusion, which is used to increase production rates, the presence of a large grain peripheral region can cause further problems. The complex nature of the flow leads to the region being distributed between the rods and this gives a crescent like effect to the macrostructure. Segregation has been found near the periphery in the zone of radial flow, leading to poor mechanical properties [1,18,31].

The surface finish of the product is important to both the customer and the producer and the defects that occur can be visible blemishes, e.g. cracks, blisters, and die lines, or invisible ones that show up on anodizing[24,25]. The control of these defects is a deciding factor in many production problems. It is doubtful if lubrication is of any use in aluminium extrusion, a good surface finish being obtained by shear at the die face[28]. Blisters on the surface occurr if any lubricant, or other foreign matter, on the side of the billet is dragged between the flowing metal and the dead metal zone[18,28] to become trapped just under the surface. Often a trace of lubricant is applied between the front of the billet and the die but, in view of the problems of lubrication in cold-extrusion[26,27], it is unlikely that this has any other effect other than easing the mind of the operator.

Many of the stiffer alloys, such as the Al-Zn-Mg range, have a very limited extrusion range[18,22]. Limited on the one hand by the press capacity and on the other by the onset of hot-shortness, where the melting point of one of the phases is reached. It is in the extrusion of these alloys that limit diagrams[32-34], section 1.4.12. can be of use.

Although this is only a brief review it can be seen that there are many conflicting factors to be considered, e.g. the type of structure required, the temperature and speed to be used, the quality of the surface finish,and the effect of the die shape on the properties. Many of these parameters can only be adequately allowed for if more research on the connecting variables is undertaken.

1.3. Hot Working

It has been the practise for centuries to work metals at high temperatures. The reason for this is shown in fig.1.1 At low temperatures the stress to deform a metal increases as the strainincreases. This is known as work-hardening and is caused by the complex interaction and formation of dislocations within the material. At higher temperatures the flow stress for a given strain is much lower , suggesting that there must be some mechanism removing the effects of work-hardening. It is these restoration processes that have been studied in investigations into hot working[35]. An examination of stress strain curves at different temperatures and strain-rates[35-41] shows that the rate of deformation is also very important, the higher the strain rate, at a given temperature, the higher the flow-stress. This observation is of importance in the metal-working industries where high strain-rates are used to deform materials to large strains at high temperatures. In aluminium extrusion the reduction ratio can be up to 200:1. The practical importance of the subject has led to hot-working becoming one of the most important subjects of modern metallurgical research. The approaches used can be classified into three methods;

1. Empirical; it is useful to have equations relating the flow stress, strain-rate, and temperature. Also it is relatively easy to adapt a standard testing technique to hot-working tests.

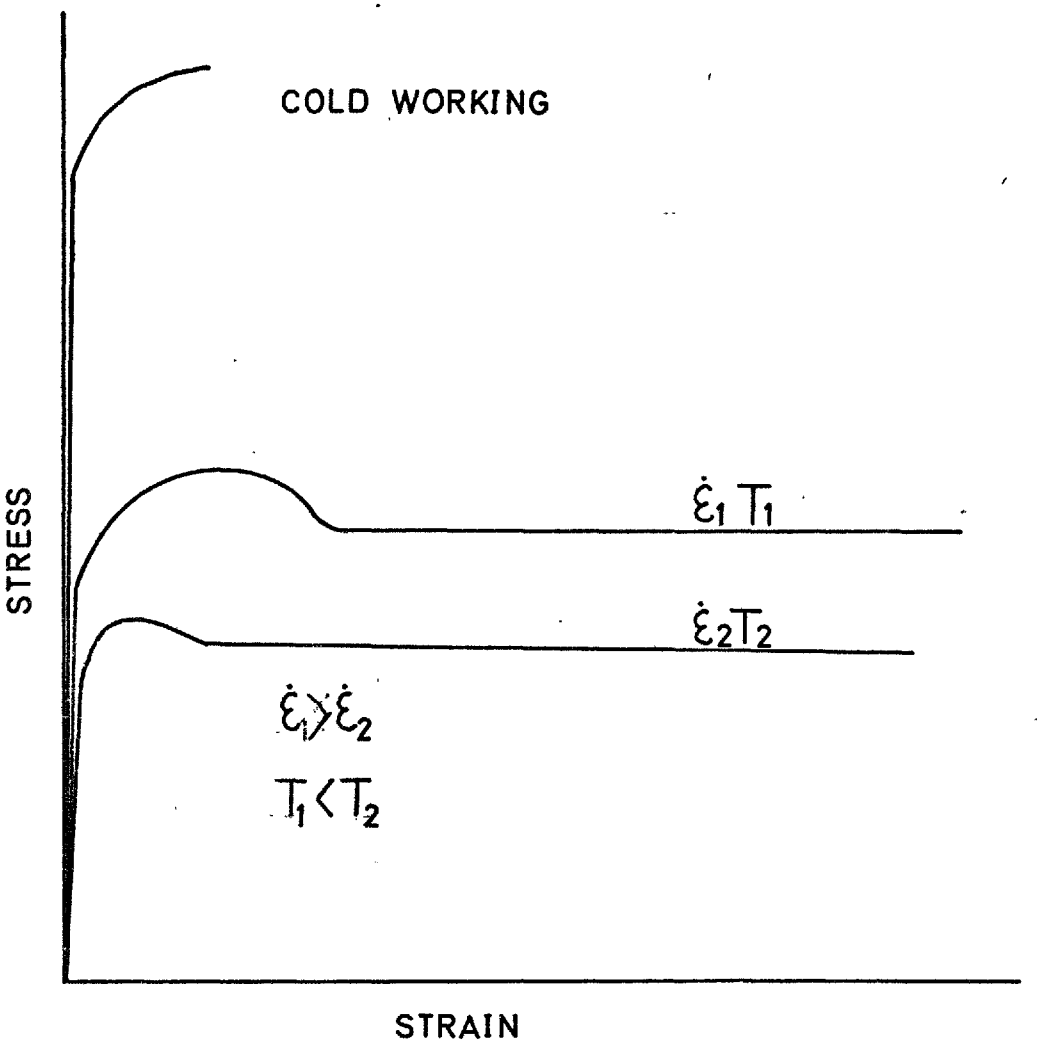


Fig. 1.1. Schematic stress strain curve for hot working

2. Structural: empirical equations are useful but their use can be extended if a knowledge of the accompanying structural changes, which control the final properties, is available. It is an experimental fact that hot-worked metals can show a non-recrystallized, partly recrystallized, or fully recrystallized structure [18,35]. There are also many similarities between the hot-worked structure and those obtained in creep, a process associated with much lower strain-rates. [35]

3. Theoretical: the similarities between creep and hot-working structures has led to the examination of creep theories to see if they can be applied to the higher strain-rates [14,35,42,43]. Any theoretical study should lead to a better understanding of the many varables controlling the deformation process.

1.3.1. Methods of Testing

Before discussing the approaches to hot-working outlined in the previous section it is useful to have a knowledge of the advantages and disadvantages of the various methods of testing used and their applicability to industrial processes. These methods have been discussed by several authors [44-47].

Tensile Tests.

These are limited by the maximum strain that can be applied, usually less than 0.5. The strain-rates available are low but by using special techniques it is possible to achieve values of 100sec^{-1} [48]. The advantage of the method is the relative ease of testing.

Compression Tests.

These can be performed to true strains of more than 0.7. The range of strain-rates possible is from 5 x 10^{-3} to 2 x 10^{3}sec^{-1}, using a modified Hopkinson pressure bar technique[49]. Constant strain rate tests can be carried out using a cam-plastometer[40,41,50]. With this equipment it should be possible to use programmed strain-rates, which would be of use in comparisons with rolling and extrusion. No work of this nature appears to have been done. The problem to be overcome in compression is the inhomogenous deformation, shown by the specimen barrelling. This can be overcome by careful lubrication, usually assisted by machining concentric grooves on the specimen surfaces, but it is never certain how successful this method is.

Torsion Testing.

This is one of the most popular means of testing[36,39,50-55]. Its advantage is the ease with which large uniform strains can be achieved at constant strain-rates, using thin walled hollow specimens. For ease of experimentation it is more usual to use solid specimens but in this case the strain-rate varies from zero at the centre to a maximum at the edge. Testing is usually carried out with axial constraint on the specimen, to maintain specimen geometry at the expense of axial load[56]. By modifying the equipment it is possible to do programmed experiments, similulating rolling or forging schedules[52]. This method is also open to variable strain-rate experiments as well as investigation into the effect of sudden changes in temperature.

The above methods are all laboratory techniques that can provide valuable data on the behaviour of metals under different combinations of strain-rates and temperatures. However, they have the big disadvantage of not being industrial processes. Compression testing comes close to rolling and forging but there is a big difference between a controlled compression test on a small well-lubricated specimen and the large forging of a billet. Often the aim of the experiments appears to be to achieve a higher strain-rate than previous workers, without any regard to the structural changes that take place. This is especially true in the Hopkinson split pressure-bar technique method of compression or torsional testing[57].

There has been some attention to the examination of industrial processes [14,15,16], but the complex deformation involved entails many assumptions in the analysis. Nevertheless experiments of this kind are the only ones that can be used if the limits of a particular process are to be found or structural changes during fabrication are to be examined. This is especially true in extrusion where true strains greater than 5 can be produced in one operation at mean strain-rates of up to 100 sec^{-1}. By the very nature of the process it involves the shearing of metal over a tool under the influence of a high hydrostatic pressure. It is this interaction between the material and the tool that laboratory tests cannot reproduce.

1.3.2. Empirical Approach to Hot-Working.

Examination of data from several workers has shown that two relationshipscan be applied to hot-working data[35,38. 39,40,41,50].

For low stresses at a constant temperature

$$\dot{\varepsilon} = A_1 \sigma^{n_1} \qquad 1.1$$

where n_1 is a temperature dependent constant that approaches a value of about 5 at high temperatures[30,38,39,41].

For high stresses at a constant temperature

$$\dot{\varepsilon} = A_2 \exp(\beta\sigma) \qquad 1.2$$

where β is a temperature dependent constant [36,41].

These relationships are very similar to those found in creep experiments, supporting the idea that creep and hot-working are two extremes of the same phenomena. Garofalo [58] has shown how these two equations for the creep case, can be combined to give

$$\dot{\varepsilon} = A_3(\sinh(\alpha\sigma))^n \qquad 1.3$$

where A_3 is a temperature dependent constant.

It can be shown that

$$\alpha = \frac{\beta}{n} \qquad 1.4$$

The validity of this equation can be shown by considering the value of $\alpha\sigma$

If $\alpha\sigma > 1.2$

$$\dot{\varepsilon} = \frac{A_3}{2^n} \exp(n\alpha\sigma) \qquad 1.5$$

which is of the same form as equation 1.2.

If $\alpha\sigma < 0.8$

$$\dot{\varepsilon} = A_3 2^n \sigma^n \qquad 1.6$$

which is similar to equation 1.1.

Garofalo showed the applicability of equation 1.3 to results obtained on copper, an austenitic stainless steel and an aluminium alloy (Al-3.1%Mg).

The similarity between steady-state creep and steady-state hot-working led Sellars and Tegart[59] to propose the relationship

$$\dot{\varepsilon} = A \sinh(\alpha\sigma)^n \exp\frac{-Q}{RT} \qquad 1.7$$

where A, α, and n are temperature independent constants and Q can be referred to as the activation energy of the hot-working process.

The expression is more applicable if it is written in the form

$$Z = \dot{\varepsilon} \exp\frac{Q}{RT} = A(\sinh(\alpha\sigma))^n \qquad 1.8$$

Z is the temperature compensated parameter originally proposed by Zener and Hollonan for low temperature tests but it has been shown to apply to hot-working data[59].

The presence of the Arrhenius term $\exp \frac{Q}{RT}$ in equation 1.8 implies that hot-working is athermally activated process and Q is the activation energy of the rate controlling mechanism.

Q is the size of the emergy barrier preventing the atomic rearrangements involved in the mechanism, and the ease of overcoming this barrier depends on the temperature and the strain-rate. It must be remembered that other processes will also be occurring but the size of their energy barriers is much lower. The activation energy for hot-working has been measured for many metals and alloys[16,36,39,59,61-65] and the values obtained fall into two classes [35,45,59]

1. $Q_{HW} = Q_{CR}$

2. $Q_{HW} \neq Q_{CR}$

In the former case the value obtained is close to that measured for bulk self-diffusion [45], and this has been used as an indication of recovery occurring concurrent with hot-working. This dynamic recovery will be discussed in more detail in the next section. The two classes of metal defined above can be related to differences in their stacking fault energies. Metals with high stacking fault energies, such as aluminium and its alloys fall into the first class[16,35,39,49]. The stacking fault energy is a measure of the ease with which a dislocation can divide into two partial dislocations. The higher the energy the stronger is the binding energy and the closer together are the partials. For dislocation rearrangement the partials must come together, under the action of the applied energy, before climb can occur, and so dislocation climb is easier in high stacking fault energy metals [66]. Where Q_{HW} and Q_{CR} are approximately equal, it is possible to correlate data over many orders of magnitude of the temperature compensated strain-rate [59,61]. Most work in this field igmores the temperature rise that occurs during the test and, in the case of extrusion, where temperature rises of over 200°C can occur, this leads to a difference of 20% in the calculated value of the activation energy[62,67]. A constant value of Q is only attained at temperatures above 0.5 T_m [68,69], below this range it is very temperature dependent and decreases with a fall in temperature. The values of A, α, and n, in equation 1.7 are temperature independent constants, but they are functions of the structure and alloy

content, although the literature is not clear on how they vary with complexity of structure. The methods of calculating these constants involves complex iteration techniques and these are never fully explained. As a result it is not always certain of the accuracy of the quoted values. More work is needed in this field but it is essential to try and standardise the method of testing and analysis of the results before measured values can be compared. What is certain is that many more experiments than are usually made are needed to obtain reliable results.

1.3.3. Structural Aspects of Hot-Working.

As the schematic stress-strain curve in fig.1.1 shows, the flow stress in hot-working rises to a maximum and levels out to a steady value, there is often a peak before the steady state is reached. The presence of a steady state region shows that the flow stress is independent of the strain, as implied by the empirical equations, and that some restoration process must be active to counter the effect of work-hardening. Dislocations must still be active to effect the plastic flow. By analysing the results of many workers Jonas et al[35] have showed that there is a qualitative agreement between the structural changes observed in hot-working.

There appears to be two classes of metals agreeing with the values of Q_{HW} mentioned previously. Aluminium and its alloys fall into the first class, where the hot-worked structure consists of small equiaxed subgrains of low misorientation. These subgrains can either be within the original deformed grains, at low deformations, or they can form a continous structure when the original bounderies have been destroyed by large deformations[43,65,70-73]. A similar structure has been observed in iron and ferritic alloys[35,74,75]. There is a marked similarity between these structures and those developed during the creep of these metals.[35]. Also a similarity with the structure developed during the heat-treatment of cold-worked metals has been mentioned[44]. This again adds to the evidence that creep and hot-working are similar processes.

A substructure is also seen in hot-worked copper and nickel, and their alloys, when they are deformed to low strains. At higher strains they develop equiaxed recrystallized grains[65,72,76,77].

This is in contrast to the substructure developed in creep and suggests thst a different mechanism is operating, as indicated by the different activation energies for the two processes.

To examine the hot worked structure it is necessary to prevent any changes occurring during cooling. The exception to this is in the technique of hot-stage microscopy. The only way that these changes can be prevented is by rapid quenching immediately after deformation, the more rapid the quench the greater the likelihood of the hot-worked structure being retained. A delay will always occur between testing and quenching and it is in this region that rapid structural changes will occur. For this reason there is always the possibility that the structure being examined is not the hot-worked structure but a transition one. It is important therefore, to know what static restoration processes can occur. One point that is often overlooked is that rapid quenching might alter the structure by thermal shock.

1.3.4. Static Restoration Processes.

Metals that have been deformed can regain their original state by two processes, recovery and recrystallization[78], the driving force for these two processes being the stored energy. Recovery constitutes all those annealing phenomena that occur before the appearance of new strain free recrystallized grains. Recrystallization is the nucleation and growth of strain free grains and leads to the gradual consumption of the cold-worked matrix by the movement of large angle grain boundaries.

Recovery is brought about by changes in the number and distribution of point defects and dislocations and Byrne[78] lists the processes involved according to the relative temperature ranges with which they are associated.

At low temperatures, like point defects pair off, defect clustering occurs and they migrate to disloations, subgrain boundaries and other surfaces. (The cold-worked metal usually consists of a cell network of dislocation free regions surrounded by ragged dislocation tangles. The dislocation free regions are known as subgrains to distinguish between them ... the matrix grains[66].)

At intermediate temperatures, dislocation rearrangement within piled up groups occurs, dislocations of opposite signs annihilate each other and subgrain growth can occur.

At high temperatures, dislocation climb occurs leading to polyganization, the rearrangement of dislocations into low energy configurations by the formation of cells. This is a different process to subgrain formation, which occurs by dislocation interaction during working.

Recrystallization involves the replacement of the cold-worked structure by a new dislocation free one. This is achieved by high angle boundaries sweeping through the structure. It is known that recrystallization is a nucleation and growth mechanism[78] but there are still arguments over the process of nucleation[79,80]. Most of these differences of opinion are caused by comparisons between specimens prepared from bulk samples and those prepared for in-situ experiments in the electron microscope. The possible mechanisms have recently been reviewed by Doherty and Cohn[81] and can be summarized as;

1. The growth of a polyganized subgrain to a greater size and increased misorientation, with respect to its surroundings, by subgrain coalescence[80].
2. The strain induced migration of a subgrain boundary that has a higher misorientation than average.

As stated earlier the driving force for these restoration processes is the stored energy in the worked metal. If the metal can lower its energy by recovery there is less available for recrystallization, which has a nucleation time, and below a critical value of the stored energy recrystallization cannot occur. Therefore in metals where dislocation climb and polyganization is relatively easy, the possibility of recrystallization is reduced.

Of importance in hot-working studies are the changes that can occur at high temperatures after deformation. It has been shown that the time for static recrystallization to occur decreases with an increase in the holding and working temperature[52,71,75,82,83]. Rossard and Blain[75] have also demonstrated that the time for recyrstallization to occur depends on the strain-rate, which is related to the flow stress or the stored energy. The amount of strain can also have an effect[71], expecially at low temperatures where the flow stress depends on the strain. The time for recrystallization to be initiated decreased with strain in aluminium deformed in torsion at a strain rate of 2 sec^{-1} and a temperature of 400°C. It is important to consider the effect of heating during the deformation but this is often ignored.

Static recrystallization occurs in both groups of metals but results obtained show that in metals such as copper, the time for structural changes is much more rapid than that for aluminium[35].

It is usually considered that static structural changes can be ignored in rapidly quenched aluminium, but the work of Evans[83] has shown that static recrystallization can occur and they use this observation to explain the presence of the recrystallized structure in aluminium extruded above 450°C, followed by rapid quenching.

1.3.5. Development of the Hot Worked Structure

There has been a limited amount of research into the structural changes during the initial part of the stress-strain curve but this region is of prime importance. It is here that the initial structure changes to that of the steady-state and any dependence of the final structure on the initial one will be related to the changes occurring in the transition region.

At the start of deformation the flow stress rises to a maximum, the dislocations causing the plastic deformation accumulate into tangles and, by a strain of about 0.2, form into rough cells outlined by the intersecting dislocations[37,72,84,85]. The increase in flow stress is caused by the increase in the dislocation density. At the same time thermal activation assists the dislocations to cross-slip and climb and either annihilate each other, or to find equilibrium positions. The net result is conflicting hardening and softening processes. The presence of a steady-state flow stress indicates that a position is reached where the rate of dislocation production is equal to the rate of softening. This region is reached at strains of about 0.3, the actual value depending on the strain rate[35,86]. The steady state region is characterized by a steady-state cell size[35]. In creep a steady-state dislocation cell size is reached at strains of less than 0.1[87]. Further straining does not change the sub-grain size but the equilibrium size increases with an increase in the temperature and decreases with an increase in the strain-rate [14,38,70,74,84]. At temperatures less than $0.5T_m$ the subgrains outlined by the dislocation cells are slightly elongated but above this temperature they are equiaxed. This happens even at the strains encountered in extrusion[14]. Therefore the subgrains must be continously reforming at the equilibrium size and this has been termed repolyganization, by analogy with the production of new grains in recrystallization[88].

The variation in subgrain size with strain-rate and temperature can be related to the value of Z, indicating the possibility of controlling the structure by keeping Z constant, and varying the strainrate and temperature to obtain the most efficient operating conditions, combined with the maximum structural properties[14,16,88,51].

In aluminium and its alloys the nature of the sub-grains consists of very sharp boundaries with equilibrium dislocation networks within the subgrains. The misorientation between the subgrains is very small but the quoted values vary considerably, from less than 1° to 7°. This can be attributed to the insensitive techniques used to measure the misorientation[70,43,73,89,65,84]. Smaller cell structures have been observed within these grains [43,84]. Raybould and Sheppard associated them with both the remnants of subgrains that have annealed out by rotation, and the formation of the subgrains during deformation. The former mechanism occurring at the end of the deformation the latter at the start. There is also the possibility that they occurred by sub-grain coalescence, in the time between deformation and quenching. These micro-cells are very similar to those observed by Hu[85], which he associated with sub-grain coalescence. In copper the cell structure is less well defined at low strains[84,77,72] At higher strains the quenched structure shows recrystallized grains, often with an internal substructure. It is still not clear whether static recrystallization occurs prior to quenching[72,77,84].

The structural changes outlined above are known as dynamic recovery because of the similarities with the changes occurring during static recovery. This softening mechanism is widely accepted but, as mentioned above, a partial or fully recrystallized structure is often seen after hot-working, even with very high rates of quenching. Structures of this nature are associated with metals of group two but can also occur in group one metals deformed at high homologous temperatures[72,77, 84,88,83]. The presence of this recrystallized structure has led to the idea of dynamic recrystallization being an important softening mechanism. Opponents of dynamic recrystallization point out that the structures observed are not usually deformed and that there is no satisfactory explanation of how the nucleation of new grains can occur during high strain deformation. The tendency would be for subgrain formation by dynamic recovery[35,90-93]. The most recent review of dynamic recrystallization has been by Honeycombe and Pethen[94].

During creep testing under constant loads the steady state condition is often interrupted by sudden accelerations in the creep rate where softening by dynamic recrystallization occurs[95-97]. Similar oscillations are observed in torsion tests on copper, nickel, and and some steels[36,98]. These oscillations could be caused by recrystallization, resulting in the original non-worked structure, followed by a rise in the flow stress as a substructure forms. At a critical value of the strain recrystallization reoccurs. When the strain taking place during recrystallization is more than the critical strain the oscillations will disappear and this is what happens at high strain rates[98]. Dynamic recrystallization can explain the observed structure and the oscillations in the stress-strain curves but the nucleation of the recrystallized grains still has to be explained. There is metallographic evidence that nucleation occurs at grain boundaries that have become serrated during deformation[36,72,98]. Honeycombe and Pethen[94] suggest that nucleation occurs when, after a critical strain, bulging of a serrated grain boundary becomes energetically more favourable than the localized sharpening of sub-grain boundaries. Once formed the bulge will expand to form nucleii. In metals where subgrain formation is relatively easy the nucleation process would be energetically unfavourable. Impurities and alloying elements can have two effects. Their presence lowers the stacking fault energy, hindering subgrain formation, and also segregation at the boundaries can occur, preventing the development of the sub-structure. On the other hand small particles can lock a grain boundary, and stop or slow down the nucleation process.

1.3.6. Theoretical Approach to the Mechanisms Operating During Hot-Working.

It is only recently that a model for dynamic recrystallization has been proposed [99]. This is based on the nucleation of a recrystallized grain followed by deformation within the grain, and enables the oscillations in the stress-strain curve to be predicted, but the validity of the theory has not been experimentally verified. A number of models have been proposed to explain dynamic recovery, most of these are based on creep theory.

Gibbs[100] derived a general equation for the strain rate

$$\dot{\varepsilon} = \phi N A b \nu \exp \frac{Q}{RT} \qquad 1.9$$

where ϕ is a factor to replace the shear strain rate by $\dot{\varepsilon}$

N = the density of activatable sites

A = the ares swept out per activated event

b = the burgers vector

ν = the attempt frequency

Q = the activation energy

Jonas rewrote this as

$$\dot{\varepsilon} = \phi_f \exp\left(\frac{v\sigma}{RT}\right) \exp\left(\frac{\Delta H}{RT}\right) \qquad 1.10$$

where ϕ_f is a structure factor

ΔH = the activation enthalpy

v the activation volume

The activation volume is a measure of the effect of the stress in aiding the dislocation to surmount the energy barriers. It may be thought of as the volume swept out by the dislocation in a single activated event.

The different models proposed are similar to the basic rate equations given above. All contain the activation enthalpy equal to that for self-diffusion. The differences lie in the values obtained for the structure factor and the activation volume.

1.3.6.1. The Jog Screw Dislocation Model

When a screw dislocation intersects another screw dislocation a jog is formed. This jog can only move by the emission of vacancies. The rate of diffusion of these vacancies will control the movement of the dislocation and the rate of vacancy emission will depend on the local vacancy concentration.

Using this approach, and treating the retarding force due to the vacancy concentration as a chemical force, Hirsch and Warrington[101] derived the equation

$$\dot{\varepsilon} = N l_j b^2 z \nu \exp\frac{\Delta S}{k} \exp\frac{l_j b \tau}{RT} \qquad 1.11$$

Here the structure factor $\phi = N l_j b^2 z \nu \exp\frac{\Delta S}{k}$

and the activation volume $= \frac{l_j b^2}{h}$

Barrett and Nix[102] found that the density of mobile screw dislocations was related to the flow stress by

$$\rho = 2{\cdot}1 \times 10^{18} \sigma^3 \text{cm}^{-2} \qquad 1.12$$

Using this experimental observation they obtained

$$\dot{\varepsilon} = 12{\cdot}5 \times 10^{-18} D' \left(\frac{b}{a}\right)^3 \sigma^3 \sinh\left(\frac{\sigma b^2 l_j}{2kT}\right) \qquad 1.13$$

This predicts that

$$\dot{\varepsilon} \propto \sigma^4 \qquad \text{at low stresses}$$

and

$$\dot{\varepsilon} \propto \exp \sigma \qquad \text{at high stresses}$$

These equations imply that specimens of increasing dislocation density should have higher initial strain-rates. Jonas[103] recognised this problem and, using an approach developed by Seeger,[104] rewrote the general rate equation in the form

$$\dot{\varepsilon} = \phi s \exp\left(\frac{\Delta H}{kT}\right) \exp\left(\frac{v(\sigma - \sigma B)}{kT}\right) \qquad 1.14$$

The back-stress σB depends on the structure and can be correlated with the steady-state stress σ required to maintain this structure. Possible sources of the back-stress are the dislocation networks within the sub-grains, the sub-boundaries themselves or the long range back stresses from concentrations of dislocations near the boundaries.

1.3.6.2 Dislocation Climb Models

The early models of creep were based on the climb of edge dislocations to a low energy configuration. Under high stress conditions this approach gives

$$\dot{\varepsilon} \propto N D^3 \sigma^2 \exp\left(\frac{D^2 b^3 \sigma}{kT}\right) \qquad 1.15$$

At the lower end of the stress range this becomes a power law and an exporential one at the higher range. The structure factor is given by

$$\phi \propto N D^3 \sigma^2$$

which is stress dependent
and the activation volume by $D^2 b^3 \sigma^2$

This model again predicts an increase in the strain-rate with an increase in the dislocation density. Both the jog screw dislocation model and the climb model do not include a simple provision for the effect of alloying on the activation volume and it has been shown that this has to decrease with an increase in the solute content, to explain the experimental observations[107].

1.3.6.3. Three Dimensional Network Model

This was proposed by Mclean[108], who assumed the sub-grains to be occupied by a three dimensional dislocation network, This network will act as a barrier to any dislocation movement .

During steady-state working the strain rate is given by[89]

$$\dot{\varepsilon} = \frac{r}{h} \qquad 1.16$$

where r is the rate of recovery and h the rate of hardening which is another way of stating that the rate of recovery and the rate of hardening are constant. From experimental work Mclean was able to justify

$$\dot{\varepsilon} = A\sigma^{4.5} D \qquad 1.17$$

Although this model has the required stress dependence and can be shown to have a qualitative agreement with the observed effects of alloying additions[35], an exact analysis has yet to be made.

The network model includes the climb of edge dislocations and the migration of jogs along the dislocations. By combining the other possible recovery mechanism the non-conservative motion of jogs on screw dislocations, a more useful theory should be obtained. A theory along these lines has been suggested by Raybould and Sheppard[45] and they arrived at the equation

$$\dot{\varepsilon} = A\sigma^2 \exp\frac{\Delta H}{kT} \exp\alpha\sigma \qquad 1.18$$

Comparing this with equation 1.7 it was shown that

$$A\dot{\varepsilon}/(\alpha \exp\frac{\Delta H}{k10^3}) \qquad 1.19$$

and plotting this relationship gave a reasonable straight line.

These dislocation theories give possible qualitative explanations of the experimental observations. However, their use as quantitative expressions is very limited.

The equations require values for the dislocation parameters and these have not been made to any degree of accuracy, one reason being the loss of dislocations that occurs during specimen preparation for the transmission electron microscope. Of the dislocations that are seen it is difficult to deduce which ones are mobile and which are sessile. However, the agreement that is obtained between theory and experiment enables the terms in equation 1.7 to be given a theoretical interpretation. By comparison with the general rate equation 1.9 it can be seen that A can be related to the structure factor ϕs. The value of α is related to the activation volume. The exact relation will depend on whether high or low stress considerations are being studied[65,86].

Structure factors, which include a frequency term, and activation volumes obtained from experimental data will depend on the methods used to determine the flow-stress, strain-rate and temperature. This is especially true in extrusion where mean values have to be used. The experimental activation energy Q is obtained from

$$Q = -k\left(\frac{\partial \ln \dot{\varepsilon}}{\partial \frac{1}{T}}\right)_{\sigma} \approx \Delta H \qquad 1.20$$

Taking the natural logarithm of 1.10 and differentiating gives

$$\left(\frac{\partial \ln \dot{\varepsilon}}{\partial \frac{1}{T}}\right)_{\sigma} = \frac{-\Delta H}{k} + \left(\frac{\partial \ln \emptyset}{\partial \frac{1}{T}}\right)_{\sigma} + \frac{\sigma}{k}\left[V + \frac{1}{T}\left(\frac{\partial V}{\partial \frac{1}{T}}\right)_{\sigma}\right] \qquad 1.21$$

The experimental activation energy is close to that of the mechanism operating only when the micro-structure is independent of temperature at constant stress, i.e. when the terms of the right-hand side of the equation are negligible. If the structure is temperature dependent these terms cannot be ignored, and the measured value of the activation energy will be higher than the activation energy of self-diffusion[65,109]. This can explain the values obtained for the hot-working of metals in group two.

1.3.7. The Dependence of the Mechanical Properties on the Structure

The constant value of the flow stress and the sub-grain size during steady-state hot-working suggests a relationship between them, as does the variation in sub-grain size and flow-stress with a change in strain-rate and temperature. Experimentally it has been found that

$$\sigma = \sigma_0 + k' d^{-m} \qquad 1.22$$

where σ_0 is usually close to zero and m has values in the range 1 to 2. The value of k' increases with alloying content[35]. The different values for k' and m obtained for the same alloy can be attributed to the different methods used to measure the sub-grain size. The three methods available are; transmission electron microscopy, X-ray microbeam techniques, and optical microscopy. The first two give consistent values but the first is limited by the very small specimen area that can be examined, and the second by the inability to measure any variation in the grain-size. The accuracy of the optical techniques depends upon the method used to detect the substructure. In the case of aluminium and its alloys sub-grains are only visible in polarised light after anodizing. - The accuracy of this method is very limited because the observed sub-grains often consist of several

sub-grains of low misorientation. Jonas[35] has suggested other relationships between σ and d

$$d^{-1} = a + b \log(\sinh(\alpha\sigma)) \qquad 1.23$$

and

$$d^{-1} = p(\sinh(\alpha\sigma))^q \qquad 1.24$$

where a,b,p, and q are constants.

These equations signify a relationship between the subgrain and Z.

The fibrous structure observed in many hot-worked metals has higher longitudinal mechanical properties than a recrystallized structure in the same material. This 'cold-worked' structure is characterized by the presence of a well developed substructure. It has been shown that the room temperature proof stress can be related to d by [16,52,14].

$$\sigma_{P.S.} = \sigma_o + k_1 d^{-\frac{1}{2}} \qquad 1.25$$

This equation is very similar to the standard Hall-Petch relationship but the implication is that the strength depends on the subgrains and not on the grains themselves. Abson and Jonas[111] found that

$$\sigma = \sigma_o + k_2 d^{-\frac{3}{4}} \qquad 1.26$$

gave a better fit to the data. The difference between this and the previous equation may reflect experimental errors rather than a different relationship.

The dependence of the subgrain size on Z and of the proof-stress on the sub-grain size has the important consequence that the mechanical properties can be controlled by varying the value of Z being used, a constant Z giving the same mechanical properties regardless of the strain-rate or temperature used.

1.3.8. A Summary of Hot-Working.

Hot-working is a very complex phenomenon involving thermally activated dislocation interaction and rearrangements. The theories that have been proposed give a qualitative agreement with the experimentalobservations but they are difficult to apply to a quantitative analysis. For practical purposes the empirical equations ahould be used but the methods of calculating the results usually involve extensive iteration. This, combined with the low number of experimental results usually considered, and the approximations

that often have to be made in calculating values of the strain-rate, flow-stress and working temperature, will lead to errors in the calculated constants. This must always be remembered when comparing different sets of data. There is a need for a comprehensive analysis of results obtained by the different testing methods available. This will involve a very large number of tests on the same material, slight variations in composition will effect the results. If creep tests are also carried out the applicability of the empirical equations to a wide range of strain rates may be verified. Correlation between creep tests and data from extrusion must be treated with some sceptism because of the assumptions made in the strain-rates and flow-stresses in extrusion section

1.4. The Analysis of Extrusion.

The pressure developed during extrusion has received considerable attention and many attempts have been made to predict it. Both empirical and theoretical approaches are used and have been reviewed[1,3,112,113]. It is doubtful whether an exact prediction of the extrusion pressure is required for press design, unless the cold extrusion of the stiffer metals is being contemplated, However, the analysis of extrusion experiments usually involves a knowledge of the mean flow-stress and an accurate value is needed if a meaningful and useful analysis of the results is to be made.

1.4.1. The Theoretical Approach to Extrusion Pressures.

Assuming homogenous deformation it can easily be shown that

$$P = Y \ln\left(\frac{A_1}{A_0}\right) \qquad 1.27$$

However, the deformation in extrusion is far from homogenous, as can be seen from experimental flow patterns. Pearson[1] has compared this equation with experimental values and shown that the error increases* as the extrusion ratio increases and can be as much as 50% at reductions of 10:1. These observations can be expressed as

$$P = BY \log \frac{A_1}{A_0} \qquad 1.28$$

where B is an efficiency factor.

In this form this equation has some practical use when predicting the load to extrude different metals under identical conditions[115], although care must be taken when comparing metals of

* slip line field theory gives a decrease

completely different charactistics.

Using the slab method of analysis it can be shown that the total pressure, including a friction term may be expressed as

$$P = Y \log R + \frac{Y 4 \mu L}{D} \qquad 1.29$$

which is similar in form to the equation 1.27.

In view of the complex nature of the flow developed during extrusion it is preferable to have a theory that incorporates this flow. There are two approaches available;

1. the slip line field solution dueto Hill[2]
2. the upper bound technique due to Johnson and others

1.4.1.2. Slip-Line Field Techniques.

This is a powerful method of solving complex plastic flow problems by establishing the maximum shear-line field, but it can only be applied to conditions of plane-strain & a rigid perfectly plastic material[2,3]. Slip line field solutions have been developed for a variety of frictions conditions ranging from perfectly lubricated to perfectly rough and for a variety of die shapes. These include square, wedge-shaped, and concave dies[116,118,122]. The calculated pressures are usually given as graphs of pressure against reduction and Johnson[119] has shown that these theoretical curves can be approximated over a limited range of reduction ratios by

$$\frac{P}{2k} = A' + B' \ln R \qquad 1.30$$

the constants A and B' being determined by the frictional boundary conditons.

A problem in the application of these equations is the value of k, the shear yield stress, to be used. A rigid perfectly plastic material assumed in the original theory, has a constant value of k. This is far from the truth in real materials except at high temperatures. Dodeja and Johnson[120] suggested that a mean value, $\bar{k}$, should be used when calculating extrusion pressures for work-hardening materials. The value of $\bar{k}$ is the mean value of k found from plane-strain compression tests to a strain of $A + B \ln R$ (by comparison with equation 1.27 the effective strain can be considered to be equal to $A + B \ln R$ [113]). More recently the slip-line field solution has been extended to enable work hardening materials to be analysed, although the reduction of 50%

consideredhas a very limited application[4, 15], a criticism that can be made to most of the theoretical solutions. The slip-line field theory is mathematically correct but the computation of a solution can be very tedious. The method that has to be used has been summarised by Johnson and Kudo[3],

1. Construct the slip-line field or net which satisfies all the given boundary conditions in the stresses, starting from certain boundary surfaces of the material and assumed rigid plastic boundary slip-lines.
2. Obtain the veloctiy distribution by means of the slip-line field and from some of the given boundary conditions in the velocities and examine whether the remainder of the velocity boundary conditions are fulfilled.
3. Inspect whether the rate of plastic work in the deformation region is everywhere positive.
4. Ensure that the yield criterion in the assumed non-deforming region is not violated.

If the boundary conditions are not satisfied then the slip-line field must be redrawn. The process is therefore a very tedious and skilled one and in view of the limitations of plane-strain flow and a rigid perfectly plastic material it is doubtful whether the solution merits the work involved. Recognizing the difficulty in solving plastic flow problems by this method, Johnson[117] developed the upperbound method of analysis.

1.4.1.3 Upper Bound Techniques.

The upper bound solution gives loads in excess of those predicted by slip-line fields, which can themselves be considered as upper bounds[3]. Although the loads predicted by this method will be greater than those from the slip-line field solution, the difference between the two can be reduced to as small a value as desired by increasing the complexity of the solution. In view of the approximations of plane strain, mean yield stress, and frictional boundary conditionsthat have to be made the upper bound solution is accurate enough in the majority of cases.

This approach is simpler because it only considers velocity and boundary conditions and the incompressibility of the material.

By assuming the material to deform as blocks of rigid plastic material, which removes the necessity of considering shear in the material, the true mean rate of plastic working can be shown to be less than the sum of the products of the tangential velocity discontinuity and the line element over which it acts.

Using this approach Johnson[117] has obtained solutions for extrusion through wedge and square dies for both perfectly rough and smooth conditions. Kudo extended these solutions by introducing the concept of unit deforming regions and finding the most suitable velocity field within these regions. A triangular field gave very good agreement with slip-line field solutions[126]. It is difficult to bring different frictional conditions into the upper-bound solution but the solution for sticking friction will be an upper bound to other cases. The assumption of the material flowing as blocks of a rigid plastic material enables the solution to be easily minimized using a computer but the minimized solution need not be the best one, and the skill is in determining the form of the original velocity field. The steps that have to be taken in obtaining a solution have been given by Johnson and Kudo[3] and can be compared with those given in section 1.4.12.

1. Assume a velocity field for the body of the material, which is restricted only by the need to conform to the velocity boundary conditions and the law of constant density.
2. Calculate the rate of work due to the plastic deformation and due to slip of the material over the tool surface, using the assumed velocity field.
3. Calculate the extrusion load from the rate of working.

Steps 1 and 2 can be simplified by a knowledge of the experimental flow pattern and the assumption of rigid plastic blocks of material.

The relative ease of the upper bound solution is readily apparent and can be favourably compared with the slip-line field method of solution.

1.4.14 Axi-Symmetric Solutions.

The amount of industrial plane-strain extrusion is very small and there is an obvious need for a simple axi-symmetric solution.

The difficulty of an exact axi-symmetric solution has been discussed by Bishop[125]. The equations governing plastic flow in plane strain are hyperbolic equations and can be handled by known mathematical techniques. In the case of axi-symmetric problems the governing equations are not hyperbolic and so cannot be solved so readily. It is possible though to derive an axi-symmetric solution using upper-bound techniques[127].

Here the idea of unit-deforming regions is extended to unit deforming rings and cylinders, and to finding a velocity field to satisfy the velocity boundary conditions. The pressures predicted by this method are slightly higher than those from the plane-strain approach. This to be expected because of the more complex flow being considered. Kudo[128] found a qualitative agreement with his experimental results but the extrusion ratios considered were low, less than 10:1. The velocity fields used by Kudo were very simple, Kobayashi assumed curved discontiniuty surfaces for the velocity fields and obtained better solutions, i.e. lower loads.

Other axi-symmetric solutions have been given by Avitzur[130], and by Halling and Mitchell[131,132]. The latter authors using an optimized double triangle pattern of velocity discontinuities. This solution included the work done by circumferential straining and can be extended to incorporate the strain-hardening characteristics of the material.

One interesting solution to the axi-symmetric problem has been given by Sheppard and Raybould[13]. Using the experimental observations of Thomsen[129] that

1. The material flow is similar for similar geometrical shapes in axi-symmetric and plane-strain extrusion.

2. The velocity during axi-symmetric extrusion is the square of the velocity during plane-strain extrusion.

They derived a simple upper bound by first calculating a plane strain minimized solution. The areas of the discontinuity surfaces were then obtained by revolving the plane-strain field around the centre axis, and the magnitudes of the velocity discontinuities by squaring these given by the plane-strain hodograph. The load is then found by summing the products of the areas and the velocities. Although this method probably violates many of the laws of plasticity, as does any upper-bound solution, it has the advantage of simplicity.

They also derived an upper-bound from an experimental flow pattern. The position of the velocity discontinuities was determined from sub-grain size measurements. This method relies on a large number of measurements and the position of the velocity discontinuities is somewhat arbitrary.

This brief description of the analytical methods of solving extrusion problems shows how difficult the subject is. When considering the claims to the accuracy of any solution the assumption made must always be kept in mind. In every case the pressure given is that to pass the material through the deforming region. No account is taken of the pressure required to overcome friction between the surface of the billet and the container liner. Therefore it is difficult to predict the load at the start of the extrusion. By assuming shear to occur along the interface a term $\pi D_B k l_B$ has to be added. The mathematical form of the expression obtained from these solutions for a given reduction is

$$P = 2kc \qquad 1.31$$

The value of the k, the shear yield stress, is needed before any result can be obtained and it is difficult to decide on the value that must be used. Comparisons between theory and experiment can often be improved by selecting a suitable value of k. The main criticism that can be made is on the range of reductionsstudied. Most theories stop at reductions of 10 :1 or less. The bulk of practical extrusion is carried out at higher ratios, over 150:1 in the case of aluminium.

In view of the difficulties involved in these mathematical models it is not surprising that the bulk of research has been in developing empirical expression to relate the yield stress in tension or compression to the pressure developed in extrusion.

1.4.2. Empirical Approaches to Extrusion Pressure Determination.

Johnson[133] extruded lead and aluminium under conditions of plane-strain and compared the results with those predicted by slip-line field theory. He determined the value of k from true-stress logarithmic strain curves. The results obtained suggest that the theory is largely correct and is a considerable improvement on the earlier expressions derived from assumptions of homogenous deformation. He also discussed the failings of the theory, the most important one being the inability to allow for work hardening and the problem of effective lubrication.

Most theory is for plane extrusion and a useful piece of work by Purchase and Tupper [135] showed that the experimental pressures for the inverted extrusion of lead, through a square die, under plane-strain conditions compared very well with those found by Pearson[1] for axi-symmetric extrusions of similar reduction. Other experimental work has shown the applicability of the following equations[120,134]

$$\frac{P}{Y} = 0{\cdot}8 + 1{\cdot}5 \ln R \qquad 1.32$$

for lubricated extrusion $2{:}1 \leqslant R \leqslant 16{:}1$

and

$$\frac{P}{Y} = 0{\cdot}6 + 1{\cdot}8 \ln R$$

for unlubricated extrusion $4{:}1 \leqslant R \leqslant 16{:}1$

In this work it is pointed out that the plane-strain results are always less than those from axi-symmetric extrusion, although qualitatively the same, and so the constants in equation 1.30 which is of the same form as the two mentioned above should be determined for the axi-symmetric conditions, preferably by using a non-hardening material. The agreement that Purchase and Tupper[135] found between plane-strain and axi-symmetric results shows the need for caution in these experiments. As Alexander [113] pointed out, theory and experimental results can be made to agree by choosing a suitable value of $\bar{Y}$, the mean flow stress.

These equations by Johnson and his co-workers can only be applied to certain experimental conditions and only give the pressure needed to pass the material through the deformation zone adjacent to the die-face. The equation derived are limited in their application because they only consider very low reductions. In aluminium and copper alloy extrusion ratios in excess of 100:1 can be used. The results should possibly apply to the extrusion of iron and nickel alloys but the difficulty of determing a value of the flow-stress still remains.

To allow for variation in die shape, or dead-metal zone angle, Wilcox and Whitton obtained an empirical formula

$$\frac{P}{Y} = (0{\cdot}9 - 1{\cdot}6\cot\omega) + (0{\cdot}5 + 0{\cdot}8\cot\omega)\ln R \qquad 1.33$$

This applies to die angles $30° \leqslant \omega \leqslant 90°$

and extrusion ratios

$$5{:}1 \leqslant R \leqslant 150{:}1$$

This equation covers a far wider range of conditions than the previous ones and the authors claim an accuracy of 6%. Again the problem of determining the value of $\bar{Y}$ has to be overcome.

Hirst and Ursell used an equation obtained by Johnson[138] for plane-strain extrusion and, by using a slab method of analysis to include the effect σ friction, arrived at the equation

$$\frac{P}{\bar{Y}} = (0{\cdot}47+1{\cdot}20\ln R)\exp\frac{4\mu l_B}{D_B} \qquad 1.34$$

This implies that

$$\frac{P}{\bar{Y}} = 0{\cdot}47 + 1{\cdot}20\ln R$$

at the die face but this is not the case as the minimum load occurs a short distance in front of the die, followed by a rapid rise as the post-steady state is reached. The length L_B should then be less than the billet length .

A useful comparison of theoretical and empirical results has been given by Thomson et al [139] who show that the slab method of analysis gave reasonable agreement, the slip-line field theory was slightly low, and Johnson's equation, 1.32, was about 50% too high; the same value of the flow stress being used in each case .

Most theoretical and experimental work is concerned with either indirect extrusion or the minimum load at the end of direct extrusion, the two should be the same. What is of more importance to the press designer and operator is the maximum load developed at the start of the extrusion.

A general relationship for the extrusion pressure [113] is

$$\frac{P}{\bar{Y}} = a + b\ln R + cl_B \qquad 1.35$$

This implies a straight line relationship between P and L_B for billets of the same length and this has been verified by Ashcroft and Lawson[140] for extrusion ratios greater than 4. The constants a and b were temperature dependent.

1.4.3. Pressure for Multihole and Complex Shape Extrusion.

The bulk of experimental extrusions have been concerned with the plane strain or axi-symmetric extrusion of sheet or rod. In industrial practise the shapes produced are far more complex, ranging from simple multi-hole rod extrusion, to increase output, to the production of complex hollow sections using bridge dies, porthole dies, and mandrels.

Theoretical application stumbles over the axi-symmetric extrusion of rod and fallsdown completely when shapes are being considered.

The only theoretical work available is for plane-strain multihole extrusion by Dodeja and Johnson[120], although Johnson has mentioned an upper bound solution to the problem[117]. Slip-line field solution were obtained for smooth and rough container wall conditions for both two and three hole conditions. The results could be written in the form

$$\frac{P}{2k} 0{\cdot}47 + 1{\cdot}2 \ln R + \frac{\Delta P}{2k} \qquad 1.36$$

for a smooth container $2{:}1 \leqslant R \leqslant 12{:}1$

and $$\frac{P}{2k} = 0{\cdot}82 + 1{\cdot}2 \ln R + \frac{\Delta P}{2k} \qquad 1.37$$

for a rough container. $2{:}1 \leqslant R \leqslant 12{:}1$

These can be compared with the expressions for single sheet extrusion

$$\frac{P}{2k} = 0{\cdot}47 + 1{\cdot}2 \ln R \qquad 1.38$$

and $$\frac{P}{2k} = 0{\cdot}82 + 1{\cdot}2 \ln R \qquad 1.39$$

By plotting $\frac{\Delta P}{2k}$ against the eccentricity ε it was found that $\frac{\Delta P}{2k}$ varied considerably with ε and that a minimum occured. The position depended on the number of holes and frictional conditions . $\frac{\Delta P}{2k}$ was positive for all values of ε for smooth containers and negative for some values of ε for rough conditions. The predictions indicate that the extrusion pressure can be reduced by choosing the most suitable value of ε but other factors, such as the non-uniform flow may be more important. Comparison with their experimental values shows several interesting points;

1. The coring point, where the familiar extrusion defect of a core starts to form occurred later for a larger number of holes. This follows from the size of the deformation zone being reduced in proportion to the absolute size of the hole.
2. The value of $\frac{\Delta P}{2k}$ increases as the number of holes increases for any given reduction ratio and that the discrepency between the theoretical and experimental value increases as both the reduction and number of holes increases.

3. A qualitative agreement was obtained between the flow pattern and that predicted from the theory.

It was expected that as the number of sheets increased the difference netween $\frac{\Delta P}{2k}$ for single hole extrusion amd that for multi hole extrusion should decrease. The experimental observation led to a contrary conclusion and it was suggested that this was due to flashing.

Some empirical work on the multi-hole extrusion of rod has been done[1, 120, 141]. The general conclusion is that the load increases as the number of holes increases. By comparing the axi-symmetric results with those from plane-strain [120] it has been shown that the plane-strain pressure is always the lower. The theory failed to give more than a qualitative correlation with plane-strain results and so only a very approximate solution can be obtained by predicting the axi-symmetric pressure from the plane-strain theory.

The results also show that $\frac{\Delta P}{Y}$ increases as the number of holes increases, and that three holes in a line produce lower values than a triangular or square distribution, the opposite is found in the larger reductions used in industry[27]. The arrangement of the holes has more importance when the degree of lubrication decreases and the reduction ratio increases.

The effect of section shape on the load has not been studied in great depth, and has been briefly reviewed by Vater and Heil[142]. Results that have shown that the shape has little effect on the pressure have probably been obtained on shapes of a very simple nature [143,144]. Other workers have shown that the deformation resistance is very dependent on the section shape, increasing sharply with complexity. A problem in comparing results from different workers is in putting a numerical value to the shape's complexity. Vater used the peripheral ratio, the ratio of the periphery of the section to that of a circular section of equivalent area, which can be as high as 16. The experimental results showed that the peripheral ratio can be used to obtain semi-quantitative results, there was no apparent effect due to the different shapes with the same peripheral ratio, but the experimental error was quite large. They also found that the different land lengths used in different die shapes had no measurable effect on the load, more detailed experiments have shown the converse to be true[148]

1.4.4. Flow Patterns Developed During Extrusion.

Extrusion involves forcing a metal through a small orifice, usually of a complex shape, and this naturally entails the metal flowing in a complex manner.

The mechanical properties, extrusion pressure and surface finish will all be related to this flow pattern, the more complex the flow the more inhomogeneous the working. It is not surprising therefore that many workers have studied this aspect of extrusion. There are several methods available:-

1. Using model materials such as plasticine.
2. Macro-etching a part extruded billet.
3. Inscribing a grid on one half of a billet prior to extrusion.

Pearson and Parkins[1] classified the flow patterns into three kinds.

A - Found in lubricated and inverted extrusion, where the billet undergoes no deformation until it reaches the deformation zone.

B - Similar to type A except that no lubricant is used, and shear occurs between the billet and the container surface.

C - A more complex form found in many industrial extrusions, where a fairly thick rim of dead material extends down the sides of the stagnant zone, under the shoulder of the die, to the back of the billet. The material at the back is gathered into the centre and eventually forms the back end defect.

In aluminium extrusion the shape of the shear region between the deforming billet and the dead metal region has been described as approximately elliptical by Smith[18] although a semi-circular approximation can be made as well. Chadwick[28], in his review paper, has shown how the flow pattern developed can be very different in lubricated and unlubricated extrusion and how this can have a profound influence on the surface finish of the product. In lubricated extrusion the surface of the billet forms the surface of the extrude. In the unlubricated case the surface is formed by shearing of the metal at the die.

Flow in multi-hole extrusion has also been studied, both in plasticine [31], and metals [120,149]. The flow that occurs is asymmetrical and depends on the distribution of the holes. This can have important consequences on subsequent heat treatment. Vater [142] has also published some flow patterns for more complex shapes. The nature of the flow pattern in multi-hole extrusion was clearly shown by Dodeja and Johnson [120]. By extruding two billets, one behind the other, and then separating them, the complex shape of the zone in the billet could be seen.

One method of considerable importance, it represents a major advance in experimental techniques, is the visioplastic technique developed by Thomson and his co-workers [139]. Here a split-billet, with a grid inscribed on one half, is extruded in incremental steps and by removing the billet at the end of each step, the instantaneous velocity of a material particle can be found. By applying basic plasticity theory the stress and strain variation in the material can be studied.

More recently Hinesley and Conrad [151] have studied the dependence of the flow pattern on temperature and ram speed of an aluminium alloy using a visioplastic technique. The applicability is limited by the low extrusion ratio of 6:1 used and by the die angle of 60°. They found two types of the flow occured. One with a single maximum (a peak in the curvature of the transverse grid lines) and one with a double maximum. They point out that this was predicted by Zimmerman and Autzur [152] for certain conditions of die angle and reduction ratio. Analysis of the results showed that this change in pattern occurred at a certain value of the temperature compensated strain rate Z.

The flow pattern is therefore a very important variable in extrusion but there is no way of predicting it from theory, apart from the slip-line field and upper bound approaches. These can only give approximate patterns in a limited number of cases. More work is needed on the pattern developed in the extrusion of complex shapes although this will involve considerable experimental work.

1.4.5. The Effect of Ram Speed on Extrusion Pressure.

The theoretical analysis of extrusion, both upper bound and slip-line field, makes no provision for the effects of variations in ram speed, other than in the value used for the mean yield stress. The operating speed of a press is very important from the production viewpoint but it has had little attention given to it. Pearson and Parkin give the equation

$$V = bP^a \qquad 1.40$$

where a and b are constants depending on the temperature and the material. The index a can be considered approxiamtely constant and its value is such that over the industrial range of speeds the variations caused by changes in speed are very slight. These slight changes in pressure were verified by Ashcroft and Lawson[140] for speeds of 15 to 75cm/min. They did notice that below 15 cm/min the pressure varied considerably. At 20°C a decrease in the speed caused an increase in the mazimum pressure, but at 300°C a similar decrease in the speed caused a decrease in the pressure. No reasons for this were put forward.

1.4.6 The Influence of Temperature on the Extrusion Pressure.

The resistance to deformation of metals decreases as the temperature increases and this is reflected in the extrusion pressure. The higher the temperature the lower the pressure required. The exact relationship netween the two is not clear. Ashcroft and Lawson[140] found a linear relationship between the maximum pressure and the temperature of working for the extrusion of aluminium and an Al-Zn-Mg-Cu alloy. Hughes found a similar relationship for steels. However Pearson quotes the equation

$$P = Ae^{-\lambda T} \qquad 1.41$$

where λ depends on the material and for an Al-5%Cu alloy $\lambda = 0.0064$

These two different relationships can be explained by considering the range of temperatures examined. Over a range of about 200°C for aluminium and its alloys equation 1.41 can be approximated by a straight line, some of Ashcroft's results could be fitted to a curve as well as a straight line.

1.4.7. The Temperature Rise During Extrusion.

The two previous sections have shown how the pressure in extrusion can be related to the speed and temperature. It is a common observation that metals heat up during deformation and it has been estimated that up to 95% of the work done reappears as heat, the rest being stored in the deformed structure[152]. This temperature rise will have a marked effect on the deformation of a metal, but it is often ignored because of the difficulty in measuring it, or providing a theoretical estimate of it. In extrusion the magnitude of this temperature rise is complicated by the heat losses that occur to the tooling; the container, die, and ram are usually cooler than the billet.

The most exact theoretical treatment available is that by Bishop[6], who calculated the temperature rise due to the work done at the velocity discontinuities in a slip-line field solution. His solution also allowed for conduction within the material. Bishop admits that the process involves a considerable amount of labour[112], and no one else has attempted to apply a similar solution to a different set of conditions. An obvious simplification is to substitute an upper-bound solution for the slip-line field. This has been done by Tanner and Johnson[153] who showed that back conduction can be ignored when the speeds normal to the velocity discontinuities exceed 5cm/sec. This approach has been extended by Johnson and Kudo[154] to axi-symmetric solutions.

No theory can be justified unless it is tested by experiment and some work has attempted to measure the temperature rise in extrusion. Work at the National Engineering Laboratory[155,156] measured the temperature rise by inserting thermo-couples into the billet prior to extrusion. Reasonable results were obtained although the relative size of the billets and the thermo-couples would have altered the metal flow. Their work suggested that the method of extrusion, direct or indirect, and the use of a lubricant had little effect on the temperature rise ΔT, but the magnitude of ΔT was very dependent on the ram speed. The size of the billets used was very small, 2.54cm by 2.54cm diameter, and it is doubtful if the results can be meaningfully applied to the industrial scale. Singer and Cookham measured the temperature rise in the extrusion of aluminium, lead, and tin, by means of a two-prong thermo-couple situated just below the die.

This was the first attempt to measure the temperature of the emergent extrude. Their work was later extended to include a simple theory to explain the results.

The results show a linear relationship netween the log of the ram speed and the temperature rise. By varying the speed during extrusion the possibility of controlling the temperature of the emergent extrude was shown[11]. This could have an industrial application when working close to the melting point of some alloys.

The theory that they proposed considered all the deformation to take place in the plane of the die. They then calculated the temperature distribution in the billet, assuming axial heat conduction from the deformation zone and a billet of infinite length. By assuming perfect contact between the billet and the container, a reasonable assumption when the pressures involved are considered, an approximation of the heat lossesto the tooling was made. Whilst this theory predicts a linear relationship between ΔT and log V, except at high and low speeds where adiabatic and isothermal condition respectively are operating, there was only qualitative agreement with the experimental results for aluminium.

Akeret[12] obtained a reasonable agreement with experimental results by dividing the billet into cells and calculating the heat flow from cell to cell. He also allowed for the temperature gradient between the billet and the container. Altan and Kobayash[157], used a more rigorous approach which entailed analysing the flow by the visioplastic method and then calculating the temperature rise. The results obtained were experimentally verified by extruding thermocouples in the billet. The low extrusion ratios used, 2 and 4, enabled this to be carried out relatively easily. Their work did indicate that the billet surface temperature was equal to the die surface temperature.

Ideally the temperature variation in the deformation zone needs to be known. The nearest that anyone has come to achieving this, for practical extrusion ratios, is to insert thermocouples into the dead metal zone of the billet. Using this technique Sheppard and Raybould[13] successfully measured the temperature rise under a variety of conditions and compared the results with theoretical productions based on an upper bound solution, similar to that used by Tanner and Johnson[153], and on an integral profile solution. The integral profile method gave good agreement with the experimental results, although

slightly lower, and the accuracy improved as the ram speed decreased. Their results showed a very brief period of constant temperature followed by a rapid rise to a region where the temperature rises more slowly. The faster the ram speed the higher the temperature rise, as adiabatic conditions are reached. At a speed of 63.5mm/sec the temperature rise was over 200°C. An important result of their work was the role played by phase changes on ΔT. Some heat is required to redissolve a precipitate and this lowers the observed temperature rise. The experimental results were only obtained for two extrusion ratios, 30:1 and 50:1, and need to be extended before the theory can be verified. A problem at higher extrusion ratios will be in successfully inserting thermocouples into the dead metal zone.

From an industrial viewpoint, the methods of temperature measurement outlined above are not practical. A two-prong thermo-couple will mar the surface finish and the dead metal zone technique is far too difficult to be used. It is possible to place a thermocouple in the die although this will only give an indication of the temperature, and cannot predict any sudden change.

To date the only really practical method of temperature measurement is by a pyrometer situated just below the die. For very high temperature extrusion the only problem is in the coating of lubricant, if any, om the extrude's surface. In aluminium extrusion the problems that have to be overcome have been discussed by Woolvet and by Reynolds.[58,59] Experimental results that they obtained show that accurate readings with a pyrometer are possible, providing a constant surface finish is maintained, and this is very difficult to achieve.

A problem that is rarely mentioned in experimental reports is the gradual accumulation of heat in the container throughout a long production run. This is a problem that merits more attention, it should not be too difficult to measure the temperature in a container. Some investigations into this problem have been carried out, using hydro-analogue techniques

1.4.8. Strain Rates in Extrusion.

The section on hot-working shows that the flow- stress of a metal depends on the temperature and the strain-rates, and that tests are usually carried out at a constant true strain-rate with the temperature rise being ignored or adiabatic condition assumed.

The previous section shows that the temperature rise can be predicted with a reasonable degree of accuracy, but that the magnitude of the temperature rise can be considerable. The strain-rate in extrusion is even more difficult to predict.

The mean strain rate will be a function of the total strain and the ram speed i.e.

$$\bar{\dot{\varepsilon}} = f(\ln R, V) \qquad 1.42$$

or

$$\bar{\dot{\varepsilon}} = f((a + b\ln R), V) \qquad 1.43$$

depending on the definition of strain used. The function will reflect the variation in deformation that occurs.

The first method of obtaining a numberical value for $\bar{\dot{\varepsilon}}$ was suggested by Feltham who assumed that the deformation occurred within a core of semi-angle 45° and that the total strain occurring in this volume is $\ln R$. The time taken to effect this strain can be found by dividing the volume of the core by the volume extruded per unit time. This gives

$$\bar{\dot{\varepsilon}} = \frac{6V\ln R}{D_B} \qquad 1.44$$

Alexander [113] pointed out that the work done per unit volume is given by $Y(a + b\ln R)$ and so the mean effective strain-rate should be

$$\bar{\dot{\varepsilon}} = \frac{6V(a+b)\ln R}{D_B} \qquad 1.45$$

Wilcox and Whitton [136] pointed out that the core of deformation does not usually contain an angle of 45° and so equation 1.44 should be multiplied by $\tan\omega$, where ω is the effective angle formed by the dead metal zone or conical die surface. Even this is an approximation as the cone of deformation rarely has straight sides.

Jonas and Chandra [162-164] examined the strain-rate developed more closely. For homogenous deformation the strain-rate at any point is given by

$$\dot{\varepsilon}_x = \frac{4VD_B^2\tan\omega}{D^3} \qquad 1.46$$

with reference to fig. 1.2.

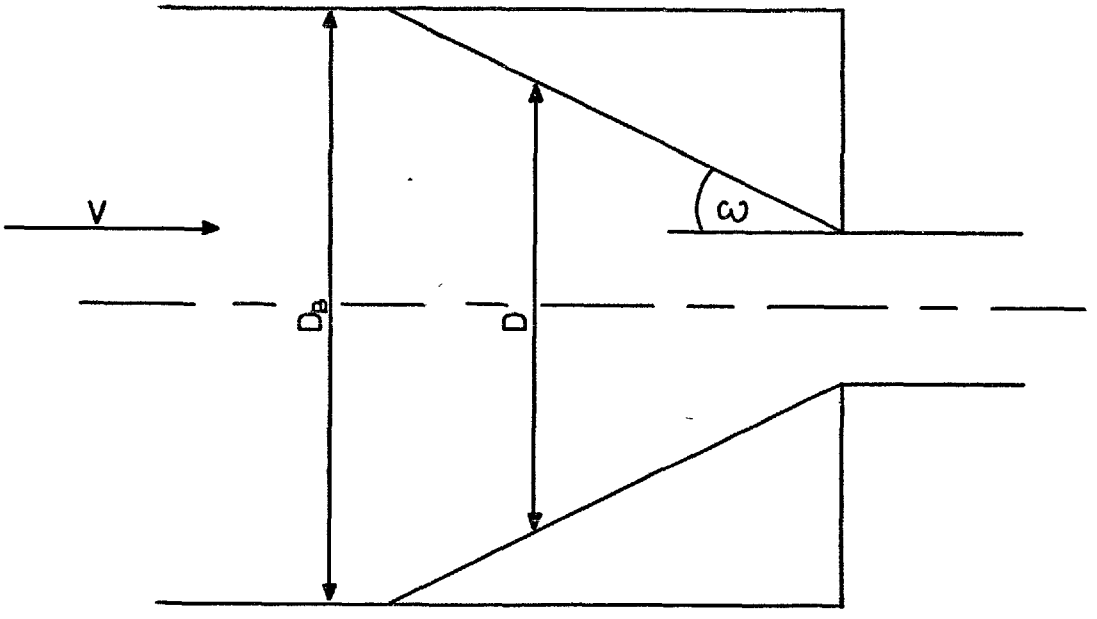


Fig. 1·2 The variation in the strain rate in the deformation zone.

For a die of 100:1 reduction and a semi-angle of 45° this gives a variation in the strain rate of three orders of magnitude in the deformation core. They also gave three possible mean strain-rates

$$\bar{\dot{\varepsilon}}_\varepsilon = \frac{1}{\ln R}\int_0^{\ln R} \dot{\varepsilon}\, d\varepsilon \qquad 1.47$$

$$\bar{\dot{\varepsilon}}_x = \frac{1}{x_f}\int_0^{x_f} \dot{\varepsilon}\, dx \qquad 1.48$$

$$\bar{\dot{\varepsilon}}_t = \frac{1}{t_f}\int_0^{t_f} \dot{\varepsilon}\, dt \qquad 1.49$$

depending on whether the mean is taken with respect to strain, axial distance, or time, within the deformation zone.

Usually $\bar{\dot{\varepsilon}}_\varepsilon > \bar{\dot{\varepsilon}}_x > \bar{\dot{\varepsilon}}_t$, but in the case of a constant strain-rate die [162] $\bar{\dot{\varepsilon}}_\varepsilon = \bar{\dot{\varepsilon}}_x = \bar{\dot{\varepsilon}}_t$; this only holds for homogenous deformation.

The equation derived by Feltham gives $\bar{\dot{\varepsilon}}_t$ and it was concluded that this should only be applied to small reductions. By considering the extrusion of a rate sensitive material, where

$$\sigma = k\,\dot{\varepsilon}^m \qquad 1.50$$

they proved that the extrusion pressure is proportional to the mean power strain-rate $\dot{\varepsilon}_\varepsilon^m$ and so the mean strain-rate that should be used is

$$\bar{\dot{\varepsilon}}_{RMP} = \left(\dot{\varepsilon}_\varepsilon^m\right)^{\frac{1}{m}} \qquad 1.51$$

This gives a mean strain-rate of

$$\bar{\dot{\varepsilon}} = 4VD^2\tan\omega\left[\frac{2}{3m\ln R}\left[\left(\frac{1}{D_E}\right)^{3m} - \left(\frac{1}{D_B}\right)^{3m}\right]\right]^{\frac{1}{m}} \qquad 1.52$$

Comparison with that derived by Wilcox and Whitton gave a difference of 24% at a reduction ratio of 4 and nearly 1000% at 169. Equation 1.52 was verified by the homogenous indirect extrusion of ice.

A more recent approach by Farag and Sellars [17] has developed this approach to materials that obey equation 1.7

$$Z = \dot{\varepsilon}\exp\frac{Q}{RT} = A\exp\beta\sigma$$

This approach gives a mean value of Z for extrusion

$$Z = \frac{4D_E^2 V\tan\omega}{(D_B \times D_E)^{3/2}}\exp\frac{Q}{2R}\left(\frac{1}{T_0}+\frac{1}{T_f}\right) \qquad 1.53$$

where T_0 and T_f are the initial billet temperature and the emergent extrude temperature respectively.

Equation 1.53 can be used to give the pressure for homogenous extrusion Ph

$$Ph = \frac{1}{\beta}\int^{\ln r} \ln\frac{Z}{A}\,d\varepsilon = \frac{1}{\beta}\left(\overline{\ln\frac{Z}{A}}\right)\ln R \qquad 1.54$$

By using a factor to allow for redundant work these expressions were used to calculate the pressures for the extrusion of aluminium through dies of reduction ratios 4.75-36 over a wide range of temperatures and strain-rates. The constants in equation 1.7 were obtained from hot torsion tests. The results obtained were surprisingly good.

It can be concluded that at the present time, there is no satisfactory method of obtaining a mean-strain rate that can be successfully applied to data derived from other testing techniques to predict extrusion pressure. The visioplasticity technique can give the true strain rate distribition in axi-symmetric extrusion but this method is difficult to apply to shapes. Any strain rate value must be applicable to both simple rod and complex shape extrusion and the only relatively simple measurement that can be made for all shapes is that of the volume of the cone of deformation. This will have a direct dependence on the shape of the extrude. Therefore the original approach by Feltham[161] appears to be the one that should be used. It remains to be seen if this approach can be successfully applied to shape extrusion. No matter what value of the strain-rate is used no direct comparison can be made with those obtained in other processes, but it should be possible to compare results from different extrusion experiments. It would be useful if the method used was always quoted when reporting any results.

1.4.9 The Peak Loads Developed in Extrusion.

For direct extrusion the pressure displacement diagram is of the form shown in fig 1.3. It can be divided into three regions.

1. The billet is upset and the load rapidly rises to a peak value.
2. The load falls from the peak value and steady-state extrusion starts. A gradual fall in pressure is usually seen in this region and this can be attributed to the decreasing billet length and the change in flow stress due to the temperature rise.

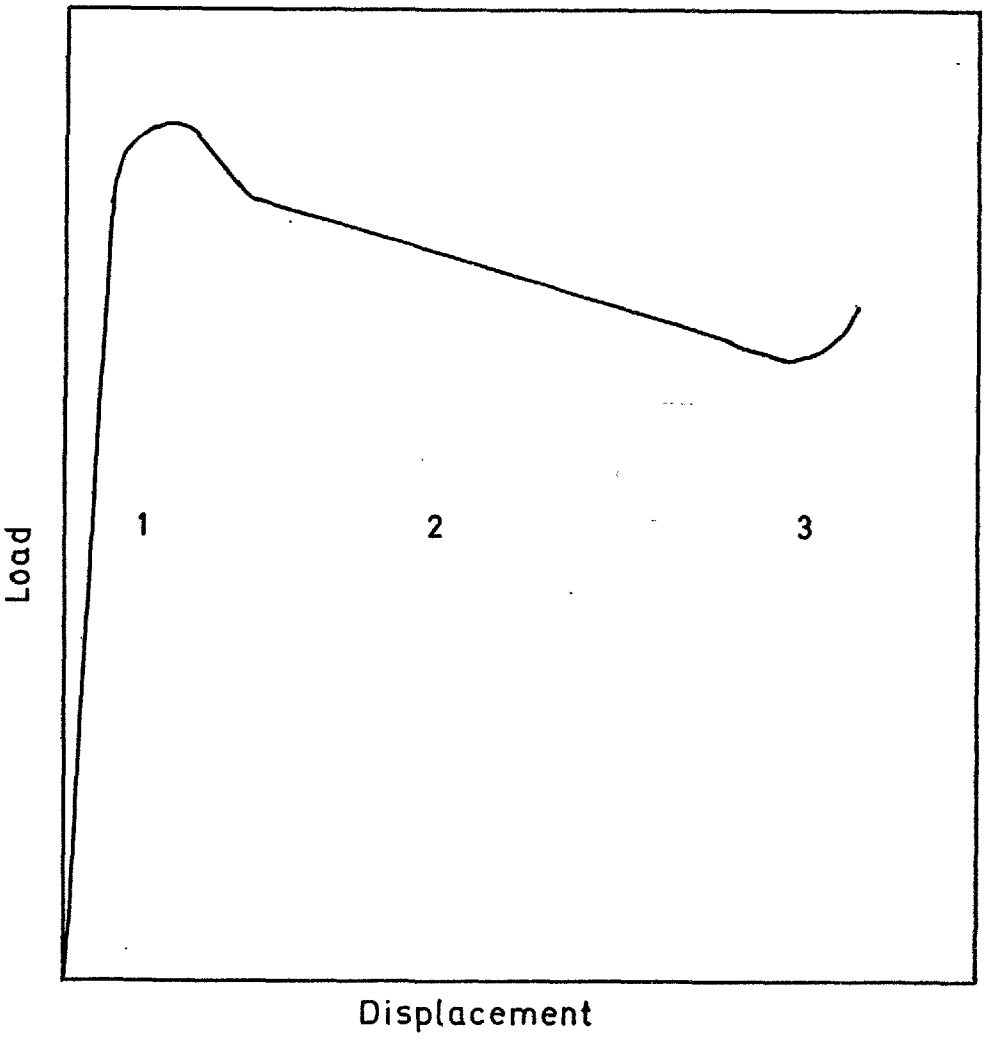


Fig. 1·3. Schematic load displacement curve for extrusion.

3. A minimum value of the pressure is reached followed by a rapid rise. This is associated with a post steady state and the onset of coring.

The factor that controls the possibility of extruding or not is the maximum load. If this is above the press capacity then extrusion is impossible.

The occurrence of a peak, which is not always seen, has been recognized many times[1,3,130], but there is no agreement on its cause. Johnson and Kudo[3] suggest that it may be due to a decrease in the friction coefficient following the initiation of metal flow, i.e. a change from sticking to sliding friction. Wilcox and Whitton[136] associate the peak with the formation of a dead metal zone. According to Avitzur[130] the possible causes are :-

1. The formation of a dead metal zone.
2. The difference between static and dynamic friction, or shear by hydrodynamic lubrication.
3. Inertia.

Ashcroft and Lawson[140] observed the occurrence of a peak above a certain temperature in an Al-Zn-Mg- alloy, and load displacement curves published by Farag and Sellars[17] for aluminium extrusion show that peaks occurred with die semi-angles less than 90°, at reduction ratios greater than 36:1. In steel extrusion the peak loads have been attributed to the cooling of the billet at the die[165]. Substantial peaks have also been seen in indirect extrusion[166] and are a well known feature of torsion and compression tests[35,75,167]. The general conclusions appear to be

1. The peak height is affected by the specimen size in torsion.
2. The ratio of the peak torque to the steady state torque decreases as the temperature increases.
3. The strain to the peak is reduced as the temperature increases.
4. Peaks are seen at high stresses.

Although peak loads have been noticed by many workers, no measurements of the magnitude of the peak appears to have been made. The peak heights can be very high, up to 15% of the total load in aluminium alloy extrusion, and up to 40% in the extrusion of phosphor bronze powders[168].

Structural changes occurring at the start of deformation have only been briefly studied[35,36,72].

The flow stress first increases as the dislocation density increases and a sub-structure begins to form, and has achieved a steady state by strain of 0.2 to 0.3 at strain rates of 0.05-1.0 sec^{-1} The height and the width of the peak, and the strain at the peak, increases as the strain rate increases, or the temperature decreases, and the magnitude of the peak depends on the metal being studied. Nickel has a large peak, copper a smaller one, and commercial purity aluminium a very small one. By quenching the speciment at the peak torque[72] the different structure in these metals have been studied. Aluminium had a continuous substructure from the surface to the centre, the definition improving near the surface. Rossard and Blain[36] noticed a similar structure in the torsion of an Fe-25% Cr alloy. Copper showed deformed original grains with a general banded structure and small recrystallized grains. Nickel had an intermediate structure. From these results Hardwick concluded that the peak in torsion can be associated with the operation of a restoration process in hot working, and that its magnitude is an indication of the ease with which this can occur. In the case of aluminium, dynamic recovery leads to a small peak.

The peak load phenomena has not been adequately explained, its dependence on the size of the specimens in torsion indicates that inertia might be important, but this does not explain the absence of a peak under certain conditions. It can be argued that the presence of a peak is of little industrial importance, especially in the aluminium industry, where the surface finish is the important factor and presses usually operate well within their capacities. This argument does not consider the possibility, if the peak can be eliminated, of being able to improve production by using longer billets, or to use larger reduction ratios leading to better mechanical properties in the as extruded rod. In the cold extrusion industry where presses operate very close to their full capacity the peak can be of major importance. The loads predicted by the various theories all give the minimum load or at best the load at the beginning of the steady state region, which is not the peak load. The actual load at the start of extrusion can be much higher. Apart from the usefulness of being able to predict the peak load its presence is a phenomena that should be explained.

1.4.10 Measurement of the Flow Stress in Extrusion.

From the experimental point of view it is necessary to have a value for the flow stress in extrusion. There are two methods that have been used. The first[14] assumes that the total extrusion pressure P_t consists of three independent parts

$$P_t = P_h + P_f + P_r$$

where P_h = the pressure for homogenous deformation.
P_r = the pressure expended in redundent work.
P_f = the pressure to overcome friction, including die land friction.

Ph is given by

$$P_h = \int \sigma \, d\varepsilon \qquad 1.55$$

the coefficient of friction was found from the rate of change of the pressure with the billet length during extrusion.

$$\mu = \frac{D_B}{P} \frac{dP}{dx} \qquad 1.56$$

where x is the axial distance along the container.
This gives

$$P_f = P_0(\exp(4\mu l/D_B)-1) \qquad 1.57$$

where l is the length up to the coring point
and P_0 is the pressure at the coring point.
The pressure for redundent deformation was estimated from

$$\frac{P_r}{\bar{\sigma}} = \frac{P_0 - P_h}{\bar{\sigma}} \qquad 1.58$$

An estimate of $\frac{P}{\bar{\sigma}}$ was made from a study of the literature and the flow stress was obtained from

$$\sigma = \frac{P_t}{\frac{P_h}{\sigma} + \frac{P_f}{\sigma} + \frac{P_r}{\sigma}} \qquad 1.59$$

This method gives a mean value of a flow stress but it is not possible to judge how this relates to the true mean flow stress if there is one. It is unlikely that P_h and P_r can be treated as separate functions, as the very presence of redundent deformation prevents homogenous deformation.

The second method involves using a slip line field or upper bound approach[13,17]. The flow stress calculated will depend on the solution used. As the upper bound solution gives an over estimate of the load then any value of the flow stress calculated will be an under estimate of the true value. It is not possible to measure the error this will cause, but the more refined the upper bound the more accurate will be the flow stress. This second method is more acceptable that the first as it considers the variation in the flow that occurs in the deformation zone.

1.4.11. Defects in Extrusion.

A major problem in the aluminium industry is the control of the surface finish of the product. This is of importance in its own right and if subsequent heat-treatment or anodizing processes are to be carried out. The usual defects[24,25] have been mentioned in section 1:2 but there has been very little work of a qualitative nature published on this subject. Ashcroft and Lawson[140] mention the occurrence of hot shortness of an Al-Zn-Cu-Mg alloy above 480°C and how it can appear midway through an extrusion as the temperature rises. It is generally believed that this defect is a result of incipient melting, causing the extrude to break up. This defect has been mentioned by Johnson and Kudo[3] and by Pearson and Parkin[1]. Another problem occurs from the tendency of aluminium to stick to the die surface and this accumulation gives heavy scoring on the surface of the product.

The only extensive work available on the subject is by Williams[169] who examined several defects and arrived at the following conclusions:-

1. The pick up defect is characterized by drag marks on the surface of the extruded section and appears above a surface temperature of 525°C in an Al-Mg-Si alloy. The metal tends to cling to the exit of the die but not to the entrance. The coating that collects on the die can be cleared by stopping and starting the press, leaving a stop mark on the surface. A possible explanation of this is deflection under the applied load, returning to its original position when the load is removed. The use of a die with a conical lead in prevents the occurrence of this defect.

2. Hot shortness occurs above a critical value of the exit temperature, measured by a contact thermocouple. The accumulation of heat in the tooling during a series of runs has a strong effect because this reduces the heat losses occuring during extrusion.

More controlled experiments are needed in this field of study, bringing in the more recent theories of hot-working and temperature rise, and the results obtained should be made available. It would be interesting to compare the occurrence of hot shortness obtained in different testing techniques.

1.4.12. Limit Diagrams.

The complex interaction of structure strain rate, and temperature occurring during hot working, and the nature of extrusion theory, makes it very difficult to predict the limiting conditions of the process. This problem was recognized by Hirst and Ursell[32] who developed a graphical method of representing all the factors, fig. 1.4 . The maximum value of R that can be extruded with a given press capacity increases as the temperature increases. By using the equation

$$P = \bar{Y}(0{\cdot}47 + 1{\cdot}2\,(\ln R)\exp\frac{4\mu L_B}{D_B}$$

and values of the flow stress from compression at an arbitrary strain rate of 30sec^{-1} a line of log R versus temperature was drawn. Above a certain temperature the metal will melt and a limiting line can be drawn corresponding to the melting point. To allow for temperature rise Hirst and Ursell assumed adiabatic conditions and calculated the mazimum value of R for this case. It should be possible to determine a diagram from experimental results and by extensive iteration Ashcroft and Lawson gave a diagram for an Al-Zn-Mg-Cu alloy[140].

The work involved in obtaining a diagram from experimental results makes it desirable to have a theoretical method for their construction. Meadows and Cutler[33] improved the original method used by Hirst and Ursell. The limiting pressure line was calculated from the same expression for the load, obtaining the yield stress from cam-plastometry work, but used the equation derived by Singer and Al-Sammarrai[11] to predict the temperature rise.

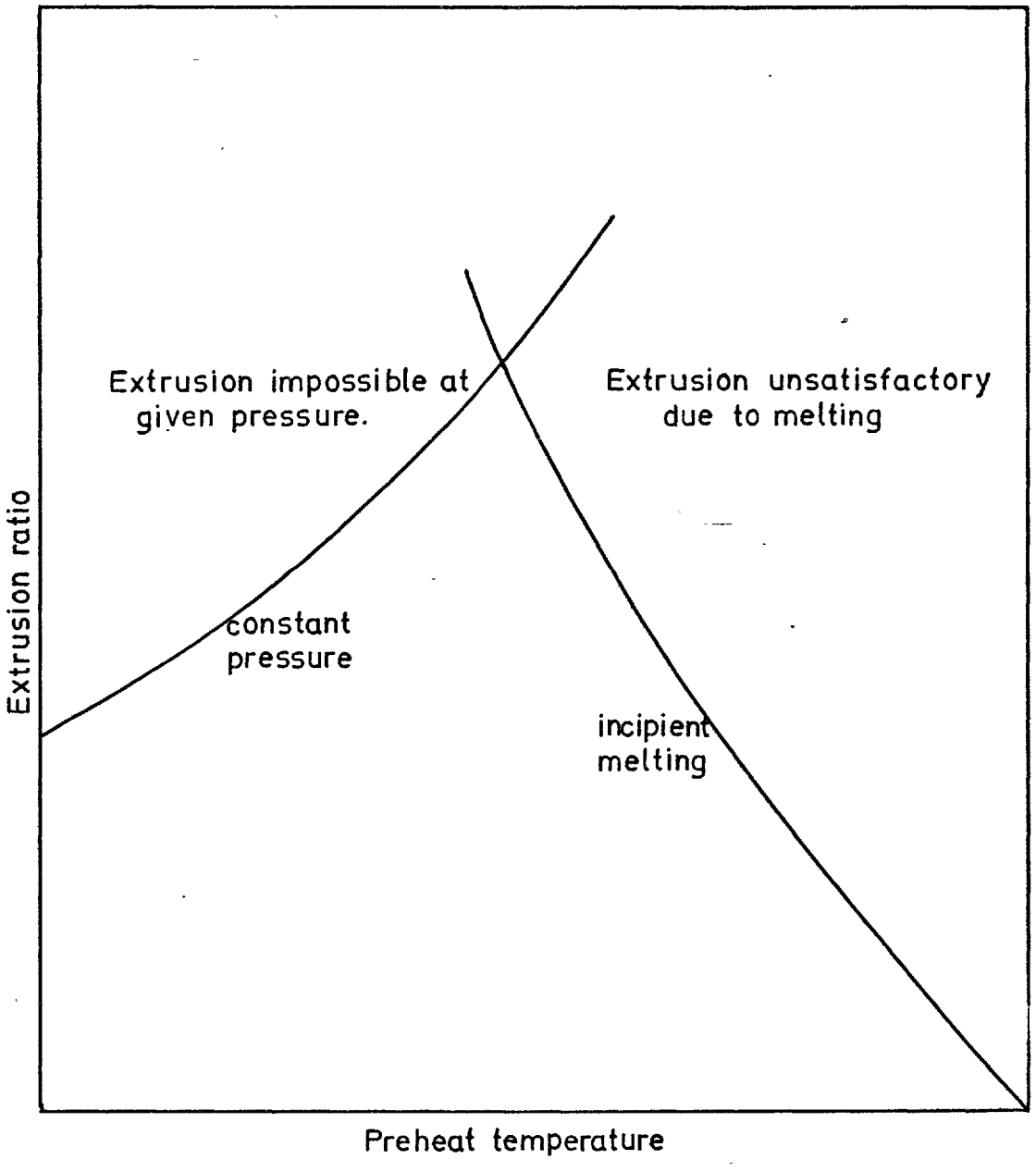


Fig. 1·4 Hirst-Ursell limit diagram.

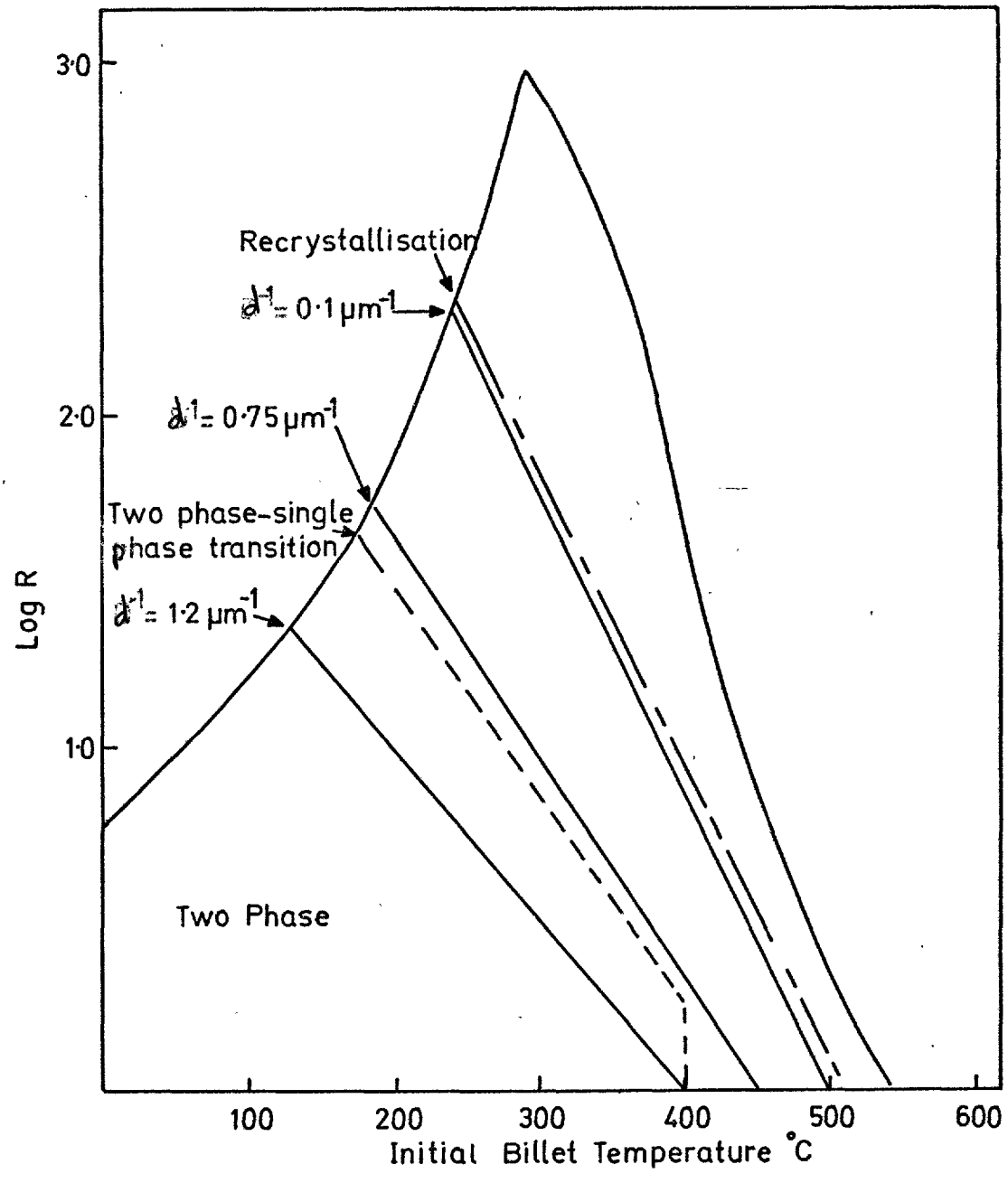


Fig. 1·5 Limit Diagram for Al 7% Zn 3% Mg. Water quenched $\dot{\varepsilon}$ = 16·0 sec^{-1}. Max. Pressure = 88N/mm^2 (from Raybould).

The diagrams in these forms are limited in their application. The method of obtaining the flow-stress is somewhat arbitrary and Singer's equation for the temperature rise has been shown to be in error[13].

A more useful form of the diagrams was developed by Raybould and Sheppard[34] who drew the diagrams for a constant pressure . Instead of plotting ram-speed curves, constant strain rate curves were plotted. The flow stresses used in the derivation were obtained from hot working theory, and the maximum value of R the reduction ratio found from a minimized upper bound solution.

The temperature rise was predictued from a derived equation that has been proved to be more accurate than Singer's[13]. By drawing lines of constant strain rate the form of the diagram fig.1.5, was noticeably different from the earlier ones, with a crest occurring. This indicates the possibility of extruding at much higher reduction ratios, by selecting optimum values of temperature and strain rate. The difficulty in controlling these limits will lower the maximum value of R possible.

There was no experimental confirmation of the upper parts of the diagrams. Experimental results demonstrated that recrystallization occurred below a critical value of Z , depending on the material and the rate of cooling[16]. This value of Z was found from a plot of log $\sinh(\alpha\sigma)$ versus d^{-1} . The critical value being the intercept when $d^{-1} = 0$. The value of Z obtained was somewhat arbitrary because the experimental points showed considerable scatter and the connecting line was assumed to be a curve at low values of d^{-1} . Accepting this idea of a critical value of Z, a value of the recrystallization temperature at a given strain rate can be calculated. Thus a line may be constructed to show the limiting value for a recrystallized structure. A similar dependence of the subgrain size on Z enables lines to be constructed to give the limits for a desired subgrain size, the mechanical properties of the extrude being related to the subgrain size, section 1.37. Obviously the position of these structure lines needs experimental confirmation but they should be applicable to industrial conditions.

The diagrams can be plotted with the temperature axis being either the calculated working temperature, or the initial billet temperature. The first gives the true temperature limits but the second is the one to be used as the operator controls the initial billet temperature.

In the latter case the temperature rise will depend on the billet dimensions and this should be mentioned on the diagrams, as should the equation used to calculate the strain rate. With a knowledge of hot working theory it should be possible to predict these diagrams from simple torsion or compression tests, although no allowance can be made for the interaction between the material and the tooling. Any diagram so constructed must be verified experimentally.

1.5. Summary.

The reauirements for a theory of extrusion were summarized by Alexander [113] in 1962 as

1. To predict the forces
2. To predict the behaviour of the material.

This excellent summary still holds today as no adequate theory has yet been found. Hot working theory gives empirical equations that can be used to relate the variables of strain-rate and temperature for a given material, the theoretical equations can only give a qualitative treatment. However, the use of these equations in extrusion is limited by the difficulties in obtaining a value for the mean strain rate and for the temperature of working. Plasticity theory enables the loads developed to be predicted but the values obtained all require a value for the mean flow stress, which can only be approximated by results from other testing methods. The concept of a specific pressure to extrude a metal is incorrect. The pressure will be a complex function of the deformation and the hot working parameters.

The temperature rise can be measured experimentally and predicted by theory but there is still no method of accurately measuring the temperature of the emergent extrude. What the theory can do is to correlate data obtained from controlled extrusion experiments and these results can be applied with care, to large scale industrial practise.

Ther are still many problems to be studied and these can be solved by planned research, preferably on a semi-industrial scale press. The relation between small scale experimental work and large scale industrial practise has not been tested.

CHAPTER TWO

THEORY

2.1 Derivation of Stress Strain Curves from Torsion Tests.

With reference to figure 2.1 , which shows the forces acting on a bar deformed in torsion, the bar is subjected to a twisting moment at the end, and this is balanced by a resisting moment, caused by shear stresses in its cross-section. At the centre the shear stress is zero and increases to a maximum at the outer surface.

The shear strain is given by

$$\gamma = \frac{r}{L} \qquad 2.1$$

Equating the twisting moment to the resisting moment

$$M_T = \frac{\tau}{r}\int_0^a r^2 dA = \frac{\tau J}{r} \qquad 2.2.$$

where J is the polar moment of inertia.

In the elastic region the shear stress varies linearly across the cross-section. This is not the case when large plastic strains are being considered. However, it is still possible to derive a shear stress - shear strain diagram from the experimental torque-twist curve by using the approach developed by Nadai, and given in Dieter.[170] Thus we may write

$$\tau = \frac{1}{2\pi a^3}\left(\theta'\frac{dM_T}{d\theta'} + 3M_T\right) \qquad 2.3.$$

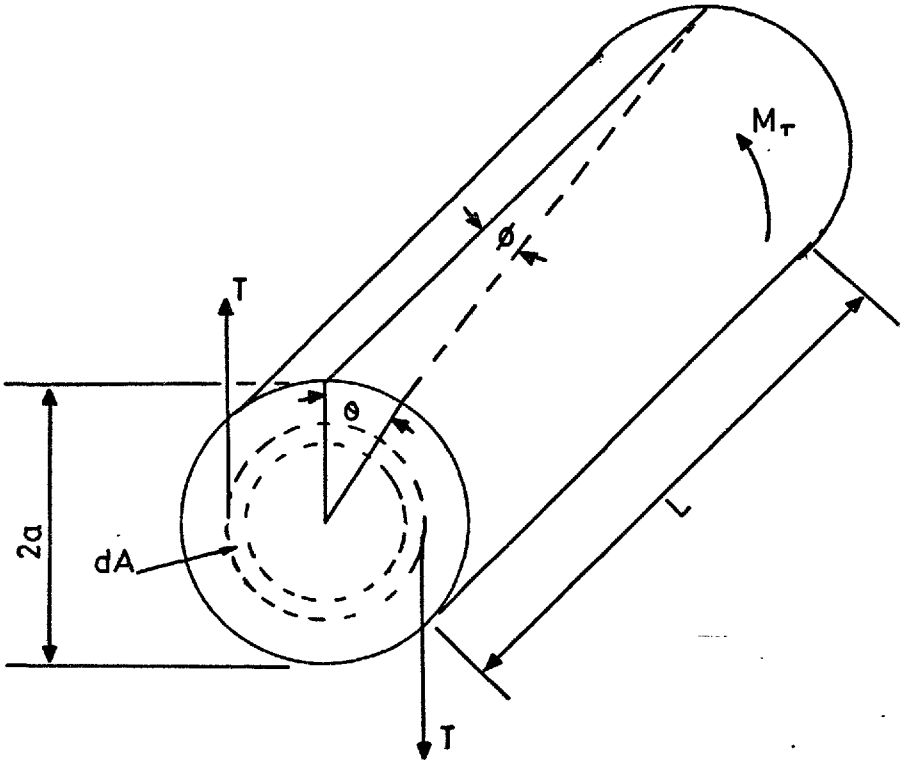
This can be rewritten in the form

$$\tau = \frac{1}{2\pi a^3}(BC + 3CD)$$

where BC and CD are shown in figure 2.1.

In hot working experiments the value of BC is small, a steady state usually being reached. Therefore

$$\tau = \frac{M_T}{2\pi a^3} \qquad 2.4$$



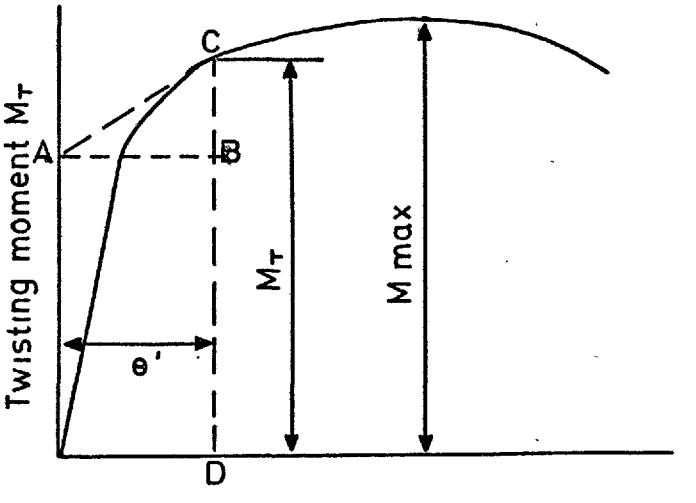


Fig. 2·1 The torsion of a solid bar.

By using von Mises yield criterion, the shear stress may be replaced by the equivalent stress in tension.

$$\sigma = \sqrt{3}\,\tau \qquad 2.5$$

The strain is then given

$$\dot{\varepsilon} = \frac{R\theta}{\sqrt{3}\,L} \qquad 2.6$$

and the strain rate by

$$\dot{\gamma} = \frac{R\omega}{L} \qquad 2.7$$

where ω is the angular speed of the test specimen.
Equation 2.7 may be rewritten as

$$\dot{\varepsilon} = \frac{R\omega}{\sqrt{3}\,L} \qquad 2.8$$

The experimental results were in the form of torque-time curves. The torque was measured at known time intervals and the true stress-true strain curves calculated by means of the computer program given in appendix I. No allowance was made for the temperature rise, because of the difficulty in calculating the heat losses from the specimen to the tooling and the atmosphere. Except for the highest strain rate used, 5.89 sec^{-1}, it is doubtful whether adiabatic conditions can be assumed.

2.2 Upper Bound Solutions for the Extrusion Pressure.

For reasons of simplicity the theoretical extrusion pressure was calculated by an upper bound approach, rather than the more complex slip-line field method.

2.2.1. Plane Strain Single Hole Extrusion.

From Johnson, the true mean rate of plastic working, which is the extrusion load, is less than

$$k\left[\int \dot{\gamma}\, dV + \int v\, ds\right] \qquad 2.9$$

where k is the shear yield stress in plane strain

$\dot{\gamma}$ is the maximum shear strain rate in an element of volume dV.

vds is the product of the absolute value of any tangential velocity discontinuity and the line element over which it prevails.

By assuming the deforming material to consist of blocks of rigid plastic material the strain rate $\dot{\gamma}$ is zero. If straight line discontiniuities are also assumed, the load is simply found by summing the products of the lengths of the discontinuities and the absolute values of the tangential velocity discontinuities.

In figure 2. 2 the deformation zone is divided into two rigid triangles. From the assumed positions of the line discontinuities the hodograph in figure 2.2 can be drawn. To calculate the load the lengths of the velocity discontinuities and the corresponding line discontinuities are needed. By simple geometry

$$AO = \frac{a}{\sin\omega}$$

$$OC = \frac{R_E}{\sin\psi}$$

$$BO = x$$

$$AB = \left(\frac{a^2}{\sin^2\omega} + x^2 - 2ax\cot\omega\right)^{1/2}$$

$$BC = \left(\frac{R_E^2}{\sin^2\omega} + x^2 - 2R_E x\cot\psi\right)^{1/2}$$

The triangles in the hodograph are similar to those in the assumed discontinuity pattern. The relative velocities are then given by

$$\overline{13} = \frac{a}{x\sin\omega}$$

$$\overline{54} = \frac{a}{x\sin\psi}$$

$$\overline{23} = \frac{1}{x}\left(\frac{a^2}{\sin^2\omega} + x^2 - 2ax\cot\omega\right)^{1/2}$$

$$\overline{24} = \frac{a}{xd}\left(\frac{R_E^2}{\sin^2\psi} + x^2 - 2R_E x\cot\psi\right)$$

$$\overline{34} = 1 + \frac{a}{R_E} - \frac{a}{x}(\cot\omega + \cot\psi)$$

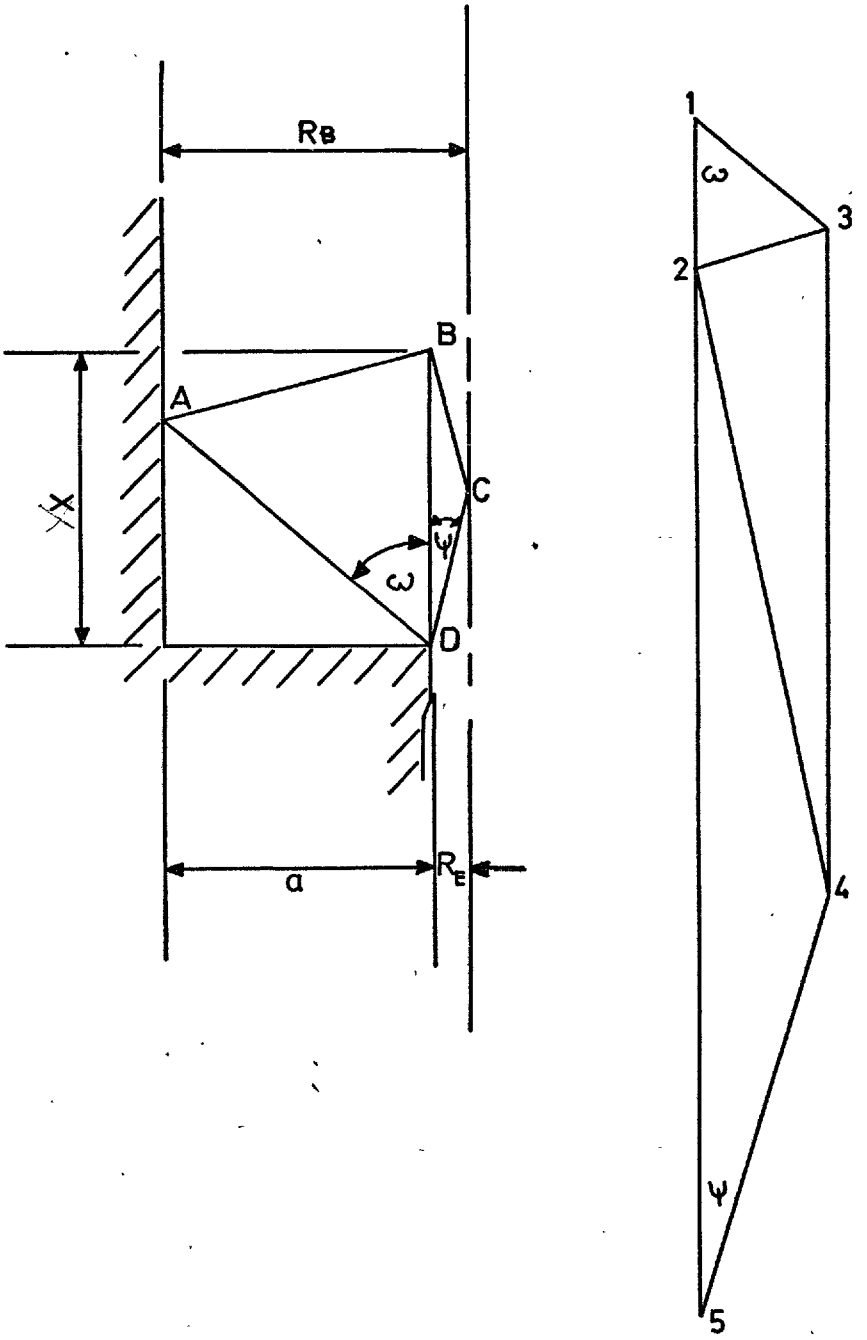


Fig. 2.2 Velocity field and hodograph for plane-strain single hole extrusion.

The load over half the billet is then given by

$$L = k(AO\overline{13} + OC\overline{75} + BO\overline{34} + AB\overline{23} + BC\overline{24})$$

$$= k(2x + \frac{2ax}{R_E} + \frac{2a^2}{x\sin^2\omega} + \frac{2aR_E}{x\sin^2\psi} - 3a\cot\omega - 3a\cot\psi)$$

$$= kC \qquad 2.10$$

where C is a constant depending on the extrusion ratio being considered.

Before equation 2.10 can be used, the values of ω, ψ, and x, that give the minimum load have to be found.

If a ω and ψ are assumed to be independent of x

$$\frac{d\,load}{dx} = k(2 + \frac{2a}{R_E} - \frac{2a^2}{x^2\sin^2\omega} - \frac{2aR_E}{x^2\sin^2\psi})$$

This expression will equal zero at the minimum value of the load. Equating to zero and rearranging gives

$$x^2 = \frac{a^2}{(1+\frac{a}{R_E})\sin^2\omega} + \frac{aR_E}{(1+\frac{a}{R_E})\sin^2\psi} \qquad 2.11$$

The values of ω and ψ can be found in a similar manner

For ω

$$\frac{-4a^2\cos\omega}{x\sin^3\omega} + \frac{3a}{\sin^2\omega} = 0$$

$$\therefore \cot\omega = \frac{3x}{4a} \qquad 2.12$$

For ψ

$$\frac{-4a^2R_E\cos\psi}{x\sin^3\psi} + \frac{3a}{\sin^2\psi} = 0$$

$$\therefore \cot\psi = \frac{3x}{4R_E} \qquad 2.13$$

Expressions 2.11 - 2.13 were derived on the supposition that x, ω, and ψ are independent of each other. This is obviously not the case and an interative technique has to be used. A value of x is selected and the angles ω and ψ calculated. Using these angles a new value for x is calculated. This process is repeated until consistent values of the variables are realized. The computer program in appendix I was used to calculate these values.

Equation 2.10 only gives the load on half of the billet. The total load is

$$L = 2Ck \qquad 2.14$$

and the pressure

$$P = \frac{2Ck}{2R_\theta} = \frac{Ck}{R_\theta} \qquad 2.15$$

Van Mises yield criterion enables the shear yield stress k to be replaced by σ, the uniaxial yield stress. The results from this simple minimuzed solution are given in figure 2.3, and can be compared with previous results.

2.2.2. A Plane Strain Solution for Two Hole Extrusion.

A similar pattern of velocity discontinuities to that used for single hole extrusion can be applied, figure 2.4. The calculation is simplified by assuming x and x' to be equal, which implies the equality of ψ and ψ'. The Location of the holes may be defined by the eccentricity

$$\xi = \frac{b}{a+b} \qquad 2.16$$

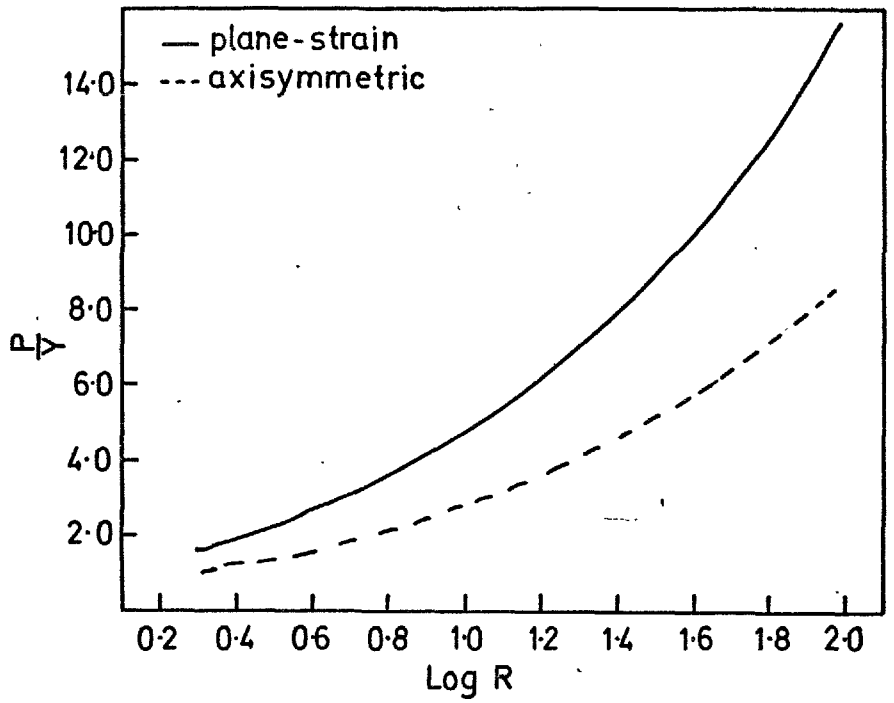
When b is zero ξ is zero and when a is zero ξ is unity. From equation 2.10, for the single hole solution, the load over half the billet is

$$L = k\left(2ax + \frac{2ax}{R_E} + \frac{2a^2}{x\sin^2\omega} + \frac{2aR_E}{x\sin^2\psi} - 3a\cot\psi - 3a\cot\omega + \frac{2R_E b}{x\sin^2\psi} + 2x' + \frac{2bx'^2}{R_E} + \frac{2b^2}{x'\sin^2\psi'} - 3b\cot\psi' - 3b\cot\omega'\right) \qquad 2.17$$

The load was obtained by finding the values of ω, x, and ψ, that make the load over region A a minimum. This is identical to the single hole solution. Using these values the load in equation 2.17 was calculated, ω being varied and the minimum load selected, a modified form of the single hole program being used. Figure 2.5 shows the variation in pressure with eccentricity for a range of reduction ratios. Also shown is the result obtained by Dodeja and Johnson for a rough container using a slip-line field approach.

2.2.3. Plane Strain Solution for Three Hole Extrusion.

A simple solution can be derived by extending the approach developed for two hole extrusion. The velocity discontinuity field is given in figure 2.4, where it can be compared with that for the two hole case. The eccentricity is defined as



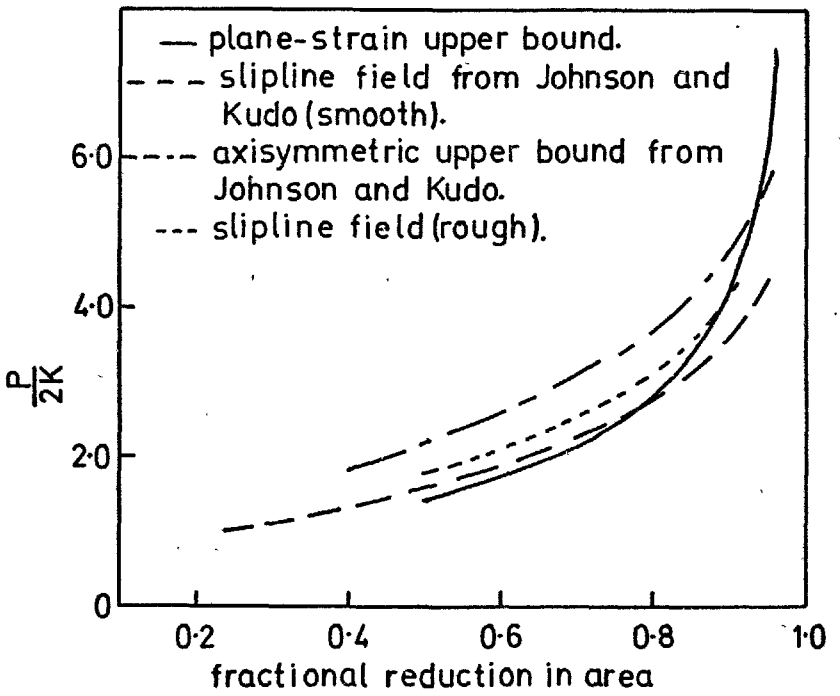
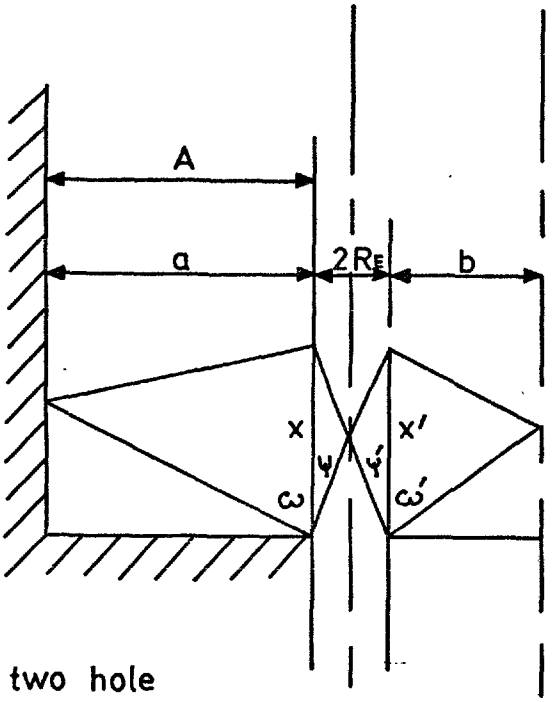
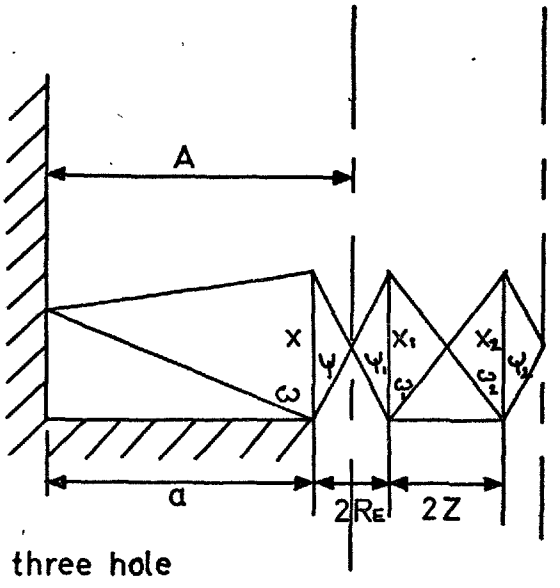


Fig. 2·33 Variation in extrusion pressure with reduction
a) calculated from simple field.
b) comparison with other results.



a) two hole



b) three hole

Fig. 2·4 Velocity fields for two and three hole extrusion.

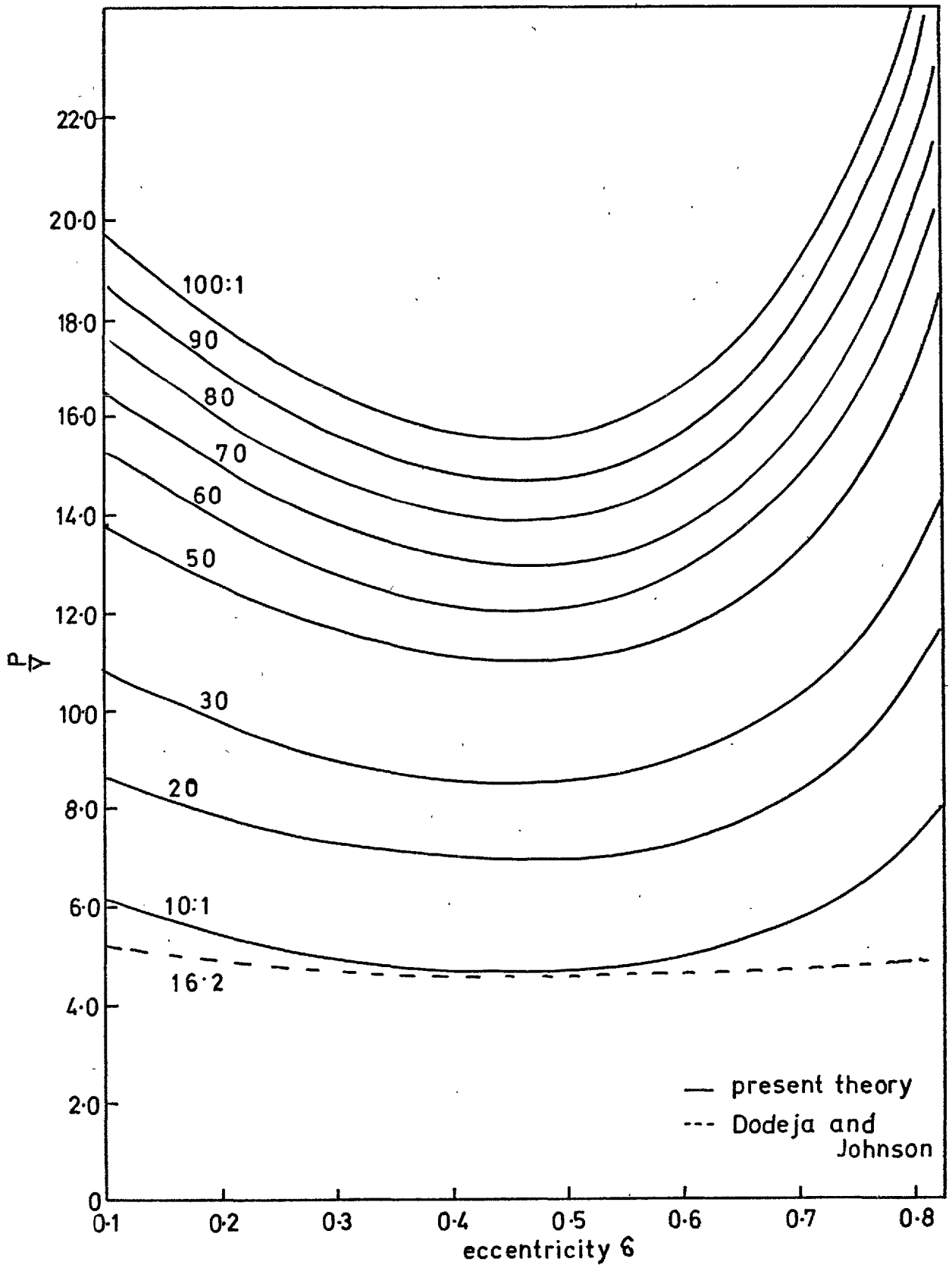


Fig. 2·5 Variation of extrusion pressure with eccentricity for two hole plane-strain extrusion.

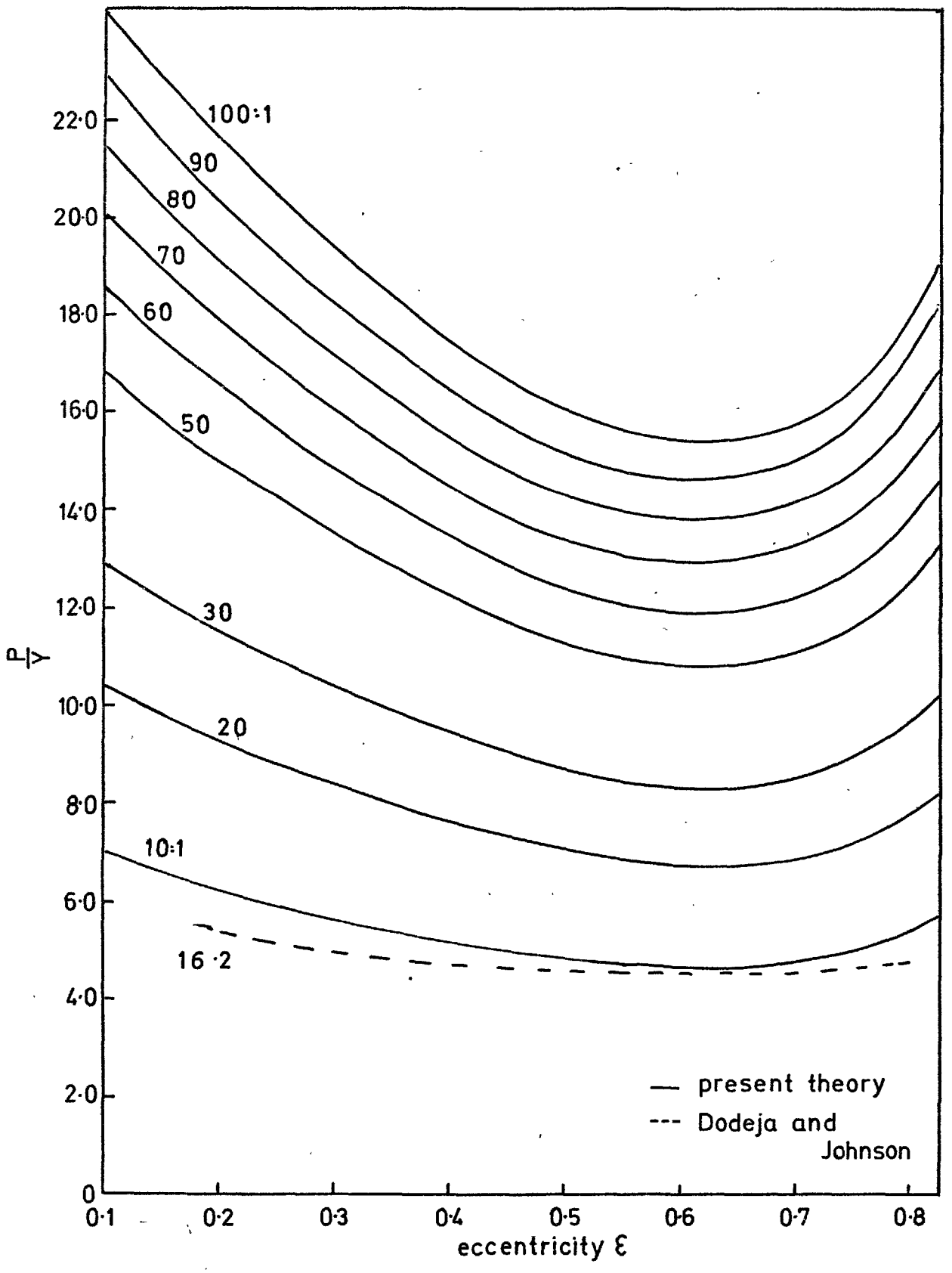


Fig. 2·6 Variation of extrusion pressure with eccentricity for three hole plane-strain extrusion.

$$\xi = \frac{2z}{a+2z} \qquad 2.18$$

which is zero when z is zero and unity when a is zero.
By making the following assumptions

1. $x = x_1 = x_2$
2. $\psi = \psi_1 = \psi_2$
3. $\omega_1 = \omega_2$

a minimized solution can be found as before. The values of w and x are obtained by treating region A as a single hole extrusion. The minimum load is then calculated by varying the value of ω_1, using a modification of the program developed in section 2.2.1.

The load over half the billet is

$$L = k\left(2x + \frac{2ax}{R_E} + \frac{2a}{x\sin^2\omega} + \frac{2aR_E}{x\sin^2\psi} - 3a\cot\omega - 3a\cot\psi\right.$$
$$\left. + 2\left(2x + \frac{2zx}{R} + \frac{2z}{x\sin^2\omega'} + \frac{2zR_E}{x\sin^2\psi} - 3z\cot\omega' - 3z\cot\psi\right)\right) \qquad 2.19$$

The variation in the pressure with the eccentricity is given in figure 2.6, for a range of reduction ratios. Dodeja and Johnson's result is also given for comparison.

2.2.4. An Upper Bound Axisymmetric Solution.

For the case of single rod extrusion, Raybould and Sheppard suggested a simple method of calculating a minimized upper bound from the plane strain solution. It is assumed that the flow pattern in axi-symmetric extrusion is identical to that for plane strain extrusion, at the same geometric reduction. The load is then found by summing the products of the surface area of the velocity discontinuity, the field is revolved around the centre axis, and the square of the velocities from the plane strain hodograph. The use of the latter is based on the experimental observations of Thomsen.

Using this approach, the values of ω, ψ and z in figure 2.2 are calculated for the appropriate geometric reduction. The surface areas of the velocity discontinuities are

$$AO = \frac{a\pi(R_B + R_E)}{\sin\omega}$$

$$CO = \frac{R_E 2\pi}{\sin\psi}$$

$$BO = 2\pi x R_E$$

$$AB = \pi\left(\frac{a^2}{\sin^2\omega} + x^2 - \frac{2ax\cos\omega}{\sin\omega}\right)^{1/2}(D+d)$$

$$BC = \pi R_E\left(\frac{R_E^2}{\sin^2\omega} + x^2 - \frac{2R_E\cos\psi}{\sin\psi}\right)$$

and the relative velocities are

$$\overline{13} = \left(\frac{a}{x\sin\omega}\right)^2$$

$$\overline{54} = \left(\frac{a}{x\sin\psi}\right)^2$$

$$\overline{23} = \frac{1}{x^2}\left(\frac{a^2}{\sin^2\omega} + x^2 - 2ax\cot\omega\right)$$

$$\overline{24} = \left(\frac{a}{xd}\right)^2\left(\frac{R_E^2}{\sin^2\psi} + x^2 - R_E x\cot\psi\right)$$

$$\overline{34} = \left(1 + \frac{a}{R_E} - \frac{a}{x}(\cot\omega + \cot\psi)\right)^2$$

The load over the half billet is given by equation 2.10 . The predicted extrusion pressures were calculated, using the computer program in appendix II, and are plotted against log R in figure 2.3 . The axi-symmetric pressures follow the same trend as those for plane strain but are much lower, the discrepency increasing as the reduction ratio increases.

2.3. The Prediction of Flow Patterns by means of an Upper Bound Solution.

The observed similarity between the flow pattern in plane strain extrusion and that seen in axi symmetric extrusion, for the same geometrical reduction, can be useful in predicting these patterns. The simple solution, section 2.2.1. will give an approximation to the pattern but cannot be used to predict any changes occurring during extrusion. From experimental flow patterns a more complex field was developed, figure 2.7 . The important difference between this and the simple field is the extension of the velocity field to the back of the billet. This agrees with the observed shear region down the sides of the billet in unlubricated extrusion. The theoretical flow pattern, for different billet lengths, can be obtained by calculating the field that gives the minimized plane strain pressure.

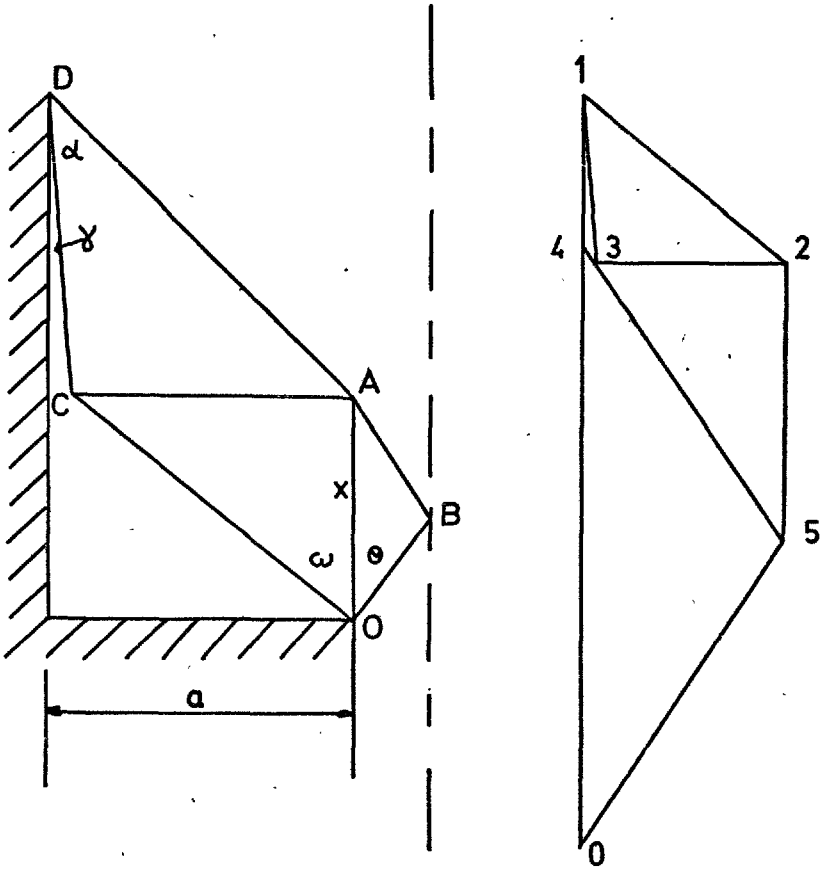


Fig. 2·7 Velocity field and hodograph for the more complex upper-bound solution used to predict flow patterns.

With reference to figure2.7

$$AO = x$$

$$OB = \frac{R_E}{\sin\theta}$$

$$OC = \frac{x}{\cos\omega}$$

$$AC = x\tan\omega$$

$$DA = \frac{a}{\sin(\gamma+\alpha)}$$

$$AB = (R_E^2 + (x - \frac{R_E}{\tan\theta})^2)^{1/2}$$

$$DC = \frac{l_B - x}{\cos\gamma}$$

The velocities are found from the hodograph

$$\overline{13} = \frac{\sin(180-(\alpha+\gamma))}{\sin\alpha}$$

$$\overline{43} = \frac{\sin\gamma}{\sin\alpha}$$

$$\overline{12} = \frac{a}{x\sin\omega}$$

$$\overline{50} = \frac{a}{x\sin\theta}$$

$$\overline{23} = \frac{a}{x} - \overline{43}(\sin(\alpha+\gamma))$$

$$\overline{45} = [(\frac{a+R_E}{R_E} - 1)^2 + (\frac{a}{x\sin\theta})^2 - 2(\frac{a+R_E}{R_E} - 1)(\frac{a}{x\sin\theta})\cos\theta]^{1/2}$$

$$\overline{25} = (\frac{a+R_E}{R_E}) - (\frac{a}{x\tan\omega}) - (\frac{a}{x\tan\theta})$$

The plane strain load over half of the billet

$$L = k(AO\,\overline{25} + OB\overline{50} + OC\overline{12} + AC\overline{23} + DA\overline{43} + AB\overline{45} + DC\overline{13}) \qquad 2.20$$

If this field is to be used to predict a theoretical flow pattern then the values of $x, \theta, \omega, \alpha$ and γ, that minimize equation 2.20, have to be found. The simplest method is to calculate the plane strain load for all possible combinations of the variables and to selct the minimum. There are various geometrical boundary conditions that limit the range that has to be considered.

1. The maximum value of ω is

$$\omega = \tan^{-1}\frac{a}{x}$$

and the minimum by

$$\omega = \tan^{-1}\left(\frac{a}{l_B}\right)$$

2. $$AO \leq l_B$$

3. $$\gamma \leq \omega$$

4. If θ is assumed to be always less than 90° then the minimum value of $\angle AOB$ is —

$$\angle AOB = \tan^{-1}\left(\frac{a}{x} / \left(\frac{a+R_E}{R_E} - 1\right)\right)$$

The upper limit is set at $(\gamma + \alpha)$.

5. The angle γ must be less than ω

$$\gamma = \tan^{-1}(A - (x\tan\omega)/(l_B - x))$$

and $$\alpha = \tan\left(\frac{a}{l_B - x}\right) - \gamma$$

A computer program to calculate the minimum load, incorporating these boundary conditions was used, appendix I. The resultant flow patterns for various billet lengths, and a diameter of 37.5mm, are shown in figure2.8 .

2.4. The Variation in Load with the Billet Length.

The theoretical flow patterns derived in section 2.3 are for an axisymmetric reduction of 60:1. Ideally a value of the change in load should also be given. However a plane strain solution for a 60:1 reduction would necessitate redrawing the field, and it is difficult to see what the corresponding billet length in plane strain would be. To compare the relative change in load with billet length, the load for plane strain extrusion through a reduction geometrically similar to that shown i.e. a reduction of 7.75 to 1 was calculated. The results are given in figure 2.9.

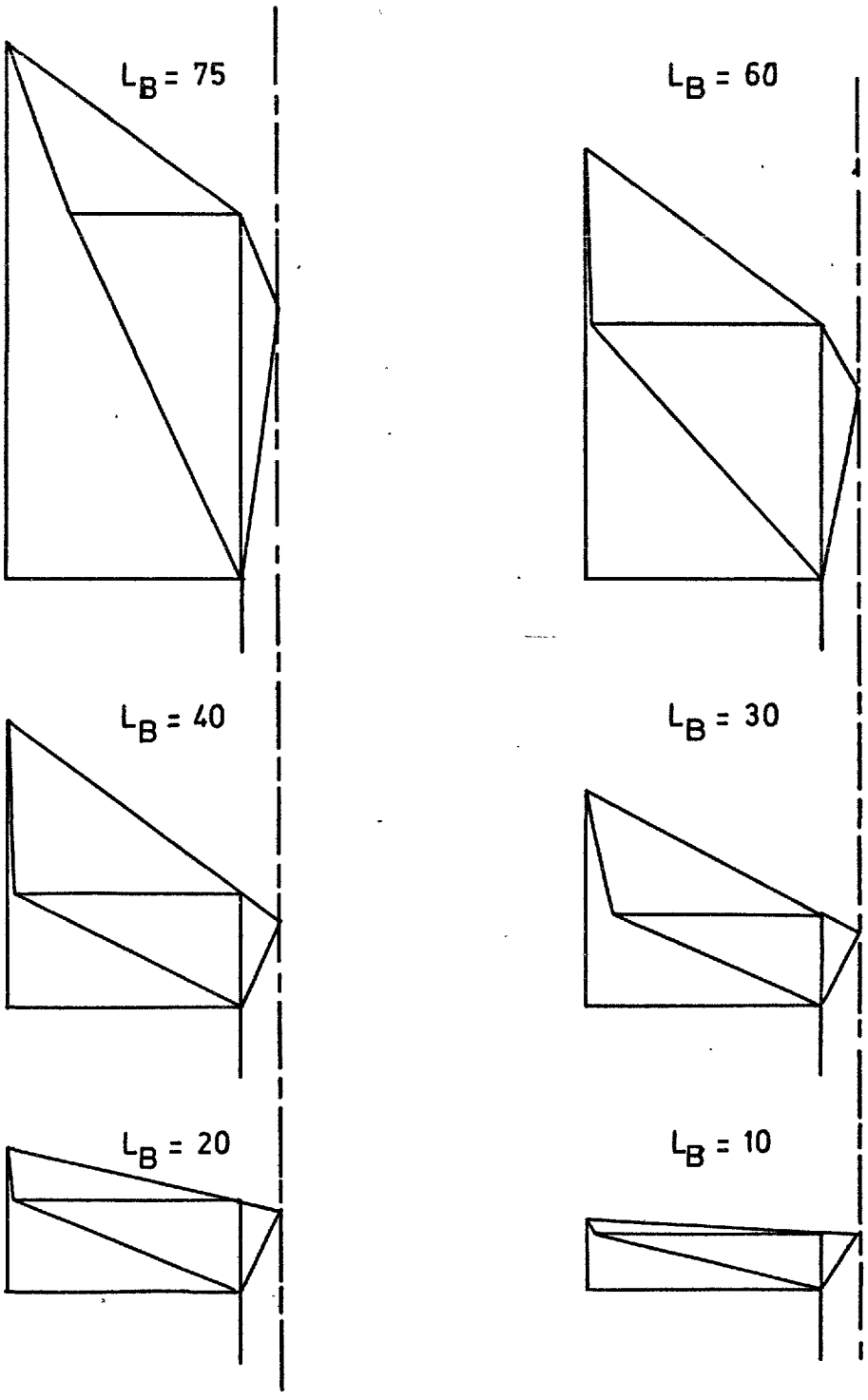


Fig. 2·8 Theoretical flow patterns for 60:1 reduction.
Billet diameter = 37·5mm.
Scale : full size.

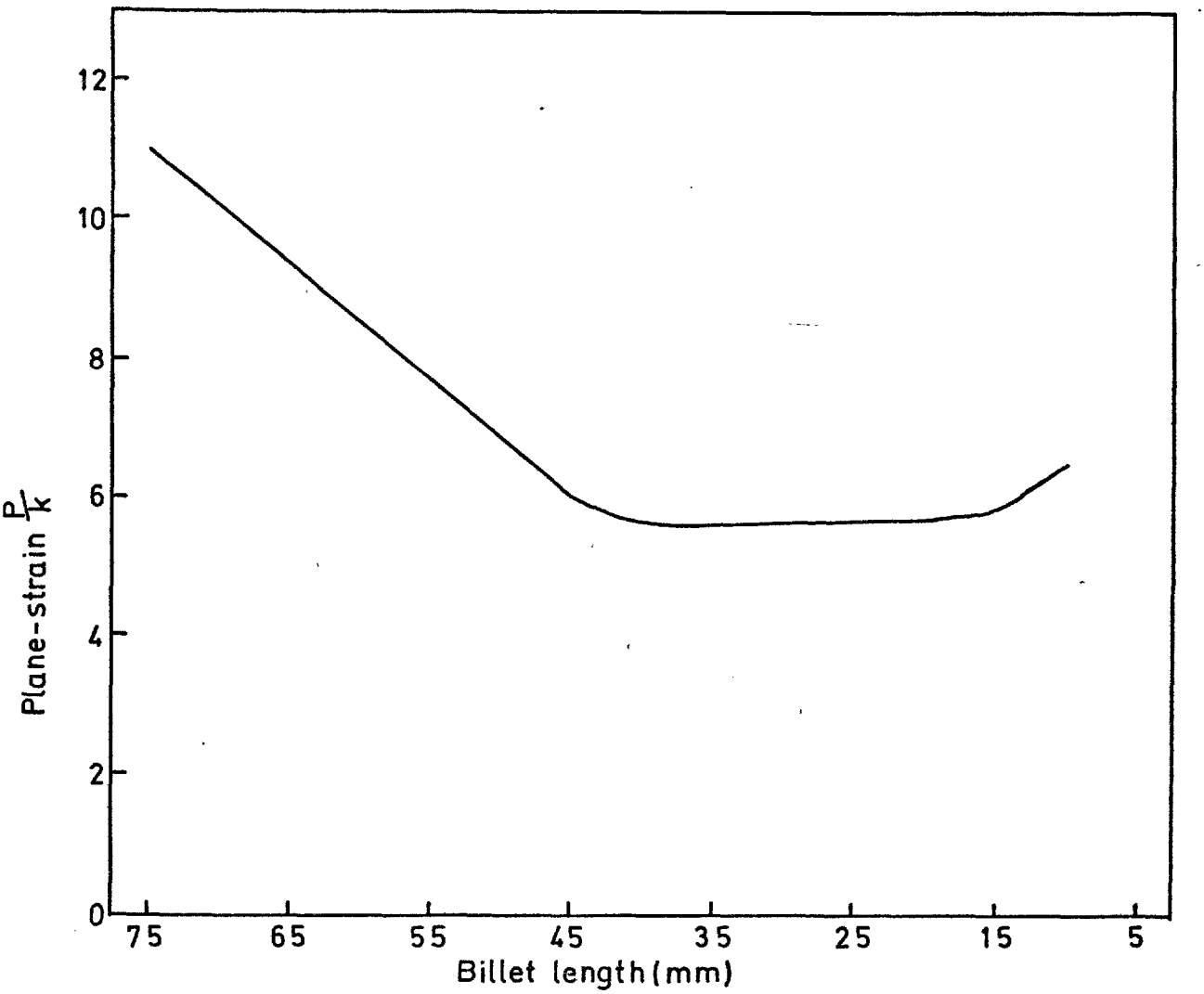


Fig. 2·9 Variation in plane-strain pressure with billet length for the fields shown in fig. 2·8
Billet diameter = 37·5mm.

2.5 The Method Used to Calculate the Flow Stress from the Experimental Results.

As discussed in section 1.4.10 there are two possible methods of calculating the flow stress. In the present work the upper bound solutions derived above were used. The minimum pressure at the end of extrusion was measured and the flow stress calculated by dividing by the local constant C. The use of the minimum pressure eliminated any frictional effects between the billet and the container. The constant C was that found from the simple plane strain field. The more complex field, section 2.3. should give a more accurate value but the difficulty in selecting an equivalent plane strain billet length precluded its use.

Also the simple field was the one used in the multi-hole extrusion solutions. For a valid comparison between single and multi-hole results the same field must be used. The values of the load constants C are given in appendix II .

2.6. The Integral Profile Model for the Temperature Rise.

The temperature rise in extrusion has been shown to be very significant [13] . The model used is derived from that given by Raybould and Sheppard, the heat losses from the billet to a cooler container being allowed for.

This model places a control volume around thedeformation zone, which is assumed to be a cone, and equates the heat leaving the volume to the work done in the zone. The temperature distribution is given by an integral profile approach. To simplify the model the heat generated by friction between the billet and the container is ignored. Approximately half of this heat will be lost to the container and work by Watkins et al [155,156] indicated that friction had no effect on the overall temperature rise in the deformation zone.

2.6.1 Assumptions Made in the IntegralProfile Model.

1. Perfect thermal contact exists between the billet and the container. In view of the high pressures encountered in extrusion, this is a valid assumption.
2. Friction is ignored for the reasons given above.
3. Uniform deformation occurs in the deformation zone. This is not found during extrusion, but any solution involving

the inhomogenous nature of the deformation will be very complex. In view of the other assumptions made deriving values for the strain rate and flow stress, the extra labour is not justified.

4. All the material that leaves the deformation zone is at a temperature ΔT, the surface of the deformation zone is also at this temperature.

5. A uniform temperature distribution across the extrude is assumed. This assumption is unlikely to introduce significant errors, because of the high thermal conductivity of aluminium and its alloys, especially in extrudes with a small cross sectional area.

2.6.2. The Calculation of the Temperature Rise.

With reference to figure 2.10, the heat flow from the deformation zone can be equated to the work done.

$$\text{Work done} = C_1 + C_2 + C_3 + C_4 + C_5 \qquad 2.\ 21$$

Under adiabatic conditions

$$\frac{\text{Load x distance}}{J} = \Delta T \rho C_{AL} V_\beta'$$

or rearranging

$$\Delta T = \frac{\text{load}}{J \rho C_{AL} A_1}$$

Calculation of C5.

Volume of metal at the surface temperature

= volume of the billet - volume of the dead metal zone

C5 = volume of metal at $\Delta T \times \rho C_{AL}$

Assuming the temperature rise at the end of extrusion is being calculated

Volume of the dead metal zone

$$= \pi \tan\psi \left(\frac{2R_B^2}{3} - R_B^2 R_E + \frac{R_E^3}{3}\right)$$

therfore

$$C5 = \rho C_{AL} \left(A l_B - \pi \tan\psi \left(\frac{2R_B^3}{3} - R_B^2 R_E + \frac{R_E^3}{3}\right)\right) \qquad 2.\ 22$$

Calculation of C1 to C4

The temperature profile in the container, tool and billet have to be calculated before C1 to C4 can be found. The

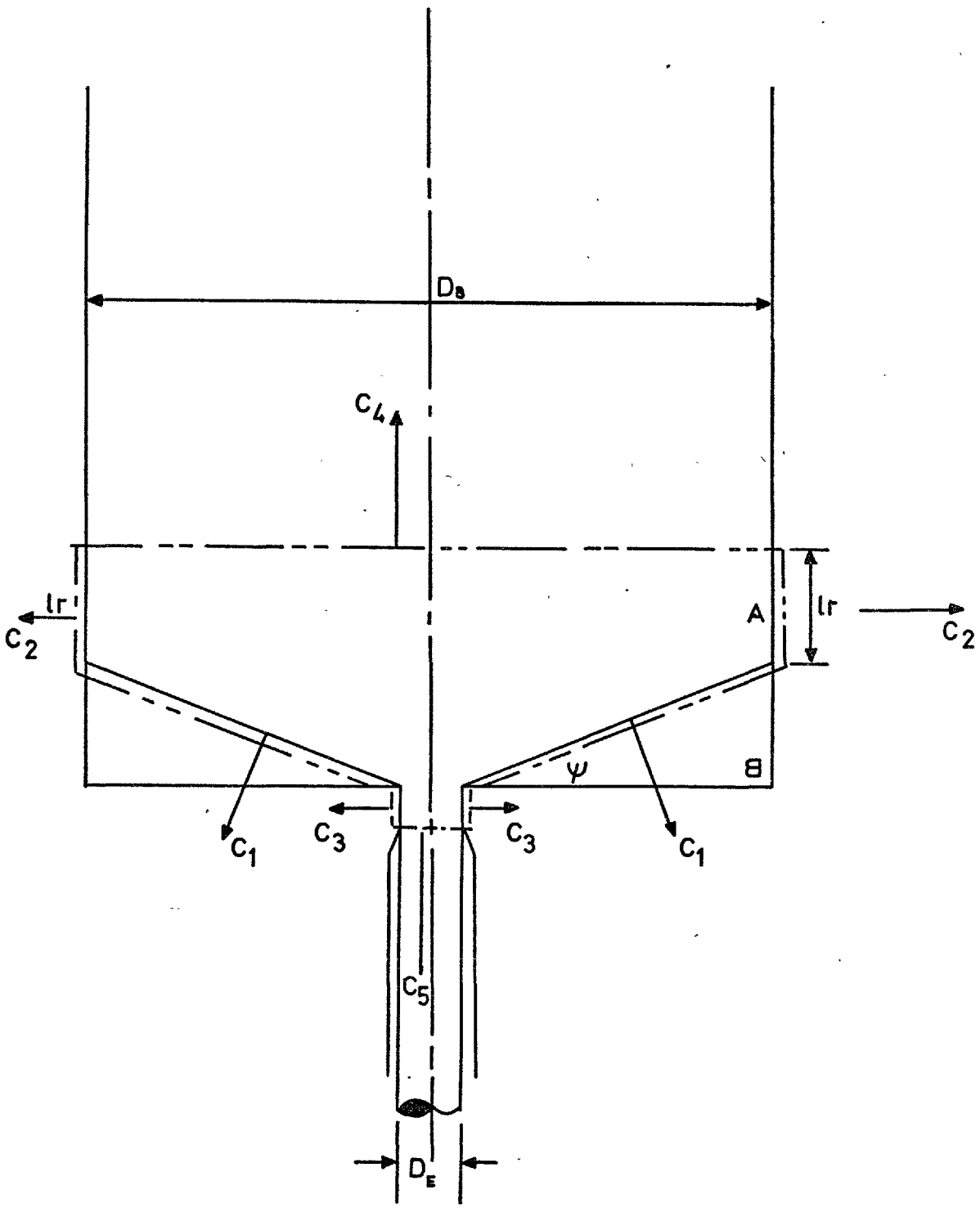


Fig. 2·10 Control volume and heat flow from the deformation zone

temperature profile around a heat source is assumed to be represented by

$$\Delta T(x_1 t) = a_0 + a_1 x + a_2 x^2$$

where $\Delta T(x_1 t)$ is the temperature at a point distance x from the heat source and at a time .

From the boundary conditions the constants a_0, a_1, a_2, can be found

$$\text{At } x = 0$$
$$\Delta T(x_1 t) = \Delta T$$
$$\therefore a_0 = \Delta T$$

At a distance S, the maximum penetration distance of the heat front

$$\Delta T(x_1 t) = 0$$

and

$$\frac{d\Delta T(x_1 t)}{dx} = 0$$
$$= a_1 + 2a_2 S$$
$$\therefore a_1 = 2a_2 S$$
$$\therefore 0 = \Delta T + S(a_2 S - 2a_2 S)$$
$$\therefore a_2 = \frac{\Delta T}{S^2}$$
$$\text{and } a_1 = \frac{-2\Delta T}{S}$$

substituting these values gives

$$\Delta T(x_1 t) = \Delta T - \frac{2\Delta T x}{S} + \frac{\Delta T x^2}{S^2}$$
$$= \Delta T \left(1 - \frac{x}{S}\right)^2 \qquad 2.23$$

If it is assumed that heat only flows in the x direction, then the heat accumulated can be calculated

$$Cacc = \int_0^S Ac\,\rho\,\Delta T \left(1 - \frac{x}{S}\right)^2 dx$$
$$= Ac\,\rho T \frac{S}{3} \qquad 2.24$$

Differentiating with respect to time

$$Cacc/sec = \frac{Ac\,\rho\,\Delta T}{3} \frac{ds}{dt} \qquad 2.25$$

From the Fourier equation

$$\frac{dH}{dt} = \frac{-KA\,dT}{dx} \qquad 2.26$$

$$\therefore \text{Cacc/sec} = -KA\left[\frac{d\Delta T}{dx}\right]x = 0 \qquad 2.27$$

equating 2. 25 and 227 gives

$$S = \sqrt{\frac{12Kt}{\rho c}} \qquad 2.28$$

This expression is valid only when the area of contact A does not vary with x. This is not the case for C2 and C3.
Here

$$Cacc = \int_0^S 2\pi x l \rho S\Delta T\left(1-\frac{x}{S}\right)^2 dx$$

$$= \frac{\pi l S \rho \Delta T S^2}{6} \qquad 2.29$$

Proceeding as before and differentiating equation 2. 29 with respect to t

$$\frac{dC}{dt} = \frac{\pi l S \rho \Delta T}{6}\,\frac{dS^2}{dt}$$

equating with 2. 27

$$S = \sqrt[3]{\frac{18KAt}{\pi l S \rho}} \qquad 2.30$$

The heat losses frpm the control volume can now be calculated.
C1

The surface area of the core $= AO\pi\left(\frac{D_B + D_E}{2}\right)$

$$= \frac{\pi}{\cos\psi}\left(\frac{D_B^2 - D_E^2}{2}\right)$$

$$Cacc = Ac\rho\Delta T\,\frac{S}{3}$$

from $S = 12\sqrt{\alpha t}$

where $\alpha = \frac{K}{\rho c}$

$$Cacc = \frac{Ac\rho\Delta T}{3}\sqrt{12\alpha t}$$

and $$C_1 = \frac{\pi}{3}\left[\frac{D_B^2 - D_E^2}{2}\right] Ac_{st}\rho_{st}\Delta T\sqrt{12\alpha_{st} t} \qquad 2.31$$

The suffix st indicating that the steel of the tooling is being considered, the thermal conductivity and specific heat of the steel is given in appendixII.

C2

The depth of the zone of working can be approximated by

$$\left(\frac{D_B - D_E}{2}\right)\tan 45$$

$$\therefore l_r = \frac{D_B - D_E}{2}(\tan 45 - \tan\psi)$$

$$C_{radial} = \frac{\pi}{6} l_r c \rho T S^2$$

where S is the distance from the heat source. This assumes the heat source to be at the centre of a long cylinder. In fact the heat source is at a distance RE from the billet centre. Therefore

$$C_{rad} = \frac{\pi}{6} l_r c T (S + R_E)^2$$

This includes the heat stored in the material, which is

$$\frac{\pi}{6} l_r c \rho \Delta T R_B^2$$

subtracting gives

$$C_{rad} = \frac{\pi}{6} l_r c_{st} \rho_{st} \Delta T (S^2 + 2SR_B)$$

$$= \frac{\pi}{6} l_r c \rho \Delta T (S^2 + SD_B)$$

$$\therefore C_2 = \frac{\pi}{6} l_r c_{st} \rho_{st} \Delta T \left[\left(\frac{18 K_{st} A_t}{\pi l_r c_{st} \rho_{st}}\right)^{3/4} D_B \left(\frac{18 K_{st} A_t}{\pi l_r c_{st} \rho_{st}}\right)^{2/3}\right] \qquad 2.31$$

This heat loss occurring through the steel of the container. Similarly

$$C_3 = \frac{\pi}{6} l_r c_{st} \rho_{st} \Delta T \left[\left(\frac{18 K_{st} A_t}{l_b c_{st} \rho_{st}}\right)^{2/3} + D_E \left(\frac{18 K A_t}{l_b c_{st} \rho_{st}}\right)^{1/3}\right] \qquad 2.32$$

C4, the heat losses by back conduction are ignored. The errors caused by this assumption will be slight, except at very slow ram speeds. The use of a pre-heated pressure pad will reduce heat losses to the ram.

The total work can now be equated to the sum of these heat losses, equation 2.21 . The resulting expression is of the form

$$\text{Work done} = \Delta T\,(a + bt^{1/2} + t^{2/3} + ct^{1/3})$$

$$= \Delta T C_{TOT} \qquad 2.32$$

At very high ram speeds the terms involving t in 2.32 will be low and adiabatic conditions are approached. To facilitate the calculation of ΔT, graphs of C_{TOT} against time were prepared for each reduction ratio considered and are given in appendix II .

2.7 An Approximate Method of Allowing for Additional Heat Losses to a Cooler Container.

The values of ΔT calculated above assume that the billet and container are at the same temperature. In the present work the majority of extrusions were carried out at higher temperatures. There appears to be no rigorous analysis of the heat losses from a short billet to cooler surroundings, but an approximation can be made by considering the heat losses through a thick cylinder of internal radius r_1 , external radius r_2 , length l , and inner and outer temperatures T_2 and T_1 respectively. This model assumes that the inner surface of the container is at the temperature of the billet and that the outer surface is at a temperature of $300^{\circ}C$.

The rate of heat loss per unit length is given by

$$C = \frac{2\pi K (T_1 - T_2)}{\ln \frac{r_2}{r_1}} \qquad 2.33$$

The value of the surface area, $2\pi l_B R_B$, is changing at a uniform rate during an extrusion.

The rate of heat loss at the start of extrusion is

$$\frac{2\pi K l_B (T_1 - T_2)}{\ln \frac{r_2}{r_1}} \qquad 2.34$$

Assuming extrusion to be stopped at the dead metal zone, the rate of heat loss at the end is given by

$$\frac{2\pi K AB (T_1 - T_2)}{\ln \frac{r_2}{r_1}} \qquad 2.35$$

The length AB being given in figure 2.10 .

Therefore the mean rate of heat loss is

$$\frac{2\pi K(T_1 - T_2)}{\ln \frac{r^2}{r_1}} \left(\frac{L_B + AB}{2}\right)$$

This occurs in a time t , given by

$$t = \frac{L_B - AB}{V}$$

V being the ram speed.

The total heat loss is then

$$\frac{2\pi K(T_1 - T_2)}{\ln \frac{r^2}{r_1}} \left(\frac{L_B + AB}{2}\right)\left(\frac{L_B - AB}{V}\right) \qquad 2.36$$

The mean heat content of the billet during extrusion is

$$\frac{\pi D_B^2}{4} \left(\frac{L_B + AB}{2}\right) \rho c T_1 \qquad 2.37$$

Subtracting equation 2.36 from 2.37 gives the mean heat content, after allowing for heat losses

$$C = \frac{\pi D_B^2}{4} \left(\frac{L_B + AB}{2}\right) \rho c T_1 - \frac{\pi K(T_1 - T_2)}{\ln \frac{r^2}{r_1}} \frac{(7{\cdot}2 + AB)(7{\cdot}2 - AB)}{V} \qquad 2.38$$

the mean temperature $\bar{T}$ can then be found by

$$\bar{T} = \frac{C}{V_B \rho c} \qquad 2.39$$

where V_B is the mean volume of the billet during extrusion.

2.8 A Summary of the Method Used to Calculate the Extrusion Temperature

1. The temperature rise is calculated using the integral profile method.
2. The heat losses to the container are estimated with equation 2.36 .
3. The mean temperature $\bar{T}$ is then calculated using equation 2.38 and 2.39 .

The temperature obtained by this method will only be an approximation, but a more rigorous treatment would be difficult. It would involve calculating the heat losses from a billet of constantly decreasing length, with a heat source at one end, to the surrounding container and tooling, all of which would be at a lower temperature.

2.9 The Temperature Rise at the Peak Load.

At the start of extrusion there is almost a linear rise in the applied load, until the peak is reached. This linear rise occurs over a short distance but will be accompanied by a rise in the temperature. If all the work is converted to heat, the magnitude of this rise can be calculated.

The work done is the area under the load displacement curve.

$$\text{Work done} = \frac{Lp \times dp}{2}$$

where Lp is the peak load

dp is the distance moved.

The temperature is therefore found from

$$\frac{Lp \times dp}{2J} = V_s \rho c \Delta T \qquad 2.40$$

The peak load is reached in a relatively short time and the magnitude of the temperature rise is low, less than $30^{\circ}C$ for a peak load of 5 MN. Therefore any heat losses may be neglected.

2.10 The Strain Rate.

As discussed in section 1.4.8 the most difficult parameter to measure in extrusion is the mean strain rate. The simplest approach is an extension of the idea originally developed by Feltham[161].
The mean strain rate is given by

$$\bar{\dot{\varepsilon}} = \frac{\text{total strain}}{\text{the time to effect the strain}} \qquad 2.41$$

The extrusion pressure can be expressed as

$$P = YB\ln R = YC$$

where C is the load constant for a given extrusion ratio.

By analagy with

work done = stress x strain

the mean strain is given by the constant C.

The time to effect this strain can be found by assuming the deformation to occur in a cone of semi-angle ω , figure 1.2. The volume of this cone is

$$V = \frac{\pi(D_B^3 - D_E^3)}{24 \tan \omega}$$

The time t = $\dfrac{V}{\text{volume of metal extruded per unit time}}$

The volume of metal extruded per unit time = $\dfrac{\pi D_B^2 V}{4}$

which gives

$$\frac{D_B^3 - D_E^3}{D_B^2 6 \tan \omega V}$$

Substituting into equation 2.41

$$\frac{6 C \tan \omega V D_B^2}{D_B^3 - D_E^3} \qquad 2.42$$

The values of C and ω were found from the minimized plane strain solution.

The multi-hole extrusion presented a problem because the volume of the deformation zone is not easily measured. The only way would be to macro-etch sectioned billets and to construct a model of the observed flow patterns. Accordingly the strain rates calculated for single hole extrusion were used, any discrepencies between the two would be observed in the results. The strain rates used are tabulated in appendix II .

2.11 The Calculation of the Constants in the Hot Working Equation.

At high stress levels the strain rate and stress are related by

$$\dot{\varepsilon} = A_2 \exp(\beta \sigma) \qquad 1.2$$

at a constant temperature.

Taking natural logarithm

$$\ln \dot{\varepsilon} = \ln A_2 + \beta \sigma$$

The values of A and B can be obtained from a graph of $\ln \dot{\varepsilon}$ against σ at constant temperature.

At low stresses

$$\dot{\varepsilon} = A_1 \sigma^{n_1} \qquad 1.1$$

and

$$\ln \dot{\varepsilon} = \ln A_1 + n_1 \ln \sigma$$

at a constant temperature.

A and n can be found by a graphical method.

The more general hot-working relationship is

$$\dot{\varepsilon} = A \sinh(\alpha \sigma)^n \exp \frac{Q}{RT} \qquad 1.7$$

Before the activation energy Q can be calculated the value of α must be obtained. At high stress levels and a constant temperature equation 1.7 can be rewritten as

$$\dot{\varepsilon} = A \sinh(\alpha \sigma)^n$$

which approximates to

$$\dot{\varepsilon} = \frac{A}{2^n} \exp(n \alpha \sigma)$$

comparing with equation 1.2

$$n \alpha \sigma = \beta \sigma$$

$$\therefore \alpha = \frac{\beta}{n} \qquad 1.4$$

If n is equal to n_1 in equation 1.2, the gradients of the graphs of $\ln \dot{\varepsilon}$ against σ and $\ln \dot{\varepsilon}$ against $\ln \sigma$ can be used to give the value of α.

Using this derived value of α, the activation energy Q can be found. A graph of $\ln \dot{\varepsilon}$ against $\ln \sinh(\alpha \sigma)$ at a constant temperature, is first plotted. From this a second graph of $\ln \sinh(\alpha \sigma)$ against $\frac{1}{T}$ at a constant strain rate, is drawn. The activation energy is given by

$$Q = -R \left(\frac{\partial \ln \dot{\varepsilon}}{\partial \ln \sinh(\alpha \sigma)} \right)_T \left(\frac{\partial \ln \sinh(\alpha \sigma)}{\partial \frac{1}{T}} \right)_{\dot{\varepsilon}} \qquad 2.43$$

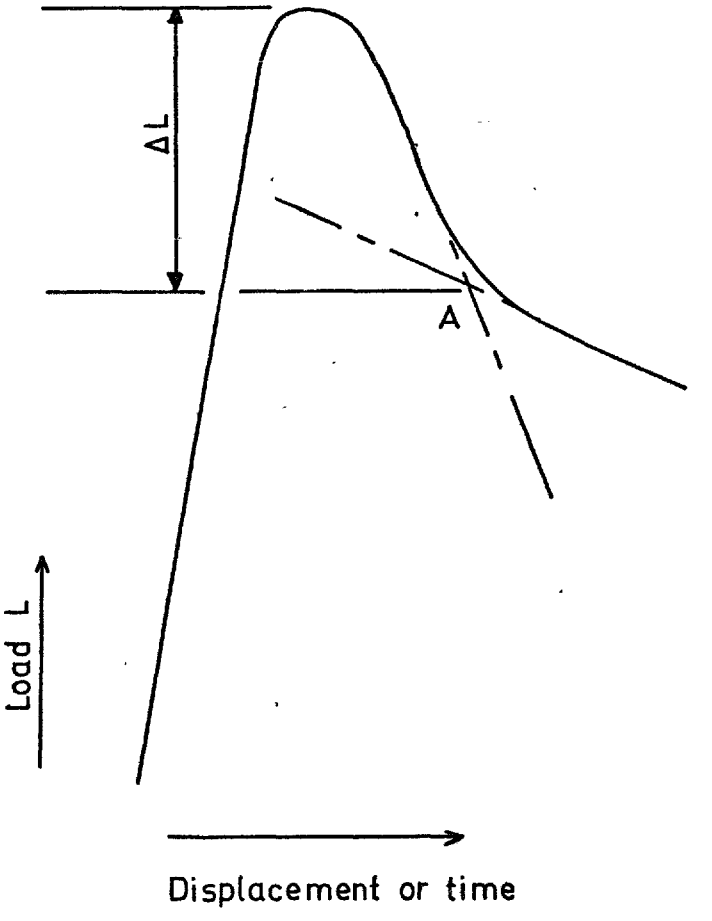


Fig.2·11 The measurement of ΔL

The accuracy of the derived activation energy will depend on the accuracy of the terms in the brackets in this equation.

2.12 The Method of Measuring The Peak Load.

A peak in the load displacement curve is often seen at the start of extrusion. The method used to measure the height of this peak is clearly indicated in figure 2.11. The only difficulty is in the accurate location of the point A. This leads to errors, when ΔL is small, and these must be allowed for when correlating the data.

CHAPTER THREE

Experimental

3.1 The Press

The experimental work was carried out on a direct operating 5MN ENEFCO vertical press, fig. 3.1 The press and its ancillary equipment have been described elsewhere [67] and the only major modifications made were to the water quench and the billet preheating system.

3.1.1. Load Measurement

The load was measured by a Mayes load cell situated directly above the ram. The output from the cell being recorded on both a Hewlett Packard 136A X.Y recorder and a Modulog data logger - the latter punching the results onto paper tape. Because of the speed of response of these instruments it was found necessary to record the load on a U.V. recorder, Southern Instruments Type F10.500/12, when using the accumulators. A visual indication of the load was provided by a dial display.

3.1.2. Ram Speed and Displacement

The ram speed could be varied over the range 2.6 to approximately 150mm/sec, using nitrogen filled accumulator bottles for the higher speed. In the range 2.6 to 14mm/sec the speed of the ram could be preset and during extrusion it remained constant, except at the very start of the cycle where the speed changed from the faster approach speed to the slower extrusion speed. When the accumulators were used the speed obtained could not be accurately predicted and decreased slightly throughout the stroke. The speed and displacement were measured by feeding the output from a rectilinear potentiometer, Penny Giles model LP/21/85/s, fixed between the crosshead and the press base, to the X.Y recorder and the data logger.

The plot of voltage against time could be converted to displacement and speed by means of a previously determined calibration chart, appendix III In the case of the accumulator runs an average value had to be taken.

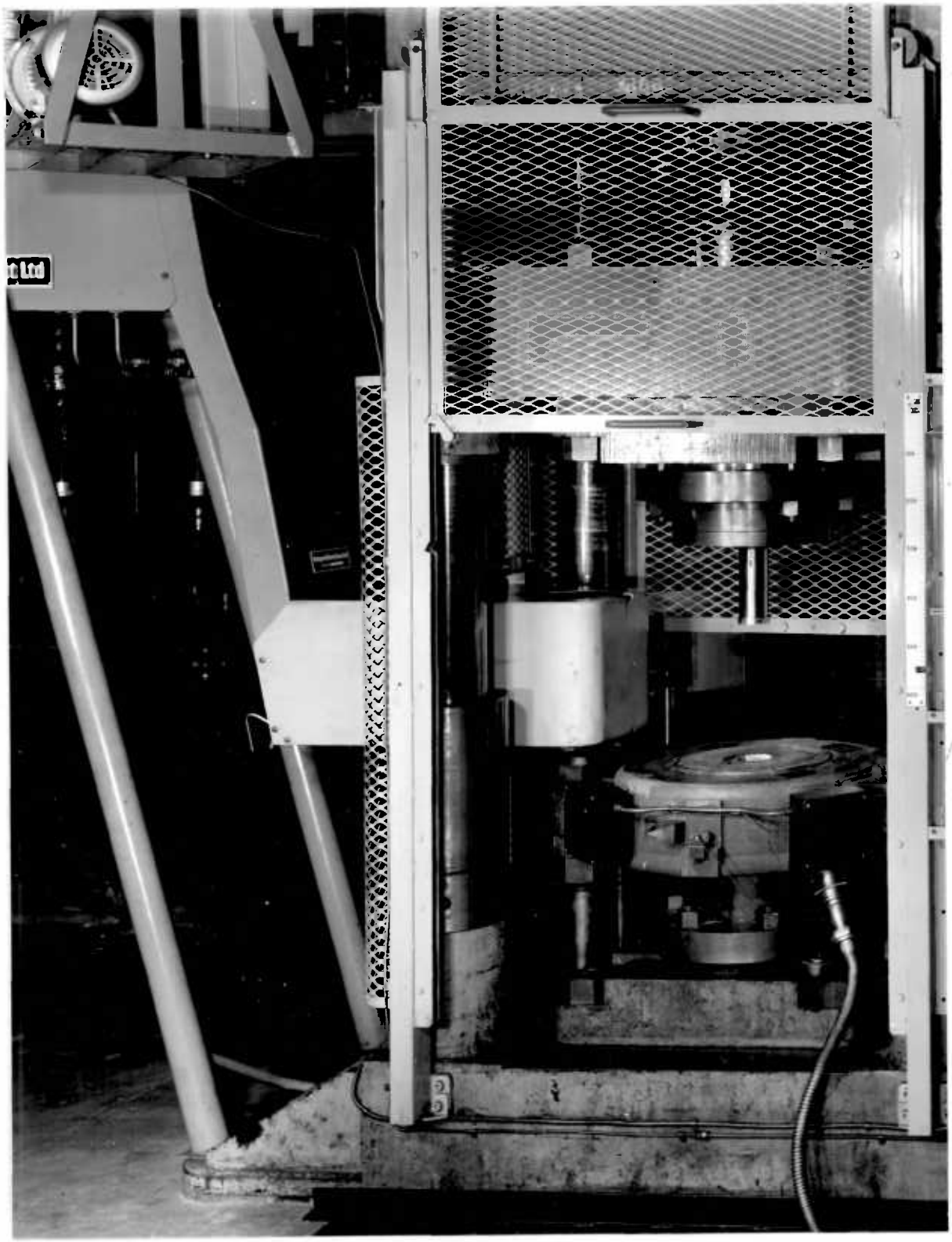


Fig 3.1 The press and induction heater

3.1.3 Container Heating

It is essential to have an accurate knowledge of the temperature of the container and to be able to maintain it at a constant value without too much difficulty.

The container was heated by eight 1.5 watt Inconel heaters, which could operate at temperatures up to 700 C. A thermocouple attached to each heater enabled the temperature to be monitered by a Eurotherm controller. Using these heaters the container liner could be maintained at 300 C throughout a series of runs. The liner temperature was measured by a thermocouple situated as close to it as possible and the output from this was fed to one of the Eurotherms controlling the heaters. The temperature of the liner was calibrated by attaching thermocouples to it at different positions and the results showed a temperature of $300 \pm 3^{\circ}C$ and a variation of less than 5 C between the top and bottom of the container.

3.1.4. Billet Preheating

Billet preheating was carried out in a Banyard Metalheat induction furnace, fig 3.1. This furnace operated at the mains frequency and the design enabled aluminium billets up to 150mm x 75mm diameter to be heated to 600 C. The temperature was originally controlled by a two prong contact thermocouple, the output being fed to a Honeywell servotrome controller. Calibration experiments showed this to give errors of up to $50^{\circ}C$ and so the billet temperature was measured by a 1.6mm dia. stainless steel sheathed mineral insulated thermocouple placed in a 1cm deep hole in the centre of the billet. This enabled the temperature to be controlled to $\pm 2^{\circ}C$.

The induction heater was suspended from two rails and could be moved over the container by means of pneumatic system operated by controls on the main control panel. When the heater was above the container the hot billet was transferred by manually removing the rod that supported the billet in the coil. Extrusion could then be started as soon as the heater had returned to its initial position.

3.1.5. Tooling

The ram stem,dies, pressure pads, scraper pads and the container liner were made from KEA145 5% Cr- V Steel.

To investigate the effect of a more complex die geometry than is usually studied in experimental extrusion work, dies were made

with one, two, and three holes in the range 30:1 to 100:1, fig 3.2 &3.3 The dimensions of the dies are given in appendix IV. With the single hole dies it was hoped to be able to measure the temperature of the billet during extrusion using the dead metal zone thermocouple technique. To accomplish this the single hole dies were drilled to accept 1.2mm dismeter stainless steel sheathed thermocouples. The distribution of these holes is shown in fig. 3.2. Because of the design of the die-holder the holes had to be drilled at an angle to allow them to come inside the die-backer. The thermocouples could then be passed through a hole in the die bolster. Some extrusions were also carried out using 30:1 square and rectangular dies, fig 3.4

3.2 Water Quench

It is necessary to quench the hot-worked material if the high temperature structure is to be examined, the better the quench the greater the likelihood that the structure will be retained.

The existing quench being unsuitable, a revised unit was constructed to the design shownin fig 3.5. It consists of two metal cylinders, the inner made of 18-8 stainless steel and the outer of brass. The diameter of the outer tube was chosen so that the quench could be positioned as close to the die as possible. To achieve a rapid quench it is necessary to have as large a volume of water as possible impinging on the product at a high velocity. To obtain these conditions holes 1.2mm diameter were drilled radially in the inner cylinder, 532 of which were in the first 26cm of the quench and the rest were in groups of 28 placed at 10cm intervals down the quench. The water was pumped by a Safran Ace F5 centrifugal pump through two 1" diameter inlets; the volume passing through the quench, operated as a closed system, being approximately 60 gallons per minute. The water in the system had to be periodically removed by a second centrifugal pump and replaced by clean water. The quench was designed for easy cleaning and this was done at regular intervals because of the tendency for dirt to collect in the holes.

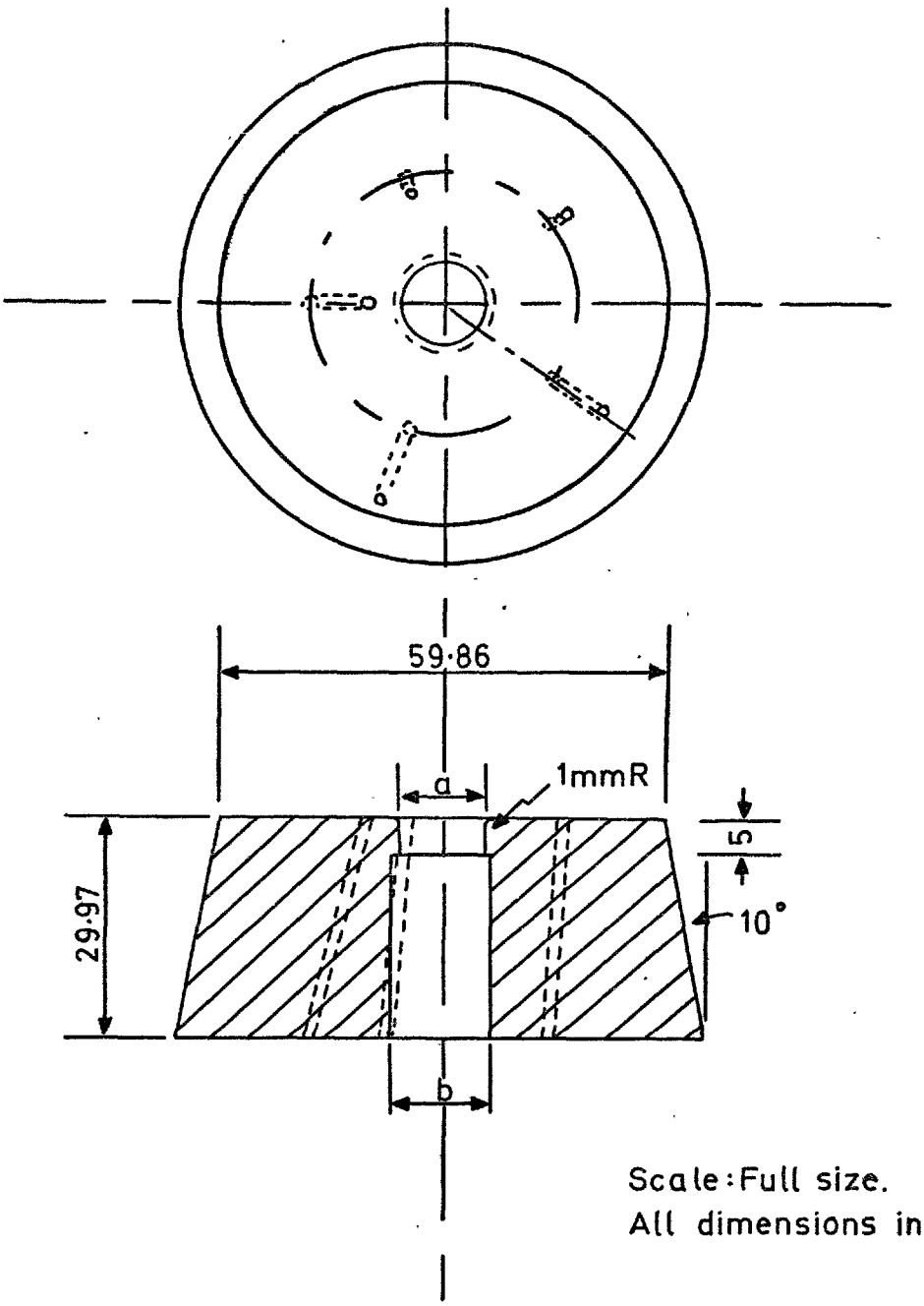


Fig.3·2 Single hole extrusion die showing the location of the thermocouple holes.

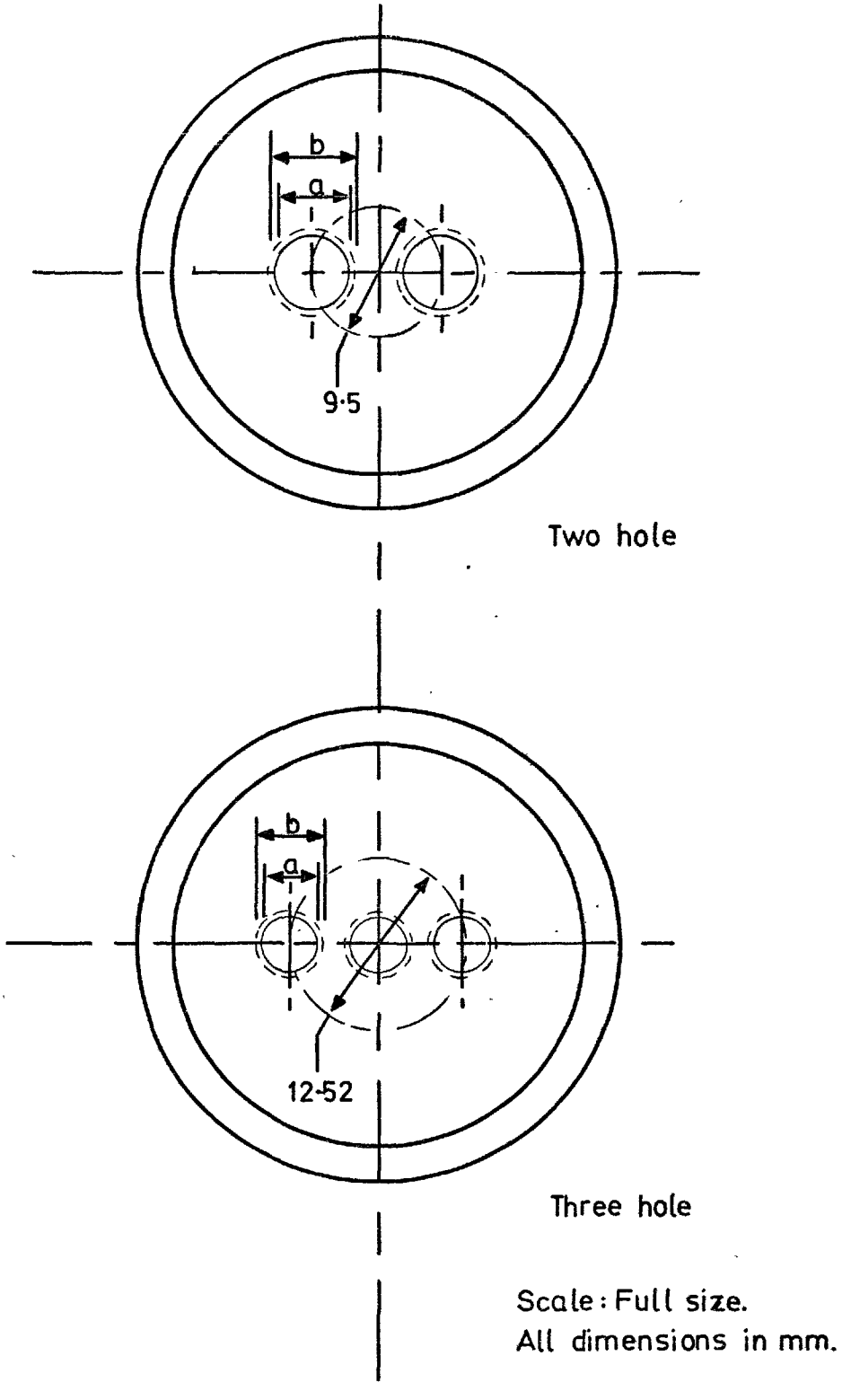


Fig.3·3 Multi hole extrusion dies.

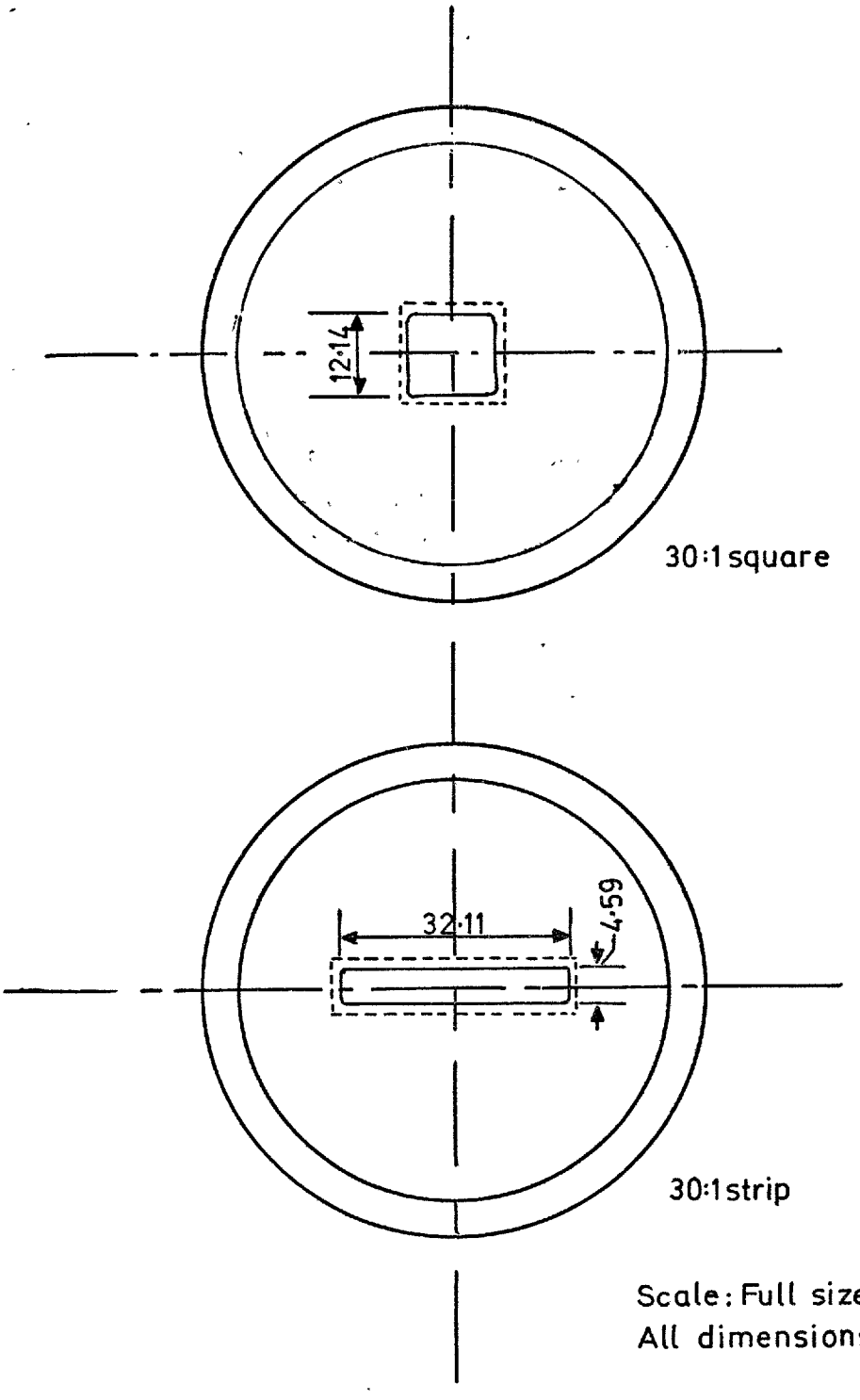


Fig. 3·4 Square and strip extrusion dies.

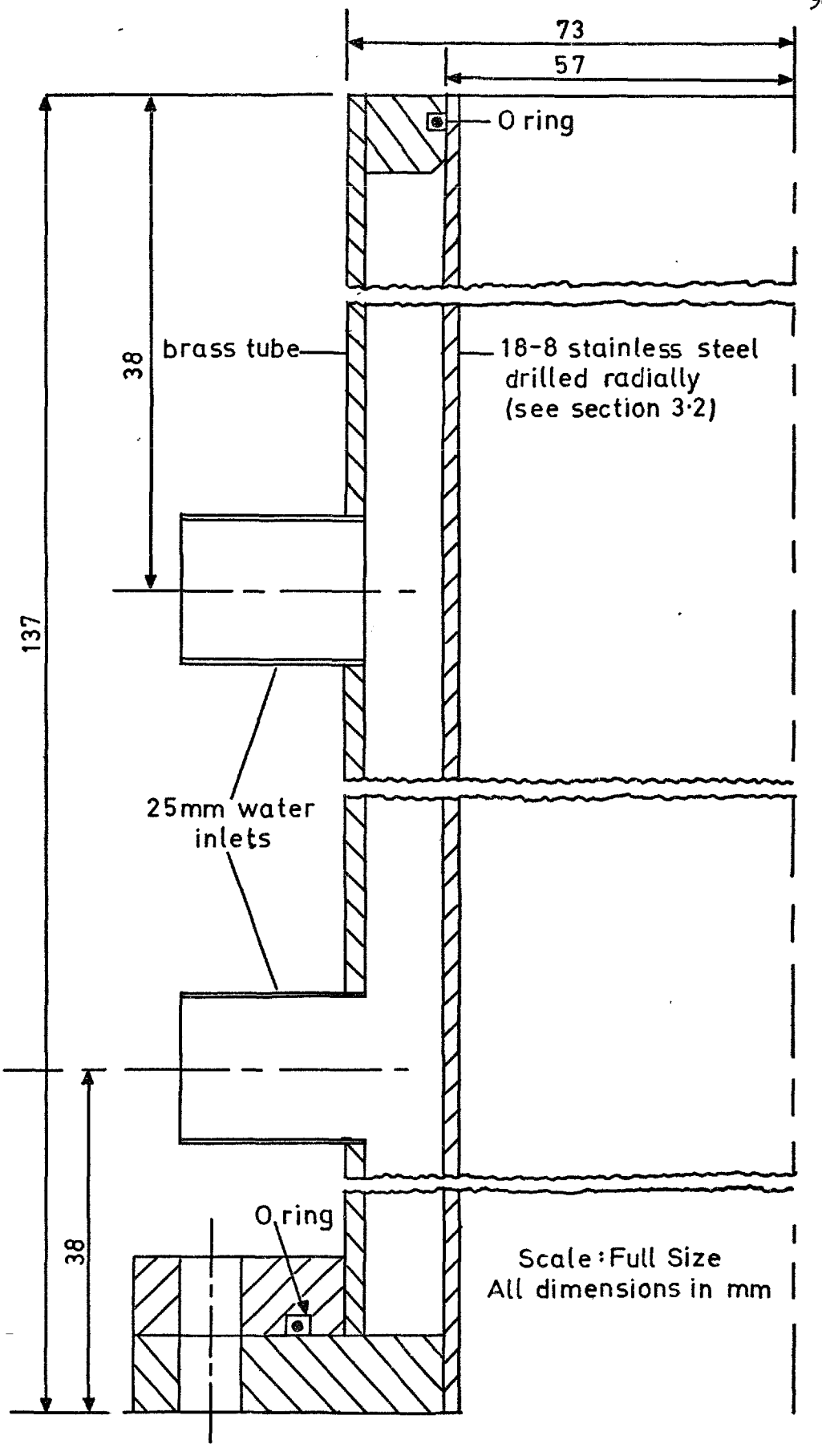


Fig. 3·5 Details of the water quench fitted under the press.

3.3 Materials

The Material was supplied by Alcan International Laboratories, Banbury, in the form of continuously cast billets of 86 mm dia. The specifications, heat treatments and experimental coding are given in Table 3.I.

The heat treatments were chosen to give an equilibrium structure prior to extrusion. After the first homogenization treatment the billets were machined to 73.5 mm diameter and 75mm length. Some billets of alloys C and D were machined to lengths of 3,6,9,12, and 15cm.

3.4 Experimental Procedure

In any experimental investigation into the hot working of metals there are many variables that have to be considered. To keep these to a minimum a standard extrusion procedure was used.

The container was heated to 300°C, usually overnight. The die was then placed in the bolster and left for one hour to enable a steady state temperature to be reached. The pressure pad was preheated on the container for at least fifteen minutes prior to extrusion. The billet, previously drilled in the centre with a No. 52 drill to a depth of 1cm, was then heated in the induction heater to the preset temperature; the time taken for this being less than six minutes at 500°C. The cycling time at temperature of the controller is about thirty seconds, and to allow an equilibrium temperature to be reached, the billet was left in the heater for several cycles.

When the billet had achieved a uniform temperature the load cycle was started by bringing the induction heater over the container and transferring the billet. The heater was then removed, the pressure pad dropped onto the rear of the billet and the ram approach cycle started. The recording instruments were operated as the ram entered the container and the water quench started as the load was applied. Extrusion was continued until the load indicator showed a sudden increase, indicating that the post steady state region had been reached. In the case of an accumulator run the ram had to be stopped by two steel half-rings to prevent damage to the container.

Alloy	Cu	Fe	Mg	Mn	Si	Ti	Zn	Cr	Heat Treatment
567D	4.00								8 hr @ 500 C, 48 hr @ 500 C
569D	4.44			0.31					"
752D	4.02	0.21	0.001	0.002	0.08	0.003	0.006	0.001	"
753D	4.00	0.18	0.001	0.30	0.08	0.003	0.005	0.001	"
817D	3.92	0.22	0.001	0.002	0.086	0.008	0.005	0.002	"
818D	3.80	0.23	0.001	0.32	0.09	0.008	0.007	0.002	"
266D	0.01	0.26	0.50	0.01	0.41	0.02	0.01	0.01	48 hr @ 510 C
265D	0.01	0.19	0.68	0.37	0.42	0.02	0.01	0.01	48 hr @ 530 C
272 D	4.36	0.40	0.74	0.70	0.77	0.02	0.01	0.01	48 hr @ 510 C

Table 3.I Alloy composition and heat treatment

In the text the following notations are used

Alloy A 567D

Alloy B 569D

Alloy CE 752D and 817D

Alloy DE 753D and 818D

After the ram had been withdrawn the container was raised and the extrude cut with a hacksaw before being punched through the die into the pit below. The discard was removed with the ram and the liner cleaned by pushing two scraper pads through it. This removed any excess metal on the liner surface and left it with a reproducible coating of aluminium. No lubricant was used at any stage during the extrusion because of the difficulty in reproducing lubricated conditions.

By measuring the time from the start of the load cycle to the point of application of the load with a stopwatch, the temperature at the start of the extrusion could be determined from cooling curves.

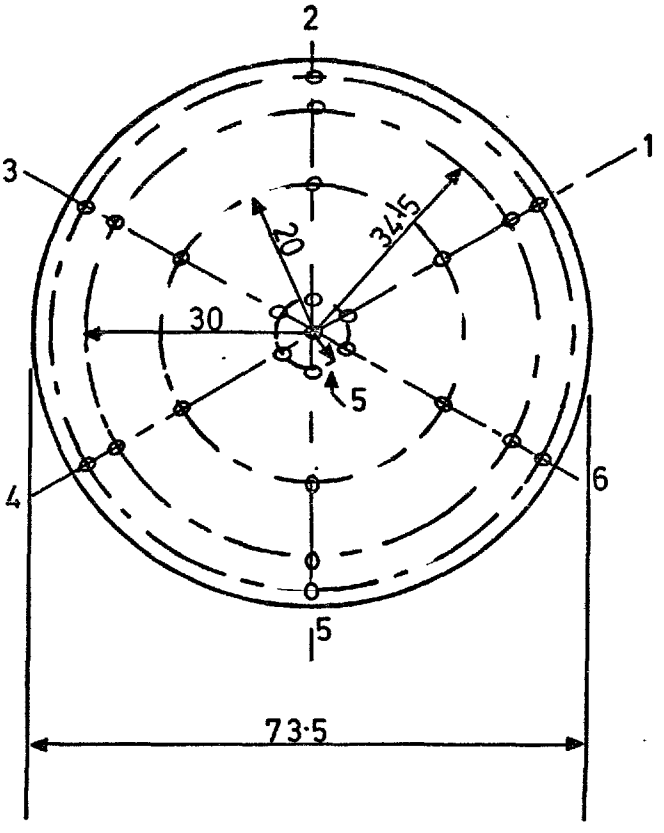
The standard procedure was used for most extrusions exceptions being those where a part-extruded billet was required or during an interrupted load test in peak load investigation. However, the starting method was always the same.

3.5 Temperature Measurements

The flow stress of a material is temperature dependent and so the temperature must be accurately known if a realistic analysis of the results is to be made.

At the start of the induction heater load cycle the power was automatically switched off; the billet was therefore cooling throughout its transfer. This cooling was measured by drilling a a billet as shown in fig. 3.6. Thermocouples were inserted into these holes and cooling curves for different starting temperatures measured. The temperature distribution during the heating cycle was similarly determined. This procedure was repeated for billets transferred into the container by the normal loading cycle, a drilled pressure pad being used to simulate experimental conditions. The results were compared with the curves obtained from a thermocouple in the 1cm deep central hole and the results found to be identical, within an experimental error of 3°C. The cooling curve from the centre hole was therefore used to determine the initial billet temperature, appendix I II

It is also important to know the temperature of the material during extrusion. Several methods were attempted.



all holes drilled for a 1·52mm dia. thermocouple.

Depth of holes
1 = 5
2 = 15
3 = 30
4 = 45
5 = 50
6 = 65

Scale: full size
all dimensions in mm
Billet length: 75
Central hole: 10

Fig. 3·6 The location of the thermocouples used in determining the cooling curves.

1) A fibre-glass sheathed thermocouple was passed through a hole in the centre of the pressure pad, and into the back of the billet. A drilled ram stem had to be used as well. This was occasionally successful but the results only served to confirm the initial billet temperature obtained from the cooling curves.
2) Stainless steel sheathed mineral insulated thermocouples were positioned in the dead-metal zone, using the drilled single hole dies. This involved drilling the billet prior to extrusion and locating the hot billet onto the projecting thermocouples. The depths of the holes were measured from the experimental flow patterns It was difficult to decide from the results obtained whether the temperature recorded was that of the billet or that of the die. A big problem was the shearing of the thermocouples during upsetting. To try and overcome this the cheaper fibre-glass sheathed thermocouples were used, with their ends covered with hardened steel caps. No meaningful results were obtained with this technique.

3.6 Flow Patterns

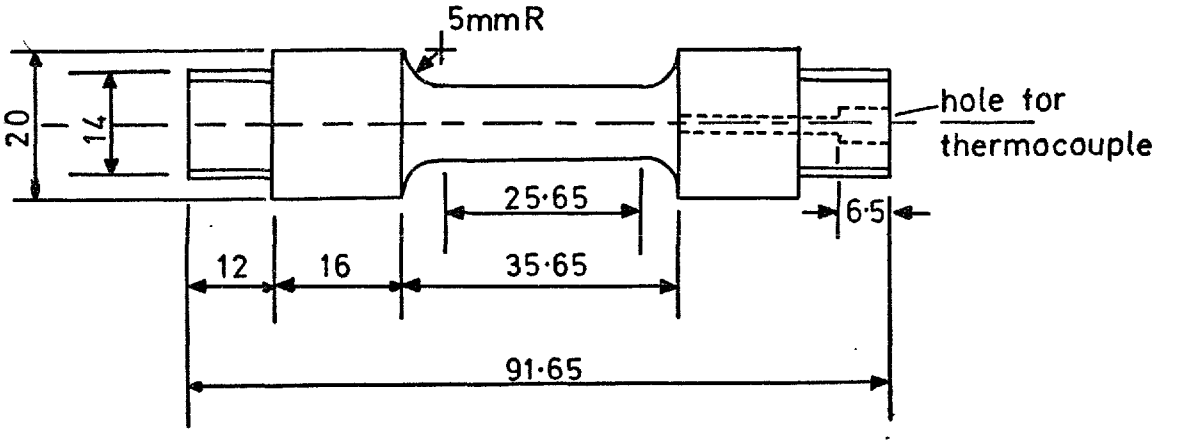
The path followed by the metal during extrusion is important in analysing the process. It can influence the surface finish of the extrude, the final properties of the extrude, and the extrusion load. It is also useful in determining strain-rate values.

The patterns were obtained from macro-etched polished sections of partly extruded billets. The etch used being a modified form of Tucker's reagent, 12% HF, 12% HNO_3, 36% HCl, 40% H_2O.

The billets to be sectioned were removed from the container as quickly as possible and quenched to minimize any structural changes occurring at the high temperature.

3.7 Torsion Testing

Solid torsion specimens, fig.3.7, were machined out of extruded rods of alloys C and D. The specimens were heat treated at 500°C for 48 hours in an air-circulating furnace to obtain a structure similar to that of the original material, Testing was carried out on a torsion machine, built in the department , over a range of true strain-rates from 0.0509 to 8.96 sec^{-1} and temperatures from 200°C to 520°C. The specimens



Scale : Full size.
All dimensions in mm.

Fig. 3·7 The dimensions of the torsion specimens.

were heated in situ by an induction heater and the temperature controlled by a thermocouple in the fixed end. Uniformity of temperature was maintained by adjusting the position of the coil with a copper specimen in position. Temperature variations in this could be more easily monitored with a disappearing filament pyrometer In the copper specimen at 750°C the temperature variation throughout the gauge length was $\pm$ 5°C. After testing to failure, or to a steady state in the more ductile specimens, the entire testing region (enclosed in a sealed container) was flooded with water to achieve a rapid quench. The torque was measured by a lever arm operating a load cell, the output being fed to the U.V. recorder.

3.8 Hot Tensile Tests

No. 12 Hounsefield specimens were prepared from extruded rods of alloys C and D. These were heat treated for 48 hours at 500°C and tested on an Instrom Universal Testing Machine over a range of strain-rates from 0.00052 to 0.31 sec^{-1} and temperatures from 200°C to 400°C. The specimens were placed in the tensile machine, using Nimonic grips and extension rods and heated in a Haddow's split furnace, controlled by a contact thermocouple. To allow equilibrium to be attained before testing specimens were left for thirty minutes at temperature.

3.9 Specimen Examination

Because of the possibility of a variation in structure along the length of the extrude, specimens were always taken from a point corresponding to the middle of the billet, i.e. a distance equal to half the extrusion ratio times the billet length from the front of the extrude. Sectioning of the extrude is shown in fig. 3.8 , other specimens were taken from the front end of some extrudes.

3.9.1 Optical Microscopy

Both longitudinal and transverse sections were prepared for examination. The samples were cut from the extrude, using a fine piercing saw, and mounted in slow setting Met Set, which has the advantage of setting without any rise in temperature. The mounted specimens were then polished in the usual way, finishing on $\frac{1}{4}\mu$ diamond paste followed by alumina. The polished specimens were

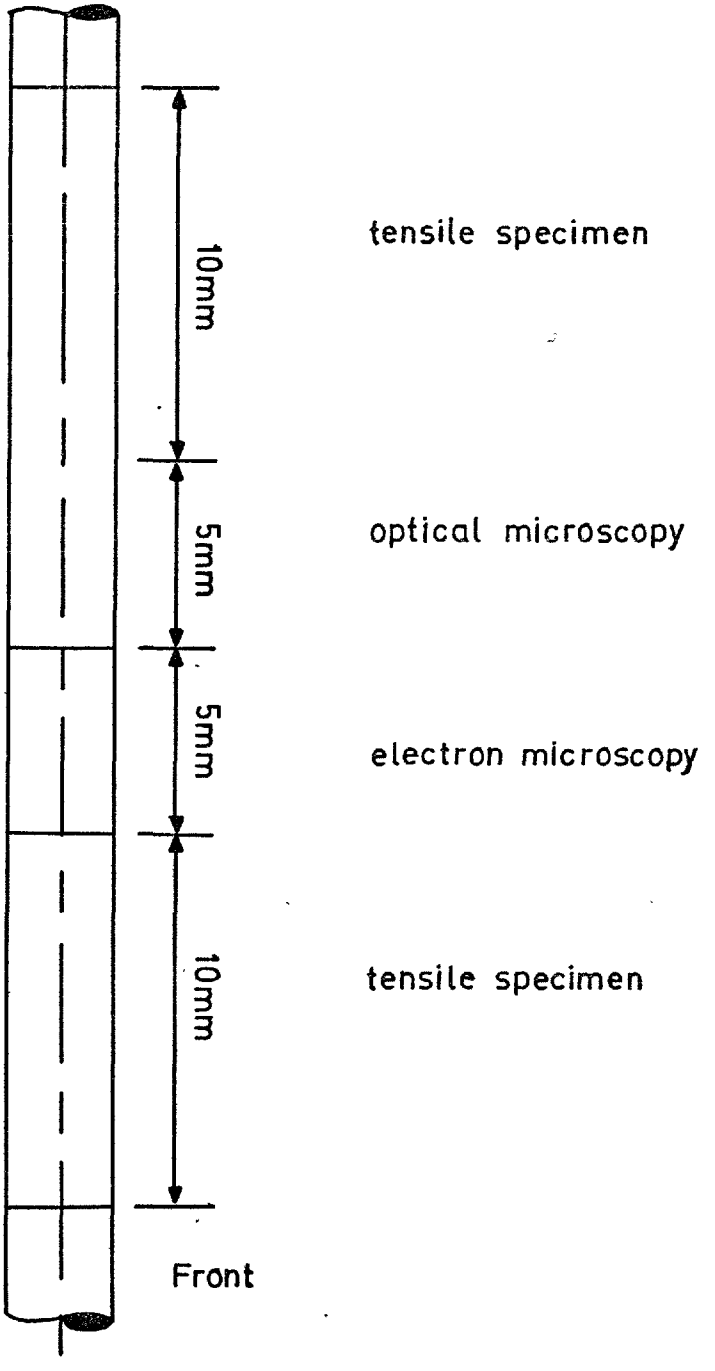


Fig. 3·8 The sectioning of the extrude.

examined in both the etched and unetched condition using the standard aluminium alloy etches.

3.9.2 Transmission Electron Microscopy

Transverse sections about 2mm thick were carefully cut from the extrude using a lubricated slitting wheel. The prepared sections were ground to a thickness of 0.15mm on rotating wet silicon- carbide papers. The specimen was mounted on perspex with double-sided sellotape, using razor blades as thickness guides, to facilitate the grinding. The thin discs were then electro-polished by the standard window technique using an electrolyte of 10% HNO_3 in methanol and a stainless steel beaker as a cathode. The best foils were obtained using a potential of 12 to 15 volts at a temperature of $-30^{\circ}C$. The thin foils were examined in a Siemens Elmiskop I electron microscope at a potential of 100 KV fitted with a stage that could be tilted through 30°.

3.9.3 Scanning Electron Microscopy

The surface of the extrude is of paramount importance in the aluminium industry and some specimens were examined on a Cambridge Stereoscan 600 scanning electron microscope. Little specimen preparation was needed other than careful cleaning. Some specimens were polished and etched in the modified Tuckers reagent to examine the relation between the surface defects and the internal structure.

3.9.4 Hardness Tests

These were carried out on the mounted specimens used for optical microscopy. Some microhardness test results were carried out but the bulk of the tests were made with a standard Vickers hardness machine using a load of 2.5 kg. Only the transverse sections were examined; in the case of the multi-hole specimens, care was taken to traverse the region showing the most complex variation in flow. A billet prepared for a flow pattern determination was also tested to see if there was any correlation between hardness and flow pattern.

3.9.5 Tensile Tests

These were carried out using No. 12 Hounsefield specimens, prepared from the as extruded rod, on an Instrom universal testing machine. The diameter of the extrudes prepared at the higher extrusion ratios precluded any tests being made on them.

CHAPTER FOUR

RESULTS

The fully tabulated results are listed in appendix V . Where applicable, the best fit straight line was calculated, using a least squares approach. A flexible computer program was used and this is given in appendix I . The discussion of the results will be left to Chapter Five.

4.1 Hot Working.

The applicability of the hot working theory, discussed in Chapter One to the hot torsion and tensile tests, and the extrusion results was examined.

4.1.1. Hot Torsion and Tensile Tests.

Using the theory given in Chapter Two, section 2.1. the torque time curves were converted to true-stress true strain curves. These are given in appendix VI , and follow the expected form, with a rapid rise to a maximum followed by a fall to an almost steady state. The exceptions to this were the high strain rate low temperature tests, where a steady state was not reached, and the high temperature low strain rate tests, where a peak was not observed. The strain to the maximum stress increased with an increase in the strain rate and a decrease in the temperature. The hot tensile results exhibited a rise in stress to an almost constant value, followed by a fall, as necking occurred. The higher strain rate tests started to neck immediately after the maximum stress was reached. In order to correlate the results a value of the flow stress for the torsion tests had to be selected. By studying the stress-strain curves, and the available literature, the stress at a strain of 1.5 was used. This value was in the steady state region for most of the tests, and fell in the region before a rapid fall in the stress occurred in the others.

Two equations have been found to apply to hot working results obtained at a constant temperature.

At low stresses

$$\dot{\varepsilon} = A_1 \sigma^{n_1} \qquad 1.1$$

and at high stresses

$$\dot{\varepsilon} = A_2 \exp \beta\sigma \qquad 1.2$$

The applicability of these equations to the experimental results was tested, figures4.1-4.4. Within the accuracy of the results, equation 1.1 could be fitted to all the data. The values of the constants n_1 and A_1 being temperature dependent, especially in alloy CE , Equation 1.2 could also be applied to the results for alloy DF. In alloy CE a linear relationship was only seen at the lower temperatures.

Assuming equation 1.1 to hold at the highest test temperature, and equation 1.2. to apply at the lowest temperature used, i.e.in the lowest and highest flow stress regions respectively, the constants can be obtained.

For alloy DF

$$\dot{\varepsilon} = 8{\cdot}0 \times 10^{-9}\sigma^{12{\cdot}30}$$

and

$$\dot{\varepsilon} = 1{\cdot}40 \times 10^{-8}\exp 1{\cdot}68\sigma$$

For alloy CE

$$\dot{\varepsilon} = 6{\cdot}2 \times 10^{-6}\sigma^{7{\cdot}65}$$

and

$$\dot{\varepsilon} = 2{\cdot}48 \times 10^{-1}\exp .2\,48\sigma$$

These constants were calculated from the results at 573° and 673° . More results were obtained at these temperatures and hence the accuracy would be correspondingly greater.

Before equation 1.7, the general hot-working relationship, can be applied, the values of α and the activation energy Q have to be determined. In Chaper Two, section 2.11 it was shown that a value of α can be obtained from n_1 and β_1 in equations 1.1 and 1.2.

$$\alpha = \frac{\beta}{n_1}$$

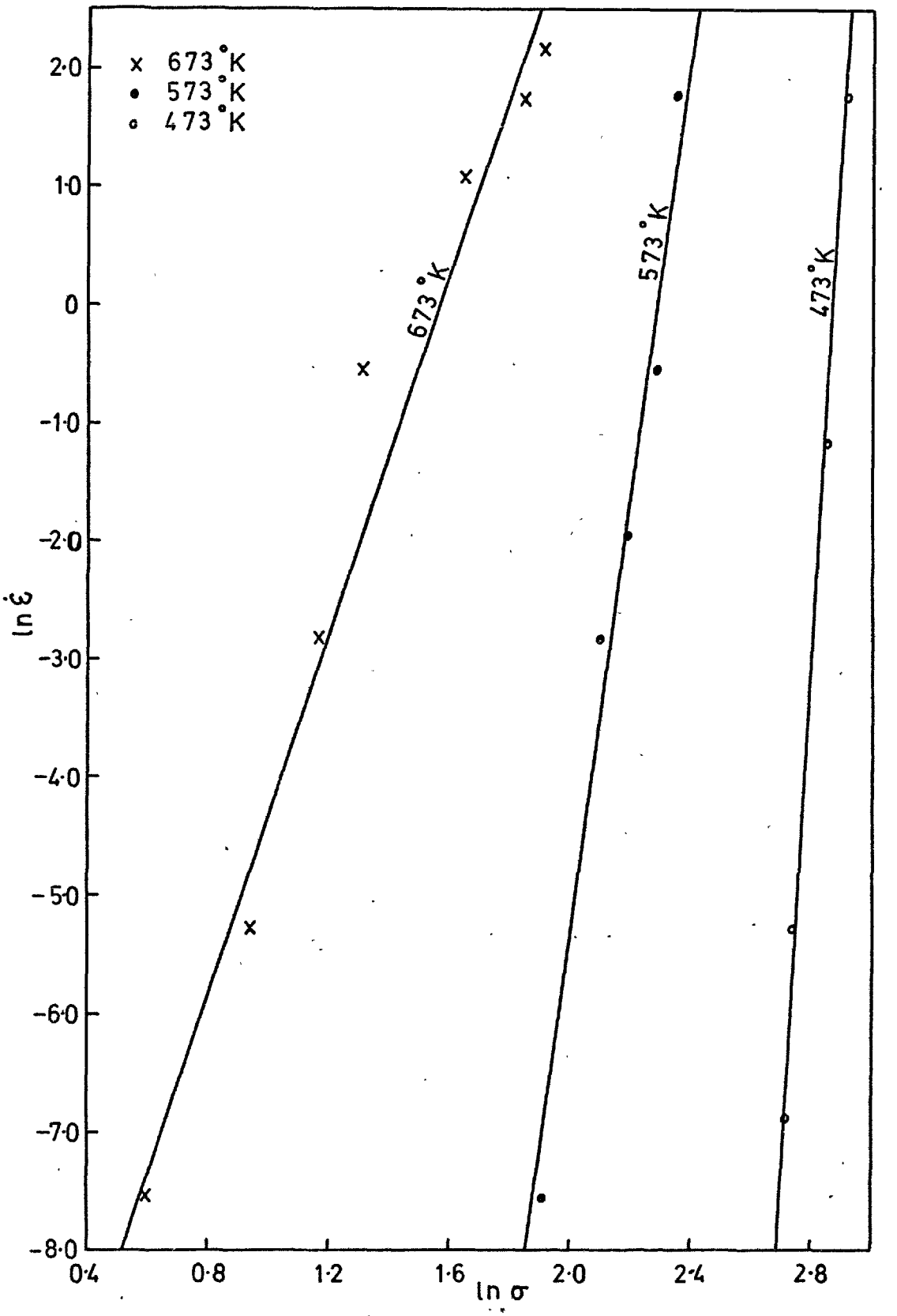


Fig. 4-1 The applicability of a power law to the flow stress and the strain rate for alloy CE.

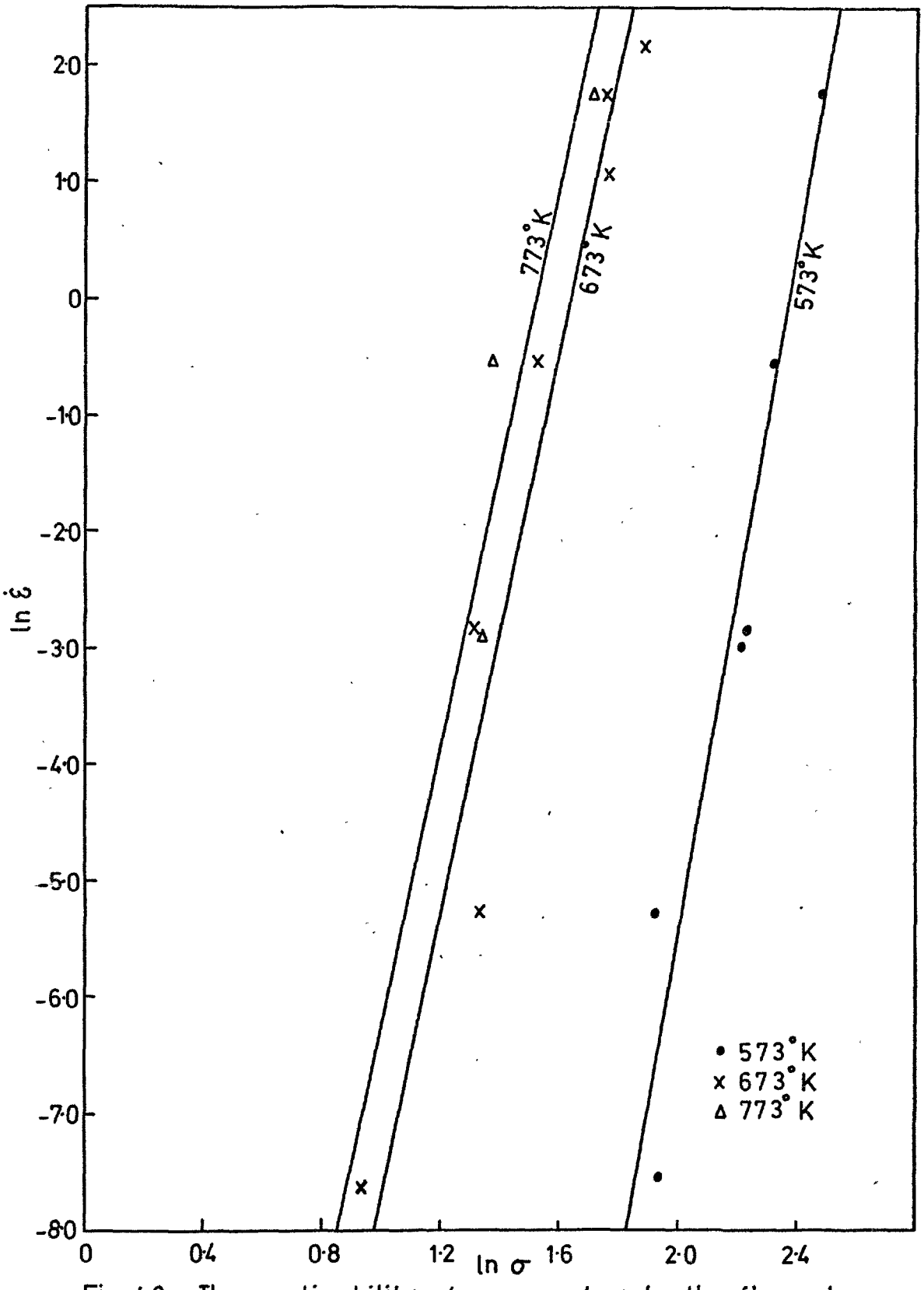


Fig. 4·2 The applicability of a power law to the flow stress and the strain rate for alloy DF.

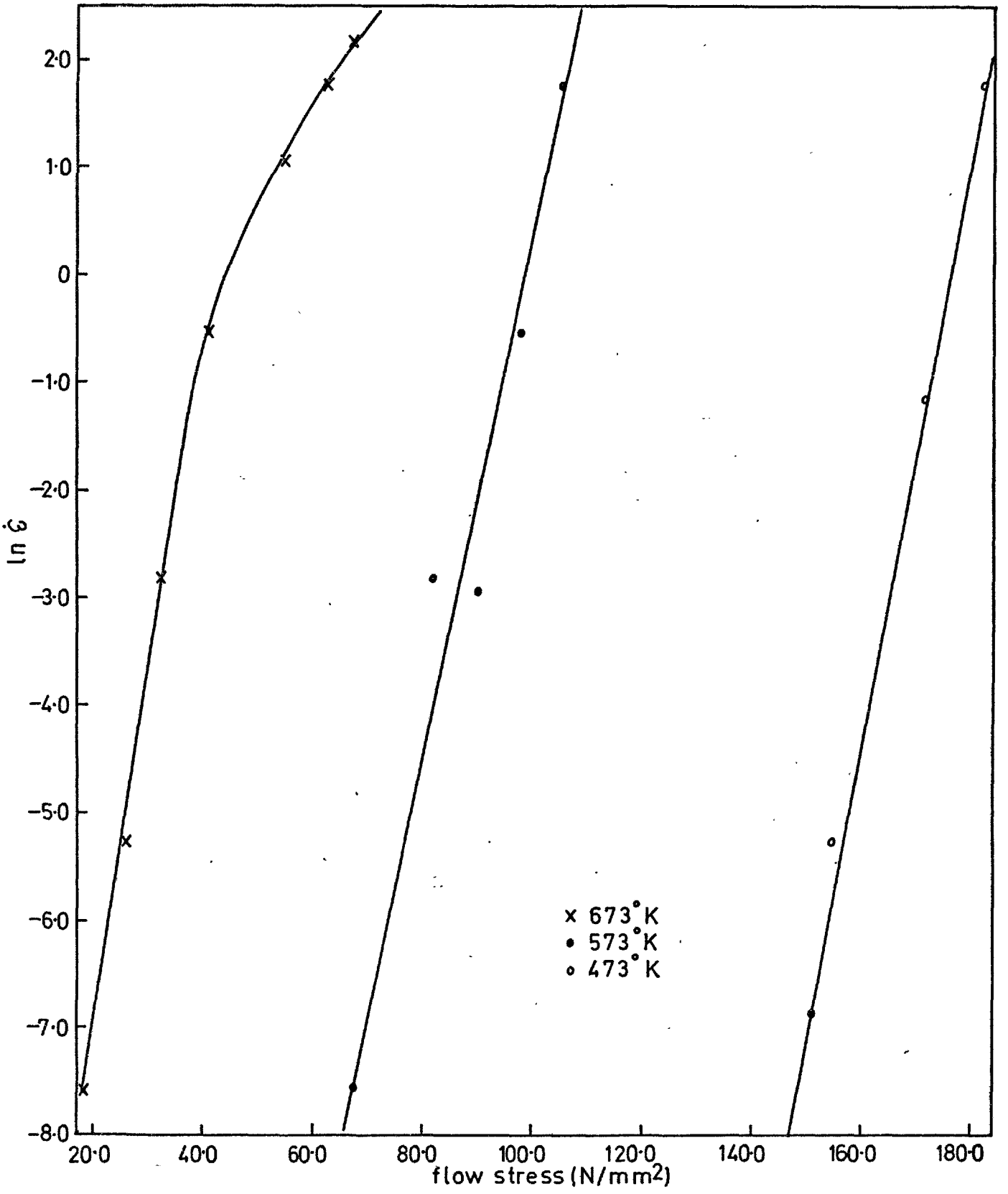


Fig. 4·3 The applicability of an exponential law to the flow stress and the strain rate for alloy CE.

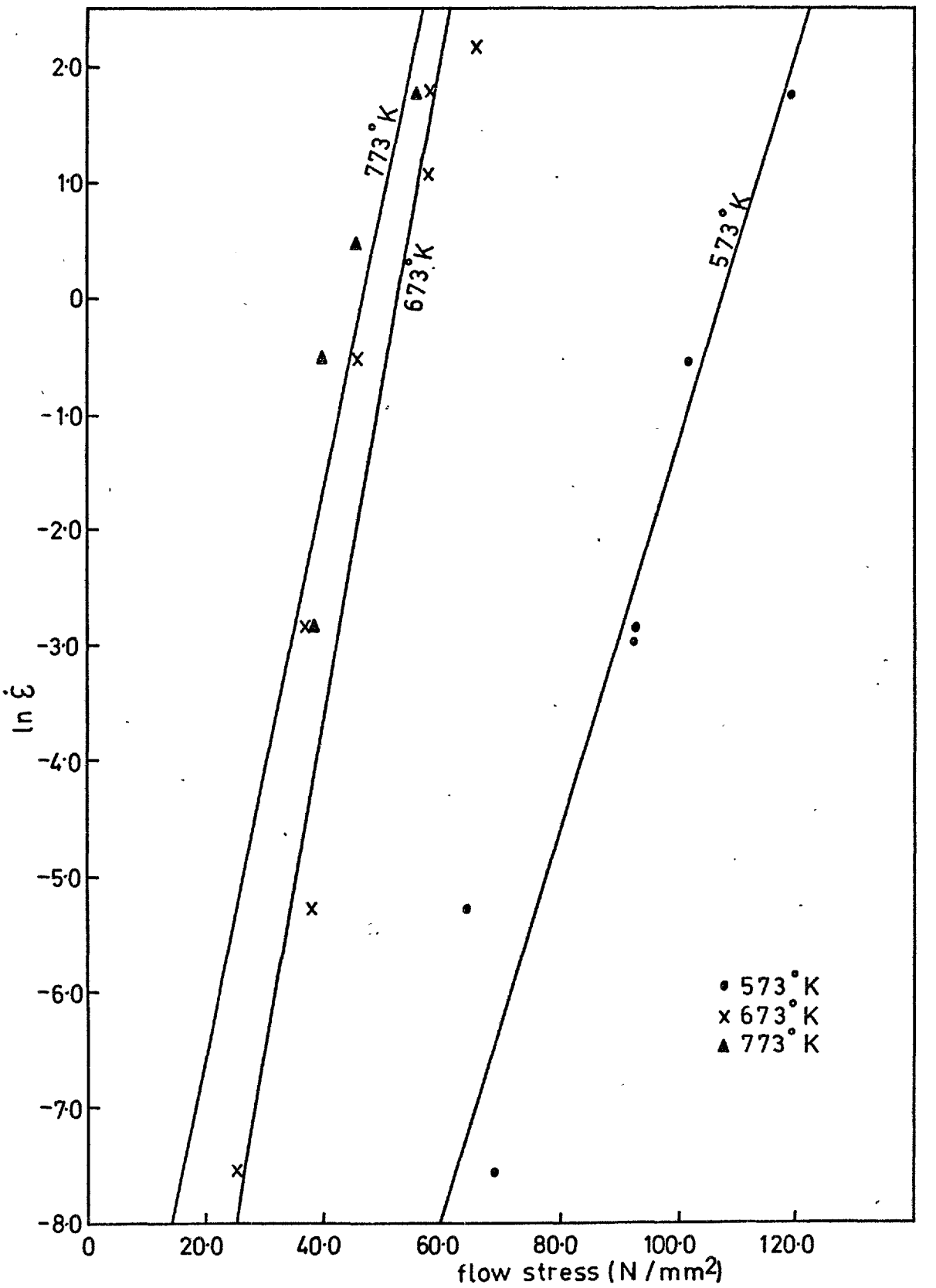


Fig. 4·4 The applicability of an exponential law to the flow stress and the strain rate for alloy DF.

Using the results obtained above
For alloy DF

$$\alpha = 0{\cdot}0137 mm^2/N$$

and for alloy CE

$$\alpha = 0{\cdot}0324 mm^2/N$$

Knowing the value of α it should be possible to determine the activation energy for hot-working, using the method given in section 2.11. This involves plotting values from the extrapolated graphs of $\ln \dot{\varepsilon}$ against $\ln \sinh(\alpha\sigma)$. A meaningful activation energy will only be obtained if a large number of experiments are carried out over a wide range of temperatures.

The number of results in the present work precluded the use of this method but examination of the results of other workers suggests that the value of the activation energy, for the hot-working of aluminium alloys, is of the order of 160,000 joules per mole. Using this value the results from the hot-working tests were plotted in the form of log Z against $\log \sinh \alpha\sigma$, figures 4.5 and 4.6, Z being the temperature compensated strain rate. Reasonable straight lines were obtained for both alloys. From the gradient and intercept the values of α and A in equation 1.7 were obtained.
For alloy DF

$$Z = 1{\cdot}99 \times 10^{12} \sinh(0{\cdot}0137\sigma)^{6{\cdot}57}$$

For alloy CE

$$Z = 1{\cdot}41 \times 10^{10} \sinh(0{\cdot}0324\sigma)^{3{\cdot}3}$$

At high stresses equation 1.7 can be rewritten in the form

$$Z = A_4 \exp(\beta_1\sigma) \qquad 4.1$$

Figures 4.7 and 4.8 show that this equation cannot be applied over the full range of strain rates and flow stresses achieved in these tests.

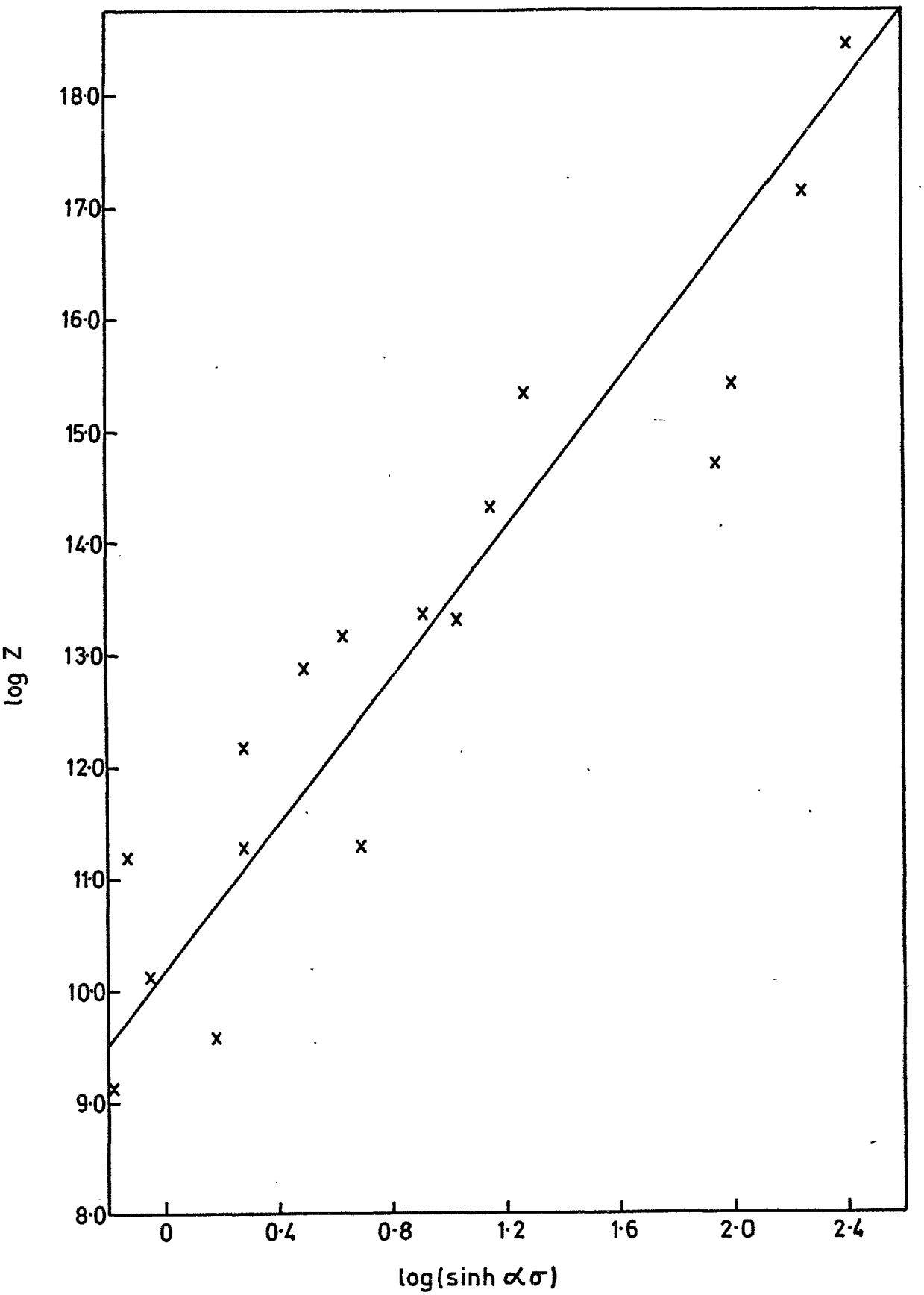


Fig. 4·5 Relationship between log Z and log (sinh $\propto\sigma$) for alloy C E (Torsion)

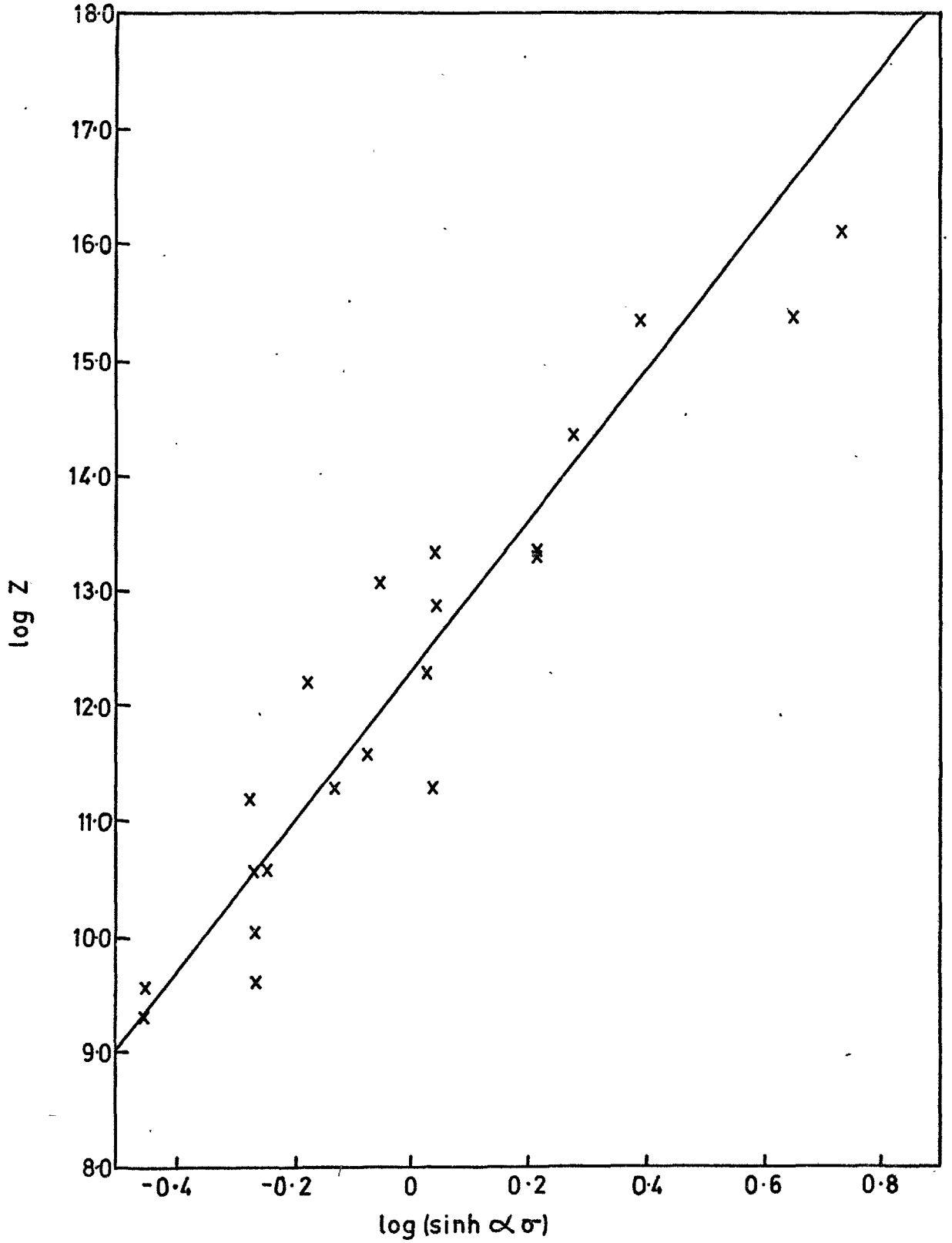


Fig.4·6 Relationship between log Z and log (sinh $\alpha\sigma$) for alloy DF (Torsion)

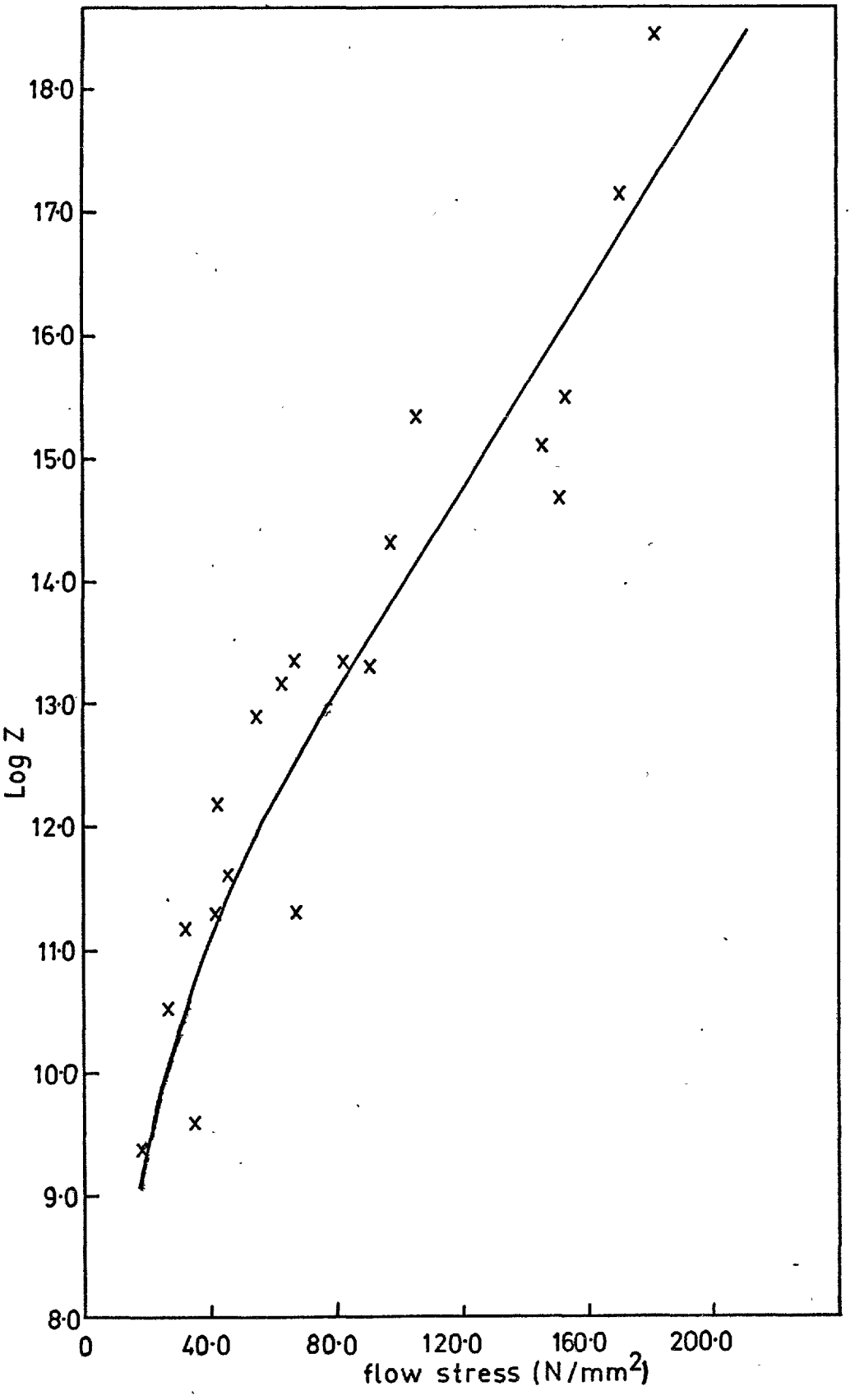


Fig. 4·7 The relationship between Z and the flow stress for alloy CE (Torsion).

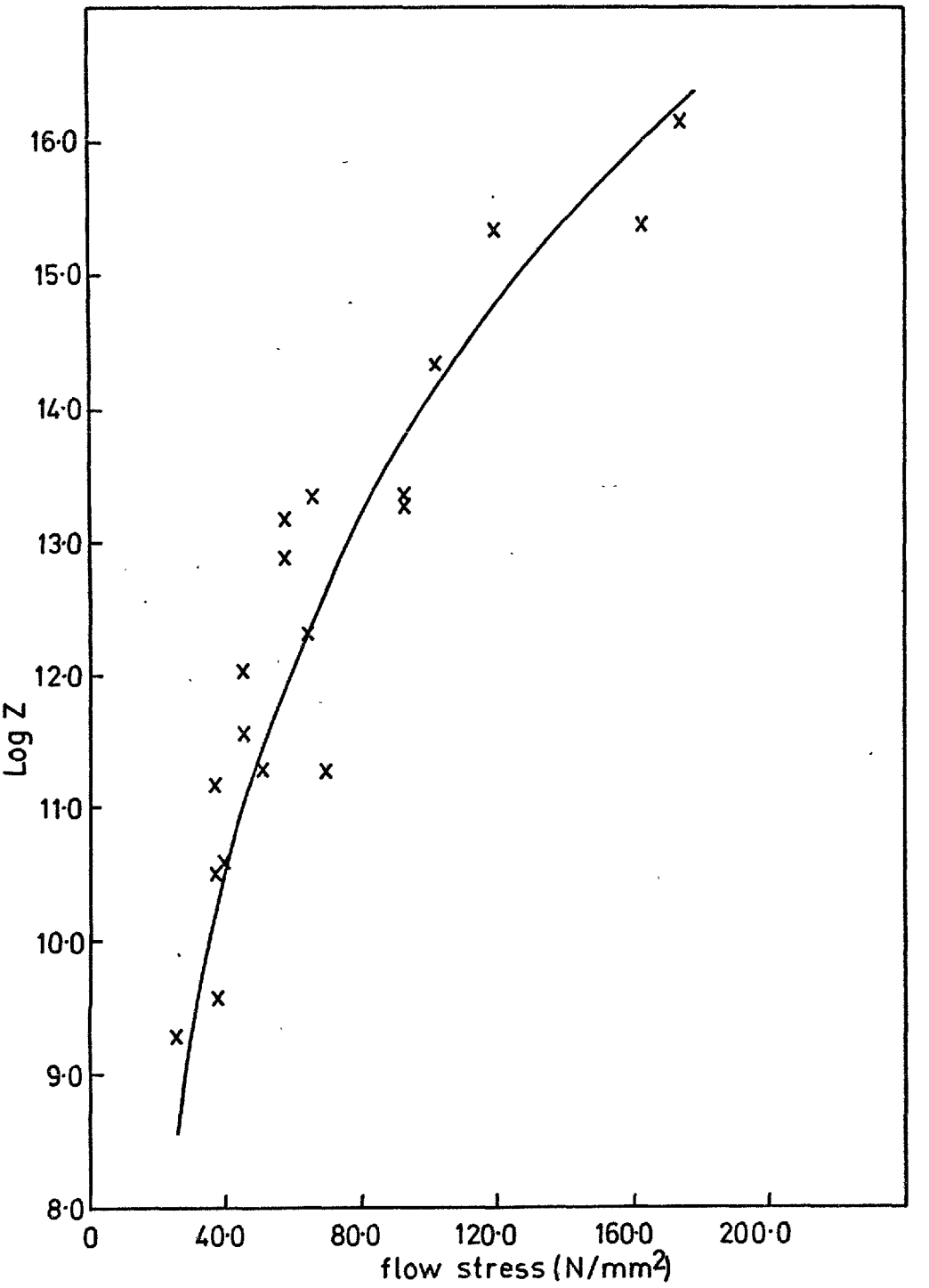


Fig.4·8 The relationship between Z and the flow stress for alloy DF (Torsion).

4.1.2. Extrusion Results

In the previous section the hot-working relationships have been shown to apply to the hot-torsion and tensile results. Their applicability to the results from extrusion will now be examined.

The flow stresses, strain rates, and temperatures were calculated using the theory given in Chapter Two. To calculate the constants in equations 1.1, 1.2, 1.7, and 4.1 graphs at constant temperatures and at constant strain rates have to be plotted. The presence of the large temperature rise precludes the first and the number of results at the different strain rates will prevent accurate results being achieved by the second. For the reason given in section 4.1.1 an activation energy of 160000 Joules per mole was assumed. Figures 4.9-13 show the relationship between log Z and the flow stress for all the alloys considered. The gradients of the lines give the values of β in equation 4.1, and these depend on the alloy being considered. In these graphs a series of approximately parallel straight lines is seen, each line being associated with one reduction ratio and hole configuration. If the correct value of the flow stress and the strain rate had been used, the results should have fallen onto one straight line. The spacing between the lines appears to be the same for all alloys and therefore a correction factor can be applied to the values of log Z, to raise or lower the lines relative to a chosen reference one. The reason for correcting the value of Z, rather than the flow stress, will be given in the discussion. The results for the 60.1 single hole reduction were used as a reference line for the simple reason that more results were obtained at this reduction. The correction factors were obtained by taking the average of the vertical line spacings for each reduction ratio, they are given in table 4.I . In other words, the validity of equation 4.1 is accepted and the extrusion results are made to follow this equation by applying empirical correction factors to the values of Z. The results are replotted using this corrected value of Z, Zc, in figures 4.14-4.17 As expected, reasonable straight lines were obtained. The constant A and B are listed in table 4.II. The effect of alloying is seen in the relative magnitudes of these constants.

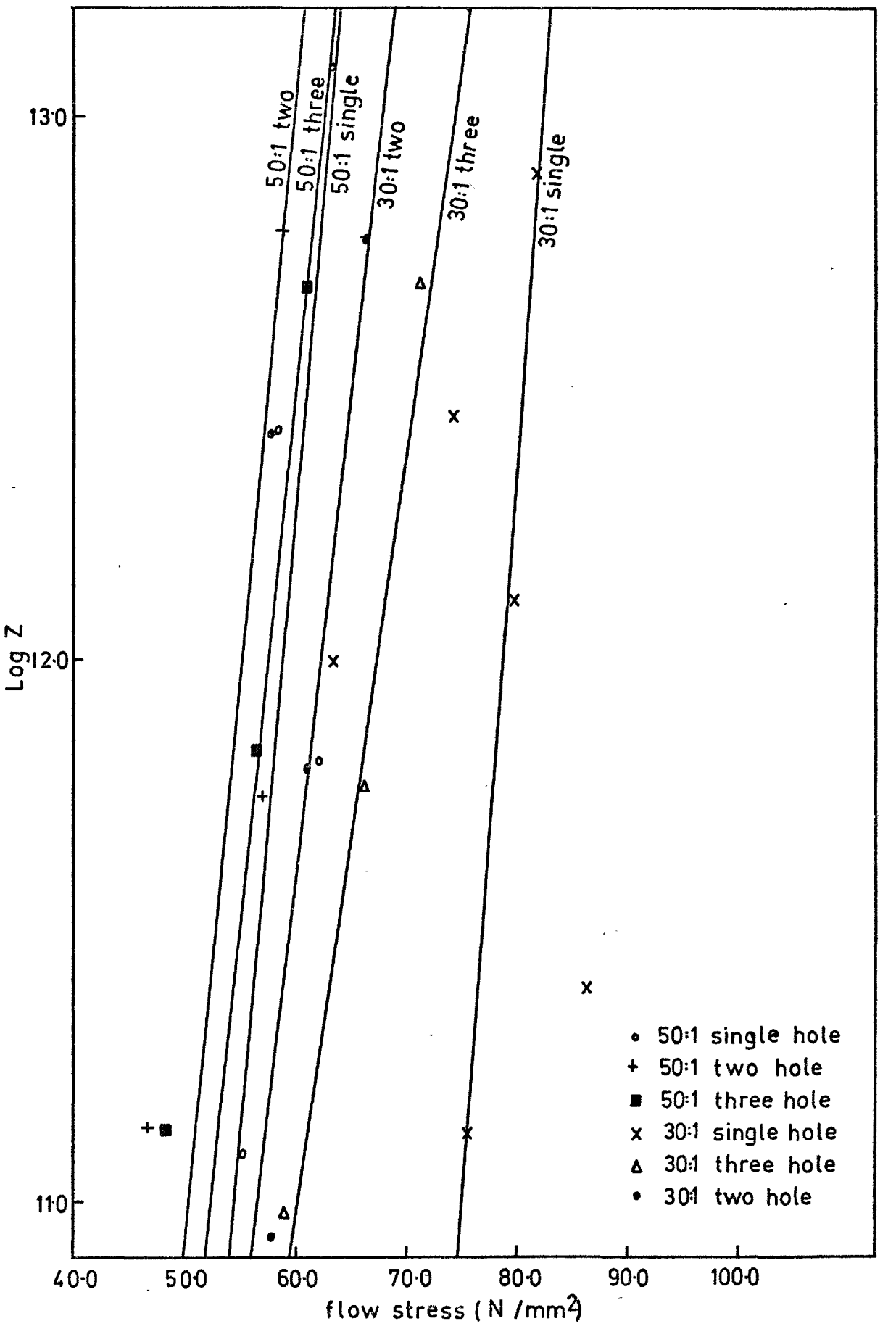


Fig. 4·9 The relationship between Z and the flow stress for alloy A.

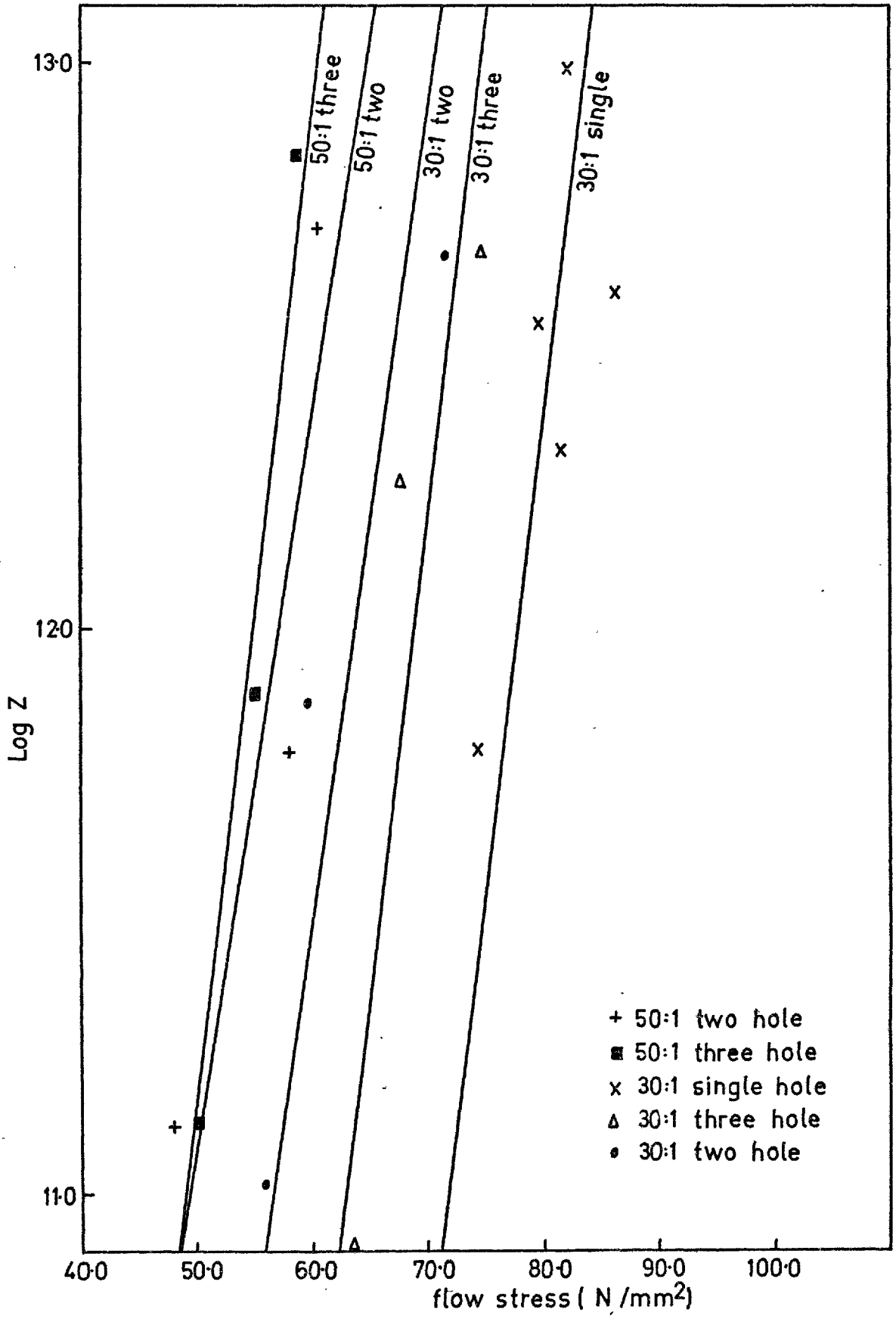


Fig. 4·10 The relationship between Z and the flow stress for alloy B.

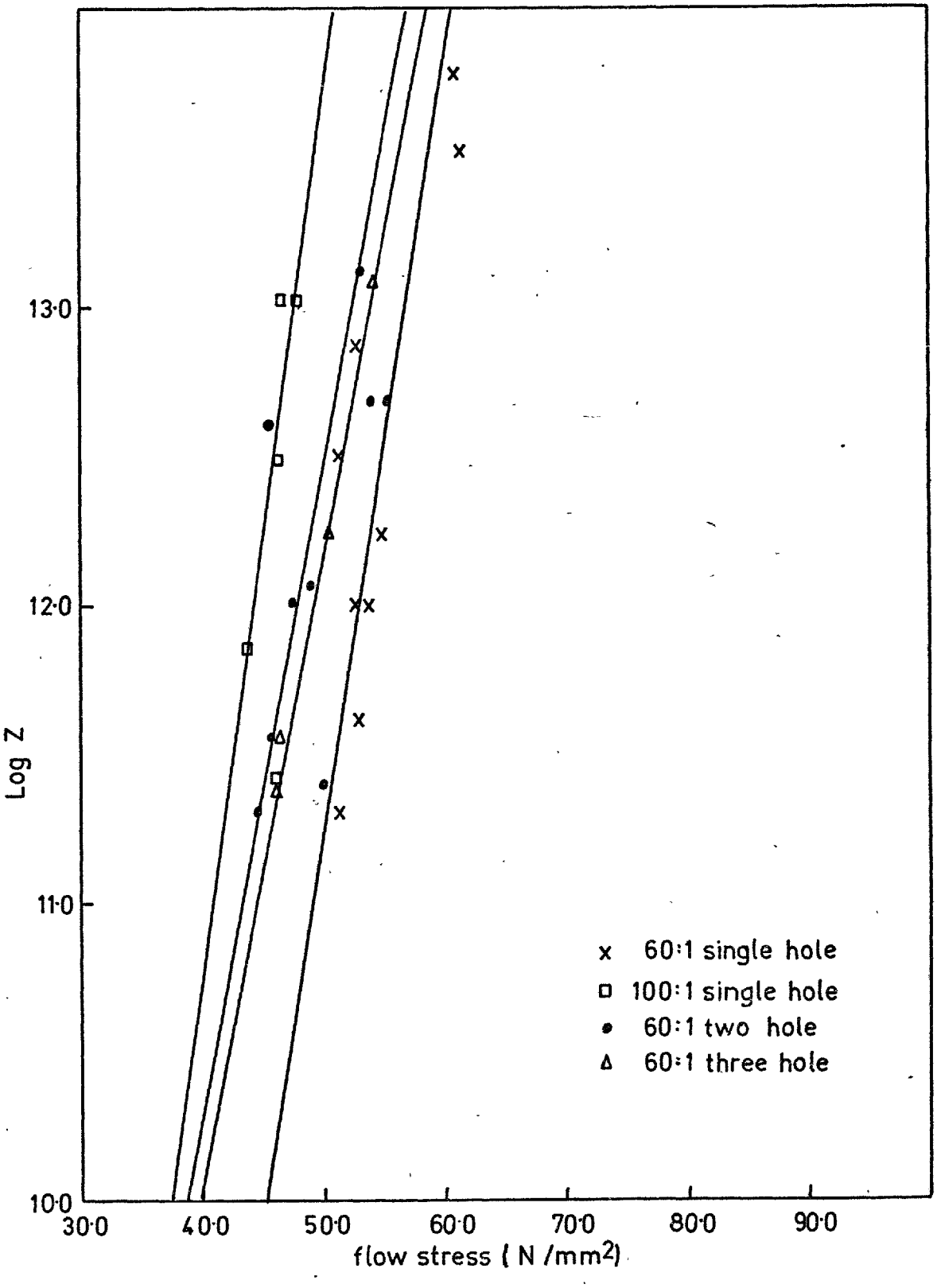


Fig. 4·11 The relationship between Z and the flow stress for alloy CE.

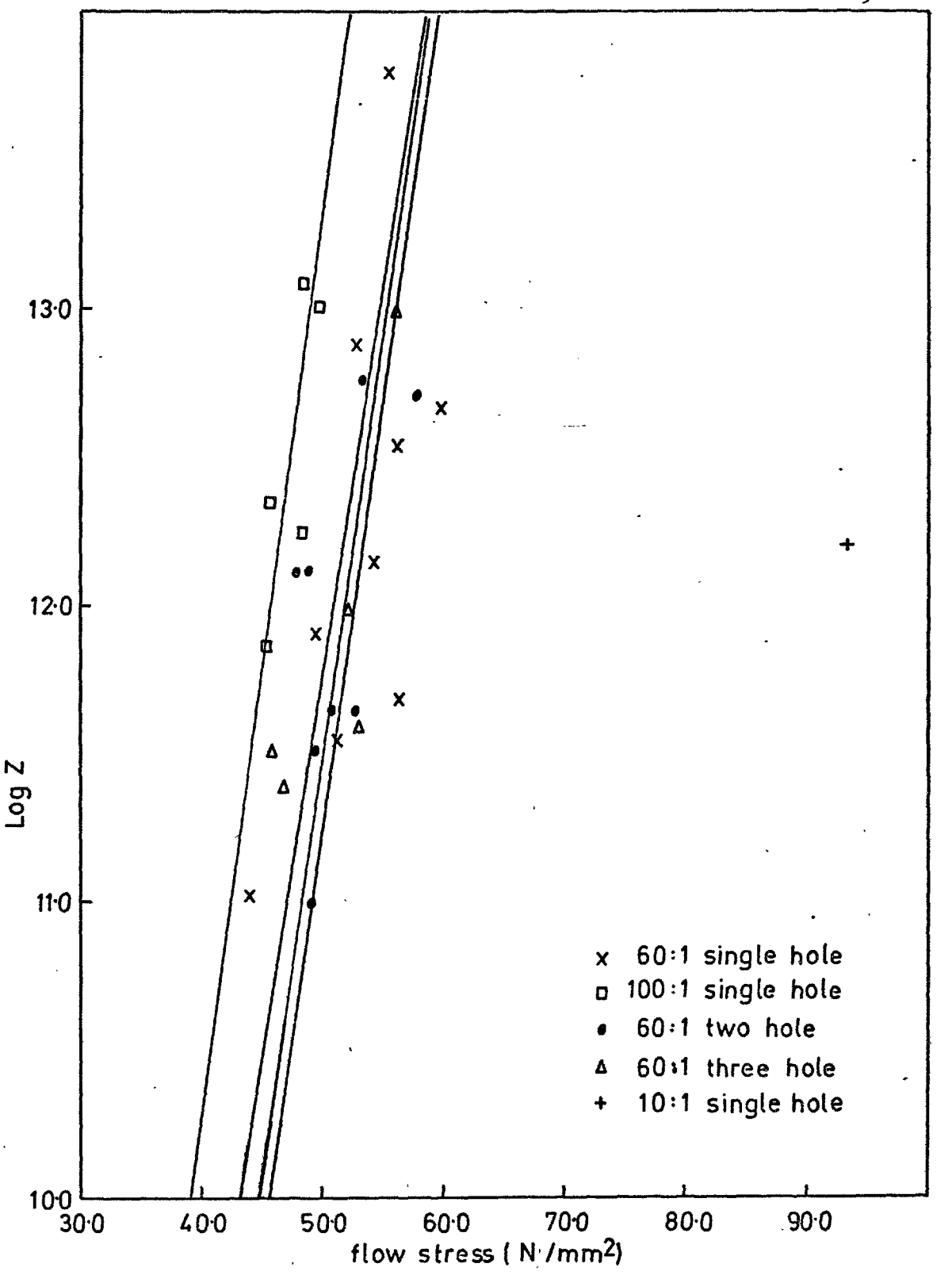


Fig. 4·12 The relationship between Z and the flow stress for alloy DF.

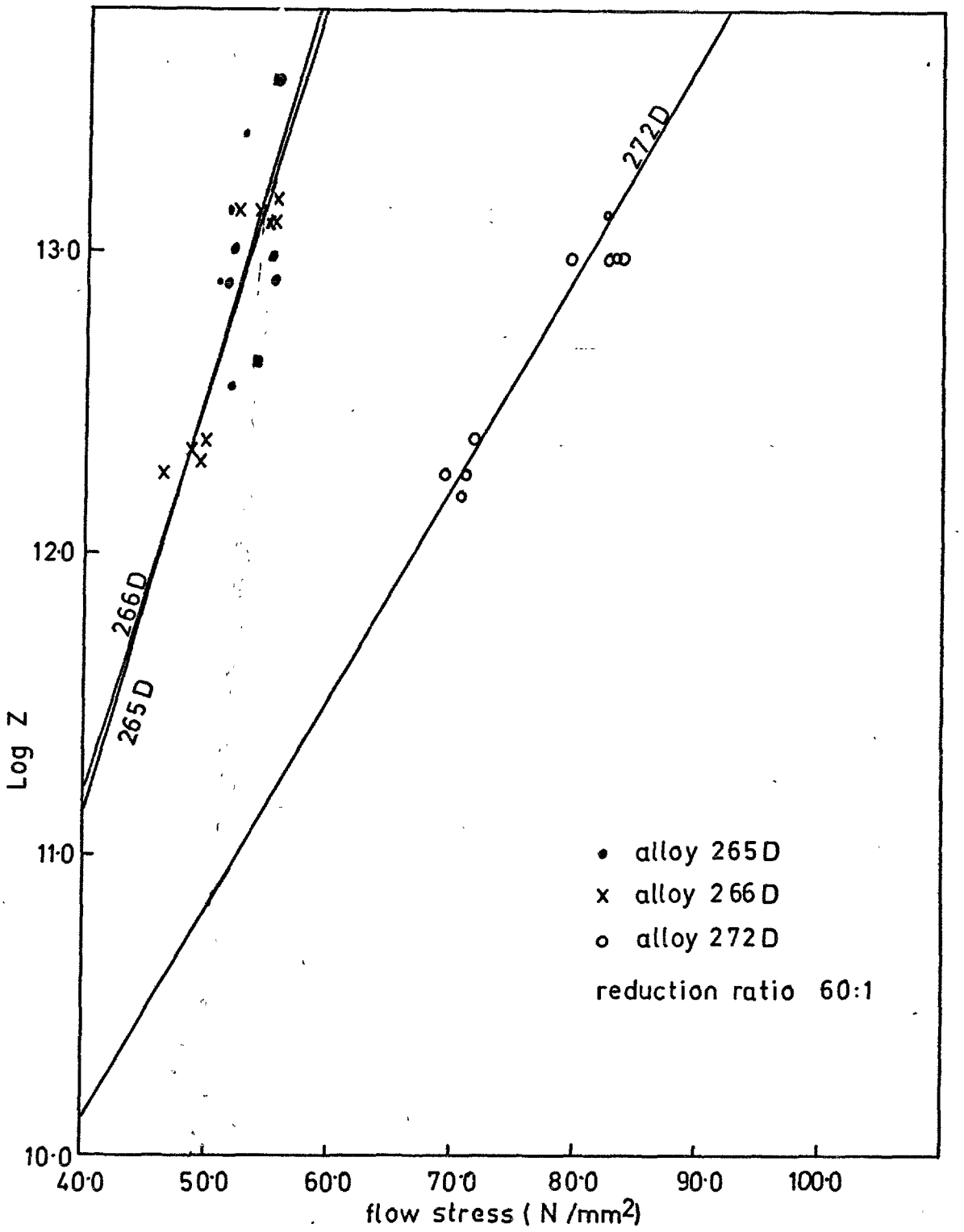


Fig.4·13 The relationship between Z and the flow stress for alloys 266D, 265D, and 272D.

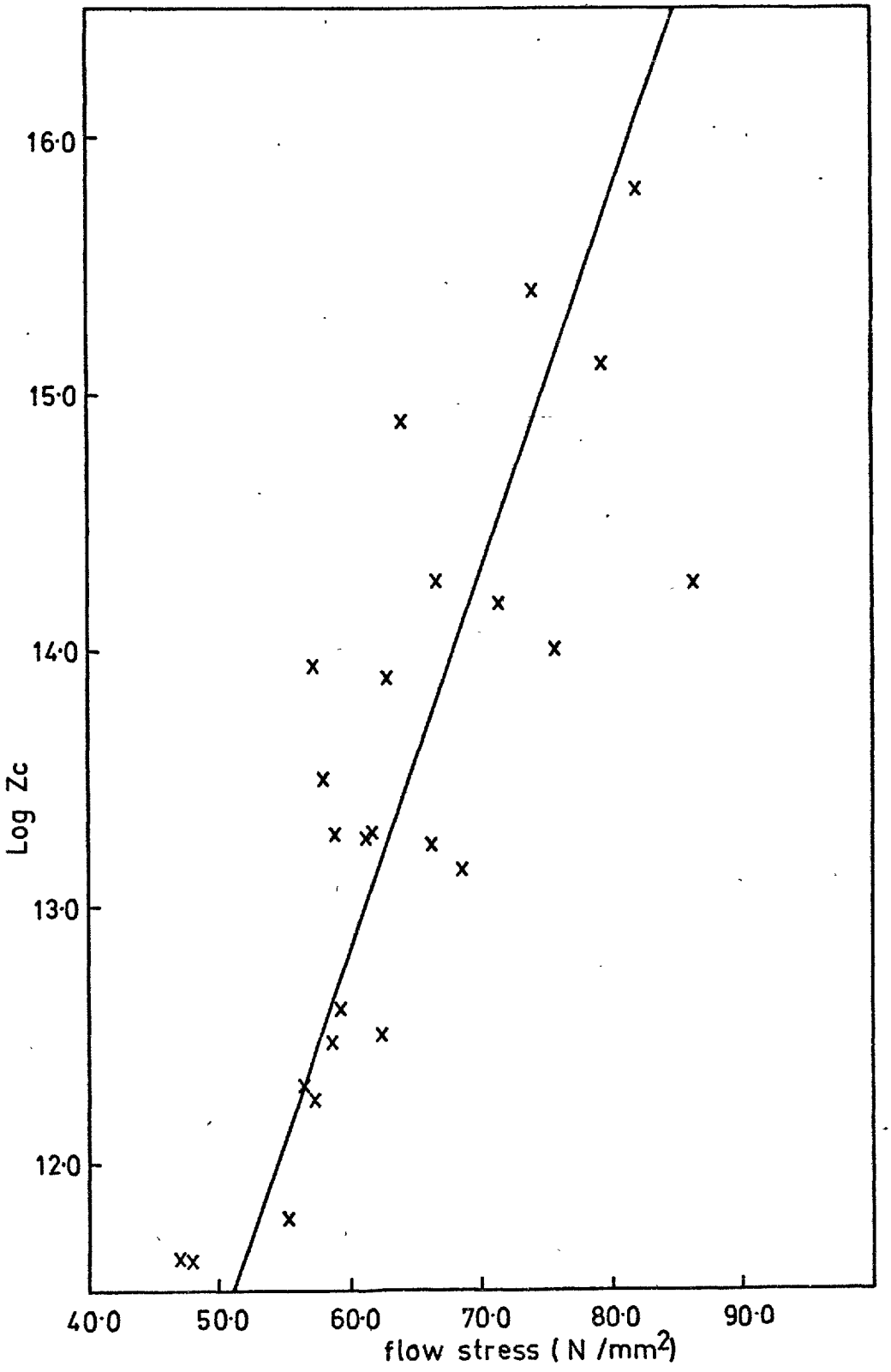


Fig. 4·14 The relationship between the corrected value of Z and the flow stress for alloy A.

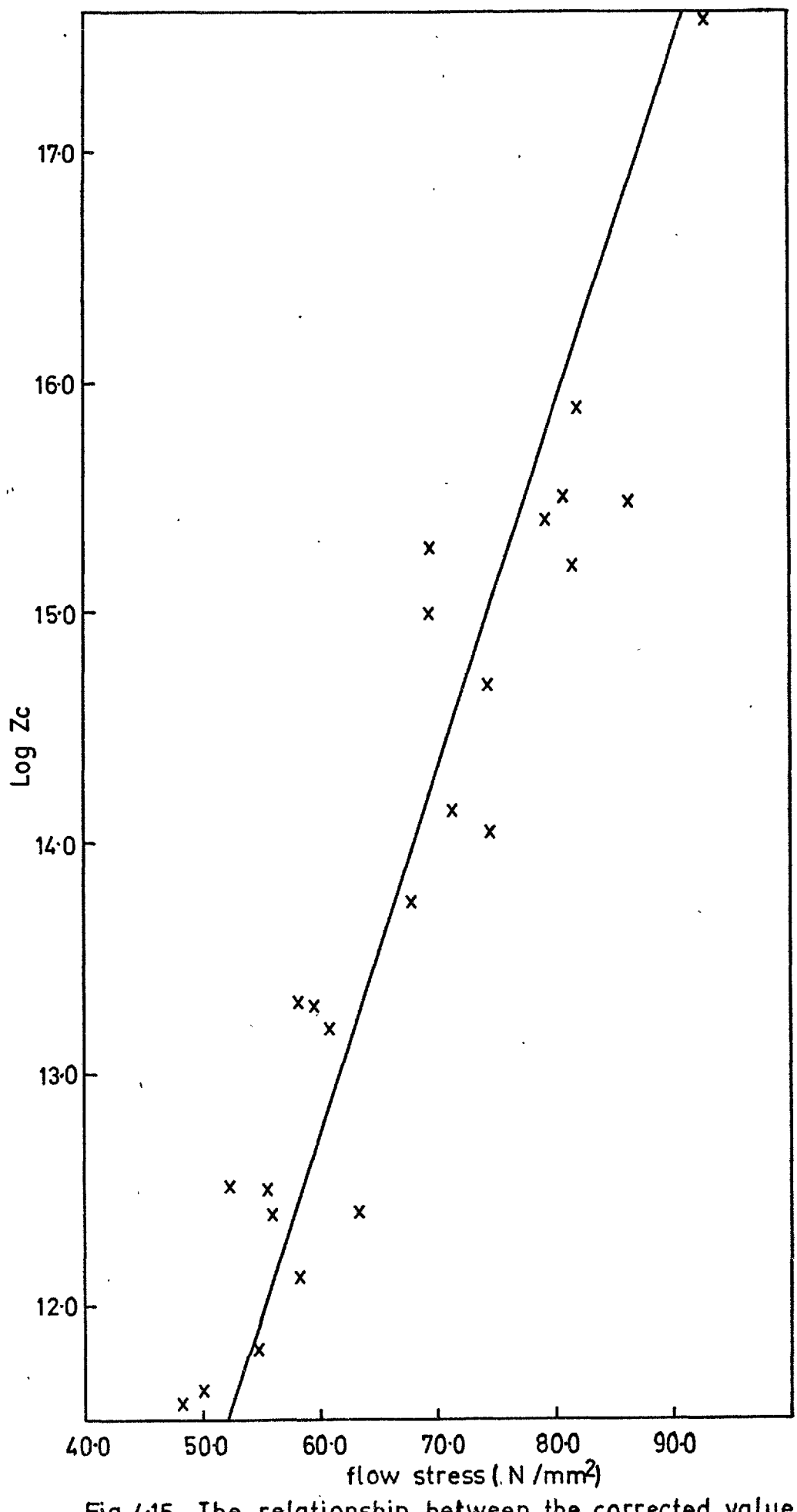


Fig. 4·15 The relationship between the corrected value of Z and the flow stress for alloy B.

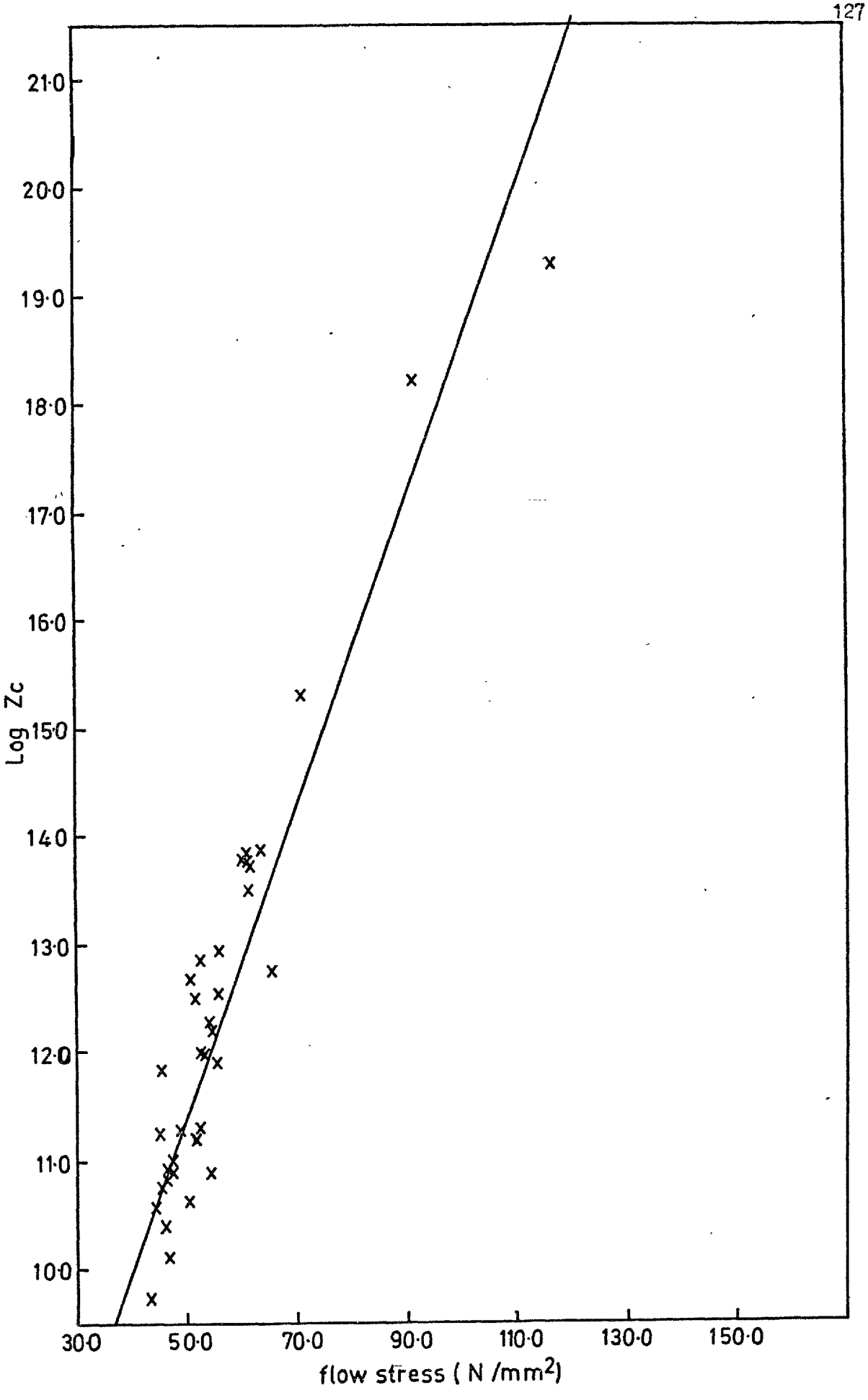


Fig. 4·16 The relationship between the corrected value of Z and the flow stress for alloy CE

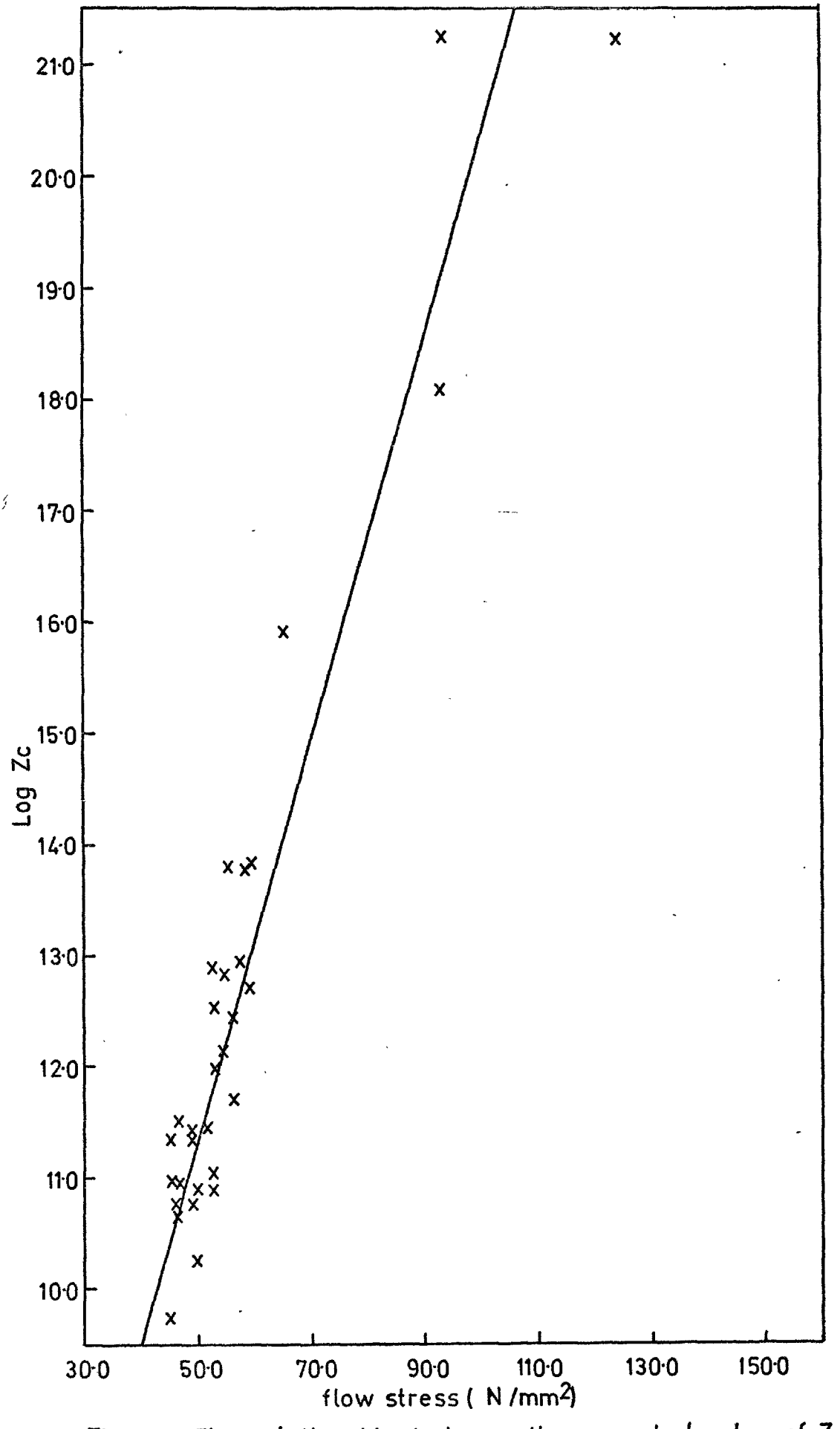


Fig. 4·17 The relationship between the corrected value of Z and the flow stress for alloy DF.

R	Correction fact : for logZ
100:1(s)	-2.1
60:1(2)	-0.75
60:1(3)	-0.50
60:1(s)	0.0
50:1(s)	1.3
50:1(2)	0.5
50:1(3)	0.5
30:1(s)	2.9
30:1(2)	1.5
30:1(3)	1.5

Table 4.I Correction factors for logZ

Alloy	A	B
	sec^{-1}	mm^2/N
272D	$1.95x10^7$	0.162
265D	$2.46x10^5$	0.334
266D	$7.36x10^5$	0.307
A	$1.68x10^5$	0.297
CE	$1.25x10^4$	0.333
B	$1.43x10^3$	0.366
DF	$1.85x10^2$	0.418

Table 4.II

To compare the extrusion results with those from the hot working tests, the corrected values of Z were used in a log Zc against log sinh$\alpha\sigma$ plot for alloys CE and DF. The values of α being those obtained from the hot torsion and tensile results. The graphs are given in figures 4.18&4.19 , where the results for the relevant hot-working tests are also given. The line representing extusion agrees with the latter in the orders of magnitude of the flow stress and strain rates, however the gradient, n in equation 1.7, is much higher. Theory dictates that the two lines should coincide. Equation 1.7 for alloys CE and DF can be written as

for alloy CE

$$Z = 6{\cdot}2 \times 10^{7} \sinh(0{\cdot}0324\sigma)^{10{\cdot}75}$$

for alloy DF

$$Z = 1{\cdot}59 \times 10^{14} \sinh(0{\cdot}0137\sigma)^{14{\cdot}20}$$

4.2 The Load at the Start of Extrusion.

The capacity of any press is limited by the peak load that occurs at the start of extrusion. The dependence of this peak load on the operating variables was studied.

4.2.1. The Dependence of the Peak Load on the Extrusion Ratio.

By extruding the same material at the same initial billet temperature and ram speed, but through dies of different reduction ratios, the dependence of the peak load on the reduction was determined for alloys CE and DF, figure 4.20 Over the range 10:1 to 100:1 a linear relationship was found. The gradient for both alloys was approximately constant but the intercept depended on the alloy. The relationships between the peak load and the reduction ratio for the two alloys can be expressed as;

for alloy CE

$$Lp = 0{\cdot}325 + 1{\cdot}725 \log R$$

for alloy DF

$$Lp = 0{\cdot}313 + 1{\cdot}65 \log R$$

Here Lp is in MN.

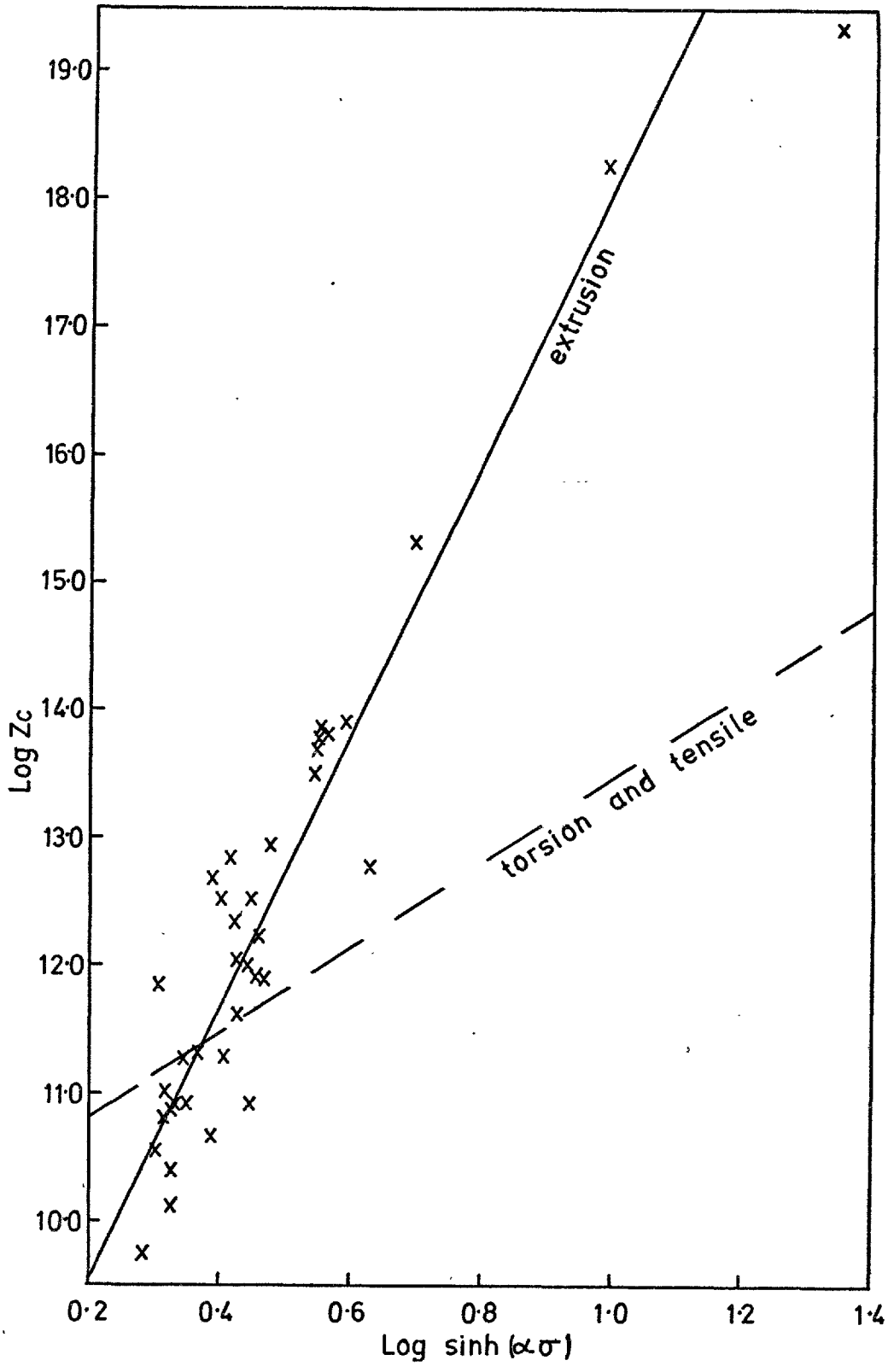


Fig. 4·18 The relationship between the corrected value of Z and sinh(ασ). Alloy CE (extrusion).

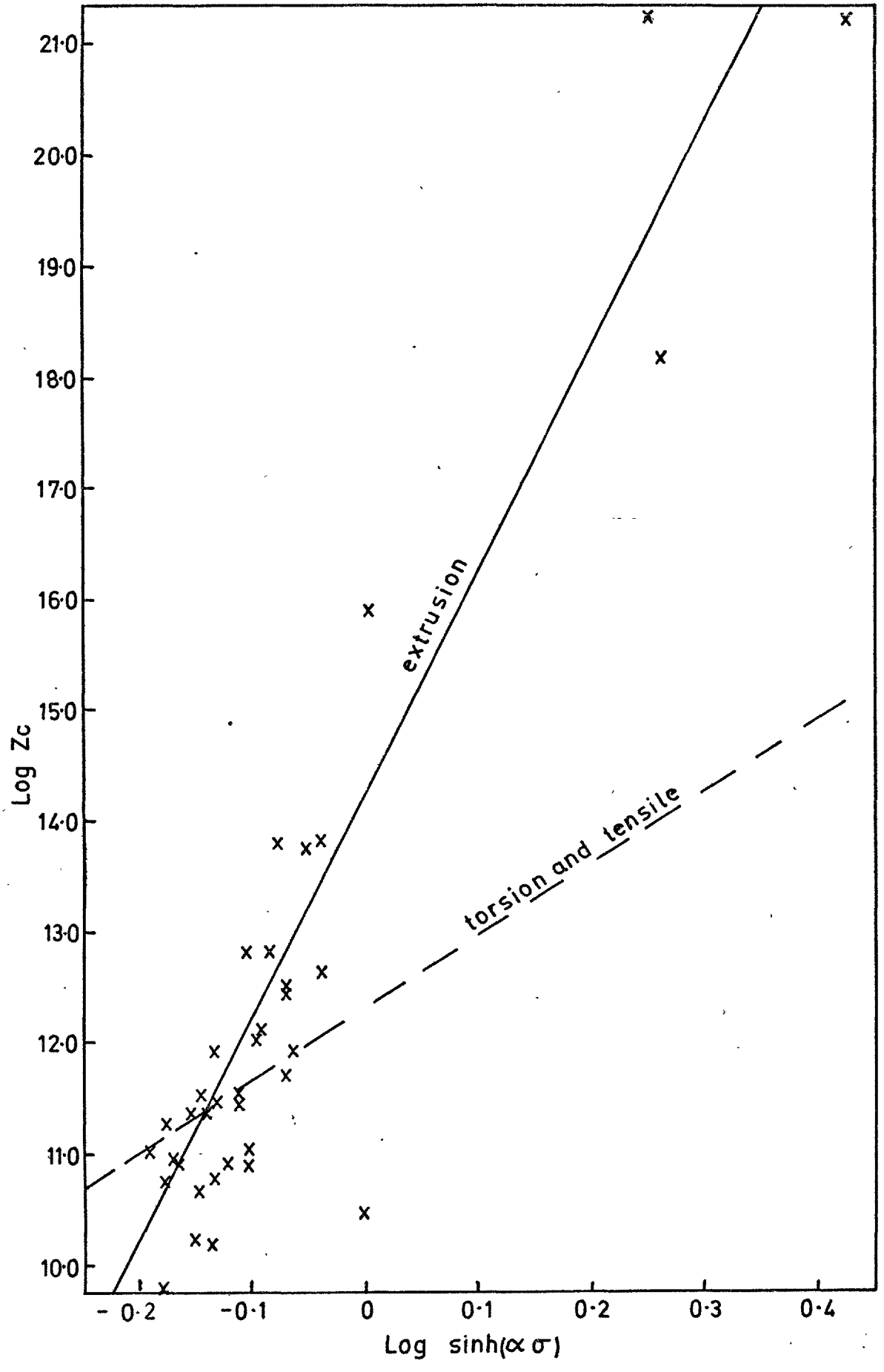


Fig.4·19 The relationship between the corrected value of Z and sinh $\alpha\sigma$. Alloy DF (extrusion).

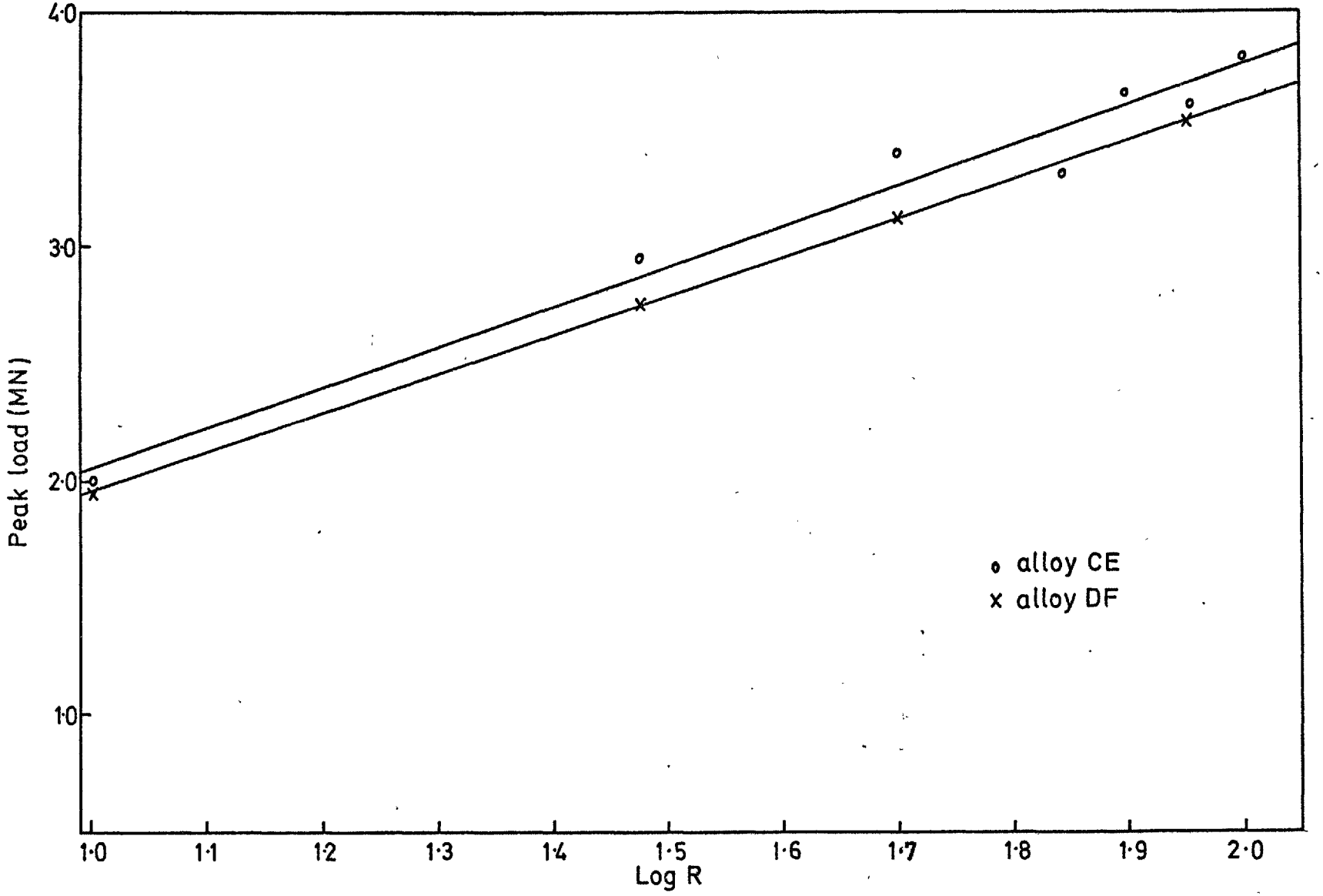


Fig. 4·20 The variation in peak load with log R.

These expressions can be rewritten in terms of the extrusion pressure
Alloy CE

$$P_p = 73{\cdot}56 + 392{\cdot}2 \log R$$

Alloy DF

$$P_p = 70{\cdot}85 + 373{\cdot}5 \log R$$

The pressure being in N/mm^2 or MN/m^2

The corresponding results for the multi-hole extrusions are not shown, but they followed a similar trend, allowing for the effect of the different eccentricities of the dies used.

4.2.2. The Effect of the Initial Billet Temperature on the Peak Load.

For a given extrusion ratio the press operator can control the initial billet temperature and the ram speed. The effect of an increase in the initial billet temperature is a reduction in the peak load, as shown in figures 4.21and4.22 . It is not possible to determine the precise nature of the relationship from these graphs, but a slight curve is indicated and this trend is followed for both single and multi-hole extrusions at different reduction ratios.

4.2.3. The Effect of a Change in the Ram Speed on the Peak Load.

Hot working theory entails an increase in the flow stress with an increase in the strain rate. In extrusion the strain rate is a function of the ram speed, consequently a change in the ram speed should have an effect on the extrusion pressure, or load. This is not seen in the peak load, figure 4.23 , if anything there is a slight decrease in the load as the ram speed increases. This is more apparent at the high speeds, over 100mm/sec, obtained with the accumulators. These latter results are not plotted for reasons given later.

4.2.4. The Effect of the Billet Length.

The results given above are for an initial billet length of 75mm. Figure 4.24 gives the peak pressures needed to extrude billets of various initial lengths. Over the range 120 to 60mm the pressure falls as l_B decreases. Below 60mm the initial pressure increases with a decrease in l_B .

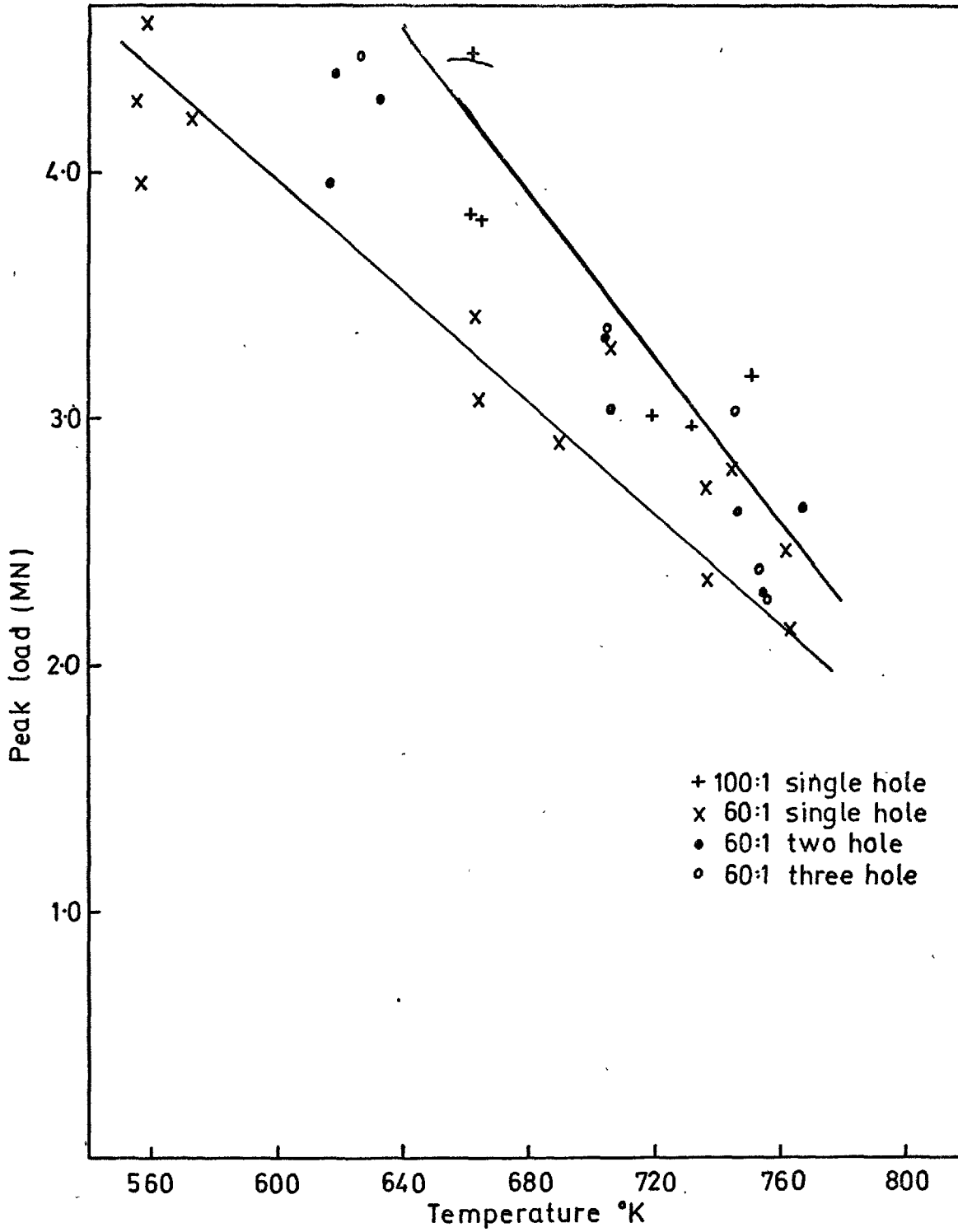


Fig. 4·21 The dependence of the peak load on the initial billet temperature. Alloy CE.

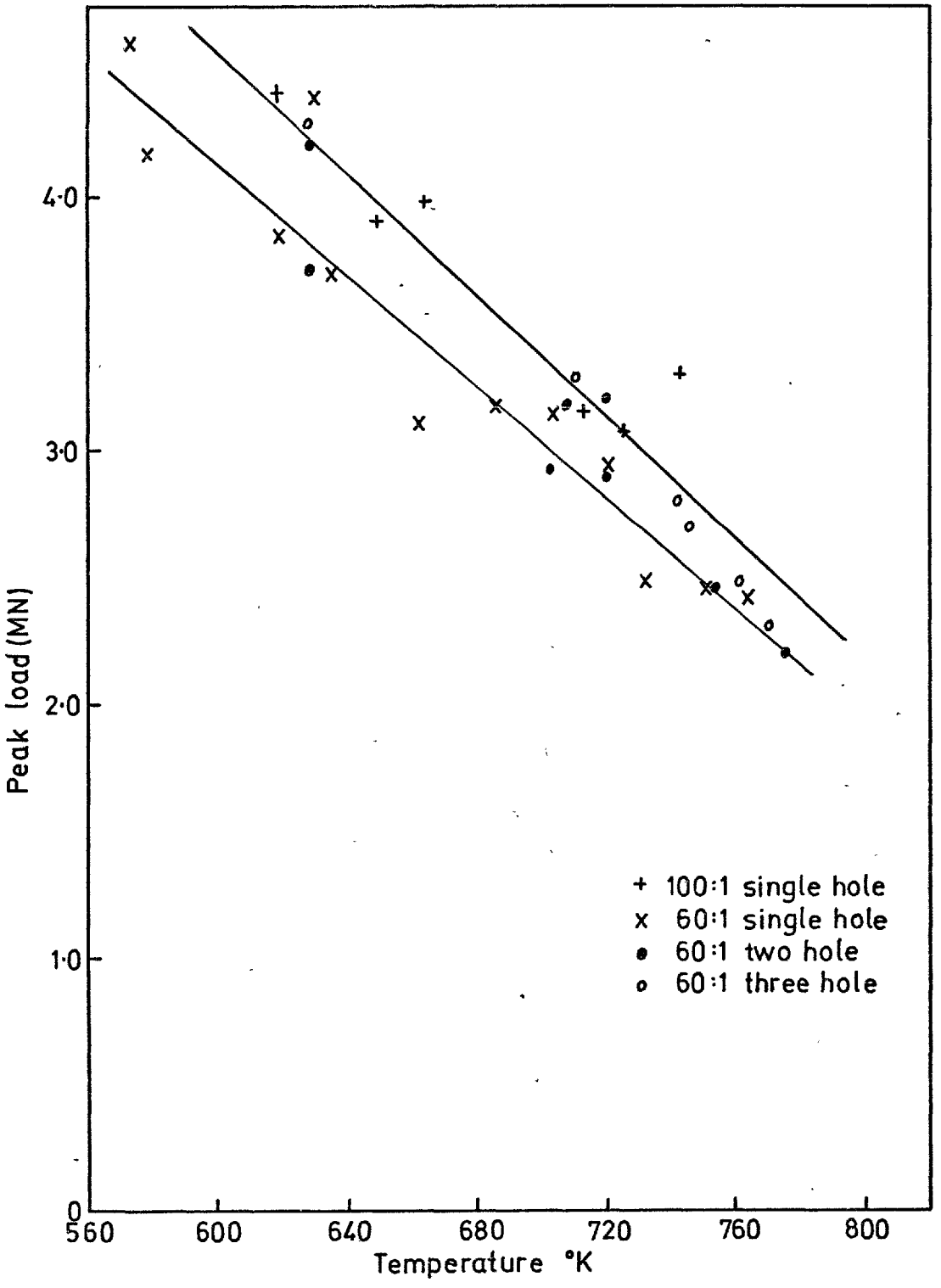


Fig. 4·22 The dependence of the peak load on the initial billet temperature. Alloy DF.

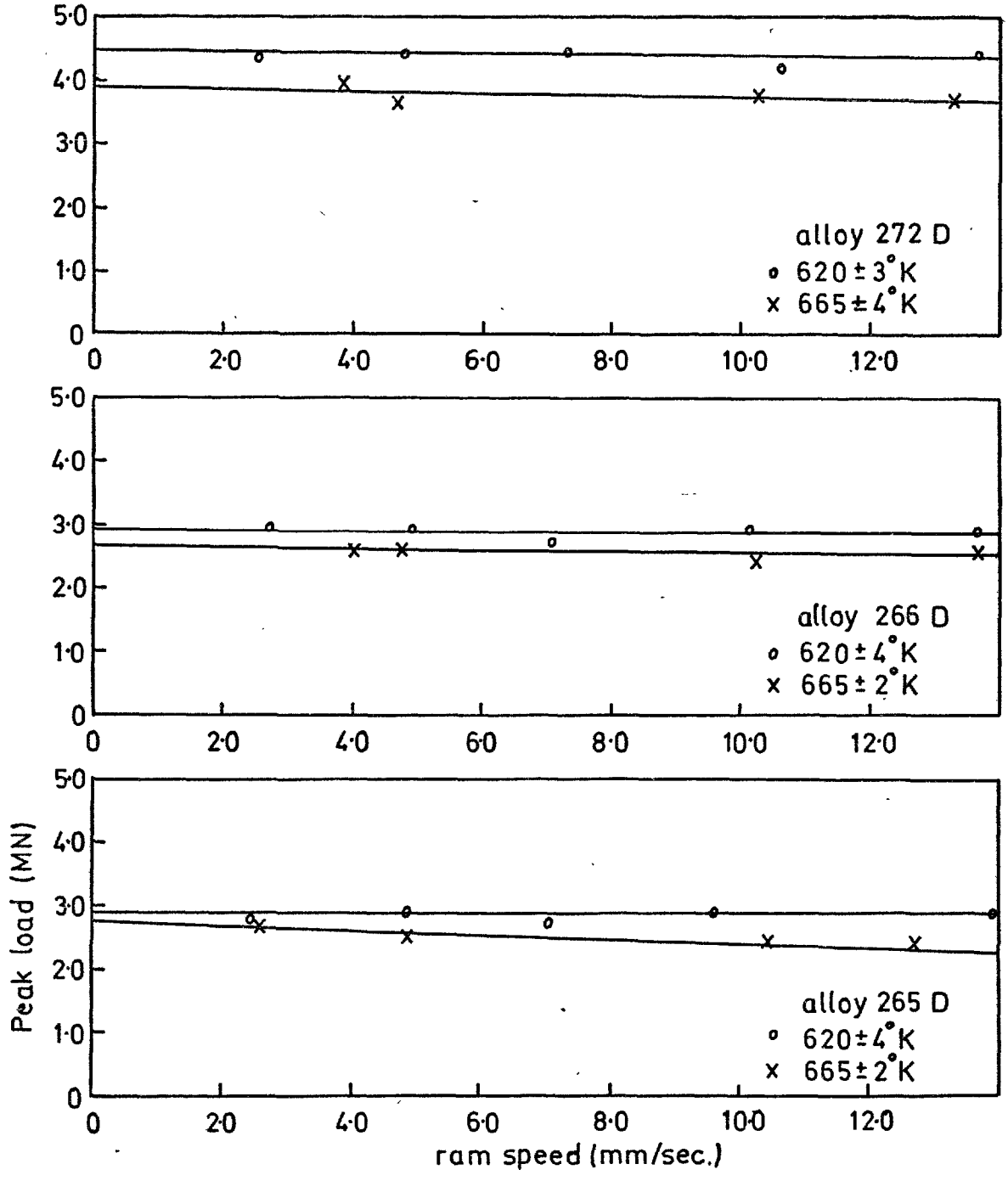


Fig. 4·23 Variation in peak load with ram speed.

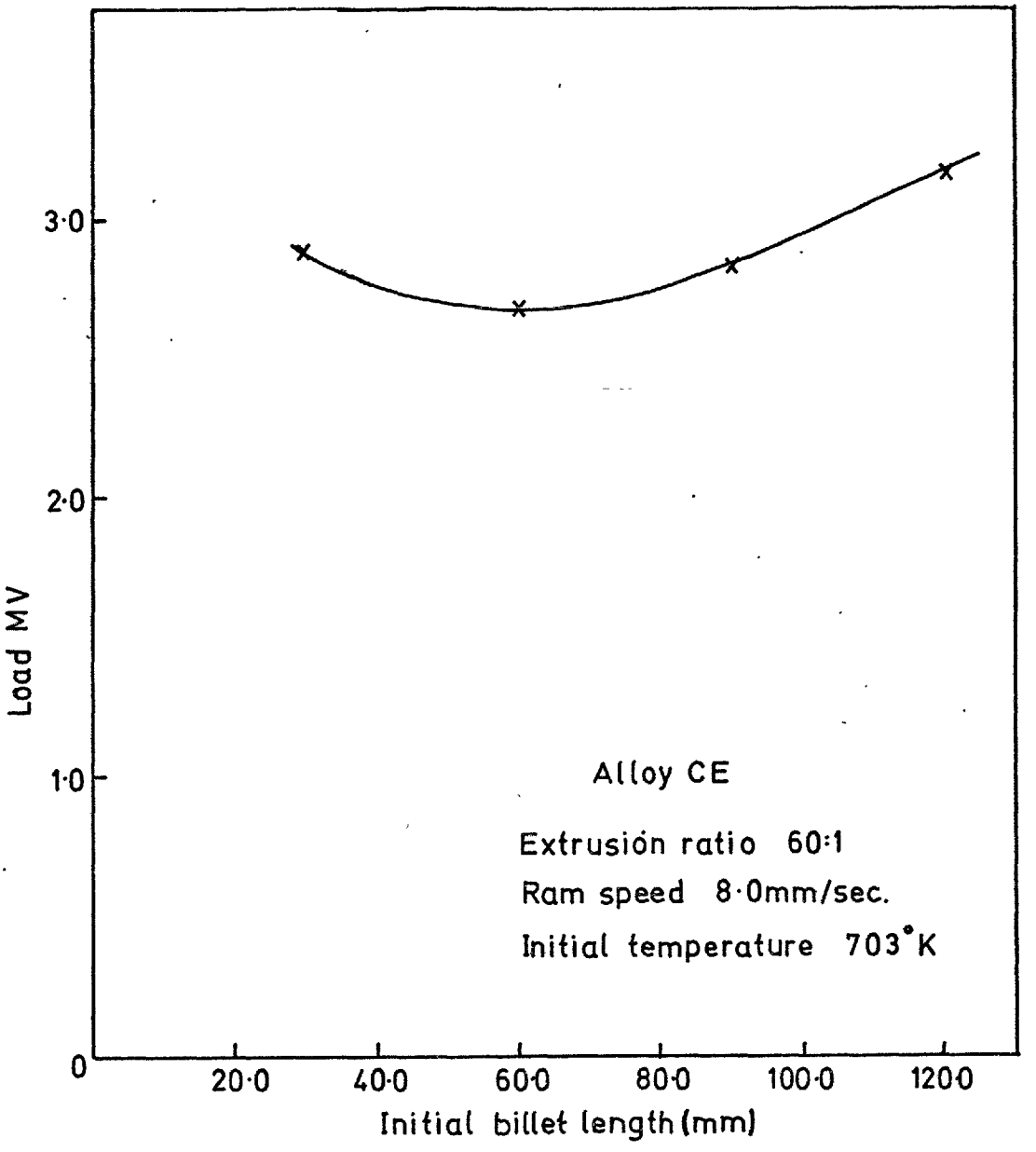


Fig.4·24 The effect of billet length on the initial load.

4.2.5. The Application of an Arrhenius Type Energy Term to the Peak Load.

If hot working theory is to be applied to the peak loads, then there should be a relationship between the temperature compensated strain rate and the flow stress, the latter being a function of the load. The strain rate to be used will be a function of the ram speed and will not be the same as that during steady state extrusion. Figure 4.23 indicates that a change in the ram speed has only a slight effect on the peak load. This does not preclude the application of a Z function, but it does mean that a value of the strain rate cannot be given. Taking the logarithm of Z

$$\log Z = \log \left(\dot{\epsilon} \exp \frac{Q}{RT}\right)$$

$$= \log \dot{\epsilon} + \frac{\exp \frac{Q}{RT}}{2{\cdot}303}$$

The results suggest that the effect of $\dot{\epsilon}$ is small, therefore a graph of the peak load against $\log \left(\exp \frac{Q}{RT}\right)$ should yield a straight line, if this type of expression can be applied. Figures 4.25 - 4.28 indicate that this is the case, within the experimental error, approximately parallel lines are obtained for the different reduction ratios used. In calculating the experimental term the temperature rise was allowed for. The gradient m of the lines depends on the alloy,

for alloy A

m - 1.30

for alloy CE

m - 0.77

for alloy B

m - 1.12

for alloy DF

m - 0.70

4.3. The Height of the Peak at the Start of Extrusion

The magnitude of the peak height was measured using the definition given in section 2.12. The values of ΔL were often very low and as a result, the errors in their measurement will be significant.

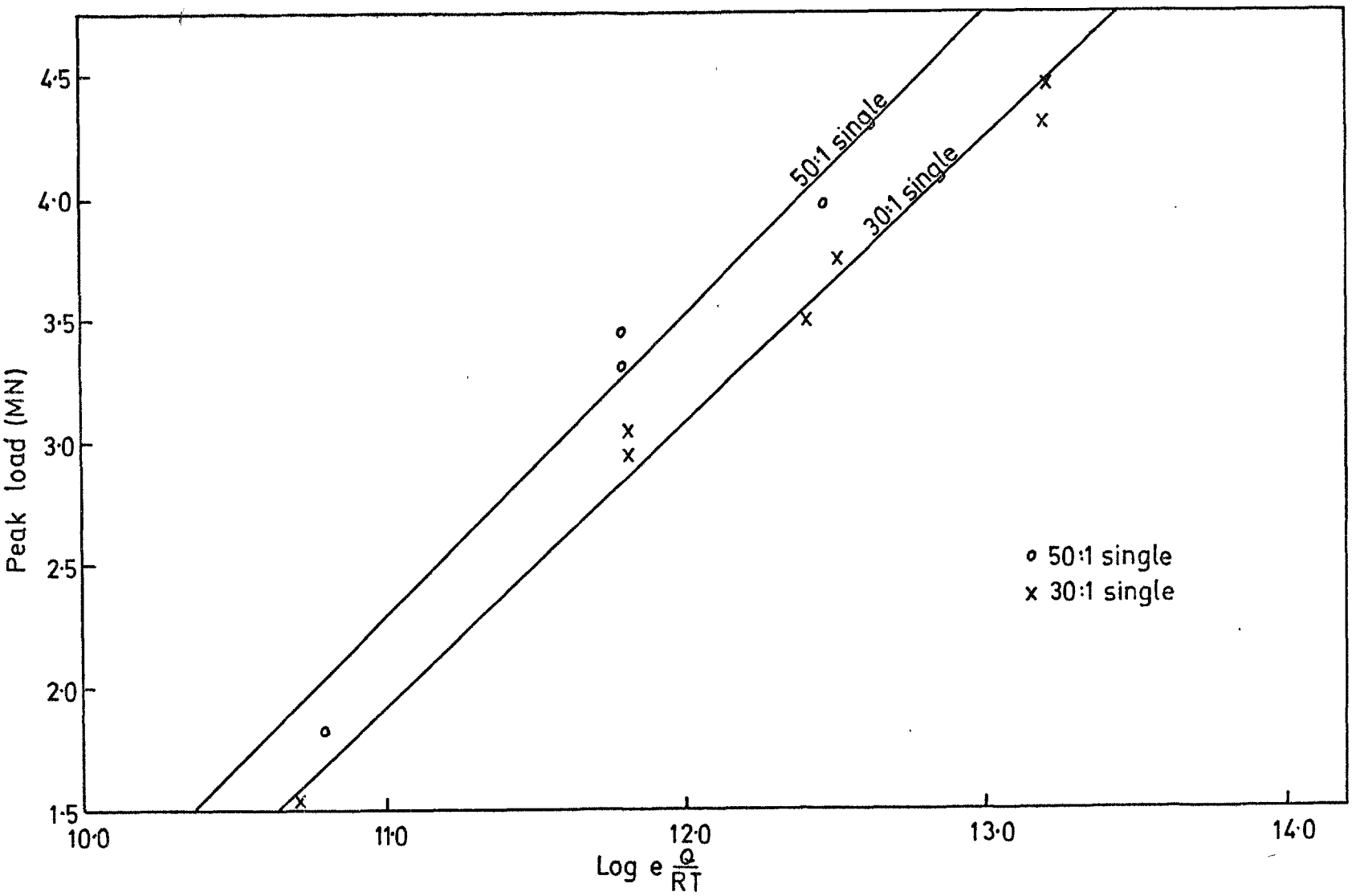


Fig.4·25 The temperature dependence of the peak load. Alloy A.

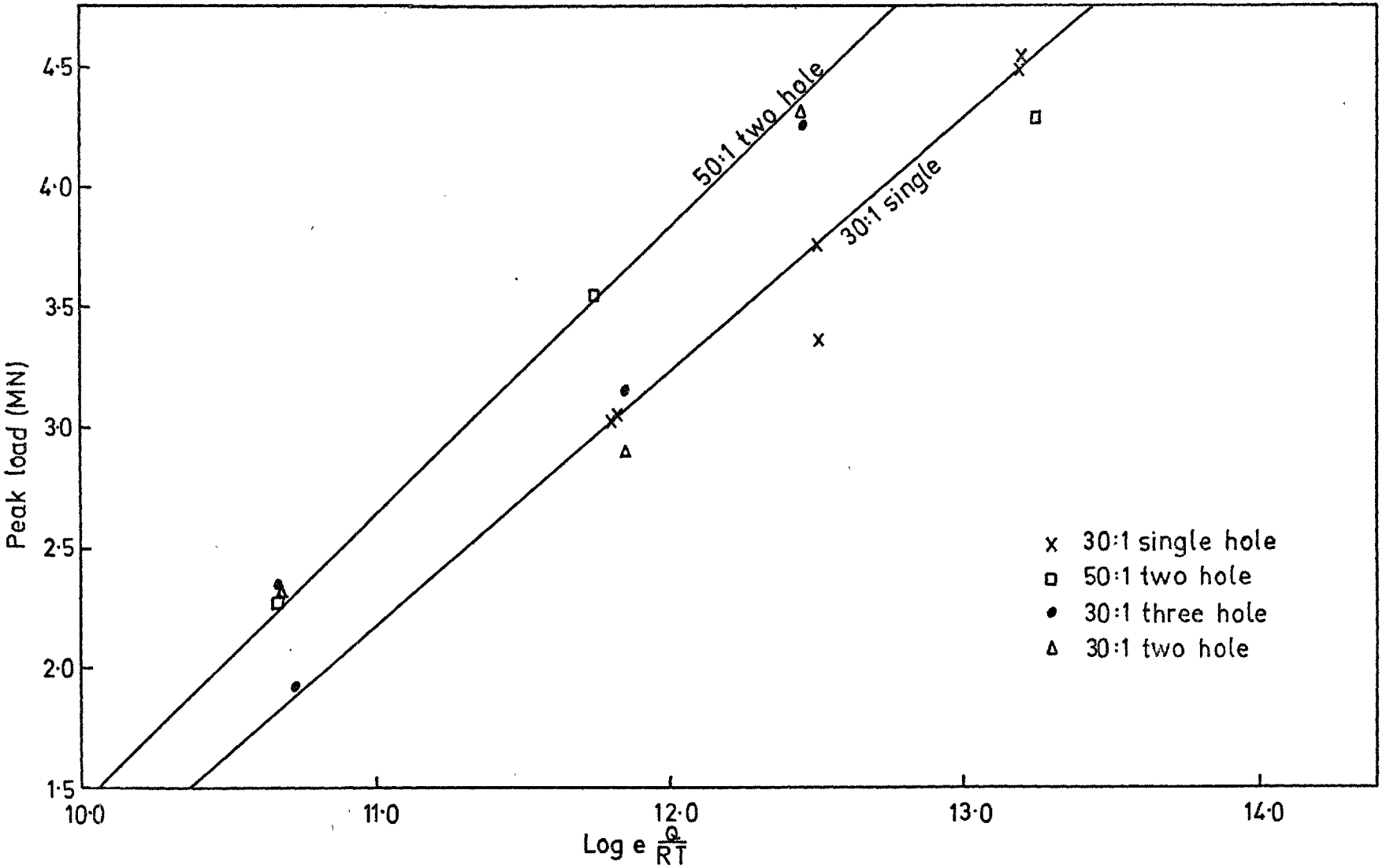


Fig.4·26 The temperature dependence of the peak load. Alloy B.

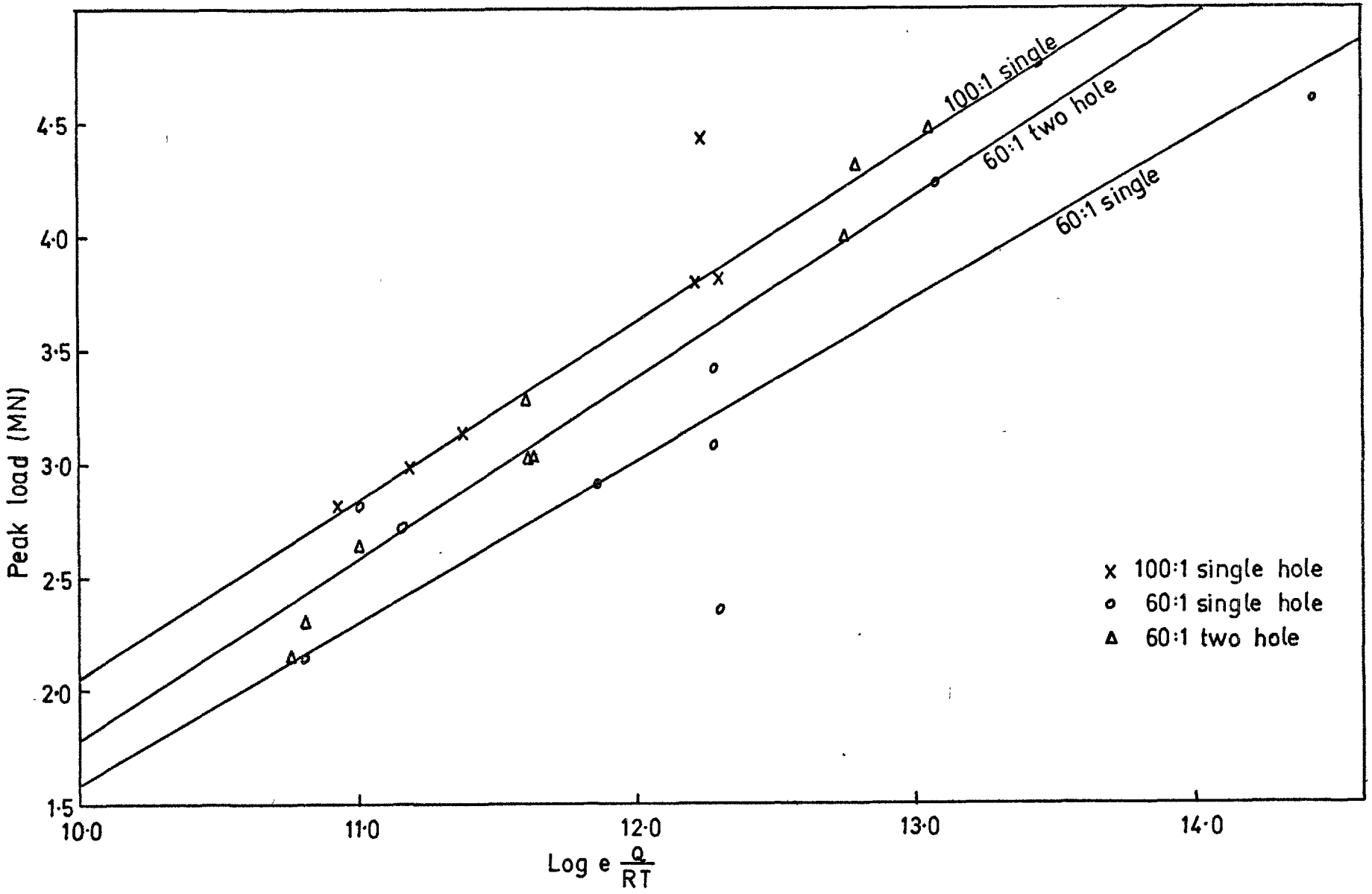


Fig.4·27 The temperature dependence of the peak load. Alloy CE.

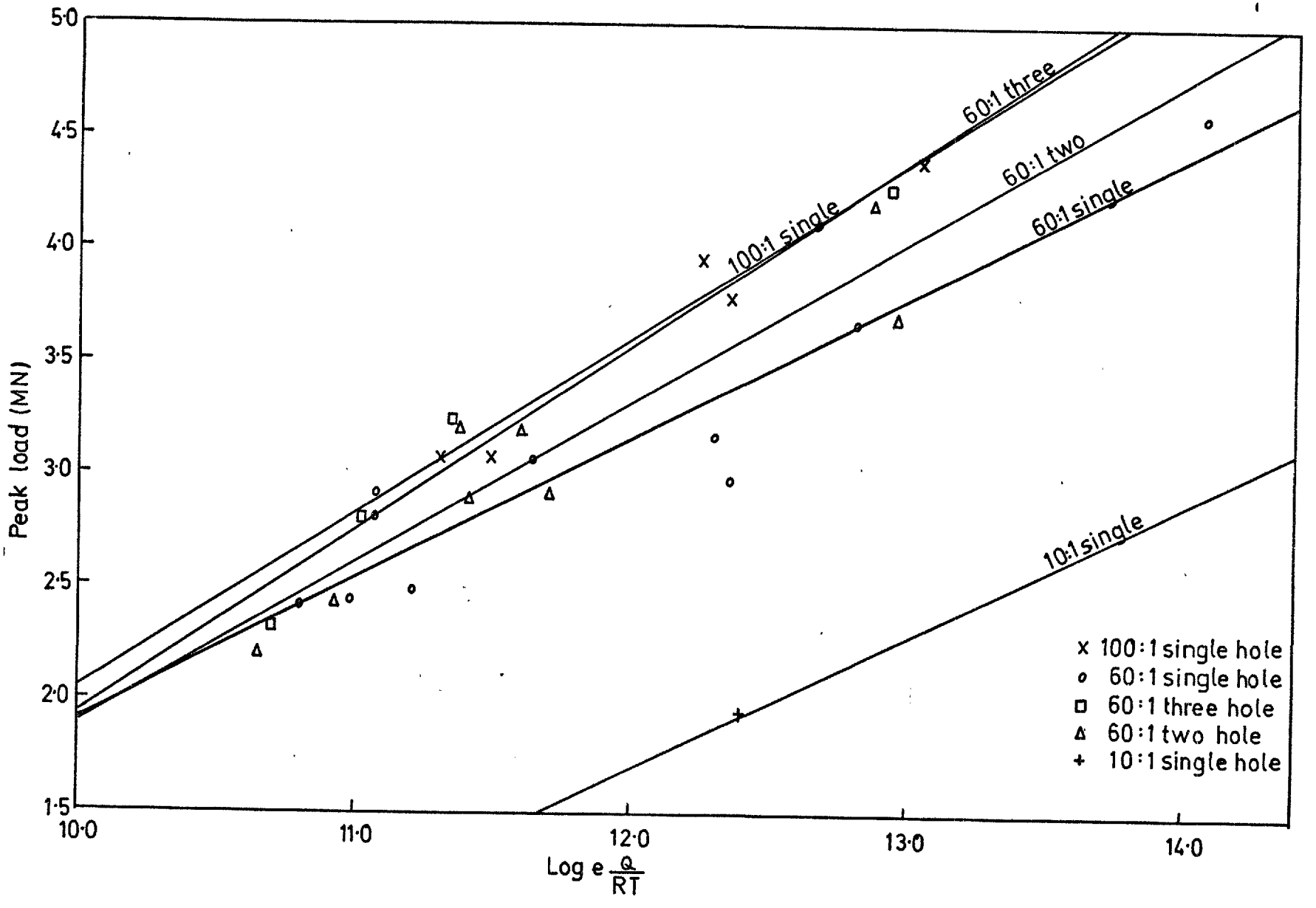


Fig.4·28 The temperature dependence of the peak load. Alloy DF.

4.3.1. The Variation in the Peak Height with the Ram Speed.

The initial load was found to be almost independent of the ram speed, over the range 2.0 to 14 mm per second. In figure 4.29 it can be seen that a similar relationship holds for the magnitude of the peak height.

4.3.2. The Effect of the Initial Billet Temperature on the Peak Height.

Again a similar dependence to that found between Lp and T was observed, figures 4.30,31 The exact nature of the relationship is masked by the experimental scatter, especially at low values of ΔL.

4.3.3. The Dependence of the Peak Height on the Peak Load.

The similarity of the relationships between ΔL and the ram speed, and initial billet temperature, with those found between Lp and the same variables suggests that there should be a correlation between the two. If ΔL is a function of the load to start extrusion then the peak load can be considered to consist of two components.

$$L_p = \Delta L + L_E$$
$$\therefore L_E = L_p - \Delta L \qquad 4.2$$

where L_E is the load required to extrude the metal if no peak was seen. It is equal to the load calculated by adding a frictional term to the deformation load. The relative magnitude of ΔL is plotted against $L_p - \Delta L$ in figures 4.32-36. A direct, almost linear correlation is indicated with the exact relationship depending on the alloy.

4.4. The Effect of Removing the Load during Extrusion.

A peak in the load displacementcurve is seen at the beginning of extrusion. To investigate whether this is peculiar to the start of the deformation or not, the load was removed midway through some extrusions. A typical load displacement curve is given in figure 4.37. After complete removal and reapplication of the

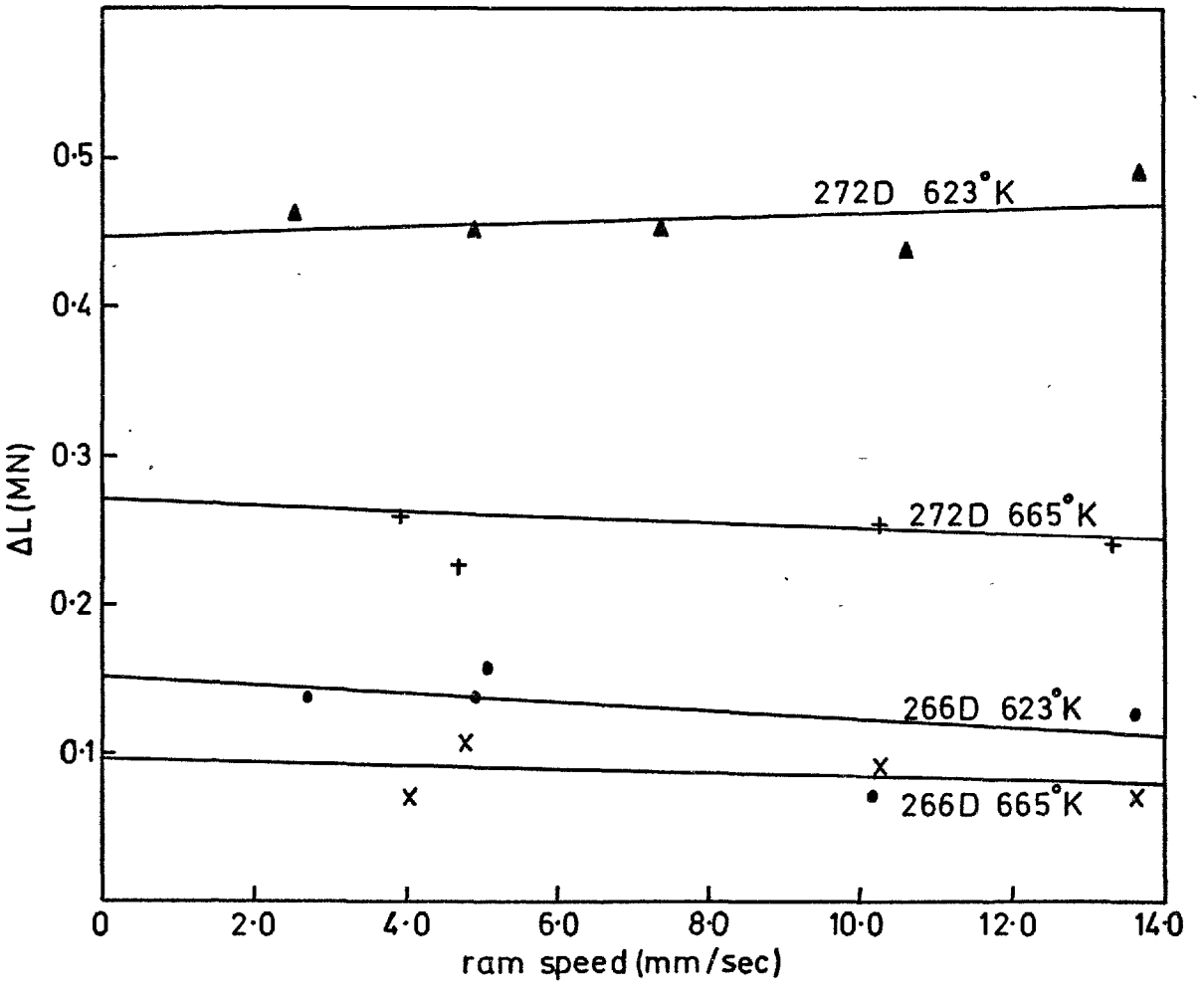


Fig.4·29 The variation of the peak height with ram speed.

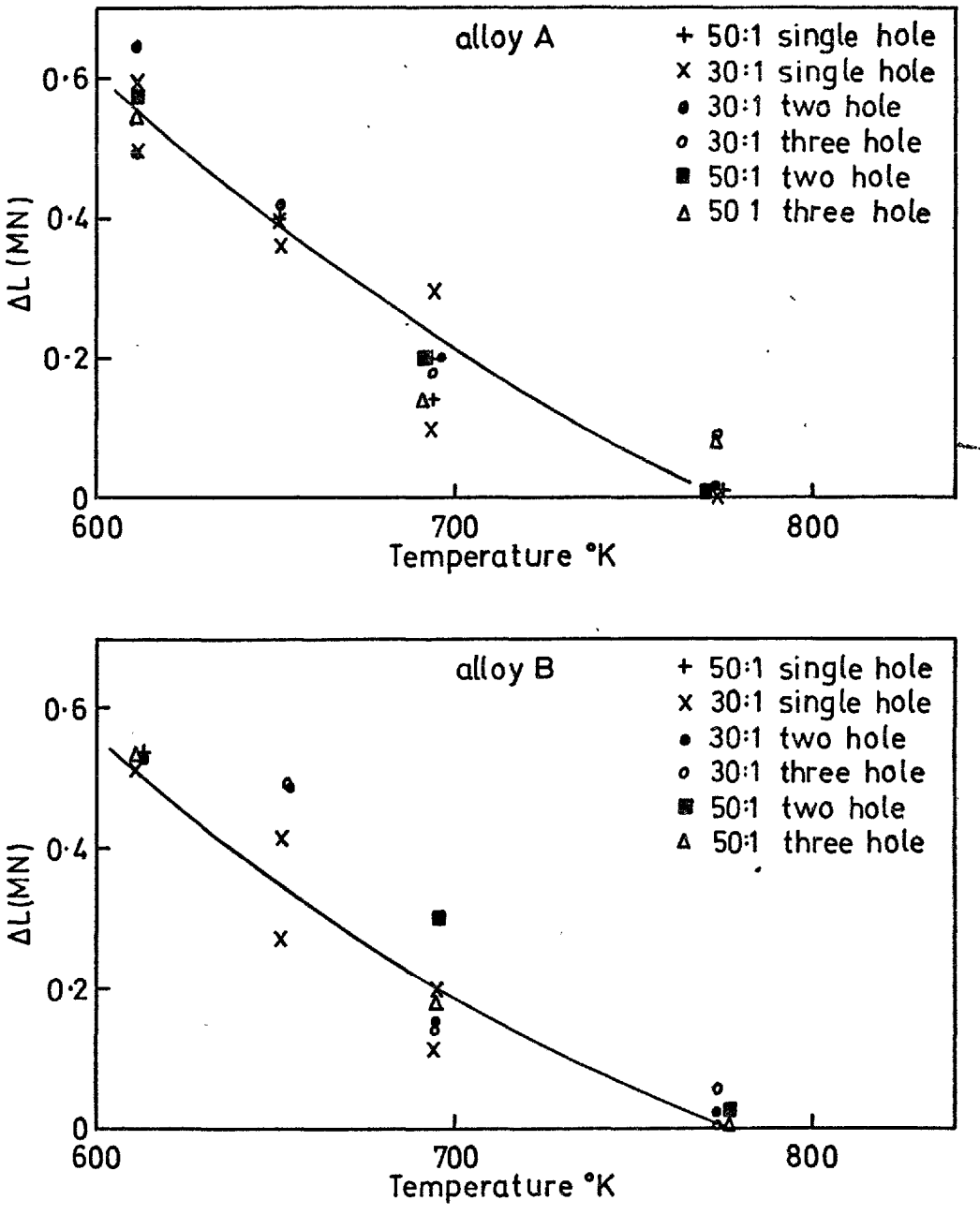
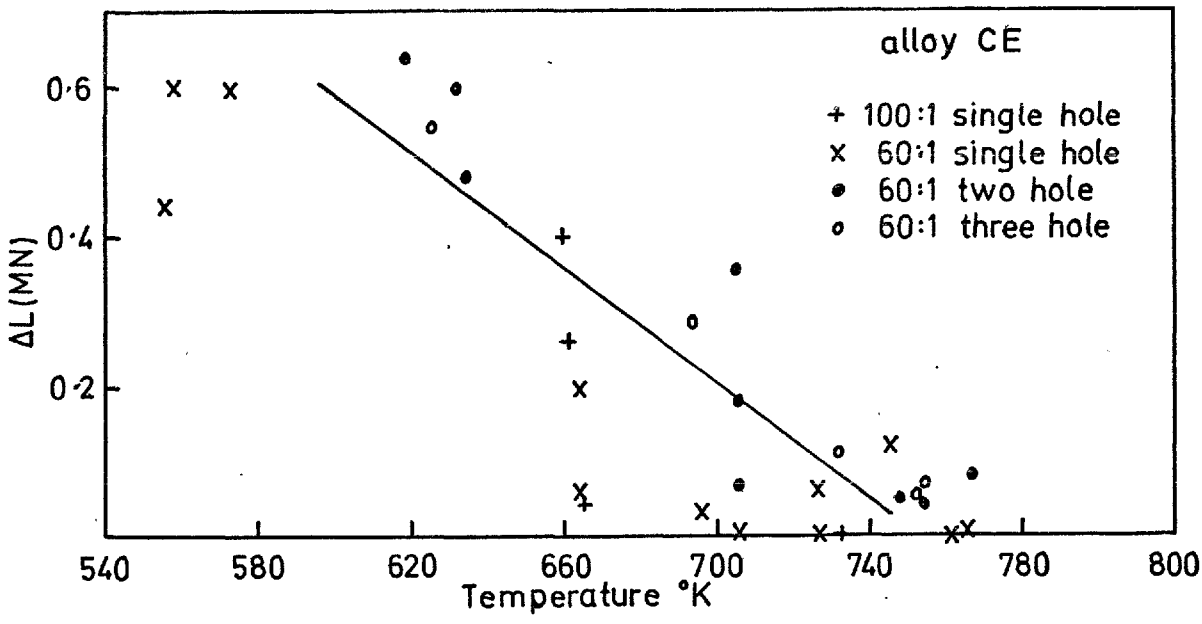


Fig.4·30 The variation of the peak height with initial billet temperature.



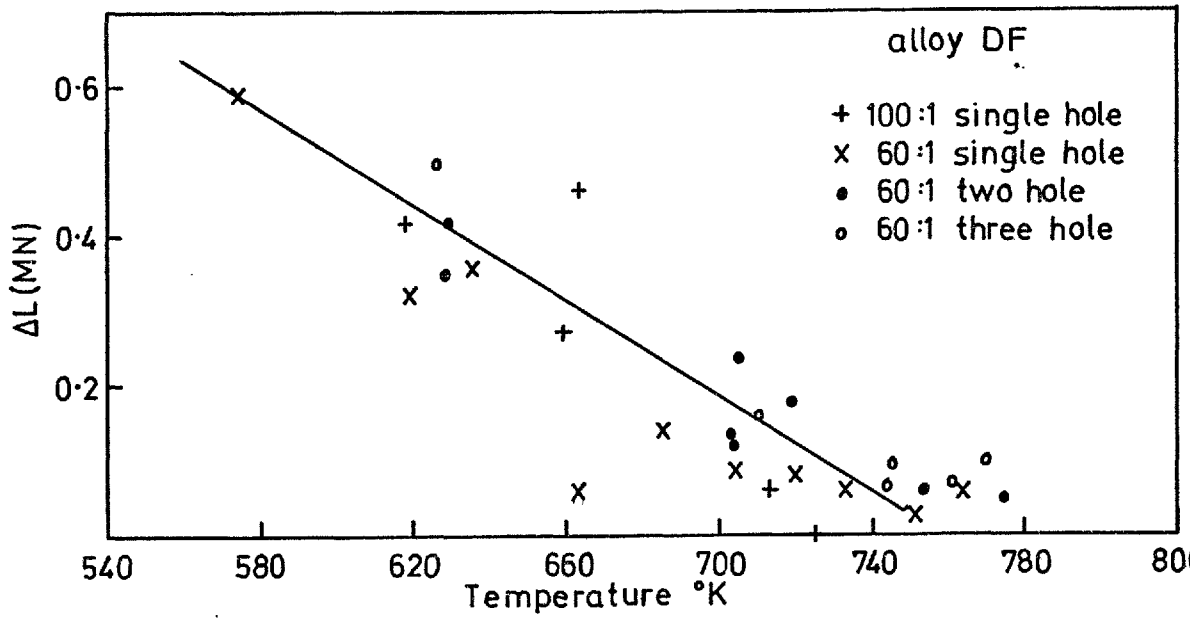


Fig.4·31 The variation of the peak height with initial billet temperature.

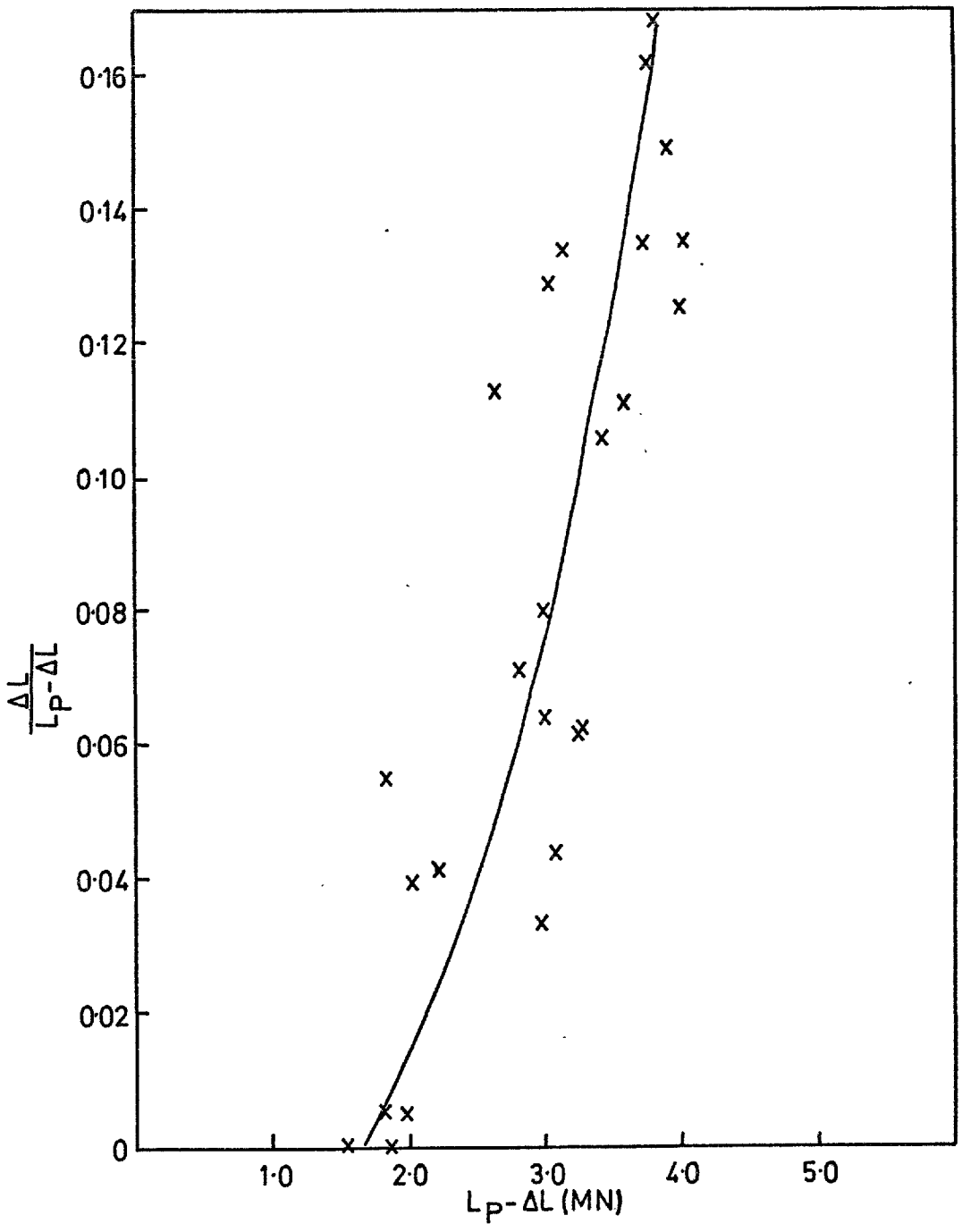


Fig. 4·32 The dependence of the peak height on the peak load. Alloy A.

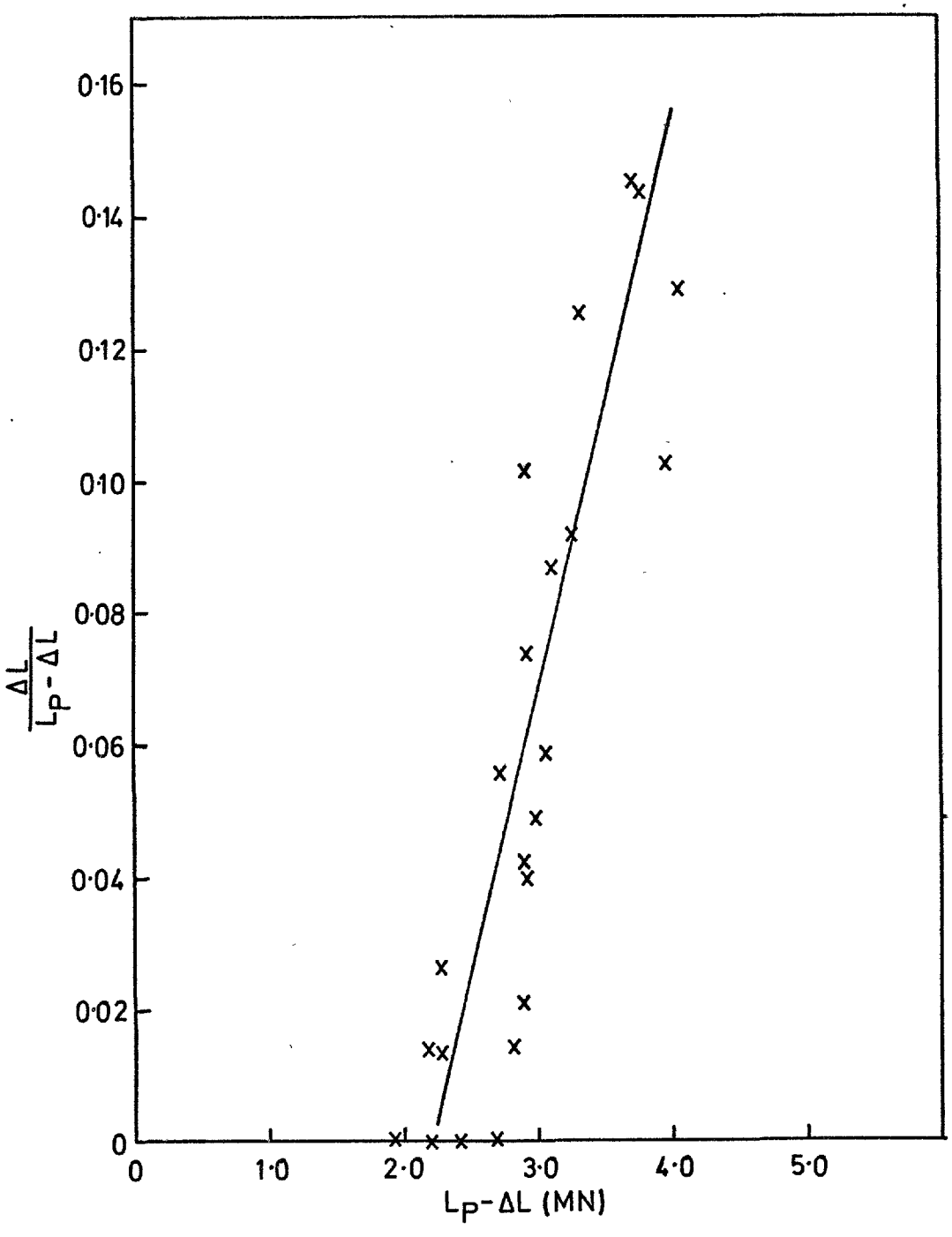


Fig. 4·33 The dependence of the peak height on the peak load. Alloy B.

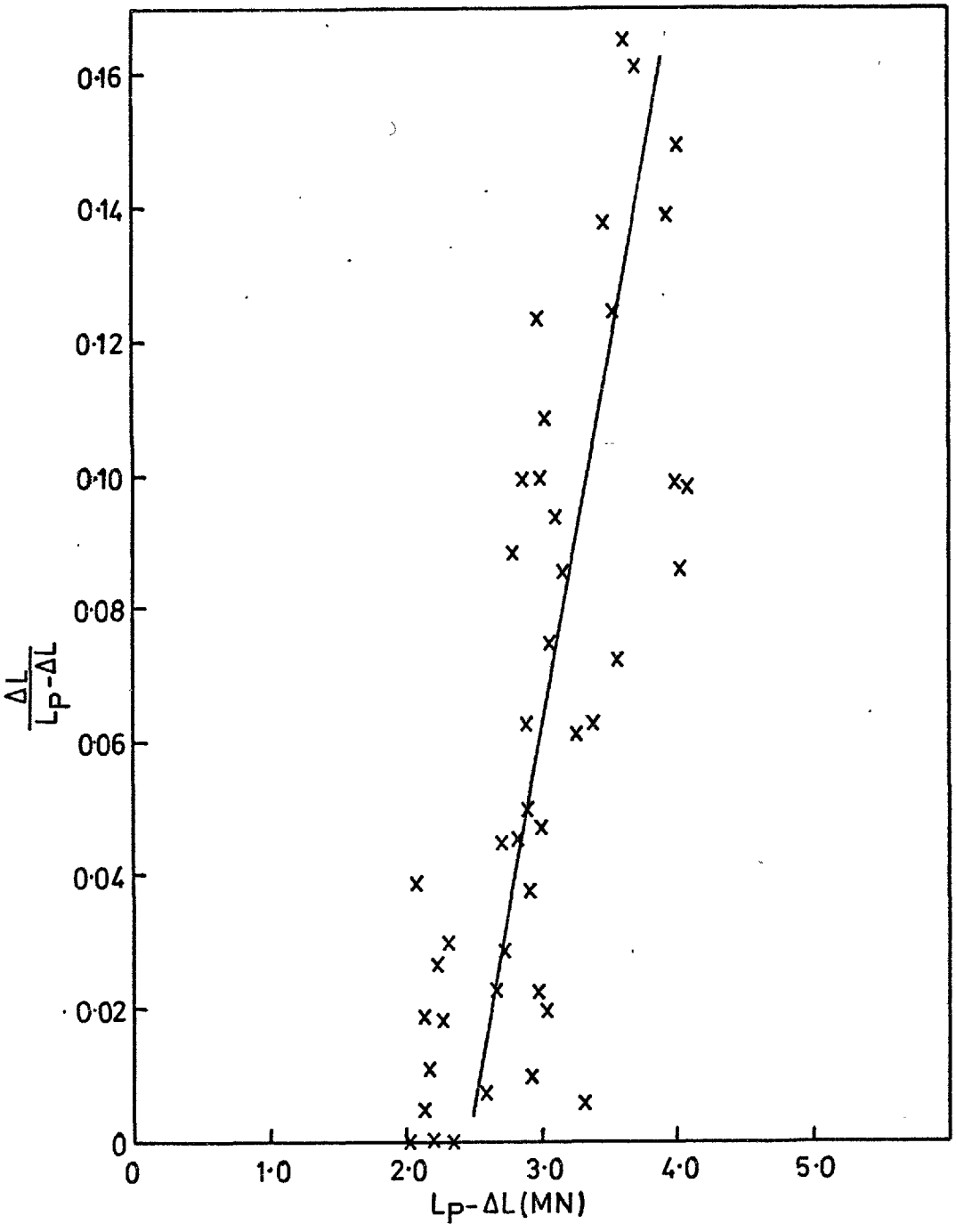


Fig.4·34 The dependence of the peak height on the peak load. Alloy CE.

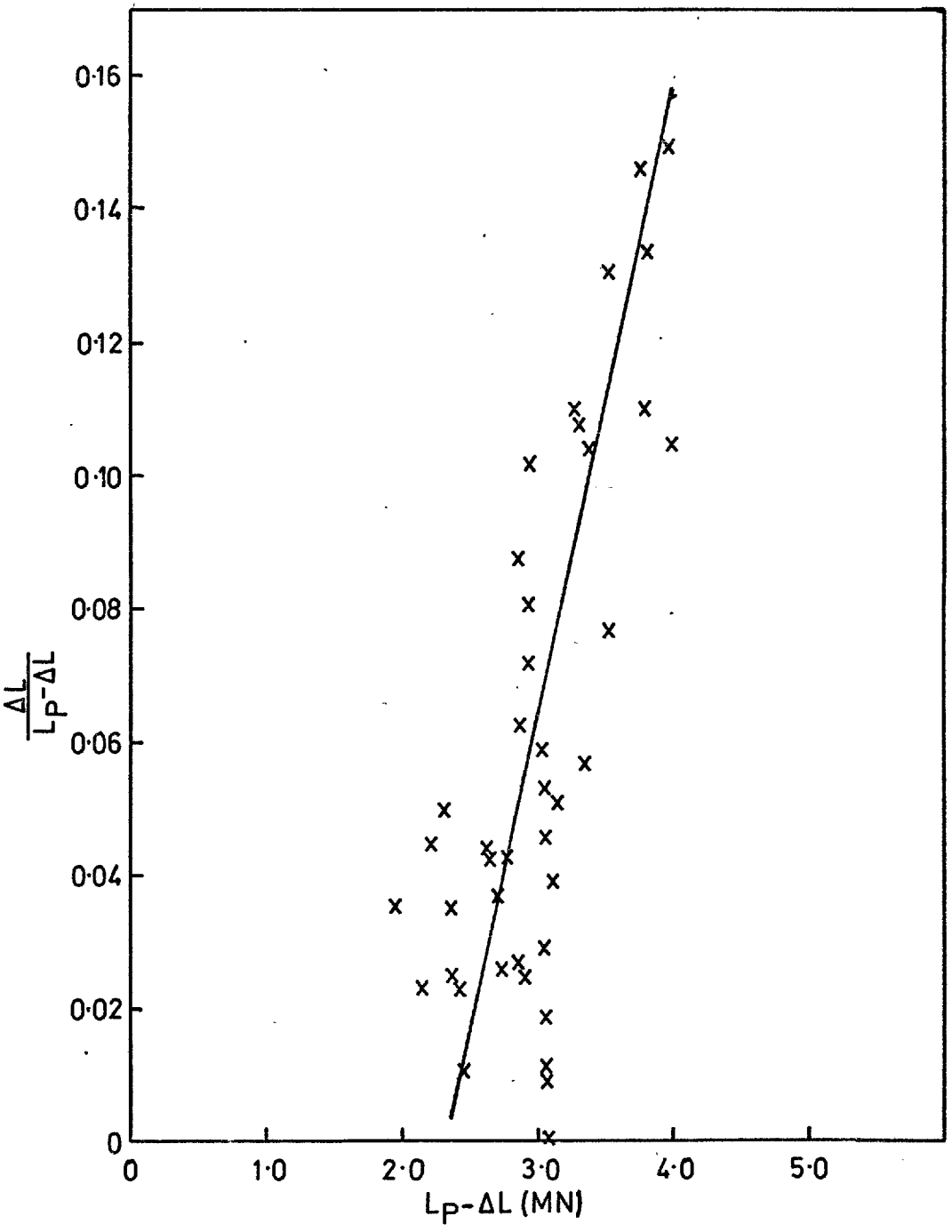


Fig. 4·35 The dependence of the peak height on the peak load. Alloy DF.

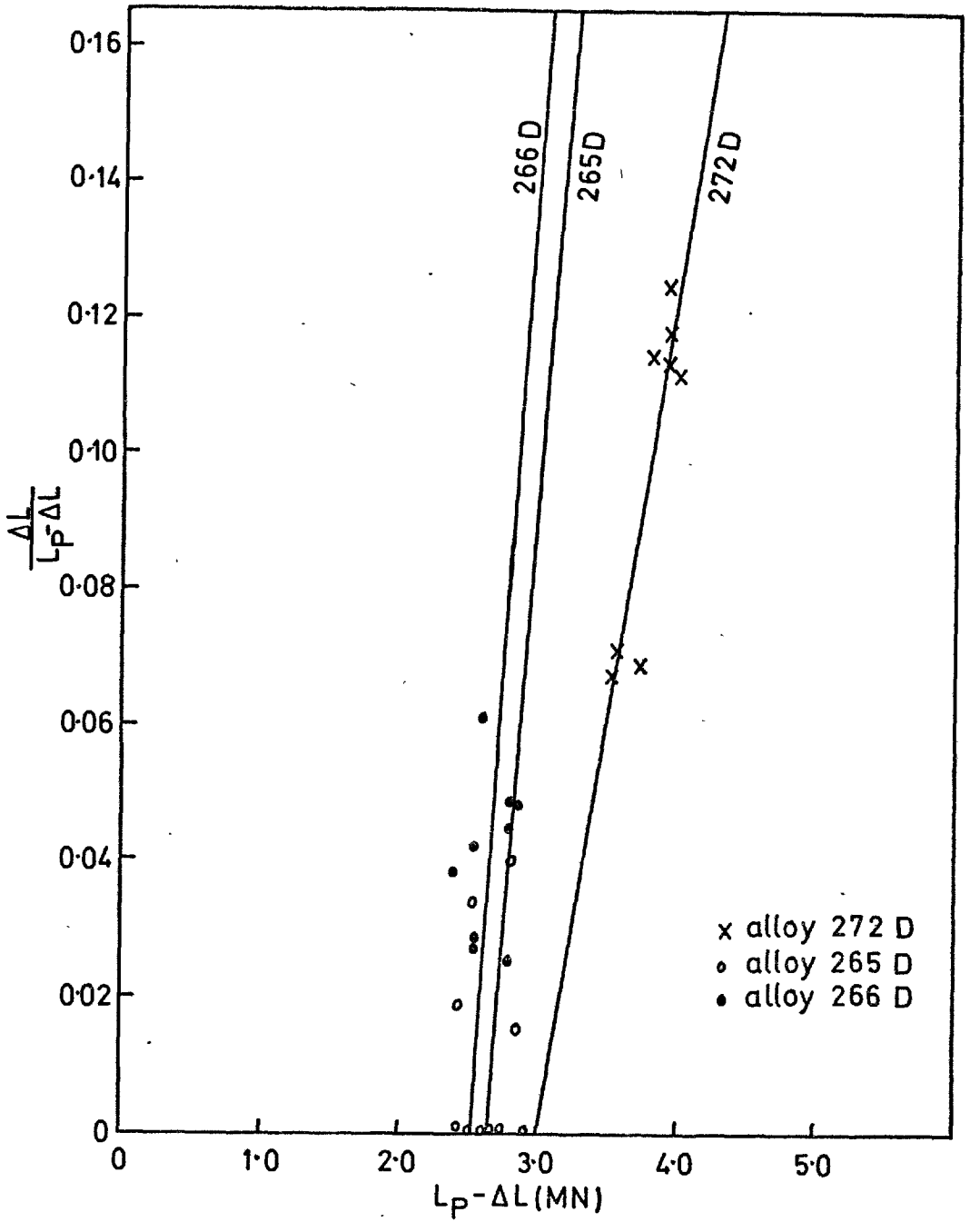


Fig. 4·36 The dependence of the peak height on the peak load for alloys 265D, 266D, and 272D.

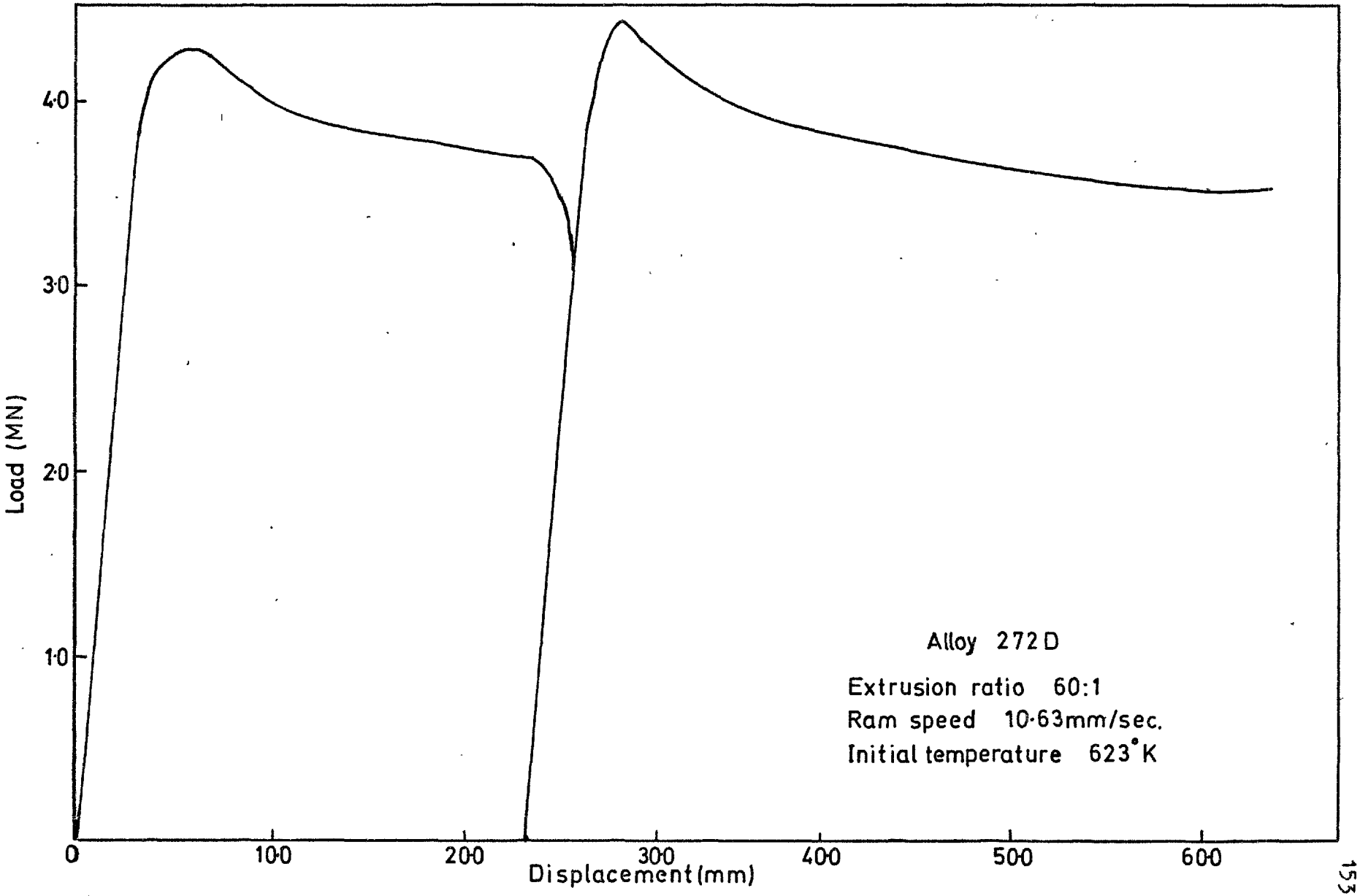


Fig.4·37 The effect of removing the load during extrusion.

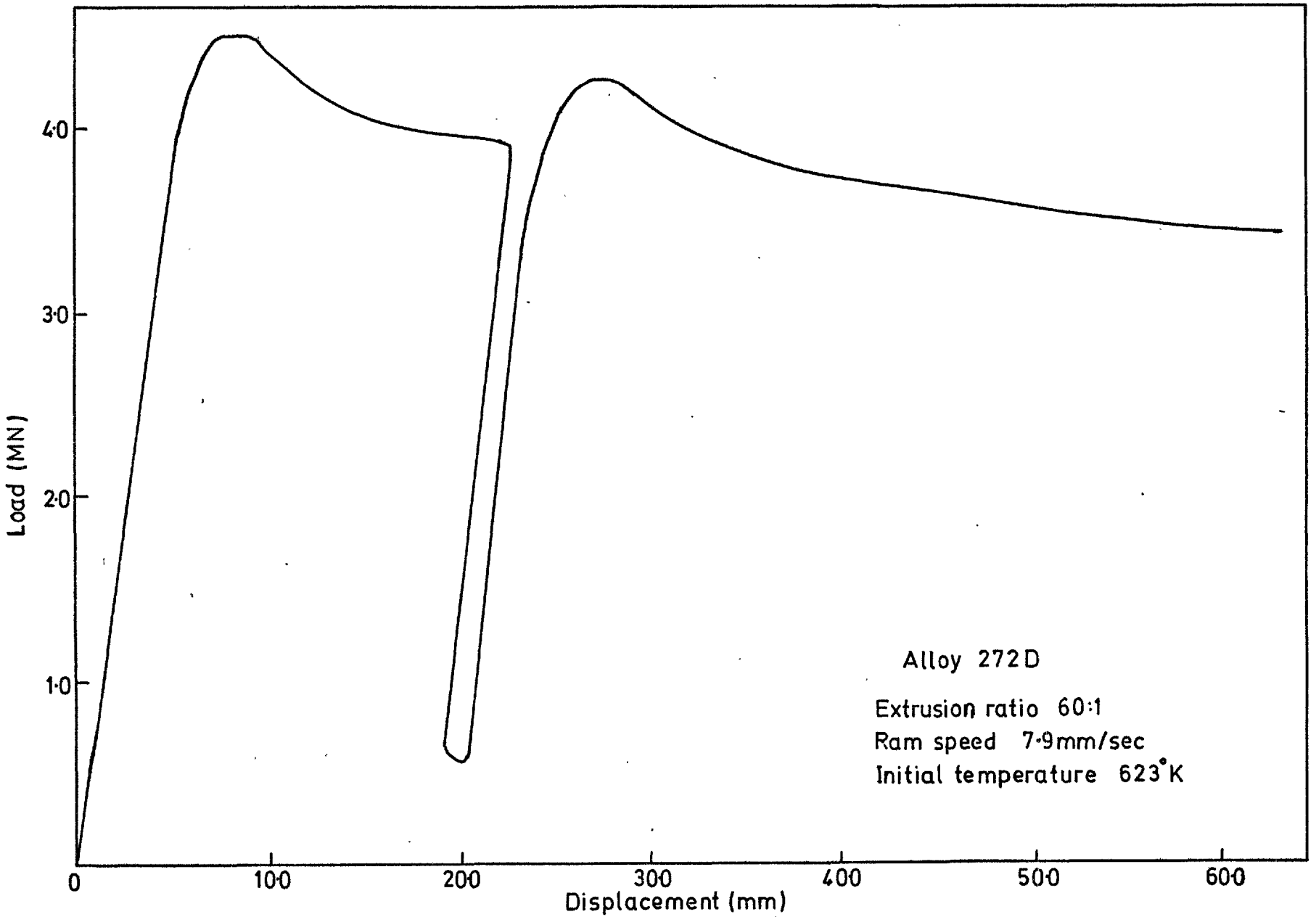


Fig. 4·38 The effect of partial removal of the load during extrusion.

load it does not return to its original position, instead another peak is seen, its magnitude being greater than the original one. This was observed in every experiment which incorporated complete load removal. In other experiments the load was only partly removed, a typical load displacement curve is given in figure 4.38 . In this case only a slight peak was seen, its magnitude being lower than the initial one.

4.5. The Effect of Section Shape on the Load.

Different shapes were extruded at the same reduction ratio, initial billet temperature, and ram speed. The load time curves are given in figure 4.39 . The peak load, and the height of the peak depend on the shape being extruded. It is highest for the three hole extrusion and least for the square hole. The loads at the end of the extrusion showed similar differences, although the effect of the temperature rise has to be remembered. In all cases the bearing length of the die was kept constant.

4.6 The General Nature of the Load Displacement Curve.

In figure 4.40 , schematic load displacement curves are drawn. These show the four types of curve seen. In the first, T_1 , the text book curve is seen. A peak load is followed by a linear decrease as the length of the billet decreases. At the end of extrusion an increase in the load occurs. At higher temperatures, T_2 a peak load is still seen but no decrease in the load occurs during extrusion. The third diagram shows the curve seen at the highest temperatures used. The load increased continously throughout the extrusion and only a very slight peak was seen. The load displacement curve for an accumulator run did not follow any of these typical curves.

4.7 The Relationship Between the Mechanical Properties and the Flow Stress.

The tensile strengths and proof stresses of the as extruded rods are plotted against the calculated flow stress in figures 4.41 -4.44. Also shown are the ranges over which the different structures, discussed later, were found. The mechanical properties were highest at the lower flow stresses, where the recrystallized structure occurred,

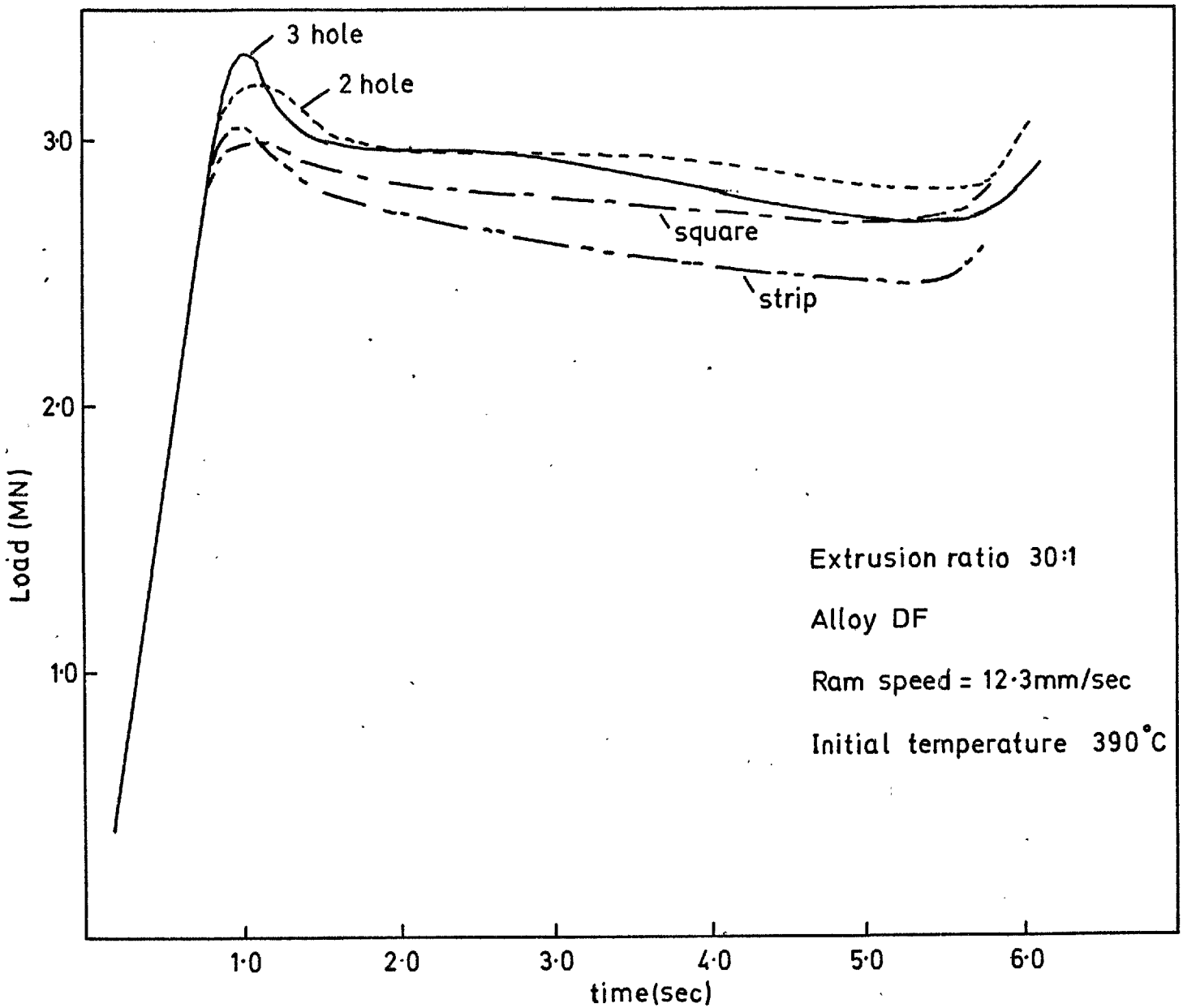


Fig.4·39 The effect of the section shape on the extrusion load.

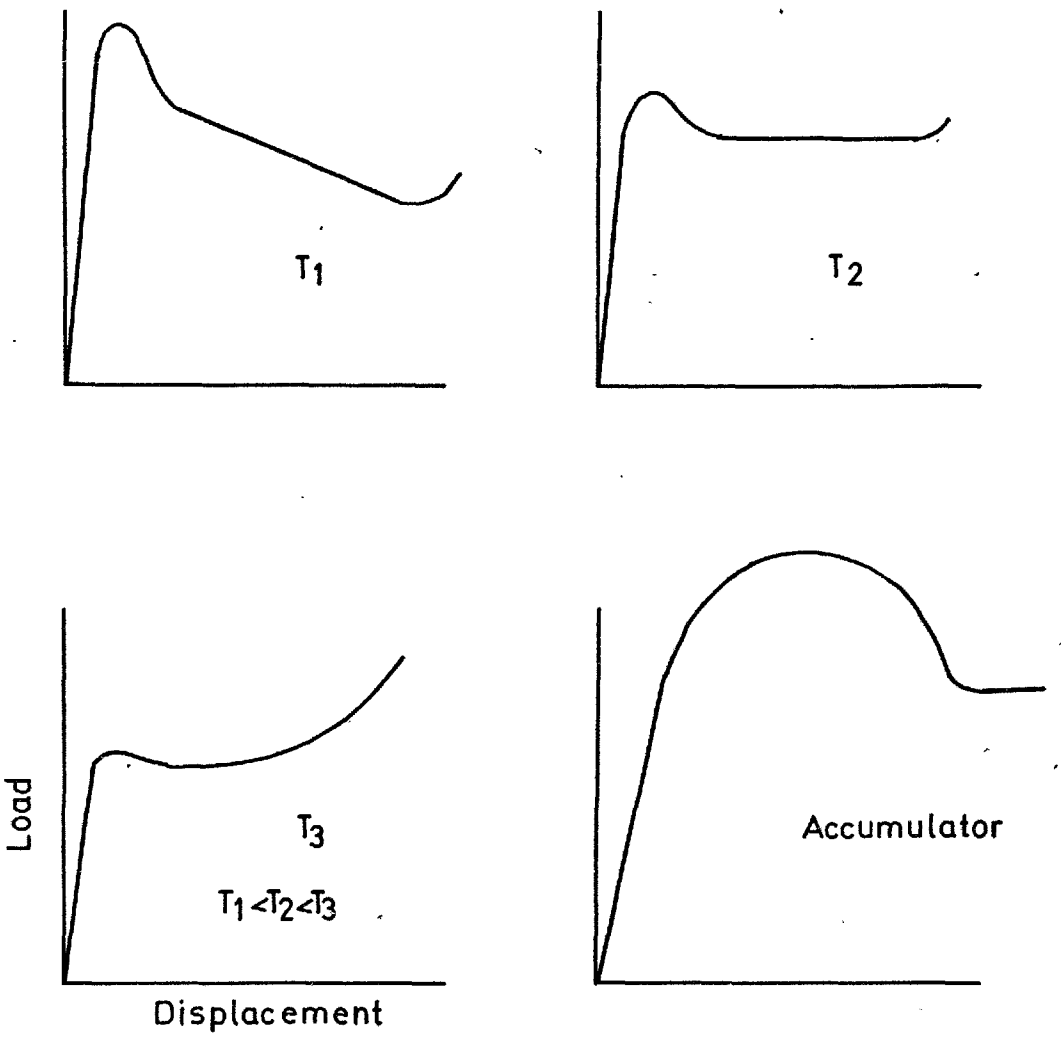


Fig.4·40 Schematic load displacement curves.

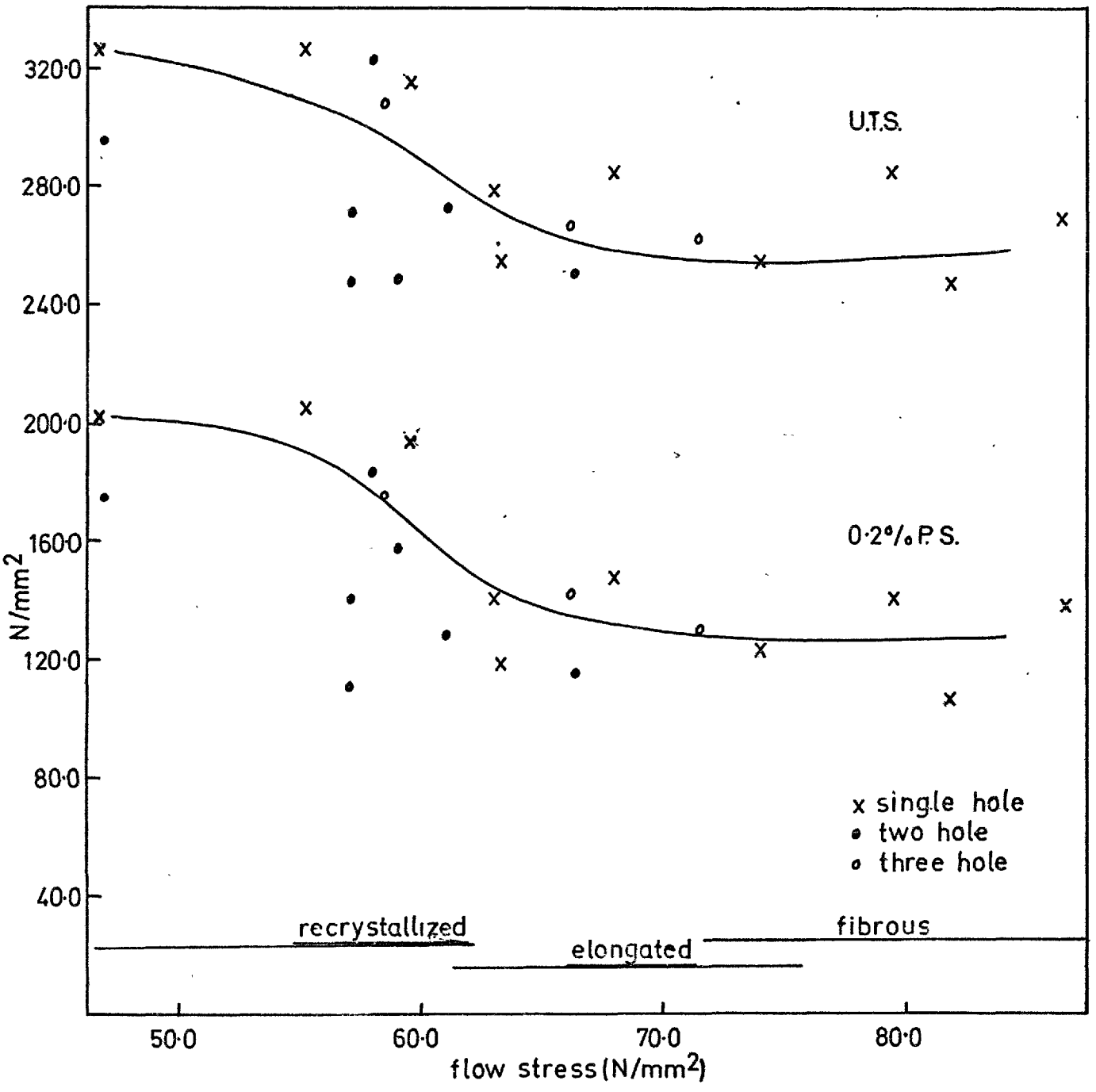


Fig.4·41 The relationship between the mechanical properties, structure, and flow stress. Alloy A.

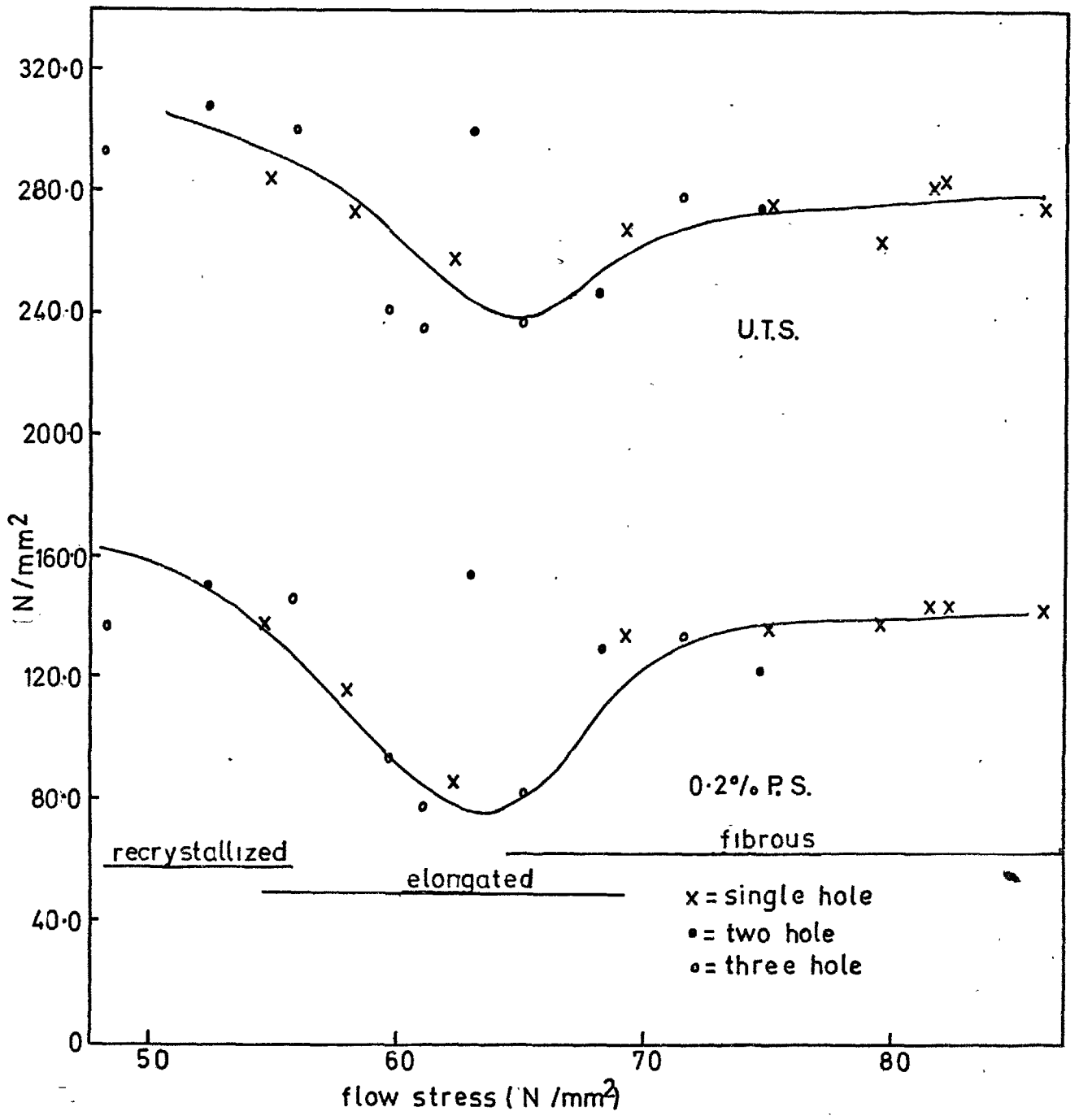


Fig. 442 The relationship between the mechanical properties, structure, and flow stress. Alloy B.

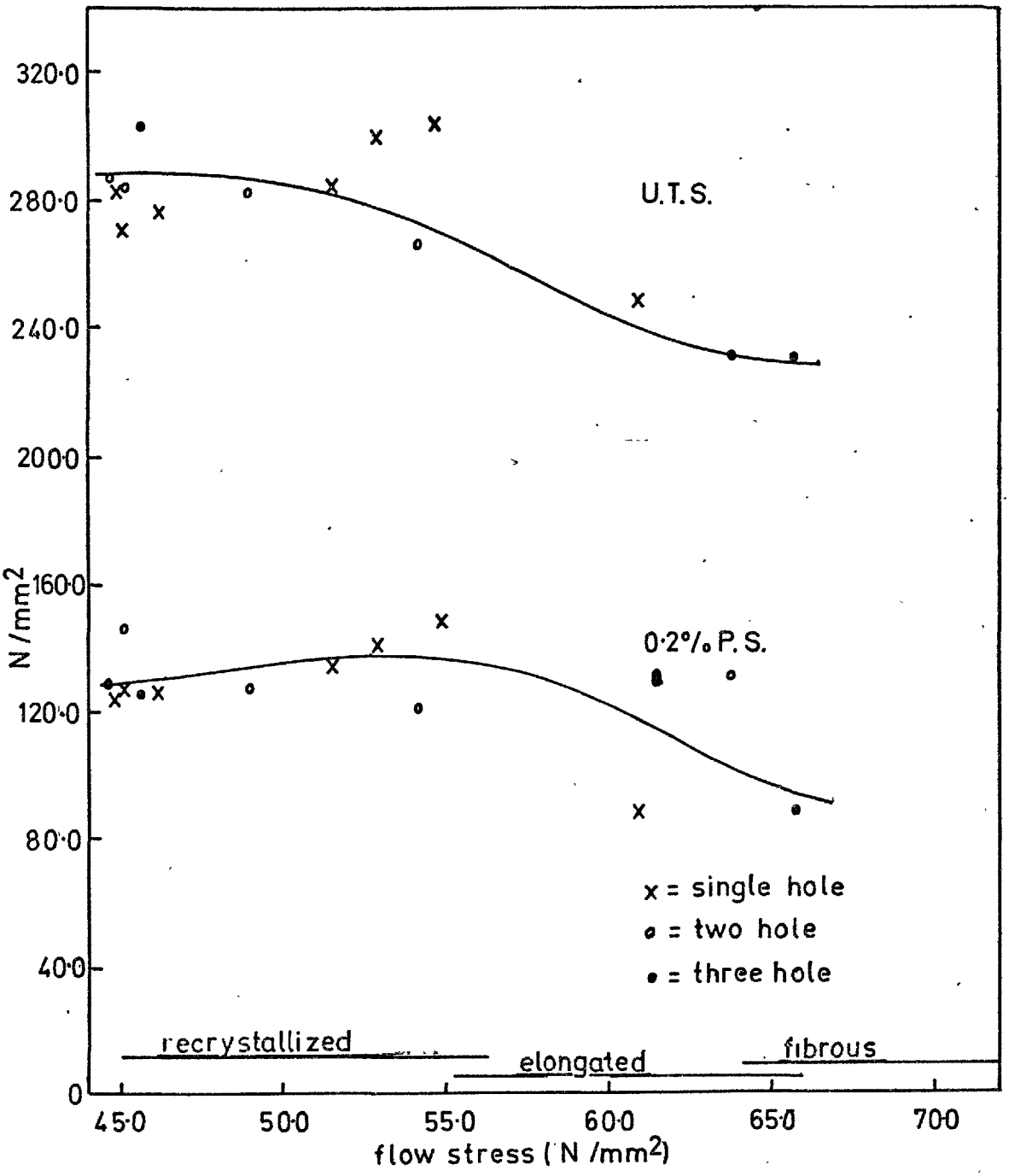


Fig.43 The relationship between the mechanical properties, structure, and flow stress. Alloy CE.

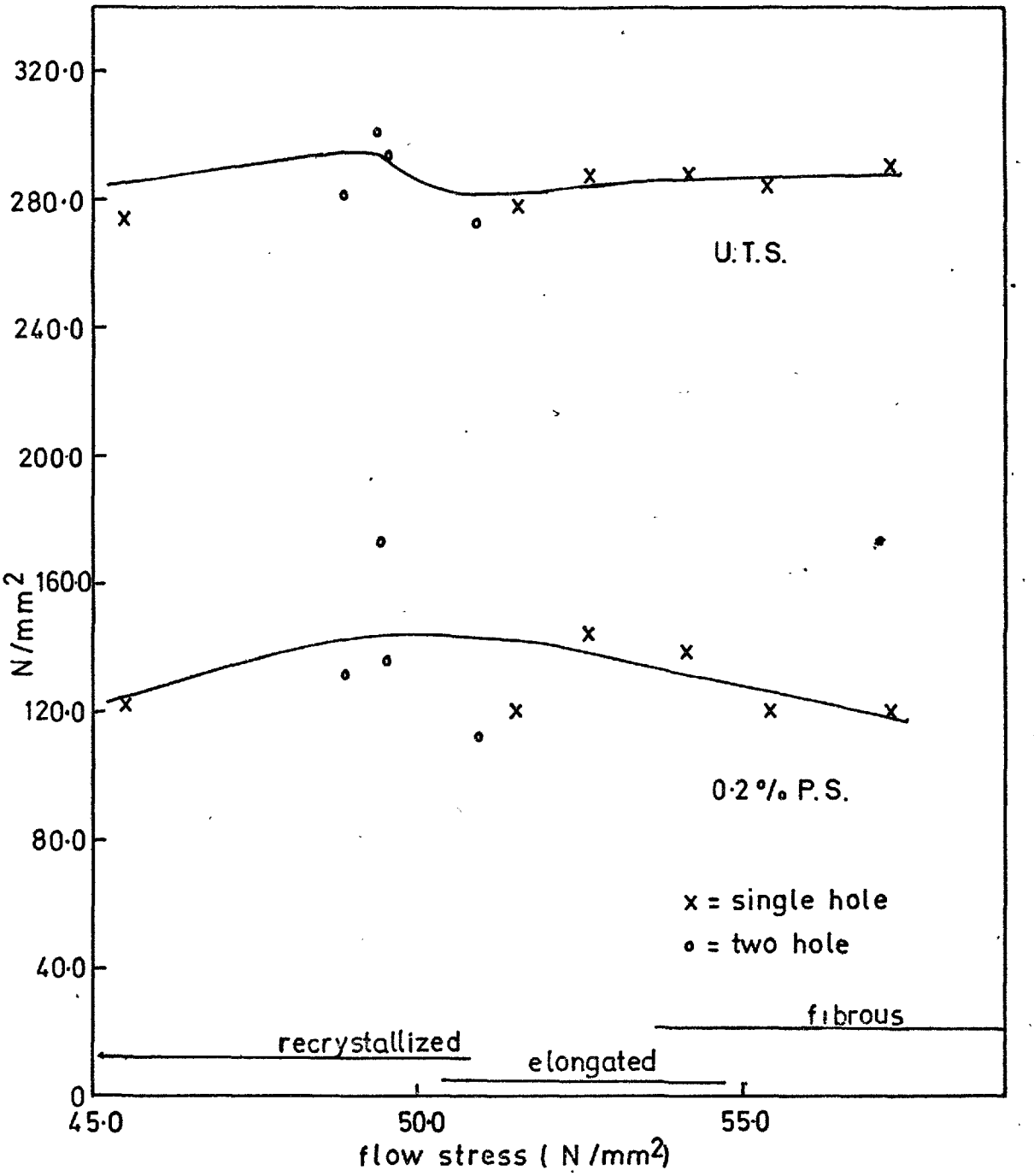


Fig.4·44 The relationship between the mechanical properties, structure, and flow stress. Alloy DF.

and there appreared to be a definite change occurring in the region where the intermediate structure, between completely fibrous and fully recrystallized, was seen. In the case of alloy B a minimum in the mechanical properties was indicated in this region.

4.8. The Dependence of the Mechanical Properties on the Grain Size.

It was not possible to determine any relationship between the sub grain size and either the mechanical properties or the flow stress. The reason for this being the limited number of results where the structure consisted entirely of subgrains. The recrystallized grain size was measured using a linear intercept technique. In the case of the elongated recrystallized structure the size across the grains was measured. The results are given in figures 4.45-4.48. Within the scatter, which is always present in grain size determination, the mechanical properties increase as the grain size increases. This differs from the expected result of a decrease in strength with an increase in the grain size. This effect is more marked in alloys A and B.

4.9. The Variation in the Properties of the Multihole Extrudes.

The difference between the properties of the as extruded rods are plotted against the flow stress in figures 4.49&4.50 for alloys A and B. They follow the same trend as that found in section 4.7 where average values were taken. There appears to be only a slight variation between the properties of the multi-hole extrudes. If anything the difference increases as the flow stress increases.

4.10. The Hardness Across the Extrude.

Figure 4.51 shows the variation in the hardness across an extrude. The single hole product shows a uniform variation with an almost constant value across the extrude, except at the edges. In the multi-hole extrude the change in hardness is much greater, only the variation across a two-hole extrusion is given but the three hole outer rods followed a similar pattern. A maximum occurs away from the centre axis. The central rod of the three hole extrusion had a variation similar to that found for the single hole, i.e. it followed a symmetrical form, but a maximum at the centre was usually seen.

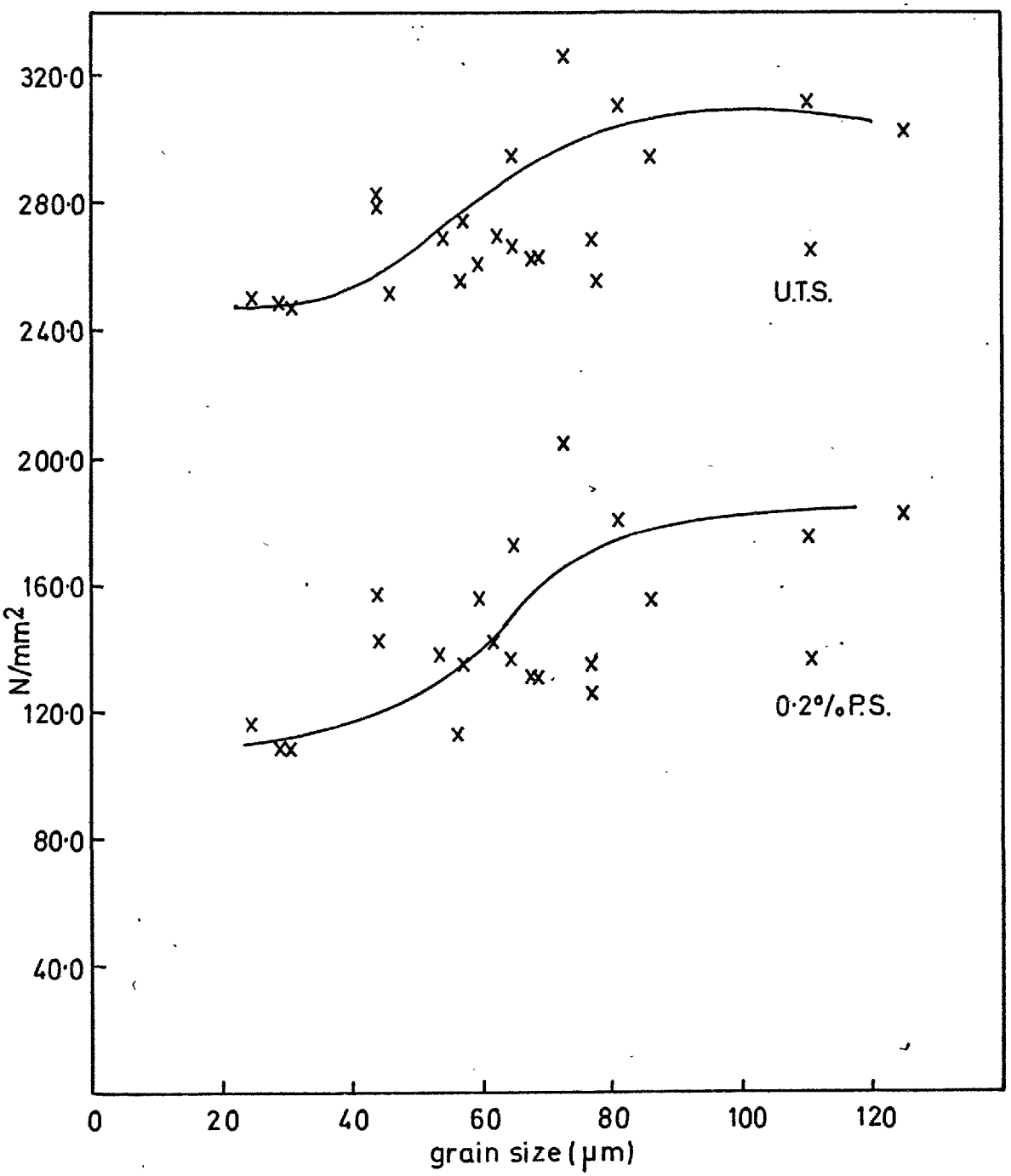


Fig.4·45 The relationship between the recrystallised grain size and the flow stress. Alloy A.

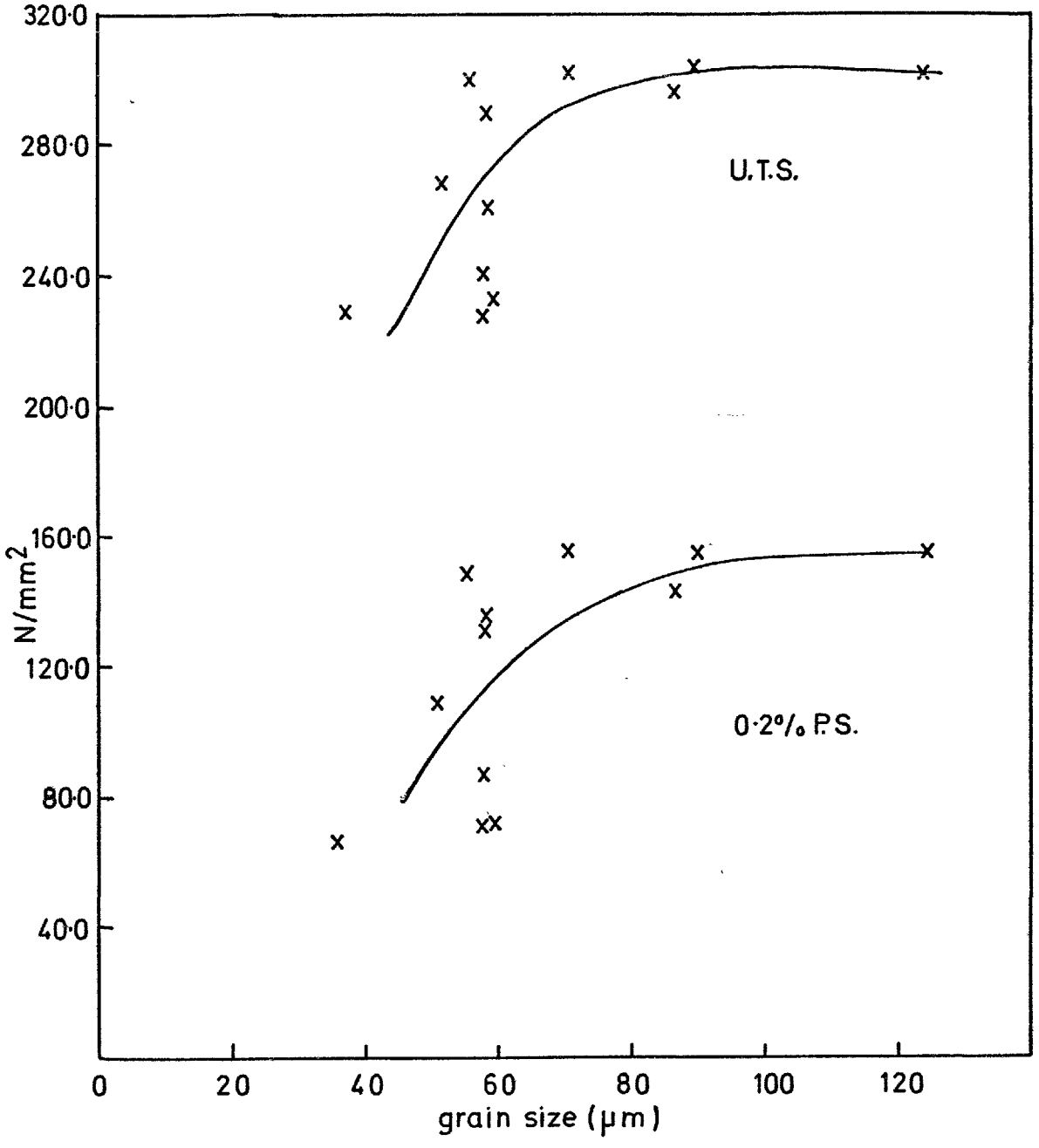


Fig.4·46 The relationship between the recrystallized grain size and the flow stress. Alloy B.

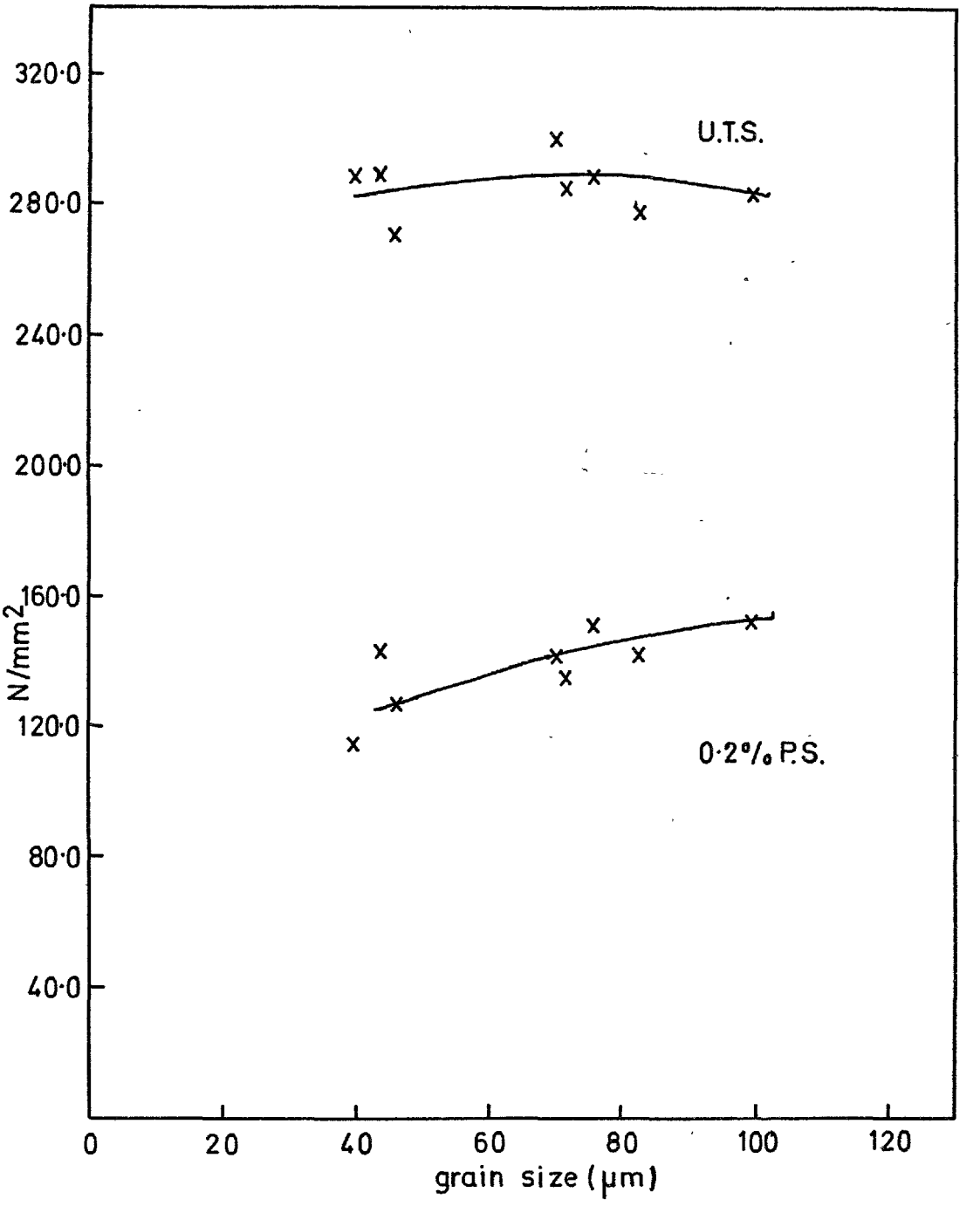


Fig.4·47 The relationship between the recrystallized grain size and the flow stress. Alloy CE.

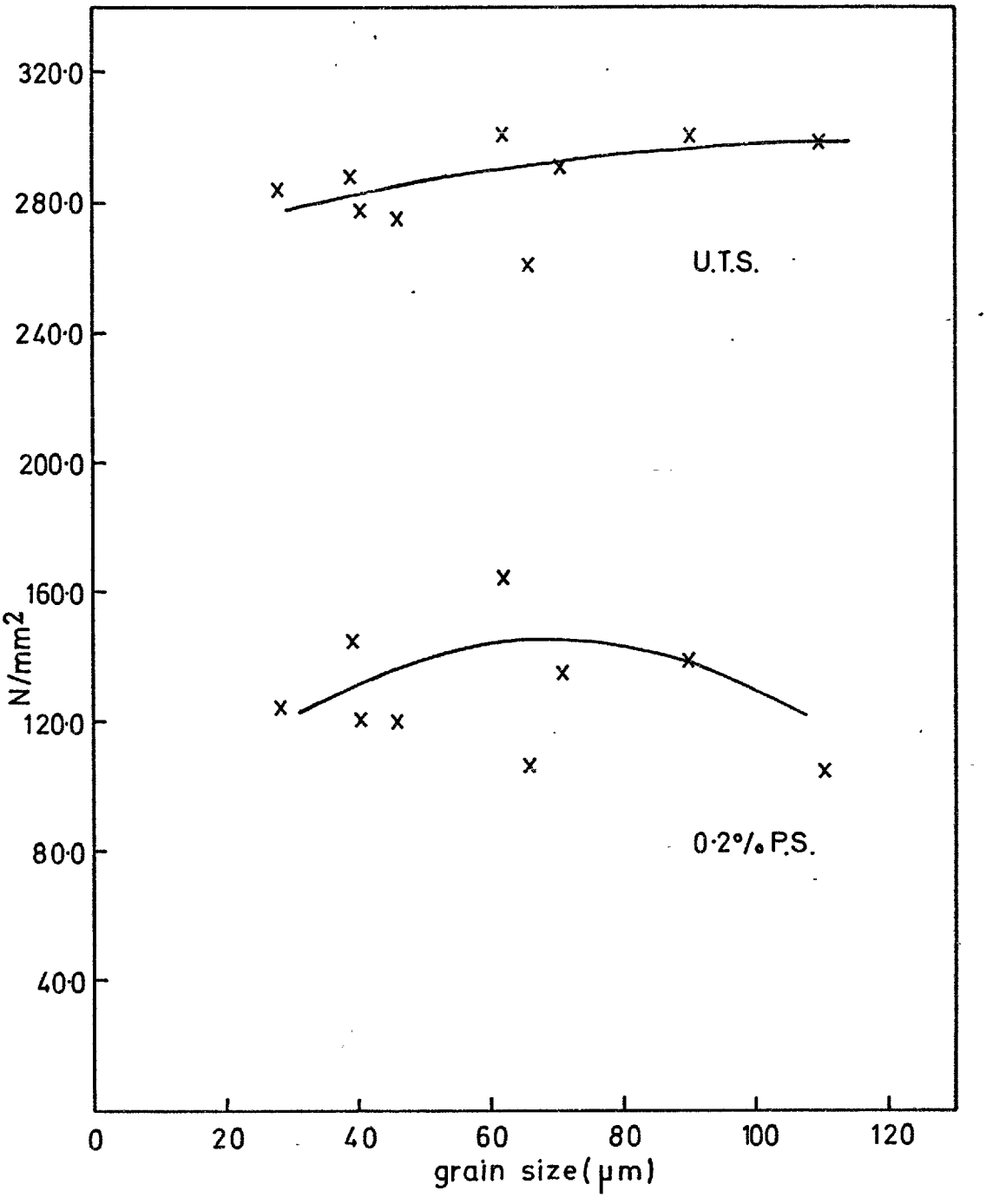


Fig.4·48 The relationship between the recrystallised grain size and the flow stress. Alloy DF.

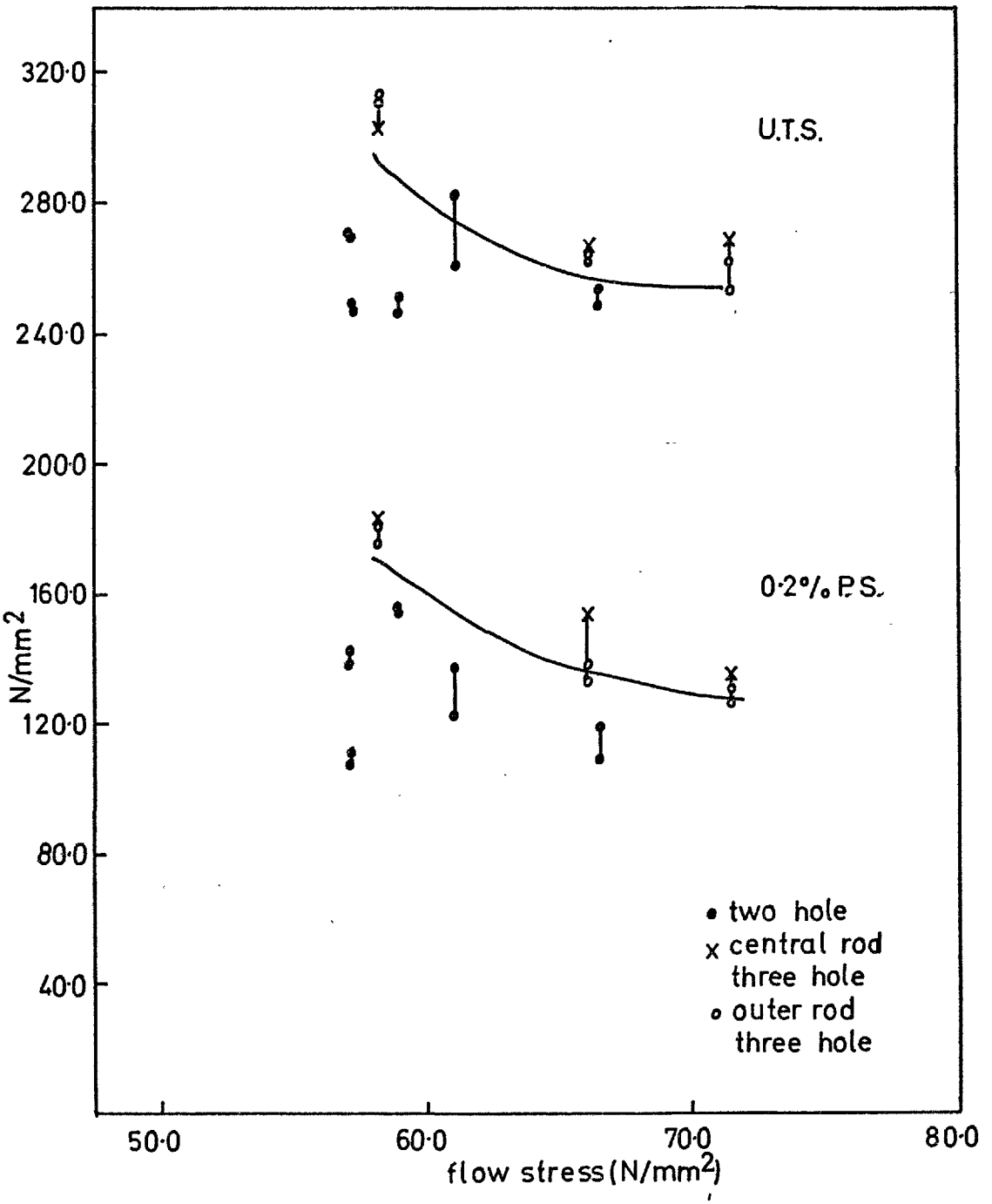


Fig.4·49 Variation in mechanical properties in multi hole extrudes. Alloy A.

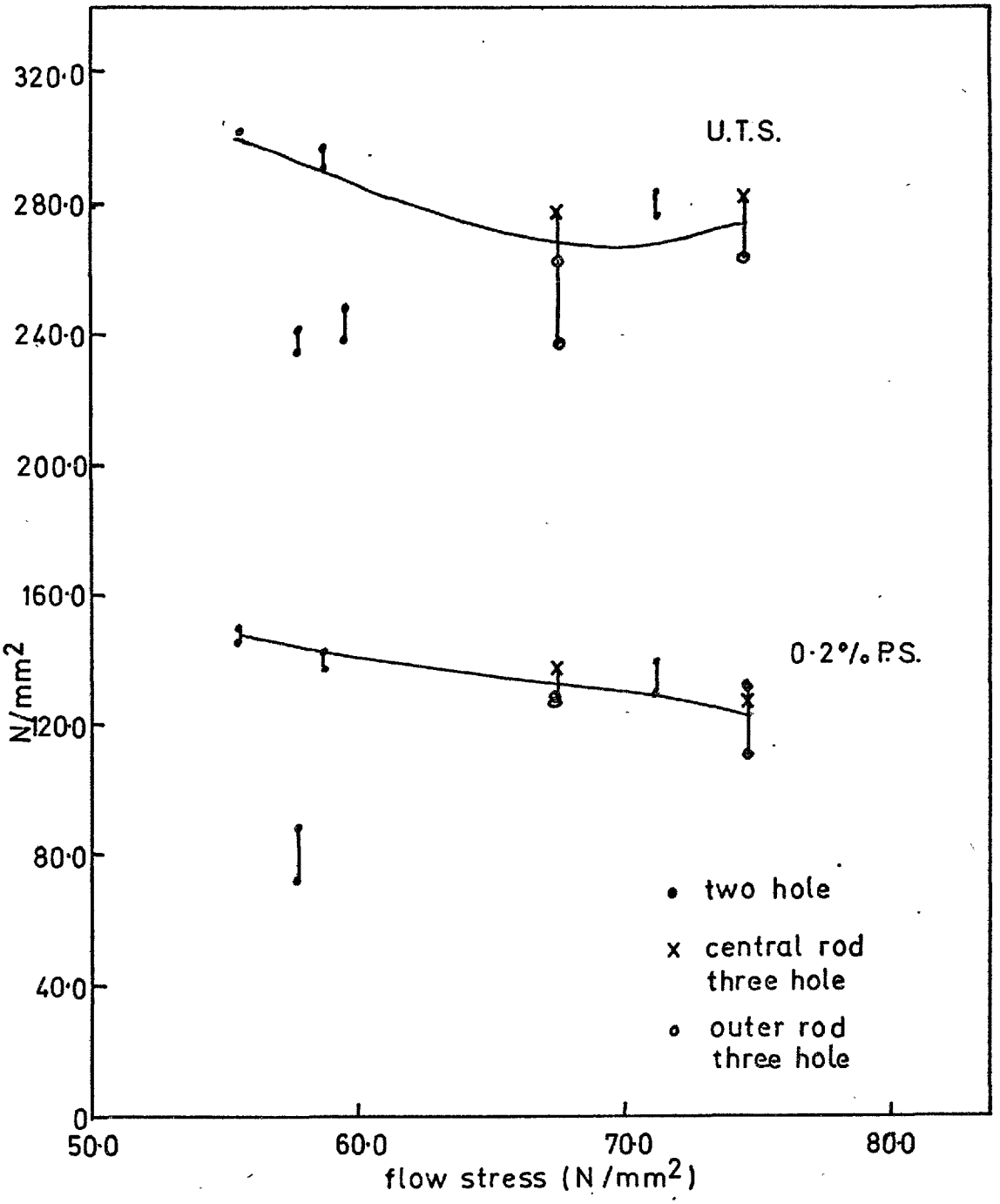


Fig.4·50 Variation in mechanical properties in multi hole extrudes. Alloy B.

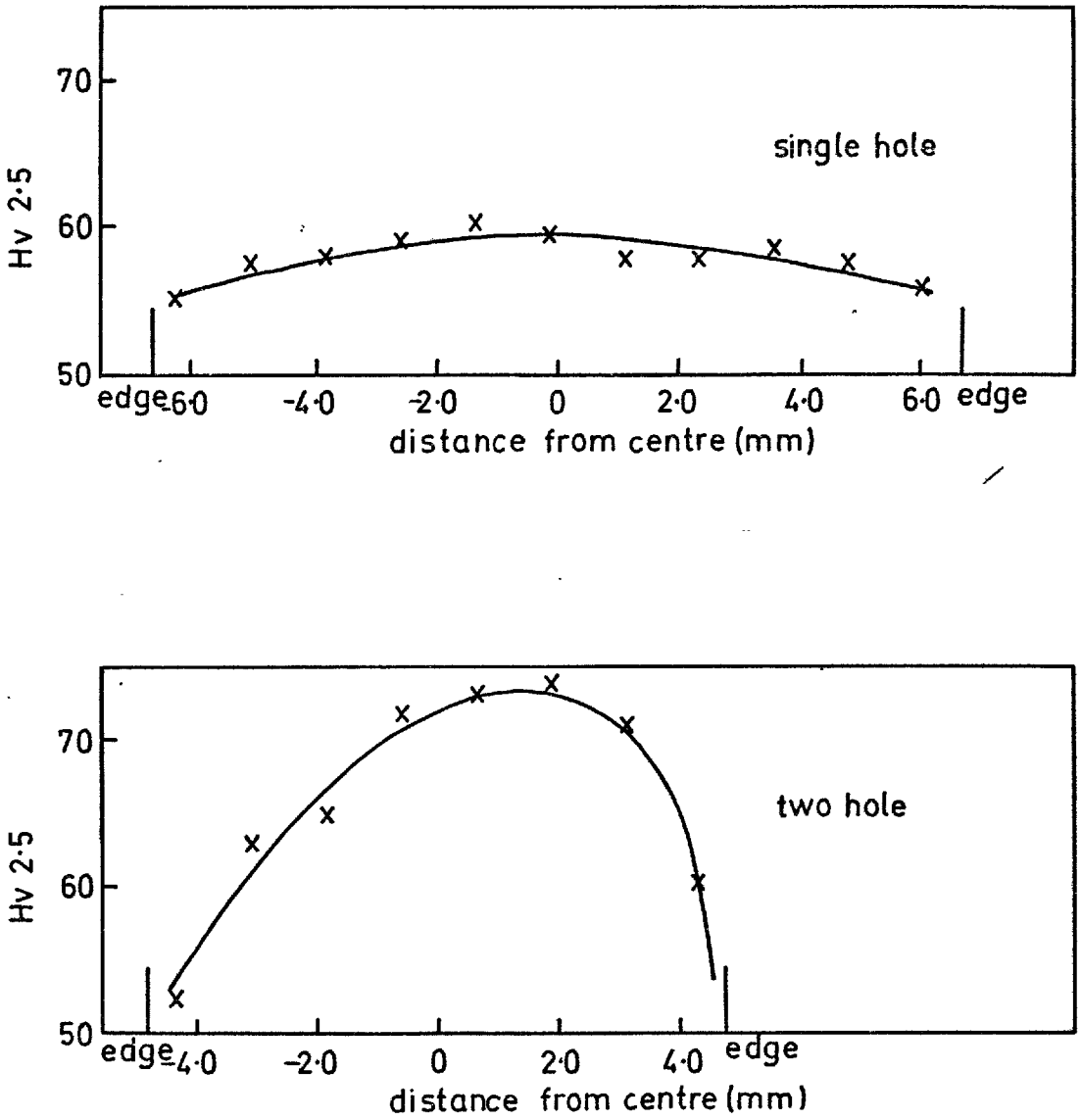


Fig.4·51 Typical hardness variation across the extrude.

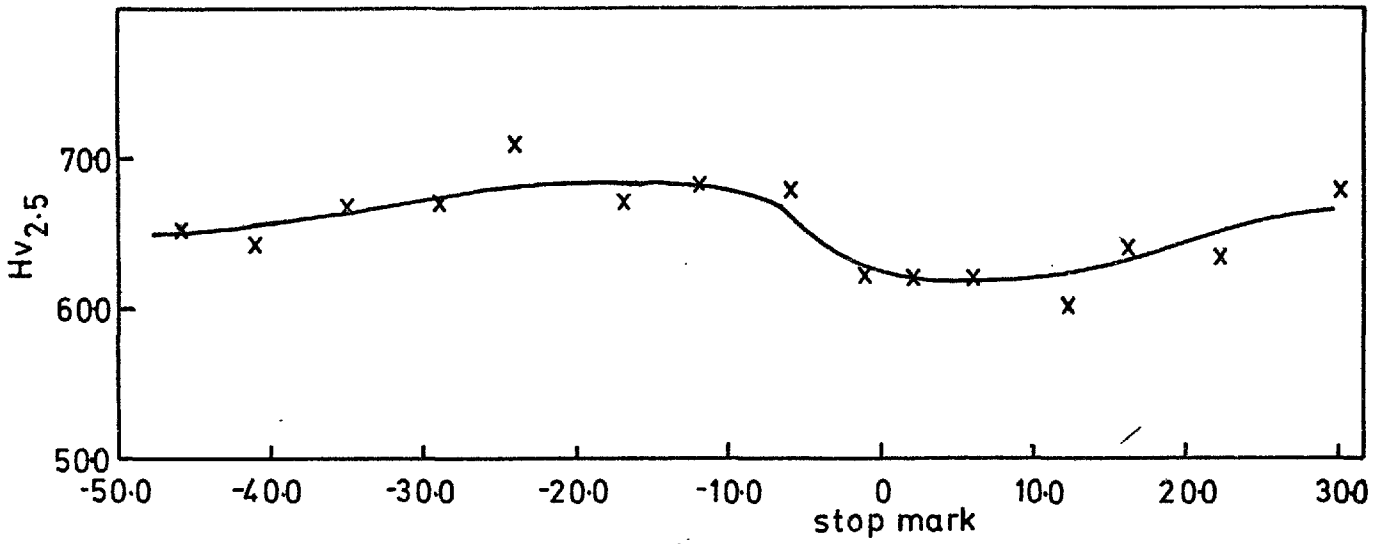
4.11. The Variation in Hardness Across the Stop Mark in the Load Removal Experiments.

When the load was removed and reapplied during extrusion, a stop mark was always seen. Hardness measurements were made along the regions adjacent to these marks and the results are given in figure 4.52. In those experiments where the load was completely removed, a sudden rise occurred about 5mm from the stop mark, towards the back end of the extrusion. This was followed by a gradual fall towards the original value. In the 5mm in front of the stop mark, the hardness showed a slight fall. When the load was not completely removed, only lowered, a slight rise occurred in the region just behind the stop mark.

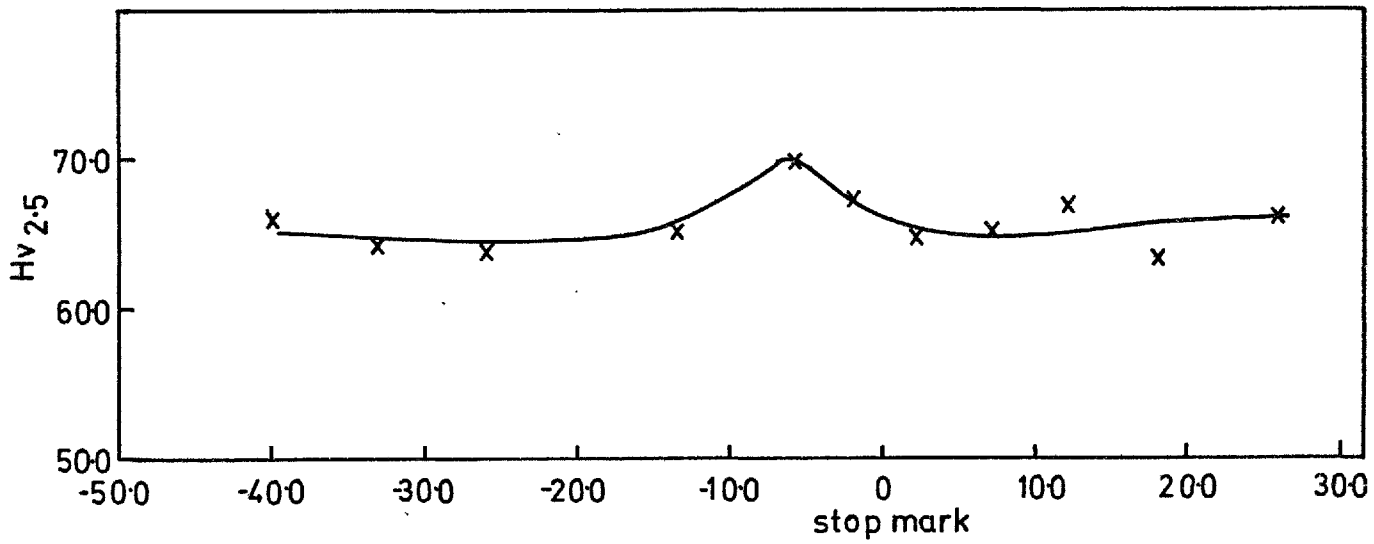
4.12. Limit Diagrams.

In the previous sections the dependence of the peak load on the temperature, ram-speed, and temperature were given. Using this information, a line can be drawn to represent the maximum extrusion ratio at any initial billet temperature. The lines in figures 4.53-4.54 were drawn for a press capacity of 5 MN, and a billet 75mm in length and 73.5mm diameter. Only alloys CE and DF were considered, because of the limited number of results available for the other alloys. The other boundary line on a limit diagram is that due to the temperature. If the initial billet temperature is being used as the axis, the maximum temperature rise has to be allowed for. A study of the results of the two alloys indicated that hot shortness shown by edge cracks almost perpendicular to the surface, did not occur below a temperature of 540°C and 560°C, in alloys CE and DF respectively. Severe scoring of the extrudes surface was also seen above these temperatures.

Taking these as the limiting temperatures the limit line was calculated for several strain-rates. The method used was the reverse of that used to calculate the final billet temperature, section 2.8. At low strain rates the calculated temperature fell above the limiting value of 540°C or 560°C. In this case the boundary was drawn at the lower temperature.



a) load completely removed.



b) load partially removed.

Fig.4·52 The variation in hardness in the region adjacent to the stop mark.

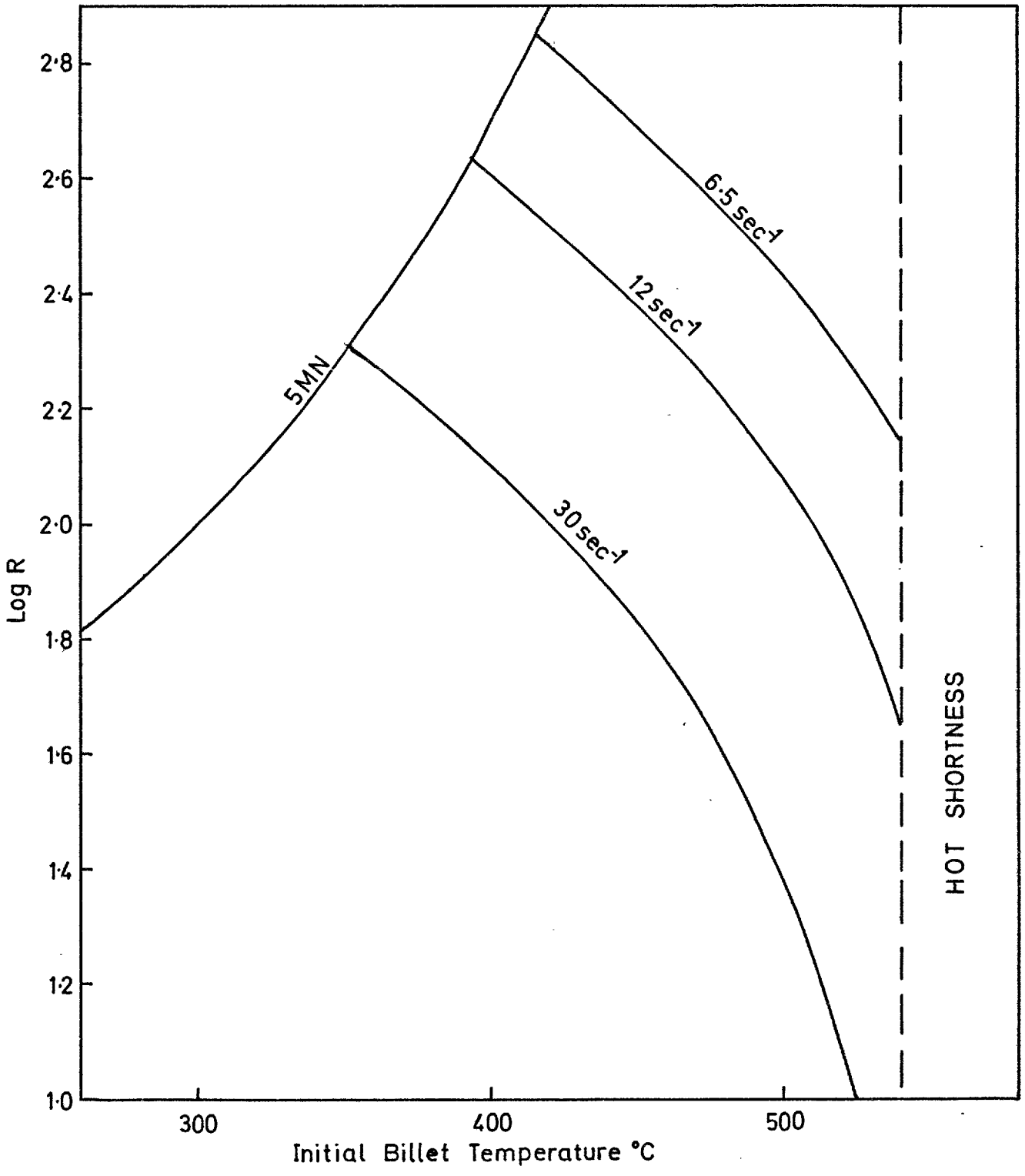


Fig.4·53 Limit diagram for alloy CE.

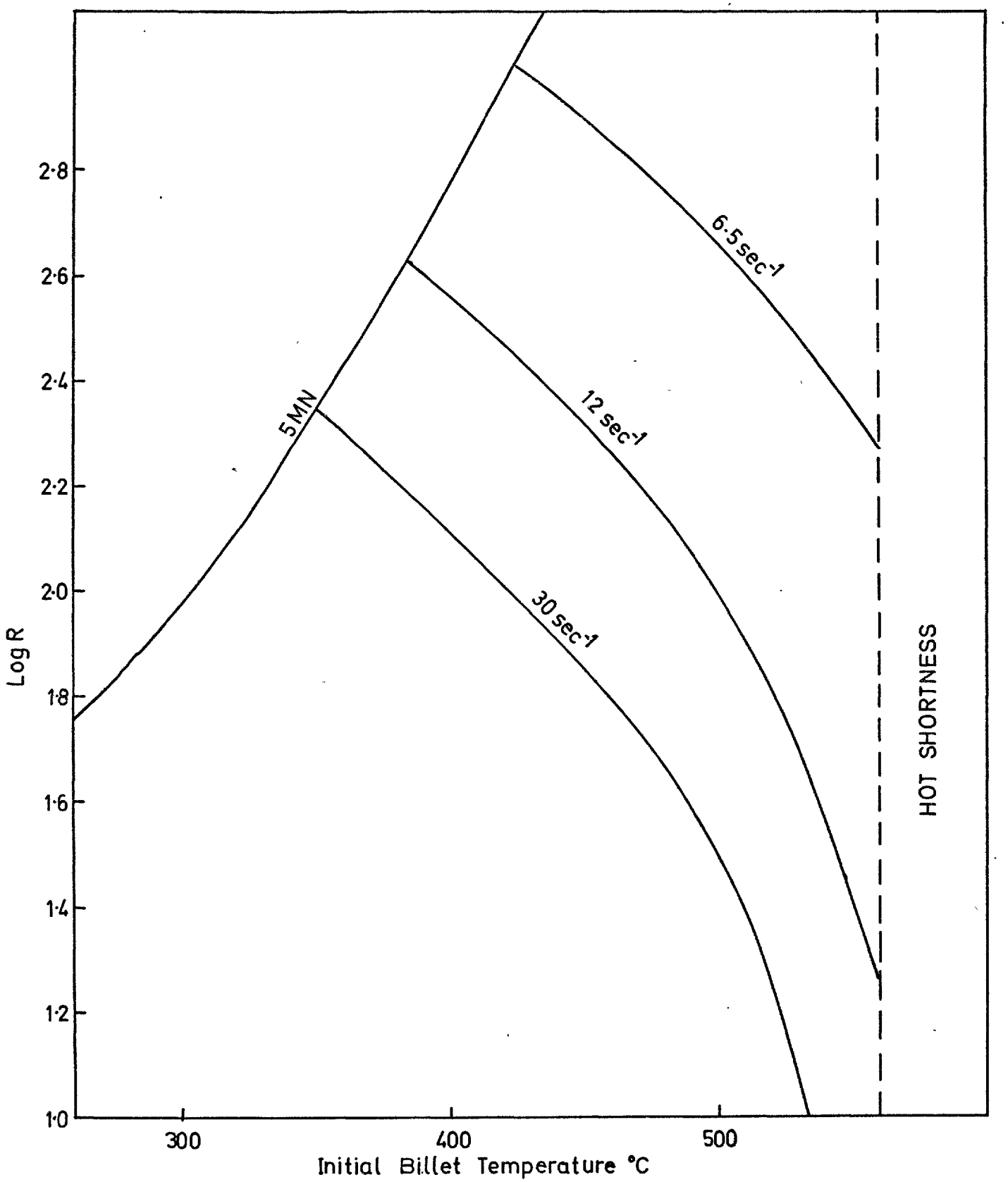


Fig.4-54 Limit diagram for alloy DF.

4.13 Flow Patterns and Microstructures.

For ease of discussion the flow patterns and micrographs are given in the next chapter.

CHAPTER FIVE

DISCUSSION

5.1. Possible Sources of Errors in the Experimental Results.

The validity of any conclusions drawn from experimental evidence will depend on the accuracy of the results. It is therefore necessary to have a knowledge of the various factors causing these errors, and to evaluate their order of magnitude.

The experiments involved the extrusion of a billet of known specification through a die of a known reduction ratio, at a fixed ram speed and initial billet temperature. The resulting extrude was quenched before being examined with both optical and transmission-electron microscopes. Tests on the mechanical properties were made on the extrude. There are several possible sources of error that can be recognized.

The material was supplied in the form of cast logs and the analysis are given in table 3.I. Alloys A and B were made with a super purity aluminium base, therefore the impurity level would be low, and only compositional variations from billet to billet would effect the results. The other alloys were not prepared with super purity aluminium, and as a result the impurity level is consequently higher. Also the more complex composition would augment the tendency for slight variations in the billet composition. This is especially true in alloys CE and DF, where two batches of material were used. The long homogenization treatments used would have reduced some of the compositional gradients but their presence should be noted.

Errors in the load measurement and ram speed measurement can be neglected, the accuracy of the instrumentation being relatively high. This is not the case in the accumulator runs. The schematic load displacement curve, figure 4.40 , shows that a maximum load was reached, followed by a fall to a constant value, Examination of the ram displacement-time curve showed that extrusion had stopped when the constant value of the load was reached. This must be due to the ram being arrested by the protecting rings on the container; the measured load being that exerted on these rings. The ram speed exhibited a continous fall throughout extrusion, in contrast to the constant value obtained at the slower speeds, this is a direct result of the mode of operation of the accumulators. The use of a U.V.

recorder enabled the load to be accurately measured but the absence of a definite maximum or minimum prevented the use of this measured load in determining a mean flow stress. The ram speed had to be recorded on the X.Y. recorder and the accuracy of the measurement was limited by the speed of response of the equipment.

The initial billet temperature could not be measured directly. Dead-metal zone thermocouples sheared off at the start of extrusion. For this reason experimental cooling curves had to be used, the readings from a thermocouple in the back end of the billet gave reasonable agreement with the temperatures obtained from these curves. This method entailed measuring the time to transfer the billet from the induction heater to the container plus the time for the ram to be brought down onto the billet. There are several sources of error. The accuracy of the induction heater was limited to $\pm$ 2°C. The time for transfer could be measured with reasonable accuracy to $\pm$ 2 seconds. The largest error would be in relating this measured time to the temperature loss. Slight variations in the cooling rate will lead to a significant difference in the heat losses, and this will be reflected in the assumed value of the initial billet temperature.

The quality of the die will have some effect on the measured load, and the surface finish. The ideal would be to repolish the die before each extrusion. This is impractical in most experiments of this nature, however the dies were examined after each run and cleaned when necessary, a strong solution of caustic soda being suitable in most cases. The nature of the die metal interface can change throughout a single experiment and the effect on the load and surface finish cannot be allowed for.

After extrusion the product was quenched. Some aluminium alloys are very susceptible to the quenching rate, but the rate of quenching is very difficult to measure. It will depend on the temperature , dimensions, shape of the extrude, and the exit speed, as well as the condition and efficiency of the quenching apparatus, and the temperature of the quenching medium.

The structures observed in both the optical and transmission microscopes would be subject to the usual errors of specimen selection. The mechanical properties were measured using No.12 Hounsefield specimens. The accuracy of these results will depend on the care in their preparation, plus the usual sampling errors. The percentage

elongation was not measured because the gauge length is small. Any measurements made on this short length will be subject to significant errors.

Although it is difficult to put numerical values to the accuracy of the results, the main sources of error can be summarized as;

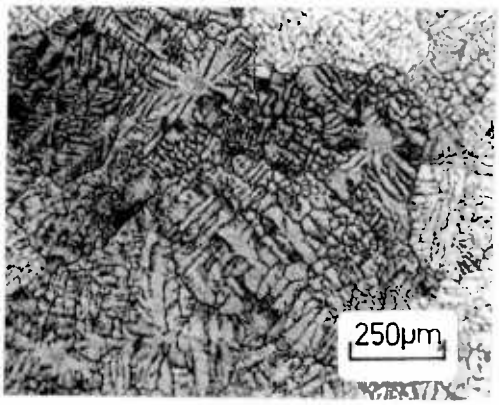
1. Variations in the material composition.
2. Errors in the determination of the initial billet temperature.
3. Variations in the quenching rate.
4. Sampling errors in examining the structures and mechanical properties of the extrude.

5.2. The Structure of the Material Before Extrusion.

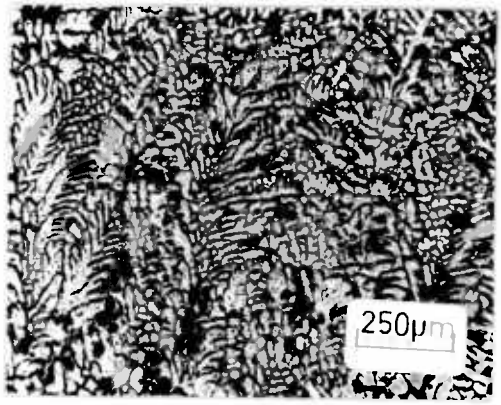
No detailed examination of the initial structures was carried out but they were examined under both the optical and transmission electron microscopes.

Alloys A and CE had very similar structures, figure 5.1 . It is still possible to identify the original cast structure and some coring is present, this was reduced in the case of alloy A. The transmission electron micrographs show an almost complete solid solution, with very few precipitates. In alloy A these could only be Cu Al_2 but the presence of iron and some silicon in alloy CE would lead to the formation of complex intermetallic compounds.

Alloys B and DF were also similar, figure 5.1. The optical micrograph shows very heavy coring with the cast structure still retained; the degree of coring being much higher in these alloys than in the previous two. The transmission electron micrograph shows that the homogenization treatment had failed to take the precipitates into solution. This difference between the two pairs of alloys can be attributed to the presence of manganese in alloys B and DF, which contained the same Cu as A and CE. In the super purity base alloy the manganese will combine with the aluminium and the copper. When iron is present it will combine with the copper and manganese in a complex Al-Fe-Mn-Cu phase. Some iron will also be tied up with the small percentage of silicon present. The nett effect of the manganese is to reduce the tendency for the formation of the equilibrium solid solution. The presence of iron and silicon will tie

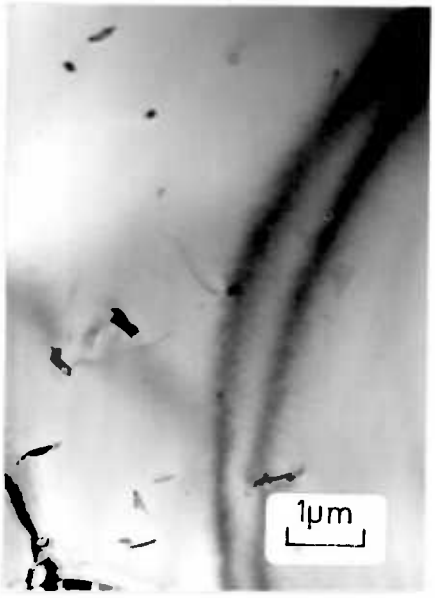


a) Alloy CE



b) Alloy DF

Optical



c) Alloy CE



b) Alloy DF

Transmission electron microscope

Fig 5.1 The billet structure after heat treatment

up some of the other elements and further reduce the likelihood of equilibrium being reached, even with the extensive heat treatments used Sometimes equilibrium is not reached in aluminium alloys even after a month at temperature.

Alloys 265D, 266D, and 272D were used because of their widely differing properties. The heat treatments of alloy 266D produced an almost complete solid solution. In alloy 265D the presence of manganese will lead to complex intermetallic compounds being formed. Alloy 272D had a very complex structure with large precipitates forming on the grain boundaries, which were associated with a precipitate free zone. The matrix of the grains had a high volume fraction of precipitates arranged in Widmanstatten type formation.

5.3. The Results Obtained from the Hot Torsion and Tensile Tests.

5.3.1. A Comparison Between the Calculated Constants in the Hot Working Equations.

Both hot torsion and hot tensile testswere used to obtain the parameters in the hot working equation, and to compare these laboratory testing methods to the results obtained from extrusion. As stated in Chapter 4, the stress strain curves derived from the torsion results followed the usual form. At high temperatures and low strain rates there was a rapid rise in the stress followed by an almost constant region, usually referred to as the state. (The term steady state is rather a misnomer as the specimen geometry is continually changing, giving a varying strain rate. There are also temperature gradients set up in the work piece during deformation.) A slight peak was also seen in the curves. At the lowest test temperatures especially at the high strain rates, the rapid rise was followed by a continuous fall in the stress leading to fracture, if the test was continued. The continuous fall masked the true magnitude of the difference between the peak stress and the steady state stress. A temperature rise will always accompany deformation, at the lowest temperature the work needed to cause deformation is correspondingly higher, and a large temperature rise will result. This is especially true at very high strain-rates where the time for the heat to dissipate is less. This increase in temperature will cause the observed decreasing flow stress. The difficulty in

calculating the heat losses has already been mentioned. Any solution must allow for heat losses by radiation and by conduction through the specimen grips, the latter is the most difficult to calculate. The most general observation that can be made from the results is that alloy CE, with the same copper content and no manganese, is more resistant to deformation at high temperatures than is alloy DF. The first alloy is almost a complete solid solution, with the associated higher properties that this entails.

On a more quantitative base the applicability of the two equations

$$\dot{\varepsilon} = A_1 \sigma^{n_1} \qquad 1.1$$

and

$$\dot{\varepsilon} = A_2 \exp \beta\sigma \qquad 1.2$$

was examined.

The results agreed with these equations, in the low and high stress range respectively, although linear relationships were obtained with both expressions for alloy DF. The two empirical equations apply to different stress ranges, but there is a region of intermediate stresses where both can reasonably correlate the data. This is the case for alloy DF.

It is not possible to compare the values of the constants A_1, n_1, and β obtained in the present work with those found previously, because no similar work on these alloys appears to have been published. Bailey [39] gave some results for the torsion of several aluminium alloys and the values of β, n_1, A_1 and A_2 that he found may be compared, on a qualitive basis, with the present work. The exponent n_1, in equation 1.2, varied from 35.1 at 200°C to 7.1 at 500°C in an Al-Cu-Mg-Mn alloy. The values obtained in the present work are 12.3 and 7.65, for alloys DF and CE respectively at 400°C. The order of magnitude agrees but obviously the absolute value will depend on the composition and structure of the particular alloy. The higher value for alloy DF means that the flow stress is less dependent on the strain rate in this alloy indicating a fundamental difference in the ease of dislocation formation, multiplication and movement between the alloys. The values of A_1 in equation 1.1, obtained by Bailey, were very temperature dependent. For the alloy mentioned previously, A_1 ranged from 10.65×10^{-50} N/mm^2/sec at 200°C to 7.65×10^{-5} N/mm^2/sec at 500°C.

At 400°C A_1 for alloy DF was equal to $8 + 10^{10} N/mm^2/sec$, and for alloy CE $6 \cdot 08 \times 10^{-7} N/mm^2/sec$. Again emphasizing the difference between the two alloys. In the other equation Bailey quotes a value of $0 \cdot 204\ mm^2/N$ for β. For alloy DF β was found to be $0 \cdot 168 mm^2/N$ and $0 \cdot 248 mm^2/N$ for alloy CE. These are of the same order of magnitude as Bailey's but the exact value of β will be very dependent on the alloy being used. It is a measure of the effectiveness of the stress in assisting dislocation motion through the structure. The higher the value the higher the velocity of the mobile dislocations which implies a high strain rate. There is therefore a significant difference between the strain rate dependence of the flow stress in the two alloys studied amd this must be a direct result of the different structures resulting from the presence of manganese in alloy DF.

5.3.2. The Use of $\sigma_{1.5}$ for the Flow Stress in Torsion.

The constants given were calculated from both the tensile and the torsion results. The use of the torsion flow stress at a true strain of 1.5 is only justifiable on the grounds that this gave the best correlation between the results. At a lower strain the stress was still in the peak region, in the lower temperature tests, and beyond 1.5 the temperature rise will have a pronounced effect on the shape of the stress strain curve. The fact that a reasonable correlation with the tensile tests, which involved much lower strain rates, was obtained implies that the correct values were used.

5.3.3. The Value of the Activation Energy.

The number of results obtained precluded the calculation of the true activation energy for the hot working of these two alloys. This is often the case in the available published work, but values are still quoted and the slight difference between different alloys discussed in detail. One fact does have universal agreement though, the activation energy for the hot working of aluminium and its alloys is similar to that found for self diffusion. The values quoted by Bailey are 159,000 J/mole for commercial purety aluminium, 160,000 J/mole for Al-Cu-Mg-Mn, and 161,000 J/mole for a dilute Al-Mg-Si alloys, three alloys with very different behaviours.

The error in these quoted values was not given but an error of only 1% will make them identical. Therefore a value of

160,000 J/mole may be said to cover the range of alloys studied. For this reason the same activation energy was used in the present work. If a significant change in the hot working mechanism occurred, such as dynamic recrystallization it would be accompanied by a change in the activation energy, and this would be reflected in a deviation in the experimental results.

5.3.4 The Application of the General Hot working Equation.

The two equations used in the above sections only apply over a certain stress range, and at a constant temperature, usually the initial temperature is the one quoted. A more general relationship is that suggested by Sellars&Tegart, equation 1.7. The values of α were derived from n_1 and β in equations 1.1 and 1.2 respectively, and are of the same order of magnitude as those found in other work. Using these values figures 4.5 and 4.6 show that equation 1.7 can be applied to both alloys over a range of Z, the temperature compensated strain rate, of many orders of magnitude. The scatter can be attributed to experimental error, including variation in the structures of the specimen, non uniform heating prior to testing, and errors in the instrumentation and torsion machine used. The exponent n, a measure of the stress sensitivity of the strain rate, for alloy DF is approximately double that found for the other alloy, agreeing with the results given from equation. 1.1 . For the alloys that he studied, Bailey gives n varying from 4.85 to 6.42, increasing with the complexity of the alloy, the values of A fell in the range $3{\cdot}2 \times 10^{10}$ to $3{\cdot}3 \times 10^{11} sec^{-1}$. These are similar to the present values of $1{\cdot}99 \times 10^{12}$ and $1{\cdot}41 \times 10^{10}$ for alloys DF and CE respectively.

In this general equation, α can be related to the activation volume, which is a measure of the effect of the stress in aiding the dislocations to overcome the barriers. A can be called a structure factor but, by comparison with various theories it also includes a term representing the frequency with which a dislocation tries to overcome the barrier. In these alloys α is higher in the 4% Cu alloy, CE, which implies that dislocation motion is easier than in alloy DF the lower value of n means that the flow stress is more dependent on the strain rate. In alloy DF the presence of the precipitates, containing aluminium, copper, manganese, iron, and silicon, will tend to hinder dislocation motion.

The effect of the stress in assisting dislocation motion will therefore be reduced and the stress will be less dependent on the strain rate. This is reflected in the values of n_1 and β respectively.
Equation 1.7 is usually expressed in the form

$$\dot{\varepsilon} = A(\sinh\alpha\sigma)^n \exp\frac{Q}{RT}$$

which is perfectly suitable for the correlation of creep tests, where the flow stress is fixed and the creep rate measured. In hot working the strain rate is pre-set and the flow stress measured. A more suitable equation will be expressed as an explicit function of the flow stress.
Rewriting 1.7

$$Z = A(\sinh\alpha\sigma)^n$$

and taking natural logarithms

$$\ln Z - \ln A = n \sinh\alpha\sigma$$

or

$$\alpha\sigma = \sinh^{-1}(\frac{Z}{A})^{1/n}$$

therefore

$$\sigma = \frac{1}{\alpha}\ln\left((\frac{Z}{A})^{1/n} + \sqrt{(\frac{Z}{A})^{2/n} + 1}\right) \qquad 5.1.$$

As α increases the flow stresses decrease accordingly. As n decreases the logarithm increases, leading to a higher flow stress, i.e. the flow stress is more strain rate sensitive. Written in this form a clearer visualization of the effect of a change in the variables on the flow stress is obtained.

No linear dependence was found between log Z and the flow stress. Therefore the equation

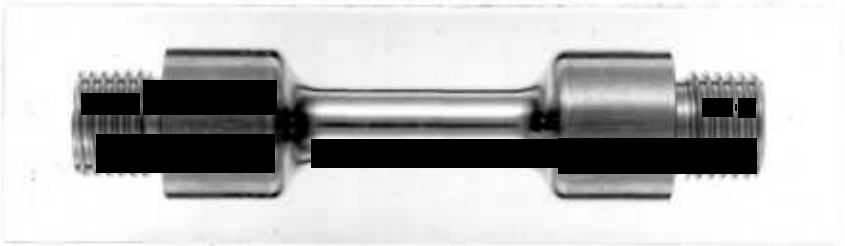
$$Z = A_4 \exp\beta_1\sigma$$

cannot be applied to the experimental data. A comparison with equation 1.2 shows that a relationship of this form will only apply at high stresses and the stress range studied straddled both the low and high stress regions.

5.4 The Importance of the Temperature Rise in Torsion.

In figure 5.2 typical torsion specimens are shown. The undeformed specimen (a) may be compared with those in (b-d). The specimen shown in (b) was twisted at an initial temperature of 400°C and a strain rate of 0.589 sec^{-1} . There is no sign of incipient melting and the only dimensional change is a slight increase in length. No evidence of necking was found. The specimen in (c) had the same initial temperature, it is also the same alloy (CE) but it was twisted at a higher strain rate of 2.99 sec^{-1} . Instead of the uniformly deformed structure there is evidence of hot shortness having occurred during the test, a slight baralleling at the centre of the gauge length can also be seen. This is direct evidence of the tenperature rise that can occur during a torsion test, and the magnitude of this rise must have been well over 100°C. The barelling at the centre and the absence of the 'hot shortness' near the specimens neck illustrates the complex nature of any calculation of the temperature rise.

The heatloss through the ends of the specimen is high enough to compensate for the temperature rise. There is also the added complication of non-uniformity of deformation throughout the gauge length. The final photograph (d) shows advanced hot shortness, the temperature and strain rate were the same as in (c) but the alloy was different, alloy DF, which contained the manganese. The peak stresses were almost identical and therefore the temperature rise must have been similar. The severe hot shortness in the latter specimen is an indication of a lower melting point phase or a higher volume of such a phase. The volume fraction of precipitates in alloy DF was much higher. An important factor will be the time taken during the heating cycle prior to testing. The induction heater used enabled the test temperature to be reached in less than five minutes. In this short time there would be very little time for any precipitates to be taken into solution. The presence of this hot shortness with its implication of a high temperature, shows that significant errors will be present if the results are correlated with the initial temperature. Nevertheless it is very difficult to calculate this temperature rise and therefore most work in this field tends to ignore it, and its implications.



a) Undeformed



b) Alloy CE, 400 °C, strain rate = 0.59 sec



c) Alloy CE , 400°C, strain rate =2.95 sec



d) Alloy DF, 400°C, strain rate = 2.95 sec

Fig 5.2 Torsion specimens

5.5. The Analysis of the Extrusion Results.

The validity of these results will depend on the assumptions made in the calculation of the flow stress, temperature, and the strain rate.

5.5.1. The Mean Flow Stress in Extrusion.

Two methods of deriving the flow stress were given in Chapter One. The first was based on an empirical approach, the second on the upper bound method of solution. The empirical method, used by Wong and Jonas [14], gives a value for the flow stress but there is little theoretical justification in the quoted figures. The agreement between their results and those obtained by other methods is no justification for its use. The value of the flow stress can be adjusted to any value by varying the constants used in its calculation. The upper bound approach is more satisfactory, on a theoretical basis, but it still has its limitations, the major one being the assumption of a constant value of the flow stress. It is possible to derive an axisymmetric solution although the calculations tend to be complex. A lot of the published work in this field seems to be more concerned with hypothetical problems rather than providing useful results in a form that can be understood and used by both engineer and metallurgist. The present work involved both axisymmetric single hole, and multi hole extrusion, the latter is not axisymmetric. For this reason a simple minimized plane strain solution was derived and compared with previous solutions.

The theoretical plane strain single hole extrusion pressure is plotted against the fractional reduction in area in figure 2.3 . It falls within the general range given by other theories, being less at the lower reductions and increasing more rapidly at the higher reductions. The solution was extended to greater reductions than are usually considered, but this is where many of the earlier theories can be criticized. It is not unusual to use extrusion ratios of over 100.1 in modern industrial practice and this corresponds to a fractional reduction of 99% in the area, a reduction of 90% is considered low in light metal extrusion. Although the theory was extended to these high reductions it is not possible to verify it, other than by seeing if the calculated flow stresses agree with those

found at the lower reductions. Figure 2.3 also shows the variation in the predicted pressure with log R and on the same graph the solution to the simple axisymmetric model, developed by Raybould and Sheppard, is also given. The general trend is the same but at an extrusion ratio of 100.1 the predicted plane strain pressure exceeds that given by the axisymmetric solution by almost 60%. The difficulty is in choosing which value to use. The plane strain solution agrees reasonably well with the other work, but it is more a case of choosing one solution, and sticking to it, rather than selecting the correct one. For this reason the method used to calculate the flow stress should always be quoted. Whichever method is used the curve of the graphs limits the application of expressions of the form

$$\frac{P}{Y} = a + b \log R$$

to a limited range of reduction, especially at high values of log R. If a graph of $\frac{P}{Y}$ against log R is available, then there is no reason to use these expressions at all.

The flow stresses for the multi-hole results were also calculated from a simple upper bound solution. As well as varying with the reduction ratio the pressures also depend on the eccentricity of the dies used. This was governed by the geometry of the die support system. For both the two and the three hole configurations a minimum load is predicted at a certain value of the eccentricity, which is practically independent of R. For the two hole die, the minimum is at an eccentricity of 0.45, which is almost identical to the symmetrical position of a and b being equal in figure 2.4. The minimum for the three hole extrusion pressure is at an eccentricity of 0.6 which again almost corresponds to the symmetrical configuration of a and z being equal. The only other work published in this field is by Dodeja and Johnson[120], who derived a slip line field solution for multi hole extrusion at low ratios. Their result for a reduction of 16.2 : 1 is shown on both graphs, after converting the shear yield stress to the uniaxial yield stress. Their predicted load lies well below the upper bound solution for a 10:1 reduction, but the minimum load occurs in approximately the same position. The reason for this discrepancy is the general difference between the two methods of solution. The more exact, mathematically, is the slip line field and the upper bound is only an approximation to this. However, the

slip line field theory underestimated the experimental loads by a significant amount, the upper bound predicts higher loads and may give better agreement, which is a surprising conclusion. Both solutions use a plane strain approach but the experimental results were not obtained for anything like plane strain conditions. The resulting more complex flow will lead to a higher load and this will counteract the over estimation associated with any upper bound solution.

These theories provide a method for calculating the flow stress from the minimum extrusion load. The question still remains, 'What has been measured?' The dimensions and order of magnitude agree with a flow stress but the true flow stress will be continously varying throughout the deformation zone and during the extrusion. Therefore a true extrusion flow stress does not exist, all that can be obtained is a mean relative value, which will depend on the method used to calculate it. The more complex the upper bound or slip line field solution the higher will be the flow stress; a more complex solution will usually predict a lower load.

5.5.2. The Temperature Rise.

The temperature rise was calculated using an integral profile method and then allowing for the heat losses to a cooler container. It was not possible to verify the accuracy of this approach to the problem. Any attempt to insert thermocouples into the dead metal zone resulted in shearing, a slight displacement of the billet during upsetting, or at the start of extrusion, would be enough to cause this. In previous work, where this method was successfully applied, the alloys used were relatively softer and lower extrusion ratios were studied. The applied loads were lower and the lower temperatures considered would have simplified the experimental difficulties of inserting the thermocouples. In the theoretical model it is assumed that all the mechanical work is converted to heat but it has been shown[152] that only 95% is converted, the rest is stored in the deformed material. Raybould was able to compare the theoretical values, using only the integral profile model, with his experimental results, and found the latter to underestimate the temperature rise by up to 20°C. The magnitude of the error decreasing as the ram speed decreased, where higher heat losses would occur. The calculated temperature rise is a mean value and he found that the difference between the predicted

and the experimental value was higher at lower reduction ratios. This is to be expected because larger temperature gradients will be found in the extrudes with the larger diameter.

The heavily deformed surface layer will have a temperature above that of the relatively undeformed inner zone. Experimentally only the surface temperature was measured by a dead metal zone thermocouple. The majority of the present work was at high reduction ratios and slow ram speeds. It can therefore be assumed that the temperature rise calculated by this model will give a reasonable estimate of the true mean value, assuming that no structural changes, such as the resolving or formation of precipitates happens during an experimental run. Such events will absorb some of the heat, the heat of solution and the temperature rise will be lowered accordingly. In general this model is the most exact one available at the present moment.

The temperature losses to the cooler container, ignored in the integral profile model, were estimated by assuming the heat flow to be the same as that through a cylinder of internal radius and temperature equal to that of the billet, and external radius and temperature equal to that of the container. Several assumptions are made in this model. The first is that the billet is at a uniform temperature throughout extrusion and that this is the same as that calculated by the intergral profile model. This is clearly not the case as the temperature increases throughout the extrusion and is not uniformly distributed within the billet. The deformation zone acts as a heat source at the end of the billet adjacent to the die. A more exact model would have to consider this variable temperature gradient within the billet. The total heat loss was calculated by considering the mean volume of the billet during extrusion.

If the billet is at a constant uniform temperature the rate of heat loss at the start of deformation will be greater than the rate at the end, and it will be directly proportional to the surface area of the billet. The increasing temperature during extrusion will t end to cancel out any errors induced by the uniform temperature assumption. The consideration of only radial heat flow is the other major source of error. The temperature of the container is not at a uniform temperature of 300°C. At the outside edge the heatersare operating at a temperature of 700°C. There is therefore a temperature gradient

throughout the container and this will have an effect on the radial heat losses. The tooling can also be considered to be at 300°C. There will therefore be heat losses from the hot billet to the cooler die, the die block, the pressure pad and the ram. To calculate these heat losses the integral profile model would have to be adapted and complex differential equations set up and solved. The use of a water quench would complicate the situation still further, because of back conduction through the extrude. The problem of the heat losses could be overcome by experimental means, measuring the temperature distribution throughout the container and tooling, and its variation during an extrusion. In Chapter One the problem of the accumulation of heat in the container during a series of extrusions was briefly mentioned. This is a problem more akin to industrial practice than laboratory experiments. In the latter the time between extrusions will enable the tooling and the container to maintain a constant temperature.

The integral profile model assumes axisymmetric extrusion. It is therefore not applicable to multi-hole extrusions. The heat losses, C_1, C_2, and C_3 in figure 2.10 , will differ, C_5 will be almost the same, for the same total reduction in area. The contribution of C_3 to the total heat losses is very small and any difference in the total land areas in the dies will have a negligible effect. The values of C_2 and C_3 depend on the surface areas of the deformation zone and these will depend on the shape of the extrude. The difficulty in measuring the size of the deformation zone has already been recognized. The dead metal zone surface area, which controls the value of C_3, will not differ from the axisymmetric surface area to a significant amount. The surface area, involving C_2, will differ but again the extent of the difference will not have a large effect on the heat losses. For these reasons the use of the single hole axisymmetric temperature rise for the multi-hole experiments should not involve any sizable error.

5.5.3. The Strain Rate.

The strain rates used were calculated according to the method suggested by Feltham. Other definitions were given in Chapter One. All of these involved the calculation of a mean value and assumed homogenous deformation. The instantaneous strain rate will differ

throughout the deformation zone and each element of material will have a complex history of changing strain rate before being extruded. The values of the strain rate will depend on the stream line followed. It is possible to measure the strain rate at any point by the visioplastic method, which involves a laborious experimental technique, or to gain an approximation to the strain rate distribution from the upper bound solution. If s is the velocity of an element of material normal to a velocity discontinuity and u is the velocity along the discontinuity the strain is

$$\dot{\varepsilon} = \frac{u}{s}$$

The strain rate can then be obtained by considering the time taken to extrude a unit volume of material of unit area past each discontinuity. This unit volume is moving at a speed V normal to the discontinuity. Therefore the strain rate at each discontinuity is

$$\dot{\varepsilon} = uV \qquad 5.2$$

The mean strain rate can be obtained from the strain rates at each discontinuity. Obviously the strain rate given by this approach will be a function of the complexity of the upper bound solution used.

These different methods will still only give a mean strain rate. There does not appear to be any reason to justify the use of the more complex approaches when the relatively simple approach of Feltham gives a working value. The strain rates given in the appendix increase with the reduction ratio and the overall strain, at a given ram speed, as expected. The variation in strain rate throughout the deformation zone will increase as the flow becomes more complex. An effect that will be dependent on the shape of the product Feltham's approach cannot allow for this and there is no model as yet that can be applied to such problems.

5.5.4. Extrusion as a Hot Working Process.

The same activation energy was used for all the alloys, 160,000 joules/mole, for the reasons discussed in section 5.3 . The linear relationships obtained between log Z and the flow stress suggest that extrusion involves working in the higher flow stress

region of hot working and that equation 4.1.

$$Z = A_4 \exp \beta_1 \sigma \qquad 4.1$$

can adequately describe the experimental results. The use of this equation simplifies the analysis of the results because equation 1.7 needs a value for α and this is almost impossible to obtain from experiments involving large deformations, such as those encountered in extrusion. Accurate and constant values of the strain rate and temperature are needed and these are not achieved.

Before equation 4.1 can be used, the temperature compensated strain rate is needed. The mean strain rate depends on the reduction ratio and the ram speed, the temperature depends on the flow stress, and the speed of extrusion, and is therefore related to the strain rate. Hence a complex interaction between the strain rate and the temperature is expected, the use of Z can only approximate to this. The calculated value will be a mean value based on the mean strain rate, and the mean temperature rise. If the correct value of the mean strain rate is given by the empirical expression used, assuming the mean flow stresses agree on a comparative basis, the graph of log Z against σ should give a linear relationship, or a curve if equation 4.1 does not apply to the range of flow stresses considered. What is seen is a series of almost parallel lines, each line corresponding to a different reduction ratio, figures 4.9-13. The results were made to fall onto one line by subtracting the average difference between log Z for the 60:1 single hole reduction and log Z for the other reductions, at the same flow stress, to give a corrected value log Zc. This correction uses the observation that the vertical spacing between the lines for the different reduction ratios appears to be independent of the material. The correction could equally as well be made to the flow stress. However it is accepted that the hot worked structure can be related to Z, in the steady state. Originally it was thought that the relationship involving Z might represent an equation of state, however, in the unsteady state region, the flowstress depends not only on the instantaneous values of the strain, strain rate, and temperature but on the previous test history or structure. In alloys A and B, a fibrous structure was seen in the 30:1 single hole reductions and an elongated or fully recrystallized structure in the 50:1 reductions.

A similar observation was made in alloys CE and DF with the tendency for a recrystallized structure increasing as the flow stress decreased, which corresponded to an increase in the reduction ratio. At a reduction of 100:1 the structures were completely recrystallized at all values of Z. A correction of the flow stress would require both recrystallized and fibrous structures at any particular value of Z. It is therefore suggested that the discrepencies are in the values of Z.

$$Z = \dot{\varepsilon} \exp \frac{Q}{RT}$$

Taking logarithms

$$\log Z = \log \dot{\varepsilon} + \frac{Q}{2{\cdot}303RT}$$

If the activation energy remains constant the correction factor must effect log $\dot{\varepsilon}$. However the magnitude of the correction factors range from -2.1 at an extrusion ratio of 100:1 to 2.9 at 30:1. These are logarithms and imply that there is an error of almost five orders of magnitude in the calculated strain rates over this range. In other words the calculated mean strain rate at 100:1 is over 100 times too high and at 30:1 it is almost 1000 times too low, leading to the conclusion that for a given ram speed the strain rate at a reduction of 30:1 is higher than that at 100:1. This is unlikely and therefore the discrepency probably lies in the exponental term, which is very sensitive to changes in the temperature or the activation energy. Without experimental verification of the temperature rise it is not possible to predict the size of any error. It is of interest to compare the values for the strain rate used with those predicted by an alternative approach. The maximum strain rates were calculated from the simple upper bound plane strain model and are given below for a ram speed

30:1 single hole $\dot{\varepsilon} = 22{\cdot}2\ V$

50:1 single hole $\dot{\varepsilon} = 37{\cdot}1\ V$

60:1 single hole $\dot{\varepsilon} = 49{\cdot}8\ V$

100:1 single hole $\dot{\varepsilon} = 68{\cdot}4\ V$

These strain rates are approximately 15-16 times the values used appendix , but the general trend is the same with the strain rate increasing with the reduction ratio for a given ram speed, and

therefore the error probably does not lie in the method used to calculate the mean strain rate.

Although it is not possible to say where the error lies, the use of the correction factors can be justified on the grounds that the same factor can be applied regardless of the alloy.

Accepting the use of these correction factors the values of β in equation 4.1 can be compared, table 4.11. The experimental values all agree in their order of magnitude. Surprisingly β for alloy DF is higher than that for alloy CE, the opposite was found for the constant β in equation 1.2. in the hot working tests. This is an effect of the temperature sensitivity of these alloys, equation 1.2 can only be applied at a constant temperature. Alloys 266D and 265D have almost identical values of A and β. They have an almost similar composition, 265D having a slightly higher magnesium content and 0.37% by weight of manganese. Equation 4.1 could not be applied to the range achieved in the hot torsion and tensile tests but the more general relationship

$$Z = A(\sinh \alpha\sigma)^n \qquad 1.7$$

gave a linear relationship.

Using the values of α, derived from the torsion and tensile data, the extrusion results could also be correlated with this expression, figures 4.18 -19. Comparing with the results from the hot-working tests there is a significant discrepancy. The trends are the same, alloy DF being less strain rate sensitive than alloy CE, and the orders of magnitude of Z and $\sinh \alpha\sigma$ are the same but the exponents n are much higher for the results from extrusion, approximately three times higher. Two reasons may be given for this and both underline the difficulties in comparing hot working data. No estimation of the temperature rise was attempted in the hot torsion and tensile data. This would lead to not insignificant errors in Z. The gradient of the graph will decrease if the temperature rise is included, as the errors in the temperature will be greater at the lower temperatures, the discrepancy would therefore increase and so there must be some other reasons for the observed difference.

The value of the activation energy used will depend on whether the temperature rise is included or not. Gagnon found a 20% discrepancy between the activation energy calculated from the initial billet temperature, and that from the working temperature, in the extrusion of zinc. However the accuracy of the work is open to question. The flow stress was calculated using the approximate method developed by Wong and only one extrusion ratio was used. The results obtained in the present work show that the empirical constants derived will depend on the extrusion ratio. The temperature rise was calculated from the theory derived by Singer. Raybould proved that this theory leads to serious errors.

The value of α is calculated from

$$\alpha = \frac{n_1}{\beta}$$

and n_1 and β are found from the gradients of graphs plotted at a constant temperature. If the temperature rise is allowed for then the gradients will change, assuming enough results at the the same temperature have been obtained. This can only be achieved with a prior knowledge of Z, α, n_1, and σ. The only solution to this problem of obtaining results at a constant temperature is to plot a three dimensional graph of $\dot{\epsilon}$, σ, T . If enough points are obtained the values of the strain rate and flow stress can be obtained at a constant temperature from the surface.

The extrusion results were correlated using the same values of α, and activation energy, but included an estimation of the temperature rise. It is therefore not surprising that a large discrepancy is seen between the two sets of data.

5.5.5 A Summary of the Application of Hot Working Theory.

Both extrusion and the laboratory testing techniques can be correlated with the empirical hot working equation, but it is not possible to combine the two sets of data, using present theory. The values of β in equation 4.1 depend only on the alloy used but the constant A, which can be related to the theoretical structure factor, will depend on the method of calculating the strain rate. Using Feltham's approach it is possible to apply correction factors to the data but, as an arbitrary datum line is used, the derived values

of A for different alloys can only be compared on a relative basis and must not be assumed to be accurate values. More important is the conclusion that the values cannot be compared with those obtained fromother data. It would beuseful exercise to compare the different values for these constants obtained from the wide range of testing techniques available. Most of the previous work on extrusion has either ignored the temperature rise or studied a limited range of reduction ratios, usually one or both. The results have then been compared with those obtained from data obtained by torsion, compression and other testing methods. By using only one or two extrusion ratios the range of Z studied is very limited. If the temperature range extends below $0.5\,T_m$ the activation energy reduces because the rate controlling mechanism changes below the hot working range. Therefore the temperature range further limits the number of results that can be obtained. Any conclusion drawn from such results can only be applied to similar experimental conditions and cannot be compared with other measurements.

The effect of neglecting the temperature rise in the present work can be seen in figures 5.3 and 5.4 , for alloys CE and DF respectively. Only the results for the 60:1 single hole extrusion are shown and Z was calculated using the initial billet temperature. It is evident that the value of n , the measure of the dependence of the stress on the strain rate increases if the temperature rise is ignored, a similar observation was found by Raybould although the value of n found was about five times less. The results for extrusion agree with those for torsion in that alloy DF is less strain rate sensitive than is CE. Comparing the values of n for the two sets of results, in the hot torsion and tensile tests

$$\frac{n_{DF}}{n_{CE}} = 2$$

for extrusion

$$\frac{n_{DF}}{n_{CE}} = 1{\cdot}86$$

Within the experimental error the strain rate sensitivity of alloy CE is twice that of alloy DF. This is a direct result of the compositional and structural differances between the two alloys. In alloy DF the presence of the precipitate will hinder dislocation movement and this will decrease the strain rate sensitivity. On the

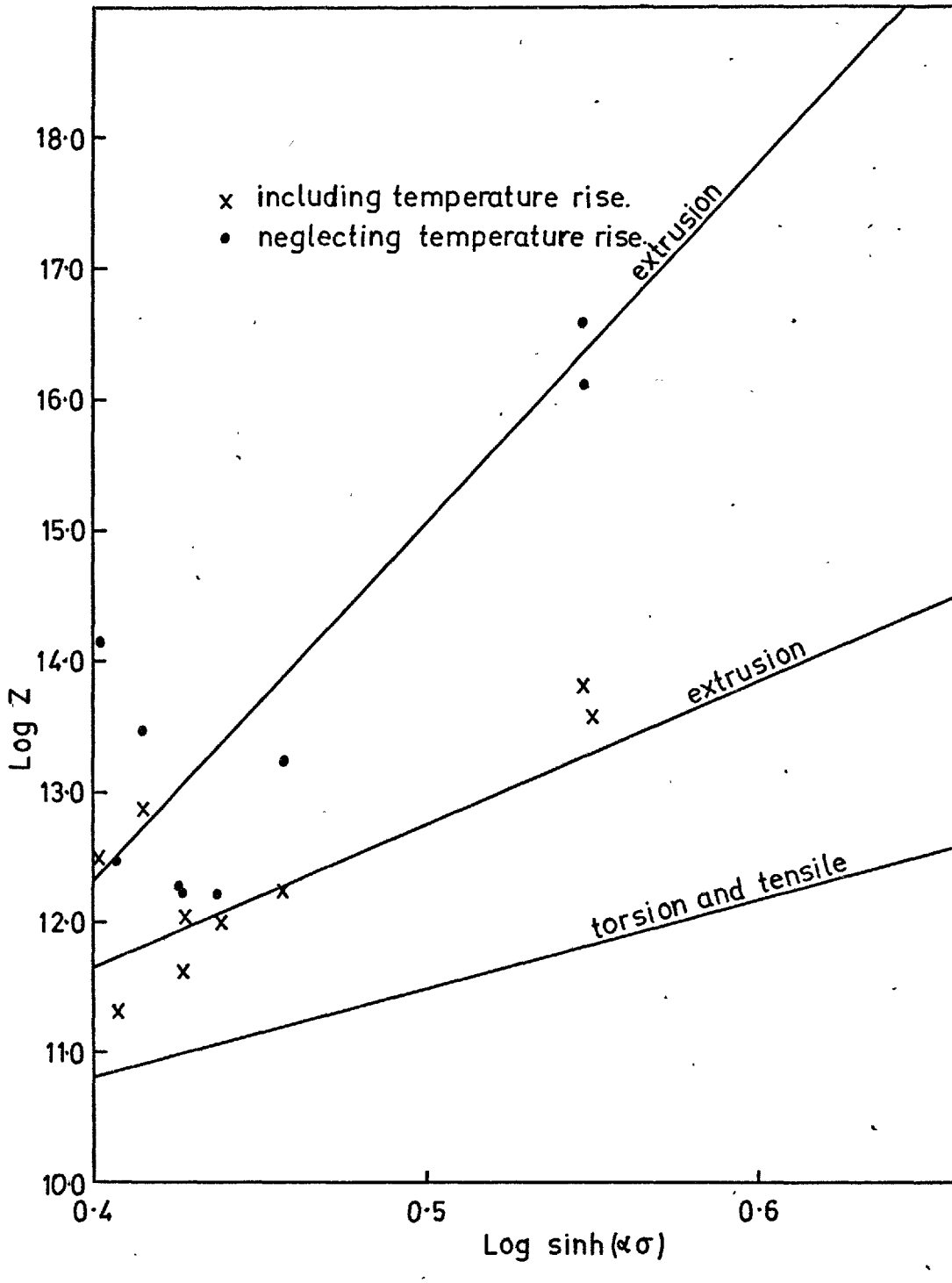


Fig.5·3 The effect of neglecting T in the extrusion of alloy CE. 60:1 single hole.

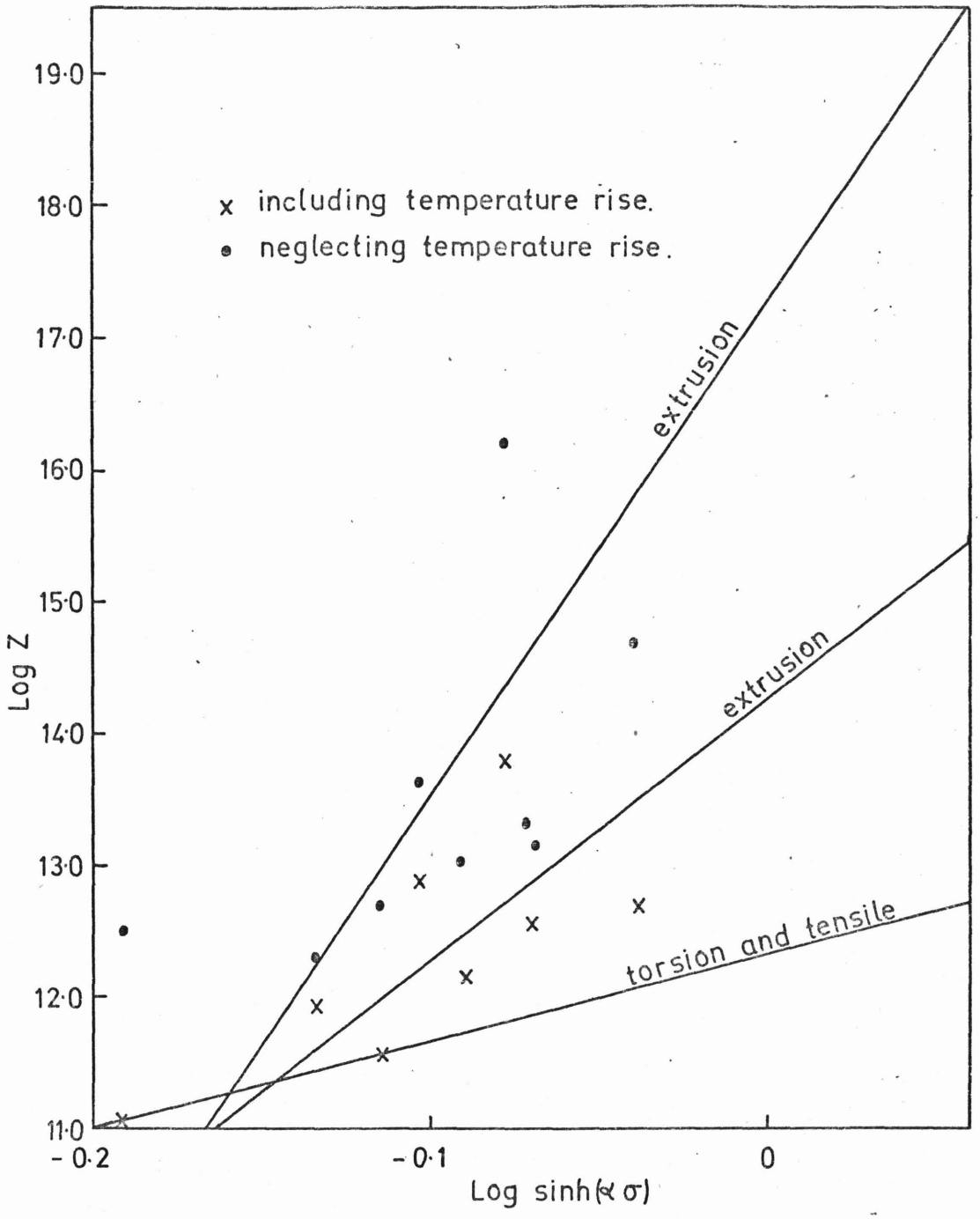


Fig.5·4 The effect of neglecting ΔT in the extrusion of alloy DF. 60:1 single hole.

other hand the flow stress at a given value of the strain rate is higher in alloy CE and this is a result of the extra solute present in the solid solution found in this alloy.

5. 6 The Peak Load Developed During Extrusion.

Over a wide range of reduction ratios there is a linear relationship between the load at the start of extrusion, Lp and log R. The exact relationship will depend on the alloy but the two studied, CE and DF, had almost the same gradient but different values for the intercept, suggesting that in alloy CE, the almost complete solid solution was stiffer than alloy DF, which initially contained a uniform distribution of precipitates. This linear relationship is of major practical importance in the effecient design and use of presses. The independence of Lp on the ram speed, figure 4.23 , is in contrast to hot working theories where an increase in the strain rate leads to an increase in the load. The ram speed is directly related to the strain rate. Pearson quotes the equation

$$V = bP^a$$

to relate the ram speed to the pressure. The values of (a) are alloy dependent and are very low. Over the experimental range studied the validity of the expression could not be verified although (a) must have been extremely small.

There are several possibilities to account for this unexpected linear dependence. At the start of deformation the billet must be upset to the shape of the container and, as shown later, at the same time some extrusion occurs. There will also be complex structural changes taking place. The net effect is non uniform deformation with a continually varying strainrate, i.e. non steady state condition. At the same time the temperature will be rising, and the flow stress is very sensitive to changes in the temperature. The overall effect must be that the mean temperature compensated strain rate is almost a constant during this initial period. By taking the logarithm Z the strain rate and temperature factors can be separated. Figures 4.21,22 show the dependence of the initial load on the initial billet temperature, the almost linear relationship does not give any insight into the controlling mechanism, other than demonstrating the effect of an increase in temperature on the ease of dislocation movement.

The experimental results could be correlated with both the linear dependence given by Ashcroft and Lawson[156] and the equation

$$P = Ae^{-\lambda T}$$

quoted by Pearson. The value of λ being of the order of 0.0064 in aluminium alloys. Plotting log exp Q/RT, assuming an activation energy of 160,000 joules/mole, against the peak load gives a linear relationship, when the temperature rise is included. The experimental scatter is high but a linear relationship is suggested. The equation of the lines is

$$Lp = A + m\log_e \frac{Q}{RT} = A + \frac{m}{2{\cdot}303}\ \frac{Q}{RT}$$

rewriting

$$\frac{Q}{RT} = -\frac{2{\cdot}303}{m}A + \frac{2{\cdot}303}{m}Lp$$

which can be compared with equation 4.1

$$\log Z = \log A + \frac{2{\cdot}303}{m}Lp \quad \text{or} \quad \log \dot{\varepsilon} + \frac{Q}{RT} = 2{\cdot}303\log A + \beta\sigma$$

the values of β for extrusion can be compared with values of $2.303/m$

for alloy A $\frac{2{\cdot}303}{m} = 1{\cdot}77MN^{-1}$

for alloy CE $\frac{2{\cdot}303}{m} = 2{\cdot}98MN^{-1}$

for alloy B $\frac{2{\cdot}303}{m} = 2{\cdot}06MN^{-1}$

for alloy DF $\frac{2{\cdot}303}{m} = 3{\cdot}29MN^{-1}$

Again the differences between the two groups of alloy are emphasized. The difference between alloy A and alloy CE, and alloy B and DF, show the significant effect of the presence of the usual impurities of Fe and Si. In this form a direct comparison between β and m cannot be made, the former has the units of mm^2/N, the latter MN. However the ratios of the constants can be compared, if Lp was converted to the pressure or even the flow stress the numerical value of m would not change but the units would become mm^2/N, agreeing with those of β.

For alloys CE and DF

$$\frac{M_{CE}}{M_{DF}} = 1.12$$

and

$$\frac{\beta_{DF}}{\beta_{CE}} = 1.25$$

For A and B

$$\frac{m_A}{m_B} = 1.16$$

$$\frac{\beta_B}{\beta_A} = 1.24$$

The suffixes referring to the alloys.

The constants can be considered to be representative of the same value, to an accuracy of 6%. This marked similarity suggests that the same hot working mechanisms are in operation at the peak load, as well as during the so called steady state region, and the linear dependence of Lp on loge $\frac{Q}{RT}$ indicates the operation of a thermally activated process.

5.7 The Height of the Peak at the Start of Extrusion.

Comparing figures 4.21-23 &29-31 the peak height ΔL and the peak load Lp have a similar dependence on the variables of the ram speed, and billet temperature, i.e. the higher the magnitude of the maximum load then the greater is the peak height, which can represent a significant part of the overall load. The load to extrude a billet is made up of the load required to deform the metal in the deformation zone adjacent to the die orifice plus the load to get the material into the deformation zone, i.e. the load to overcome the friction between the billet surface and the container. As the billet length decreases the load will correspondingly decrease and this is the usual explanation given to the alomost linear decrease in the load throughout extrusion. The sum of this extrusion load can be represented by LE and empirical expression of the type

$$\frac{P}{\bar{Y}} = (a + b\ln R)\exp\frac{4\psi L_B}{D_B}$$

are often quoted in calculating this value.

However the load to initiate extrusion is usually higher than LE by an amount ΔL that is a peak in the load displacement curve is observed. Figures4.32-36 show the dependence on the relative magnitude of ΔL on LE, which is given by Lp- ΔL. There is almost a linear correlation and figure4.36 for alloys 266D, 265D, and 272D, indicate that ΔL also depends on the alloy composition. The graphs for the other alloys are almost indentical with no peak below about 2MN rising to almost 16% of the extrusion load at 4MN. If the peak is only an inertia effect of the press it would have passed through the origin, i.e. at zero load there would be no peak load and as the load increases the peak would increase with a linear relationship. The experimental observation of no peak being found for L_E below 2MN precludes this effect. Another possible source of the peak is the increased flow stress caused by the billet cooling at the front end, the heat losses occurring to the cooler container. This is more serious in the hot extrusion of steel or other high temperature metals.

The effect of this cooling was eliminated by heating a billet in the container overnight and thenextruding. The billet container and tooling would have all been at the same temperature but a substantial peak was still seen. Its magnitude agreed with the other data obtained.

The peak must therefore be related to the deformation mechanism of the material at the start of extrusion and, before any suggestion can be made to its cause, it is necessary to examine the structural changes at the start of extrusion.

5.8 The Development of the Flow Pattern at the Start of Extrusion.

In figure 5.5 the flow patterns seen at different stages of the load displacement curve for a 60:1 reduction are given. No noticeable differences were found between the flow patterns for different alloys. In photograph (i) the billet has been almost completely upset to fill the container. The macro section is similar to that expected from a cast billet that has been slightly compressed with the columnar grains being clearly visible. At the top of the billet container interface is a region that has been subjected to a shear stress, this shear zone extends approximately half the length of the billet. This will be a direct effect of the removal of

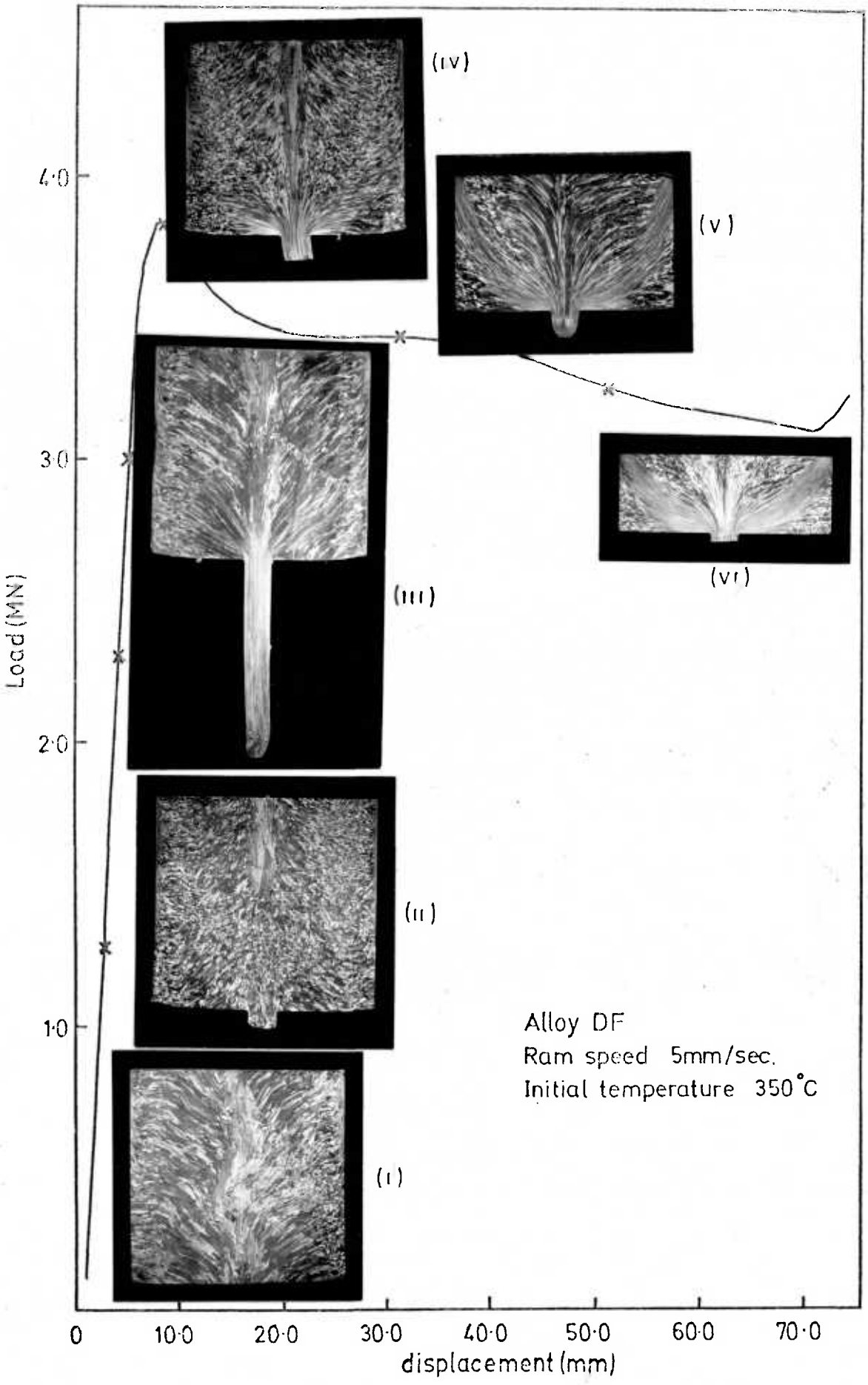


Fig. 5.5 The development of the flow pattern during extrusion.

the billet from the container, and shows that upsetting is not complete, which would be indicated by a shear zone running almost the full length of the billet. Photograph (ii) is at a slightly later stage. The load has been increased but there has only been a slight increase in the ram displacement. A very small amount of material has been pushed through the die orifice but there is no trace of the typical extrusion flow pattern. The shear zone down the sides of the billet extends to three quarters of its length. At a higher load still, but before the peak load is reached. photograph (iii), some material has already been extruded and shows a heavily worked fibrous structure extending almost to the front of the extrude. The shear zone again extends to about three quarters of the billet length and the start of a flow pattern can just be seen in the region surrounding the die orifice. The next flow pattern (iv) is taken at the peak load and can be compared to (iii). The length of the surface shear zone is the same and the extrude shows the heavily worked fibrous zone. The difference between the two is the extent of the formation of a true flow pattern. The dead metal zones can be clearly distinguished in the corners and the curved shear zone running from the point of exit, over the dead metal zone, to the shear zone at the side is just visible. Comparing with (i) the bulk of the billet has suffered very little deformation. Over the peak load the steady state region occurs and deformation proceeds at a uniform rate. Photographs (v) and (vi) are taken from different stages in the load deformation curve. The curved region of intense shear over the dead metal zones are very clearly defined, and are very similar in spite of the differing billet lengths. In (v) some flow is seen towards the central axis in the bulk of the billet. In (vi) shearing along the top of the billet is visible, suggesting some flow between the billet and the pressure pad. The net conclusion is that the peak load is associated with the formation of the steady state flow pattern and not with the upsetting of the billet or the start of extrusion, as is sometimes stated.

5. 9 Structural Changes Prior to the Peak Load.

In section 5.8 the macro structures at different stages of the load displacement curve were discussed. The flow patterns in (i) and (iii) were studied in more detail. Sections were taken from the regions given in figures5.6-7 and examined under the transmission

electron microscope. It is experimentally impossible to quench the billets immediately deformation ceases and consequently static restoration processes must be operating in the time taken to remove the billet from the container before quenching. The structure will therefore be a modified version of the true structure. Figure 5.8 shows the structures observed in (i) at a low magnification. The structures are very similar to those seen after homogenization, figure 5.1 but some variation is seen throughout the billet. The rapid billet heating achieved by the induction heater will have influenced the structure but this was not examined. In (c) and (d) the precipitates still have their original orientation with each other. In (a) and (b) they have been misorientated, showing that some significant deformation has taken place in this region.

This variation in structure is evidence to the inhomogenous deformation during the early stages of deformation, the location of (b) being close to the shear zone and (a) being near the axis. Micrograph (a) was similar to that seen in the specimen taken from the region adjacent to the die orifice. Figure 5.9 shows the same region at a higher magnification. In (d) the dislocation density is low but some precipitate dislocation interaction is seen, this corresponds to micrographs c and d in figure 5.10. In the areas where more deformation occured a much higher dislocation density is visible, (a), (b), and (c). The most interesting is (a), taken from the same region as (a) in figure 5.9 . The dislocations have started to outline cells with a relatively low internal dislocation density, the precipitates pinning these dislocation cells. These micrographs may be compared with those taken from flow pattern (iii), figures 5.10 and 5.11 , at low and high magnification respectively. Figure 5.10 , (a) and (d) are typical of the bulk structure and are very similar to those found in the previous billet section, with little evidence of deformation. Micrographs (b) and (c) were taken from the deformation zone surrounding the entrance to the die. In both of them subgrains can be seen but they are more clearly defined in (a), where the deformation would have been higher. The precipitates in (a) have been aligned and indicate the direction of flow in extrusion. Alignment is just starting in (b) and this marks the boundary of the deformation zone in the billet. At higher magnifications, figure 5.11, the dislocation structure can be examined, (a) and (b) represent the

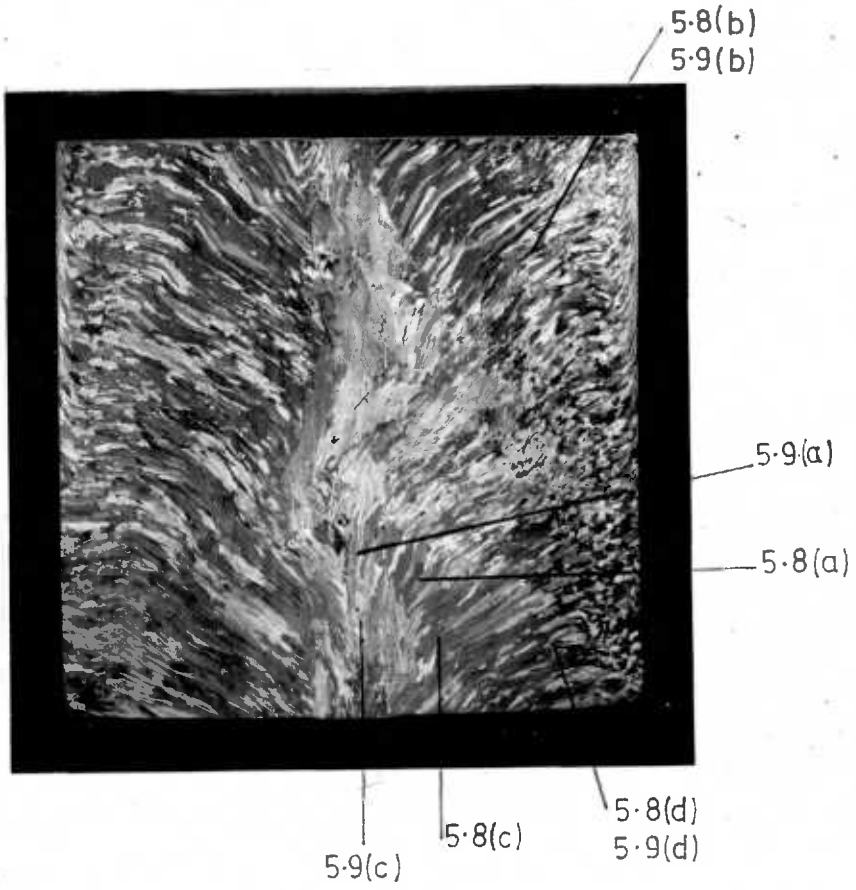


Fig 5.6 The location of the micrographs in figures 5.8 and 5.9
Alloy DF , 360 °C

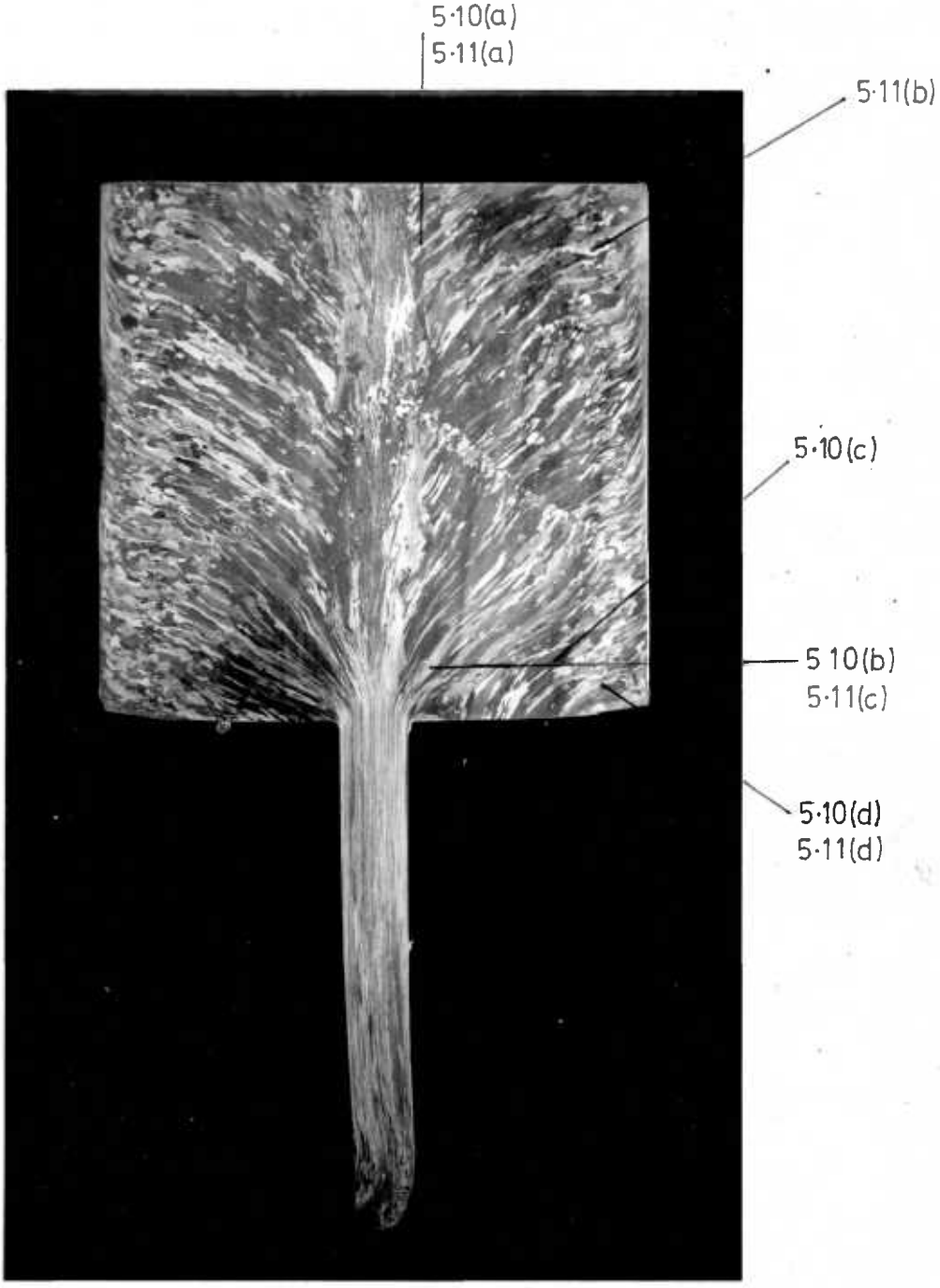


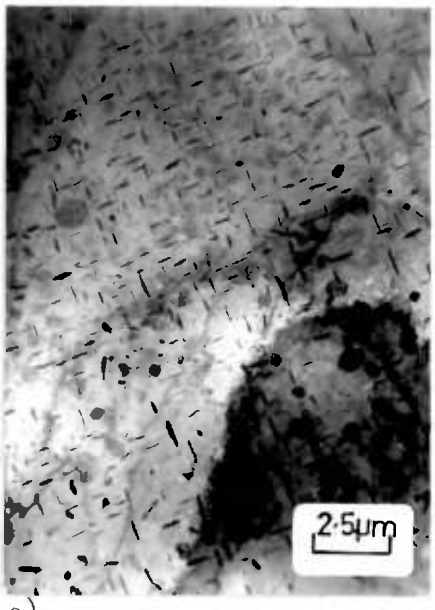
Fig 5.7 The location of the micrographs in figures 5.10 and 5.11
Alloy DF ,350 °C ,extrusion ratio 60:1, ram speed 5 mm/sec



a)



b)

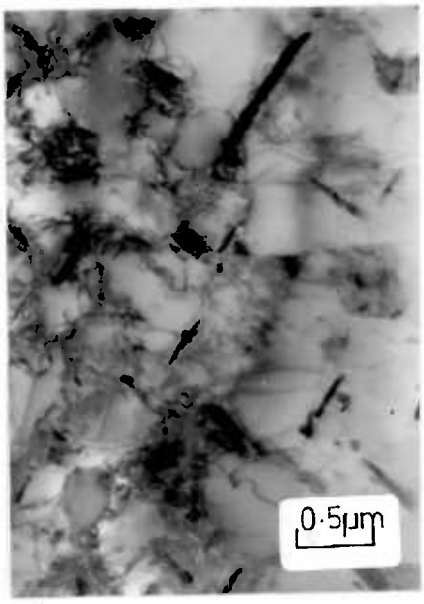


c)

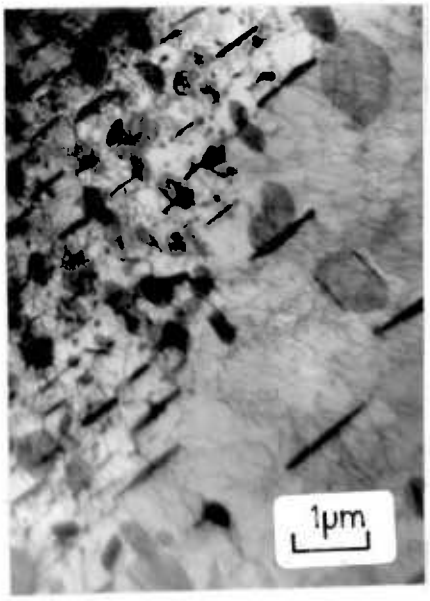


d)

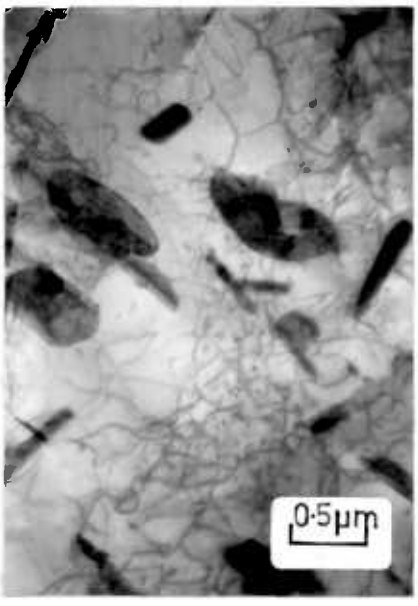
Fig 5.8 Transmission electron micrographs showing the structure immediately after the application of the load. Specimens taken from the billet in figures 5.6 and 5.5(i)



a)



b)



c)

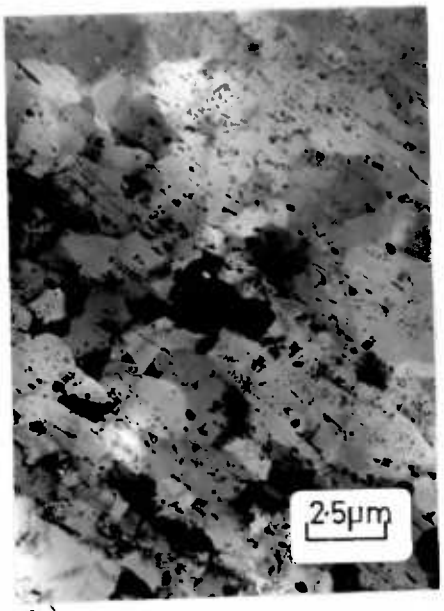


d)

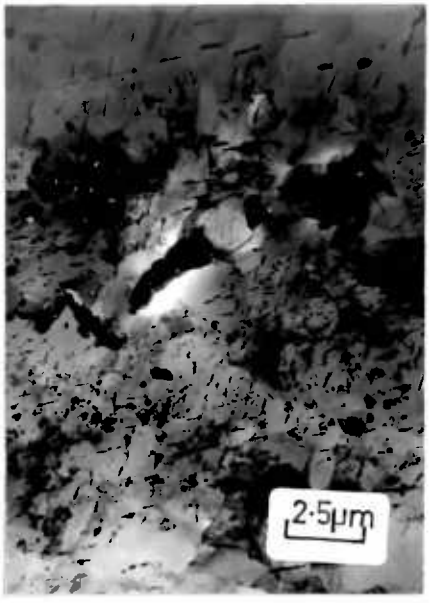
Fig 5.9 Transmission electron micrographs showing the structure immediately after the application of the load (higher magnification). Specimens taken from the billet in figures 5.6 and 5.5(i)



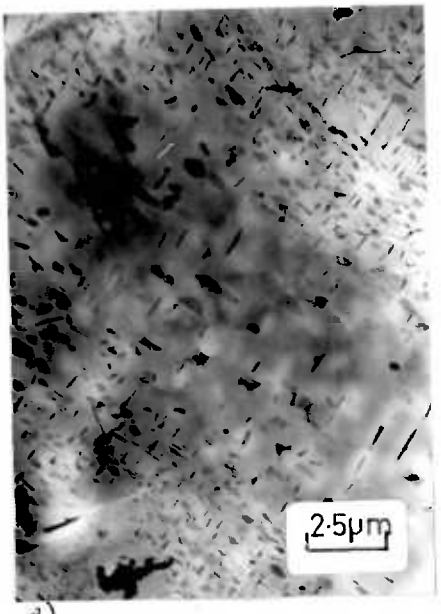
a)



b)

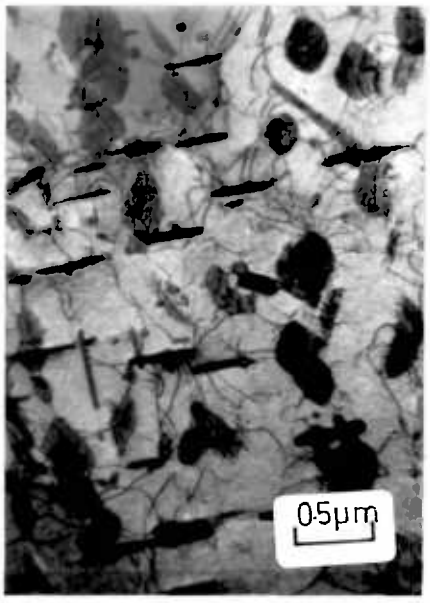


c)



d)

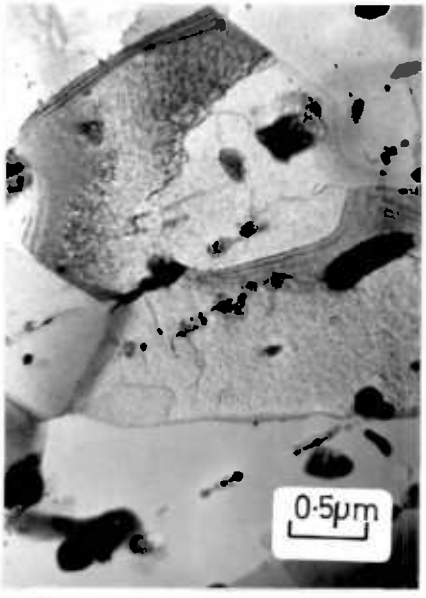
Fig 5.10 Transmission electron micrographs showing the structure at the start of extrusion. Specimens taken from the billet in figures 5.7 and 5.5(iii)



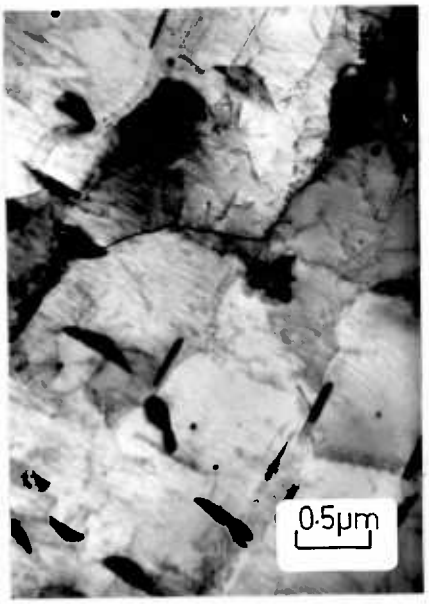
a)



b)



c)



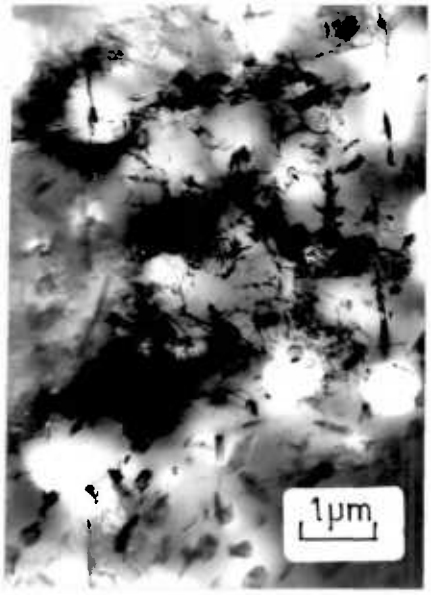
d)

Fig 5.11 Transmission electron micrographs showing the structure at the start of extrusion(higher magnification). Specimens taken from the billet in figures 5.6 and 5.5(iii)

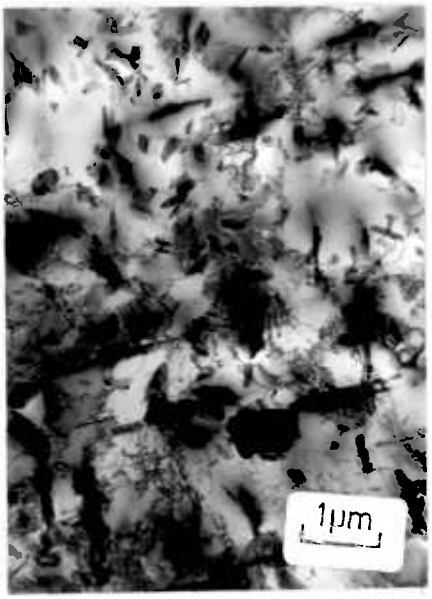
bulk of the material and a dislocation density similar to that found at the earlier stage in the deformation, figures 5.8-9 , can be seen. The precipitates play a significant role in pinning the dislocations. In the regions where more deformation was seen, near to the die, micrographs (c) and (d) are representative. Adjacent to the die orifice, agreeing with (b) figure 5.10 , a subgrain structure is well defined. The cells are almost dislocation free and the cell walls are not uniquely associated with the aligned precipitates, i.e. the cell size is larger than the inter precipitate spacing but some precipitates are still assocaited with the cell walls. In (d) there is no definite subgrain structure but a ragged dislocation cell structure is present. The walls of these cells consist of dislocation networks, seen in the bottom left hand corner, and the size of the cells appears to have some dependence on the spacing of the precipitates. Comparing (c) and (d) the precipitates act as barriers to dislocation motion at the start of deformation, they can also be dislocation sources and the cells that start to form are related to the spacing of the precipitates. As deformation continues the precipitates are elongated. There is a limit to the deformation that they can withstand, and eventually they break down into smaller particles. Their effectiveness in pinning the cell formation is then reduced and the subcells formed are not directly related to the inter precipitate spacing.

The micrographs discussed above were taken from a billet that would have extruded without any difficulty. A useful comparison can be made with the structure found in a sticker, i.e. a billet that required a load higher than the press capacity. Figure 5.12 shows micrographs taken from such a sticker in alloy 272D, the complex Al-Cu-Mg-Mn alloy. Also shown are the locations of these micrographs. A complex dislocation cell structure between the precipitates is seen in (a) and (b), showing that some deformation had occurred during upsetting, but no well defined subgrains are seen, even in the region close to the die entrance. Micrograph (c) was taken from the corner where the dead metal zones would be formed. The structure is almost dislocation free.

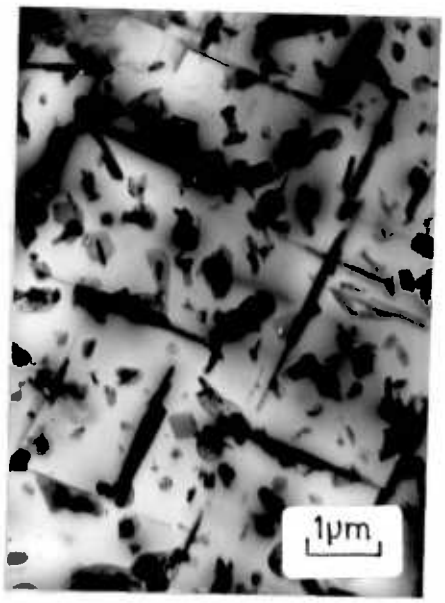
These micrographs may be compared with those published by Raybould and Sheppard for an Al 7% Zn alloy, figure 5.13 . This section was taken at a later stage of extrusion. Subgrains are seen throughout the deformation zone, except in the dead metal zone. In the area close to the die entrance the subgrains are aligned in the flow direction.



a)



b)



c)

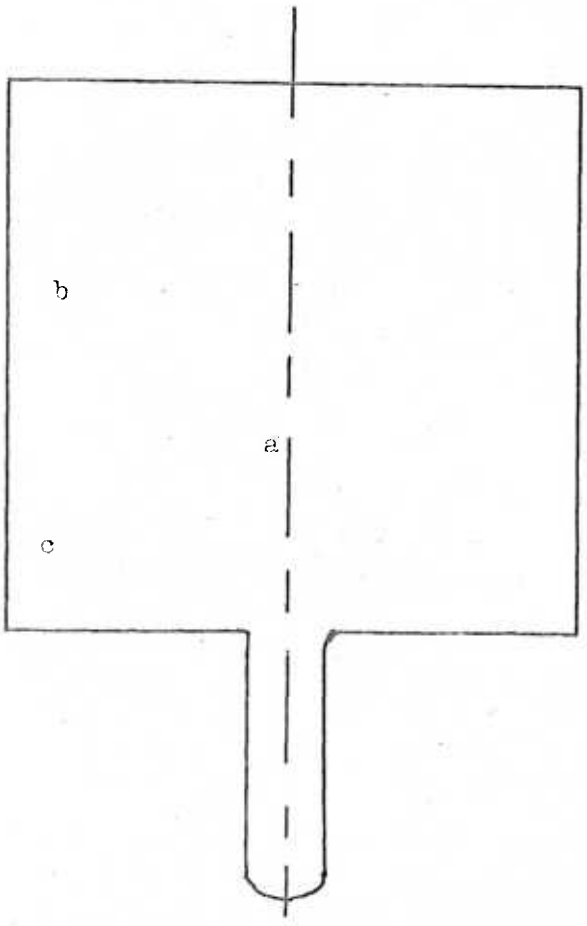


Fig 5.12 Transmission electron micrographs from a "sticker".
Alloy 272D, extrusion ratio 60:1, initial temperature 305°C

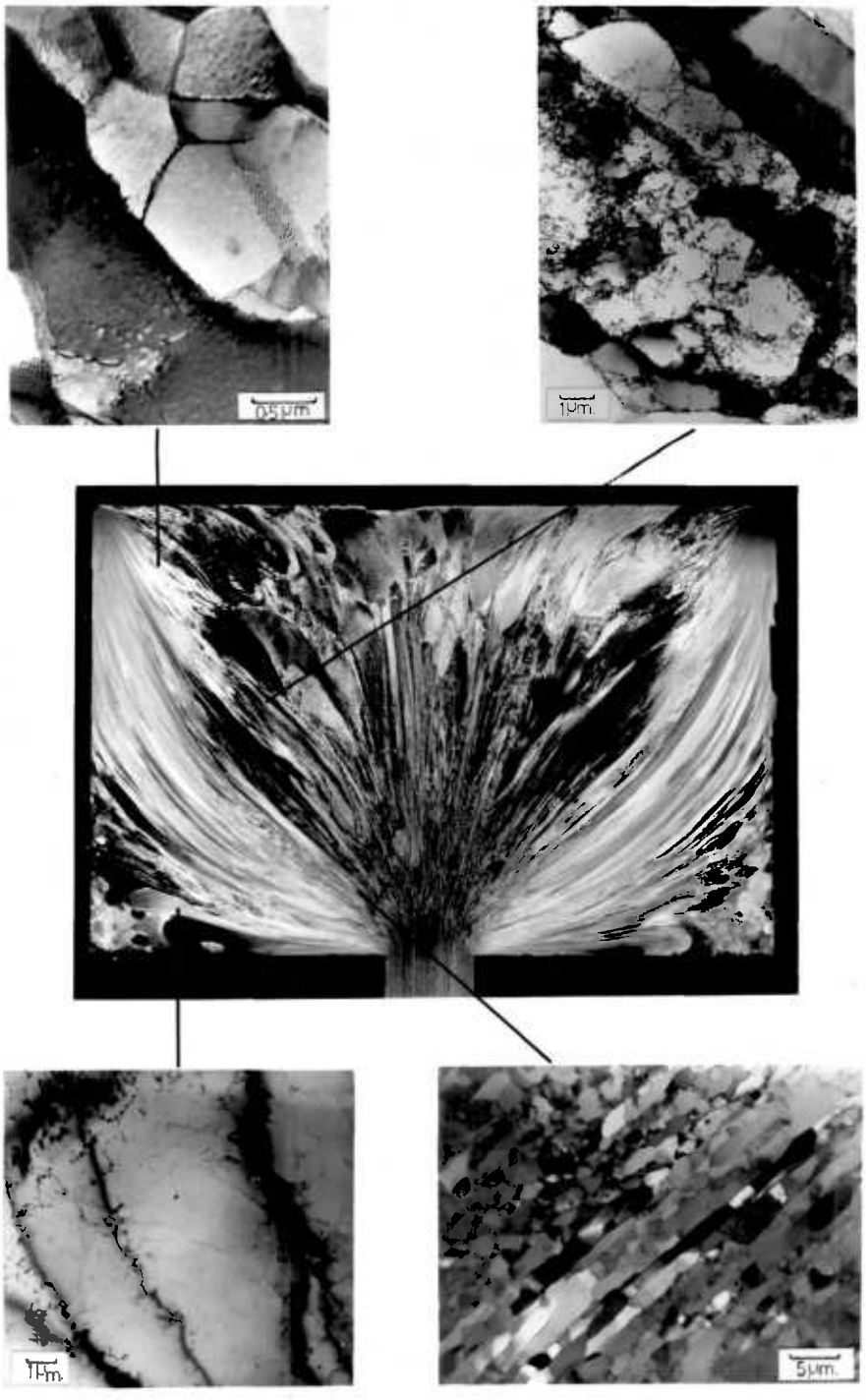


Fig 5.13 Micro-structure variation within the deformation zone
Al 7%Zn , log z/A = 4.60 , air cooled (from Raybould)

5. 9.1 A Summary of the Micro Structures Developed at the Start of Extrusion.

When the load is first applied the billet starts to deform and dislocation multiplication and migration occurs. These dislocations interact with each other and with the precipitates present. The presence of these dislocation inhibits the nucleation and movement of others, and this results in a net increase in the load required to continue deformation. Providing the press capacity is not exceeded, the applied load will increase and dislocation motion continues. In the bulk of the material deformation is halted by the restraint applied by the container and ram. Adjacent to the die the material can continue to deform by extrusion. The deformation undergone in this region must be intense, and to accomodate the strain a high dislocation density and rapid dislocation motion is needed. At these high densities the tendency is for cells to form, the walls consisting of the interacting dislocations and the interiors being almost dislocation free. The degree of perfection of these cells increases as the amount of deformation increases. As extrusion starts, which is before the peak load, the deformation region only extends back a short region into the billet. For extrusion to continue material must be able to flow into the deformation zone and the deformation zone therefore extends back into the billet, the load increasing accordingly. Eventually a stage is reached where extrusion can continue without any further extension of the deformation zone, the strain required in extrusion can be supplied by the number of dislocations being produced, and the peak load is reached. The rate of dislocation production causing the plastic flow has reached equilibrium and the load is a measure of the ease of dislocation formation/motion. Beyond the peak load the deformation proceeds at a uniform rate. Before a dislocation can move, enough energy has to be supplied to overcome the barriers to its motion, represented by the activation energy. The ease of overcoming this energy barrier will depend on the temperature expressed by the thermal activation term $\exp Q/RT$. At higher temperatures the dislocations are thermally assisted in overcoming these energy barriers and the load needed for the same deformation will be reduced. The correlation between $\exp Q/RT$ and Lp in figures 42528 show the validity of this explanation. The fall in load ΔL still has not been explained.

At high temperatures, above 0.5 T_m , dynamic restoration processes can occur and the rate of dislocation production is balanced by the rate of dislocation annihilation. The higher the temperature the easier it is for dislocation to intersect and annihilate each other, the number of barriers to dislocation motion is decreased and the rate of dislocation production can increase. A dislocation source will only operate if the dislocations that are formed can migrate away. Also once a dislocation has overcome the barrier it will require a lower stress to keep it moving, analagous to sticking and sliding friction. The fall in load is probably a combination of both the operation of an equilibrium dynamic restoration process and the ease of dislocation motion, after it has been initiated. It is not possible at the present time to predict a theoretical value of ΔL. At lower temperatures there is less tendency for a restored structure to be formed but the higher dislocation density will increase the difficulty of dislocation motion being initiated. Once started the acting stress will assist in the dislocation movement and a lower load will be needed to sustain this motion.

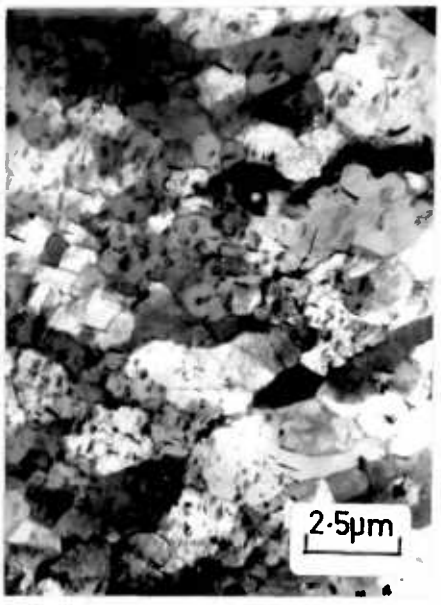
This qualitative explanation agrees with the observed micrograph and peak loads seen. The dependence of the peak load on the extrusion load will depend on the structure and composition, which controls the barriers to dislocation motion. Below a critical value of Lp a peak in the load curve does not occur. It is in this region that the energy supplied by thermal activation minimises the effectiveness of the dislocation barriers. No explanation can be given to Ashcroft and Lawson's observation of a peak occurring above a certain temperature, the possibility of a phase change cannot be excluded.

5. 10 The Structure at the Front of the Extrude.

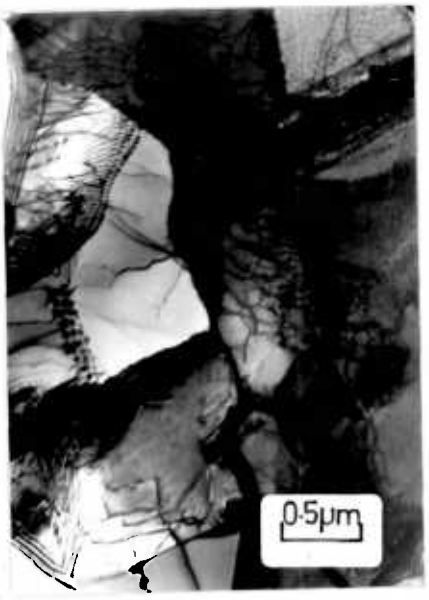
It is usually claimed that the front end of an extrusion consists of almost as-cast material, pushed through the die, with very little deformation. The previous sections confirm that extrusion starts before the peak load, and that the extrude at this early stage has the typical heavily worked fibrous structure found in many hot worked metals. This clearly demonstrates that sufficient deformation occurs to radically effect the homogenized structure, even at the vary start of extrusion. The extrusion ratio will obviously have some effect

because all of the critical deformation is in the shear at the edge of the die entrance, and if the diameter of the rod is relatively large the centre will suffer very little deformation.

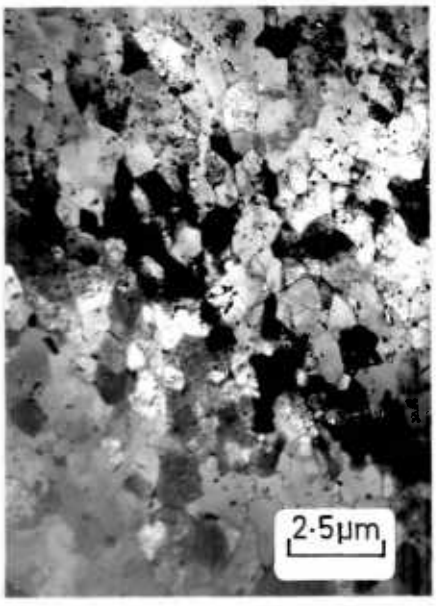
Figures 5.14 and 5.15 show transmision electron micrographs taken from the front end of two extrusions. In the first alloy DF extruded at a reduction ratio of 60:1, a substructure is seen at a distance of only 5mm from the very front of the extrusion, micrographs (a), (b) shows the same region at a higher magnification. A complex cell structure which is only found at strains approaching unity, is seen, with networks of dislocations and dislocation free regions. The micrographs are transverse sections and in (a) some of the precipitates still retain their original orientation with each other. In (b) the substructure is more defined indicating higher strain, although dislocations are still present in some of the cells. The precipitates do not have any orientation with each other in the transverse plane. The precipitates seen will be sections of the long rods that will be aligned in the extrusion direction, discussed later. Micrograph (d) is taken 8cm from the front of the extrude, but will have been extruded before the peak load. The substructure has improved in definition still more, and the subgrain walls have reached a high degree of perfection. Associated with the subgrain region are two grains with a high angle boundary between them, indicated by the difference in contrast, and no subgrains are seen in this region. Examination at a higher magnification revealed narrow well defined subgrain boundaries with a very low dislocation density region in between. Similar structures are seen in figure 5.15 , for the relatively softer alloy 265D, also extruded at a reduction of 60:1. In (a) and (b) the structure found 5mm from the front of extrusion is depicted. A cell structure is seen with ragged walls of intersecting dislocations surrounding dislocation free regions. At a higher magnification the nature of the walls can be seen in greater detail. The boundaries have a very high dislocation density, and these dislocations have lowered their energy by combining into networks. The network structure seen in the interior of the cells is generally recognised to be a polishing artefact, although there must be an explanation for its similarity to the observed dislocation networks. Further along the extrude, (c) and (d), the cell walls



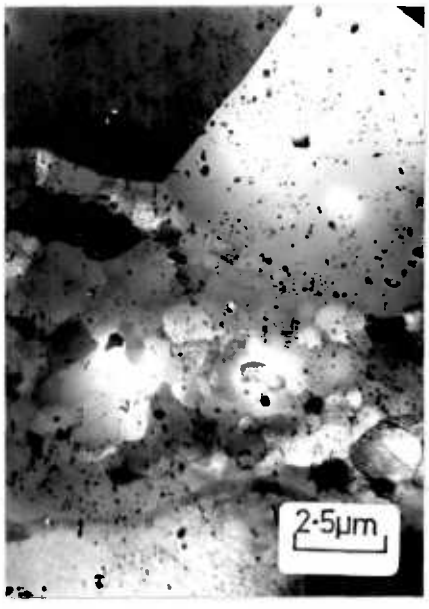
a) 5mm from the front



b) 5mm from the front

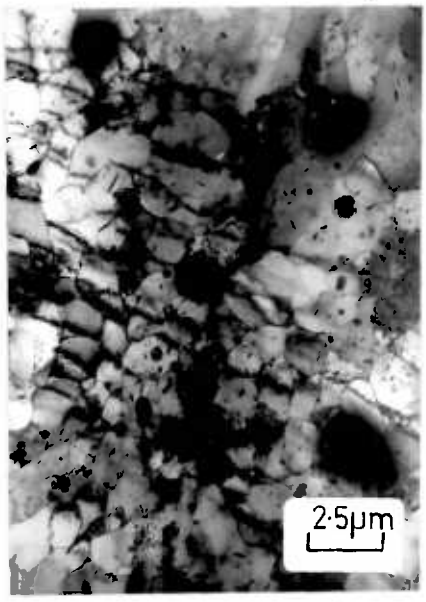


c) 35mm from the front

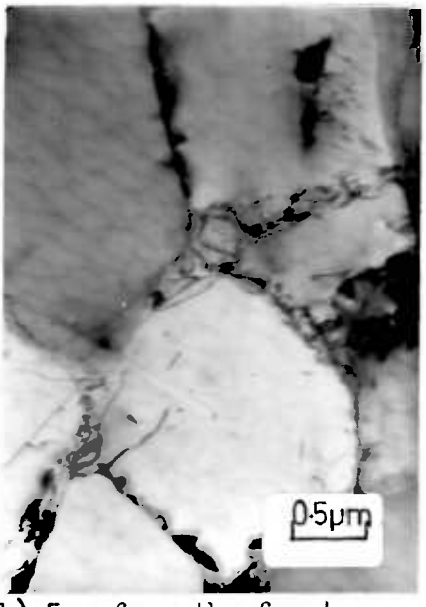


d) 80mm from the front

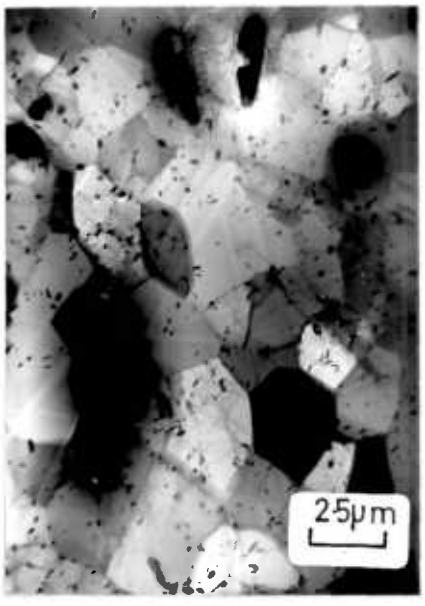
Fig 5.14 Transmission electron micrographs of the structure at the start of extrusion. Alloy DF, extrusion ratio 60:1 single, initial temperature 350°C, ram speed 5mm sec^{-1}



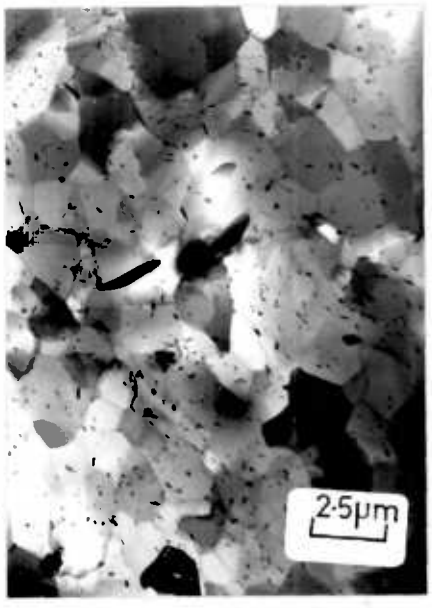
a) 5mm from the front



b) 5mm from the front



c) 120 mm from the front



d) 165 mm from the front

Fig 5.15 Transmission electron micgographs of the structure at the start of extrusion. Alloy 265D ,extrusion ratio 60:1 single, initial temperature 330°C, ram speed 9.5 mm sec^{-1}

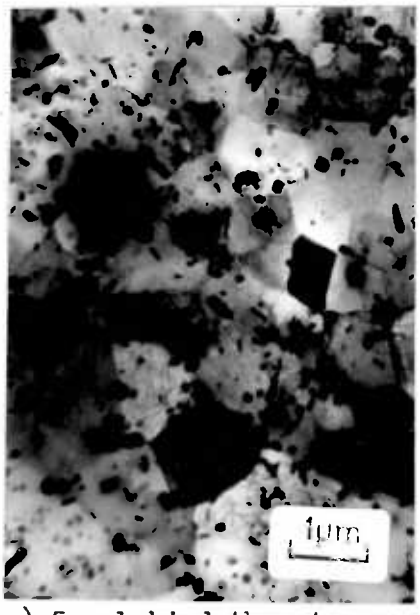
have increased in perfection and well defined subgrains are seen, the size of these subgrains being slightly higher than the cell size in figure 5.14, a direct effect of the difference in the resistance to dislocation movement between the two alloys.

These results agree with those observed in the development of the flow pattern, section 5.9, but in this case the structure is more representative of the true deformation structure. Within the region of the die entrance some deformation occurs relatively early in the cycle. The strains reached are high enough for the dislocations causing the strain to form into a cellular network, As the deformation zone starts to form the elements of material have to suffer a higher degree of deformation before passing through the die, this is reflected in the formation of the subgrains found at a short distance from the very front of the extrude.

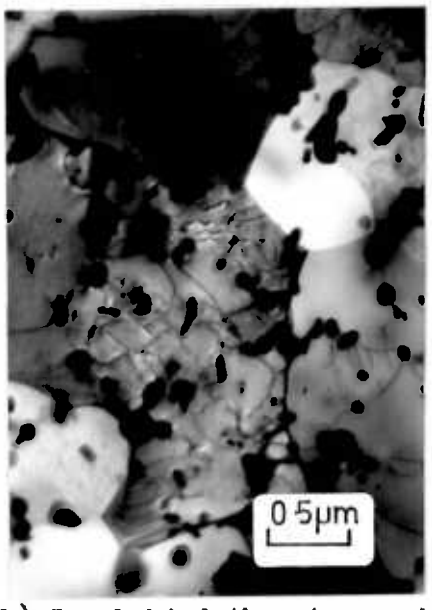
5.11 The Effect of the Removal and Reapplication of the Load During Extrusion.

Two different effects were noticed when the applied load was reduced during an extrusion run. When the load was removed completely and reapplied almost instantaneously, the load instead of returning to its original position, exhibited a peak similar to that seen at the vary start of the extrusion, however, the height of this peak was always greater than the initial one. If the load was only lowered and then reapplied a slight peak was again seen, but this time the peak load was less than the initial one and the load displacement curve followed the expected extension of the original curve, figures 4.37 &4.38. The difficulty in achieving this experimentally precluded any control over the magnitude of the load reduction. The hardness variation across the stop mark in the two cases is given in figures 4.52. The stop mark consists of a small ridge in the surface of the extrude. The reason for this mark is usually stated as being die deflection and relaxation on load removal. When the load was completely removed and reapplied a rise in the hardness occurred about 5mm, which is the length of the die land, behind the stop mark followed by a gradual fall. There was a slight fall in the hardness in front of the stop mark. The hardness variation in the extrude which had been subjected to only partial removal of the load, had a

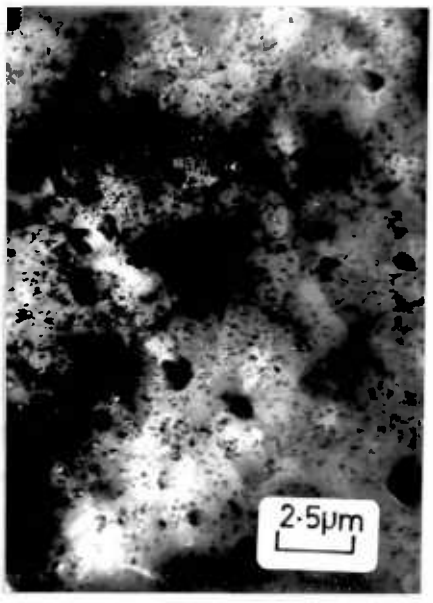
slight rise in the hardness behind the stop mark, these differences in hardness may be correlated with the structures found. In figure 5.16 transmission electron micrographs from either side of the stop mark in the first case are given. Both show regions of subgrains with well defined walls but the dislocation density is higher in that taken from behind the stop mark. A slight increase in the dislocation density in the region immediately behind the stop mark was also found in the second case, figure 5.17 . When the load is removed the tendency will be for static restoration processes to occur throughout the billet, whether they are recovery or recrystallization will depend on the magnitude of the stored energy which will be a function of the temperature and the strain rate. Both restoration processes result in some rearrangement and annihilation of dislocations. At the high deformation temperatures used these restoration processes will be extremely rapid. On reapplication of the load the dislocation density will have to increase before deformation can occur and a process akin to that at the start of extrusion will take place, with the load increasing until the rate of dislocation production and motion can satisfy the requirements of the strain and strain rate. This accounts for the observed peak but does not explain the higher peak, possibly the deformed structure after static restoration in the deformation zone, has more barriers to dislocation motion than the original homogenized structure, where there will be no regular sub-structure present at the start of deformation. When the load is only lowered there will still be a stress exerted on the dislocation and as a result they will be in a higher energy configuration than in the previous example. Some static restoration will occur but on reapplication of the load the dislocations acted upon by the stress willmove relatively easily and only a slight peak will be seen. Dislocationstend to pile up behind each other during deformation and their spacing is a function of the applied stress, the higher the stress the closer together are the dislocations. When the combined pressure exerted by these dislocations is high enough the barrier blocking their movement is overcome. The removal of the stress reduces the restraint acting on one side of the piled up dislocations and they separate to their equilibrium positions, similar to the coils of a compressed spring when the load is removed. Dislocations of thesame sign repel each other. Before deformation can occur the same



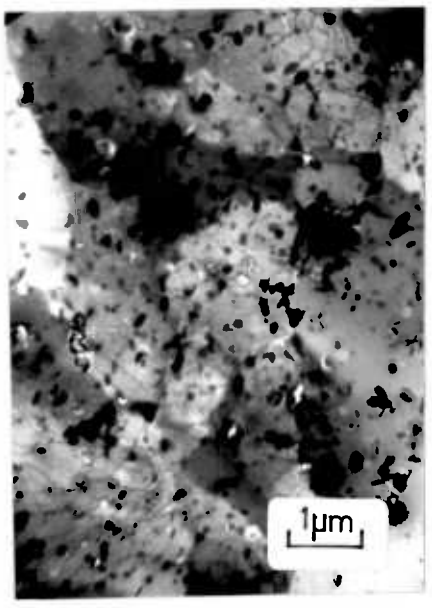
a) 5mm behind the stop mark



b) 5mm behind the stop mark

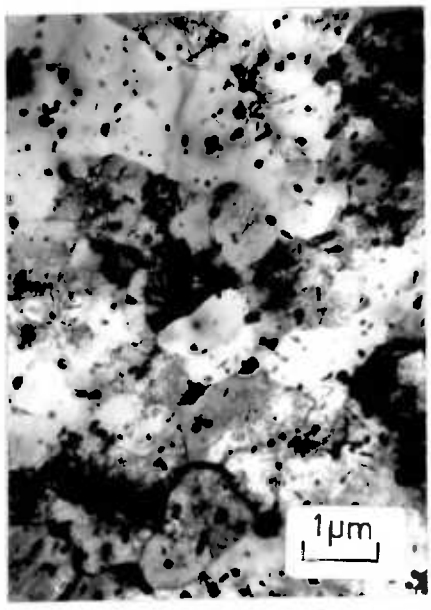


c) 5mm in front of the stop mark

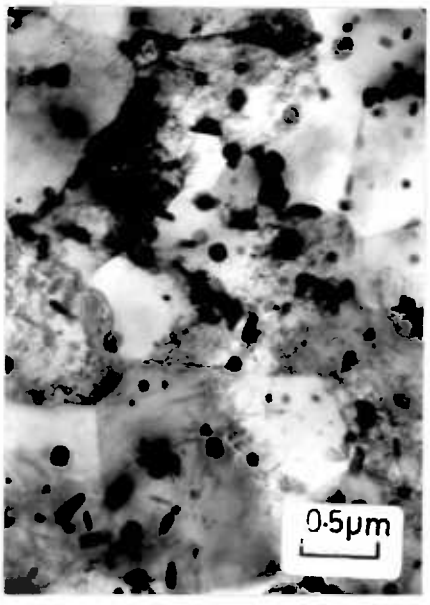


d) 5mm in front of the stop mark

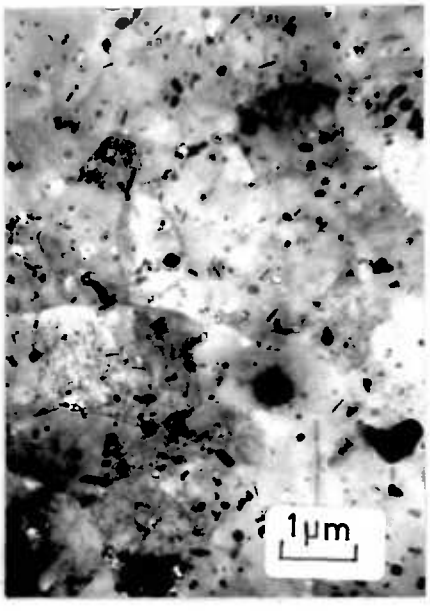
Fig 5.16 Transmission electron micrographs from either side of the stop mark, after complete load removal. Alloy272D extrusion ratio 60:1 single, initial temperature 350°C, ram speed 10.4 mm sec^{-1}



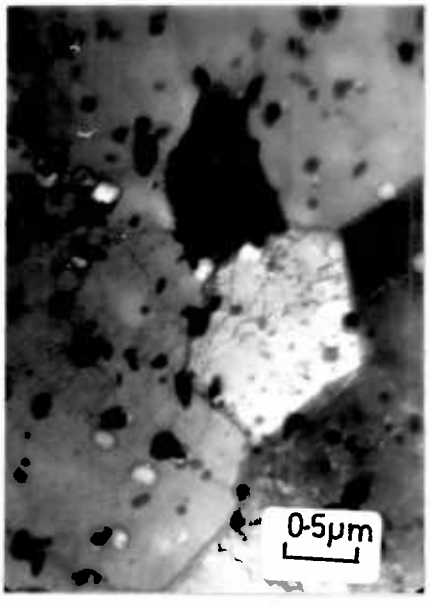
a) 5mm behind the stop mark



b) 5mm behind the stop mark



c) 5mm in front of the stop mark



d) 5mm in front of the stop mark

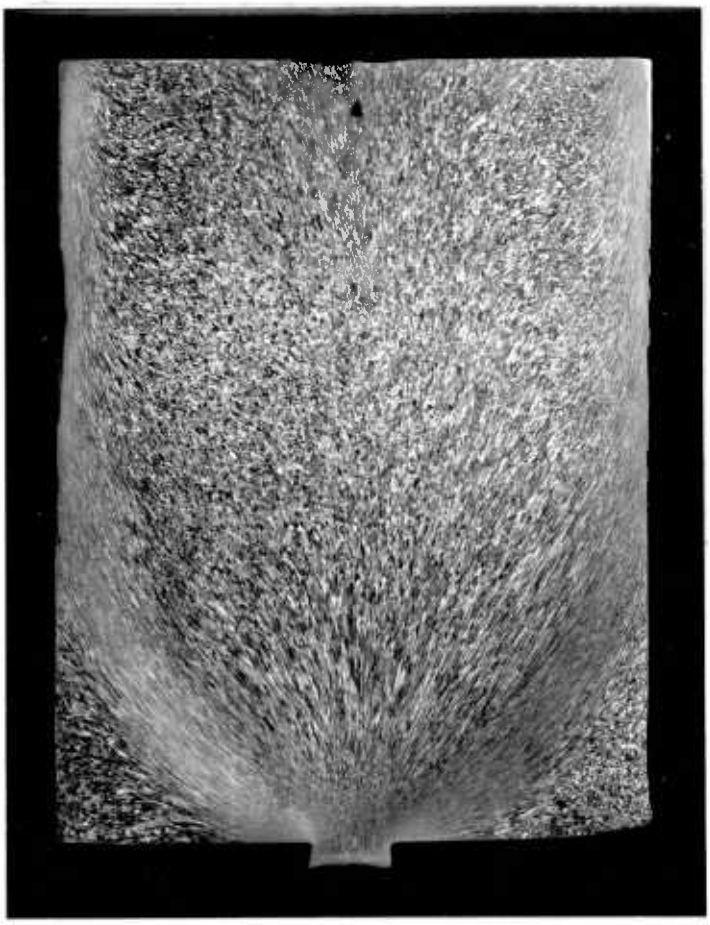
Fig 5.17 Transmission electron micrographs from either side of the stop mark, with only partial removal of the load. Alloy 272D, extrusion ratio 60:1 single, initial temperature 356°C, ram speed 7.3 mm sec^{-1}

dislocations have to be returned to their piled up configuration. The observed differences between the structures on either side of the stop line is a direct result of static restoration followed by deformation. In front of the stop mark, which corresponds to the exit from the die, static restoration is not followed by more deformation. Behind the stop mark some deformation must occur.

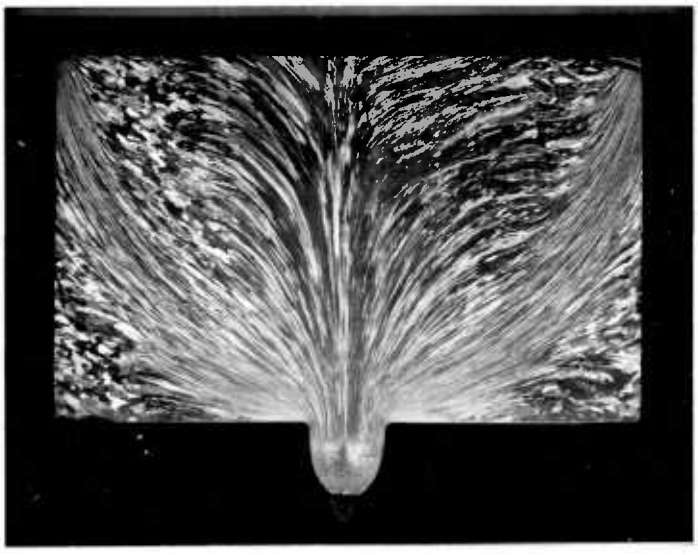
5. 12 The Effect of the Billet Length on the Flow Pattern and Load.

Flow patterns at different billet lengths are given in figure 5.18. The bottom two, (b) and (c), were from an original billet length of 75mm, (a) was from an initial length of 120mm. All three were taken well into the steady state region, where extrusion proceeded at a uniform rate. They all have well defined dead metal zones with a region of intense shesr directly above. (Macrographs (b) and (c) are also depicted in figure 5.5). In (a) there is a shear zone down the sides of the billet due to the friction between the billet and the container during extrusion. The depth of the shear zone is greater than that seen in the previous flow patterns, figure 5.6-7, and therefore cannot be due solely to the friction in the removal of the billet. This shear zone runs into the dead metal zone boundary shear region. At the back end of the billet no deformation has occurred and a fine grain homogenized structure is seen. No deformation on the macro scale can be observed until $\frac{2}{3}$ of the billet length from the back end. A comparison with (b) and (c) shows the boundaries to the deformation zone to be almost identical. From this it can be concluded that, for the flow pattern only, a steady state is reached, with the form of the boundary shear zones being independent of the billet length.

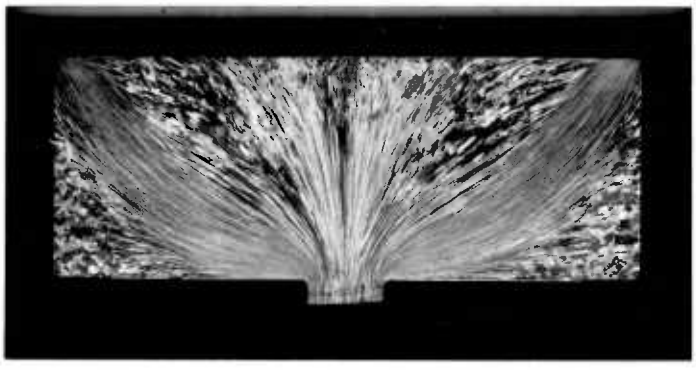
These results may be compared with the predicted flow patterns in figure 2.8. Below a billet length of 40mm the theoretical flow patterns calculated from a minimised plane strain analogue, agree very well with the experimental observations. The shape of the shear zones agree with the theoretical boundary lines. A slight difference is expected because the theory necessitates lines of velocity discontinuity, implying an infinite strain rate. In practise the shear zones have a finite width. Above a billet length of 40mm the theory predicts a much larger dead metal zone than is



a)



b)



c)

Fig 5.18 The effect of the billet length on the flow pattern
extrusion ratio 60:1

observed, the difference increasing with the billet length. A simple explanation is found in the selection of the rigid triangle velocity field used in this solution. A more complex pattern of discontinuities would be expected to give a better agreement, but the analysis would be involved. This approach to predicting flow patterns could be developed to the extrusion of solid shapes. Any vertical section through a shape can be likened to a plane strain extrusion with a displaced die exit. By calculating the flow pattern for each vertical section it should be possible to build up a model of the flow pattern and to compare it with that observed experimentally, accuracy will depend on the type of solution used. In figure 6.18a the flow pattern predicted by the simple plane strain theory shows only very approximate agreement with the experimental one, the location of the dead metal zone boundaries are similar but, by reason of its simplicity this solution is not capable of predicting the rest of the deformation field.

Billets of different lengths were extruded and the peak load plotted against the initial billet length, figure 4.24. A minimum is indicated between 60 and 30mm, followed by a rise. In the range 120mm to 60mm the billet is large enough to contain the steady state deformation and some undeformed material, towards the back of the billet. But in the shorter billets the deformation zone is limited by the position of the pressure pad and the steady state deformation zone will not be able to form. The measured load will depend on the length of the shear zone between the billet and the container and the load to pass the material through the deformation zone. As the latter is the same in all cases a linear relationship between Lp and L_E might be expected. The experimental results show a slight deviation from linearity. As well as the load to overcome the friction of the material there is also the extra load ΔL needed to initiate dislocation movement and to form the deformation zone. This will increase as l_E increases, the longer the billet the greater the deformation needed. There will therefore be a nonlinear relationship between the length and the initial load, and the gradient $\frac{dL_p}{dL_B}$ will increase as L_B increases. This is what is observed. At short billet lengths no steady state is reached.

A qualitative comparison can be made by referring to the theoretical plane strain extrusion pressures obtained from the flow patterns shown in figure 2.8 .

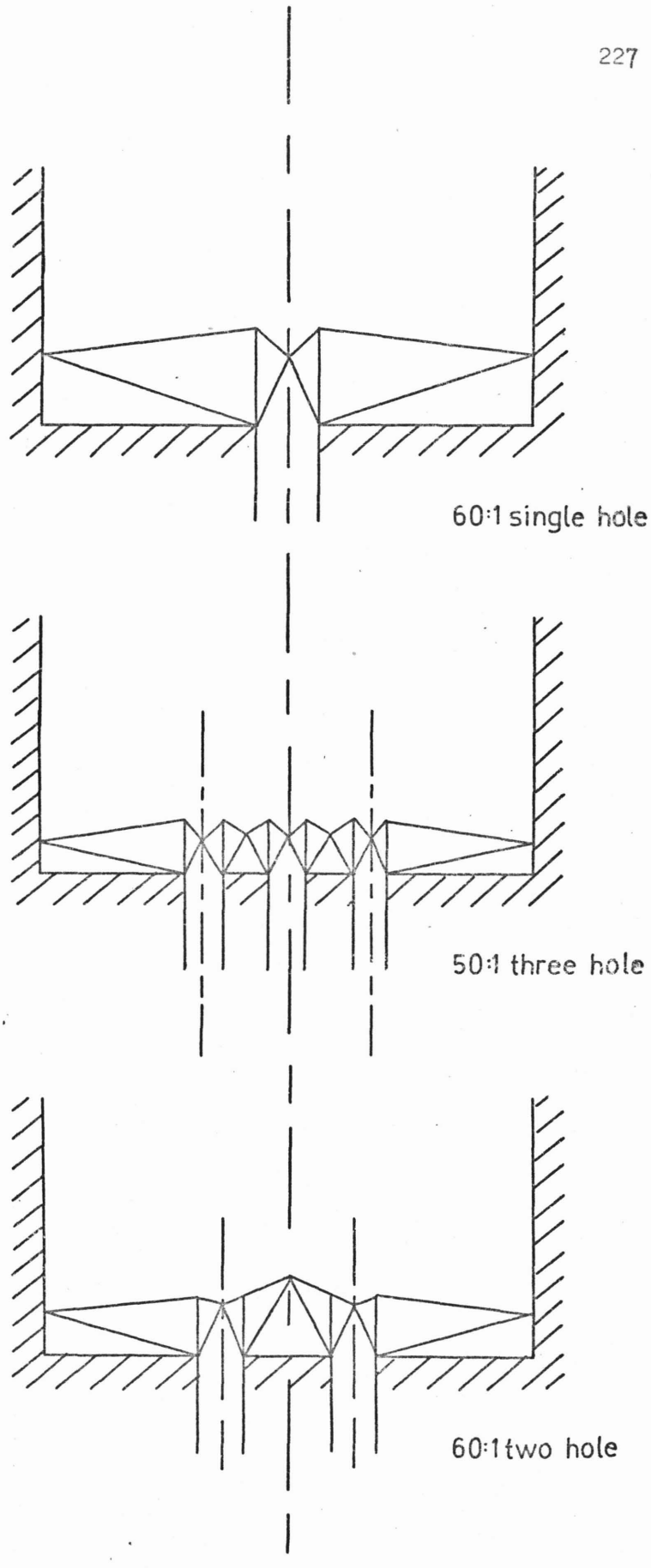


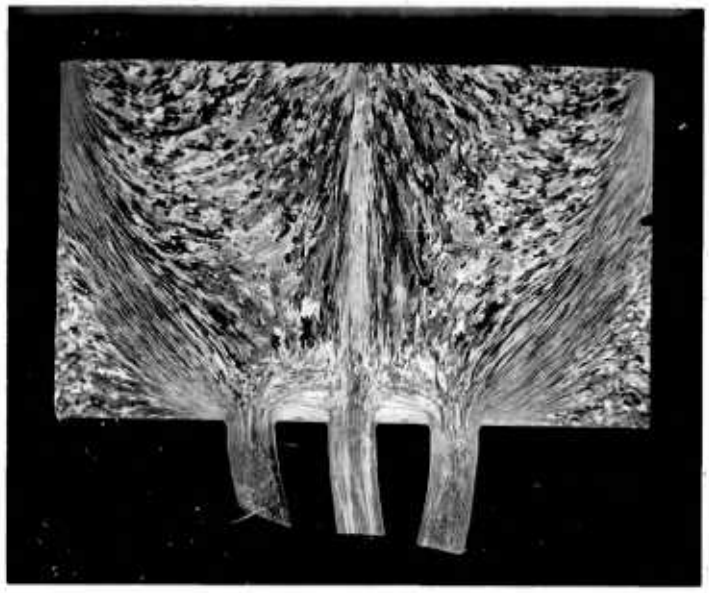
Fig 5.18a Single and multi hole flow patterns from the simple upper bound solution.

This is depicted in figure 2.9 where the expected linear relationship, (no account being made of ΔL) is seen down to a billet length of 45mm. Between 45mm and 15mm there is a very slight rise followed by a larger rise as the length decreases still further. A qualitative agreement is therefore seen between the experimental and theoretical variations.

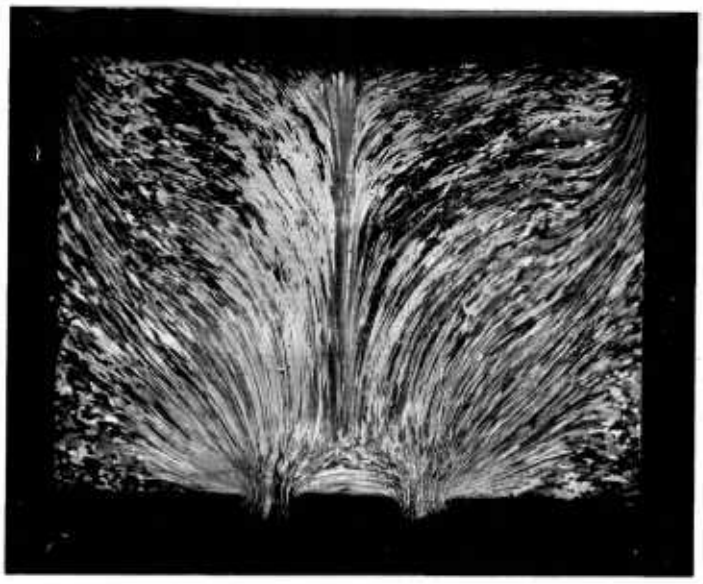
5. 13 The Flow Patterns in Multihole Extrusion.

The flow patterns for the multihole extrusions were all taken in the vertical plane containing all the holes and typical examples are given in figure 5.19 . Dead metal zones are seen in the circumferental extremities and can just be discerned in the area between the holes. There are many basic similarities to the single hole extrusions with regions of intense shear bordering the dead metal zones, but there is also a shear region down the central axis in the case of the three hole extrusion. In between these zones of shear the metal flows in a curved path to the exit. The angle the outer dead metal zone boundary makes with the die is greater than that seen in single hole extrusion but the region extends back to approximately the same depth, roughly equal to half the billet diameter. In fact the geometry of these outer dead metal zones, in the plane studied, appears to be only a function of the distance between the outer rod and the billet edge, and not by the number of holes being extruded. If this is true then a similar flow pattern should be observed for the extrusion of a rod equal in diameter to the distance between the outer surfaces of the outermost rods. Comparing (b) and (c), different reduction ratios, there is very little difference between the two patterns as the change in reduction ratio does not alter the geometry to any significant extent.

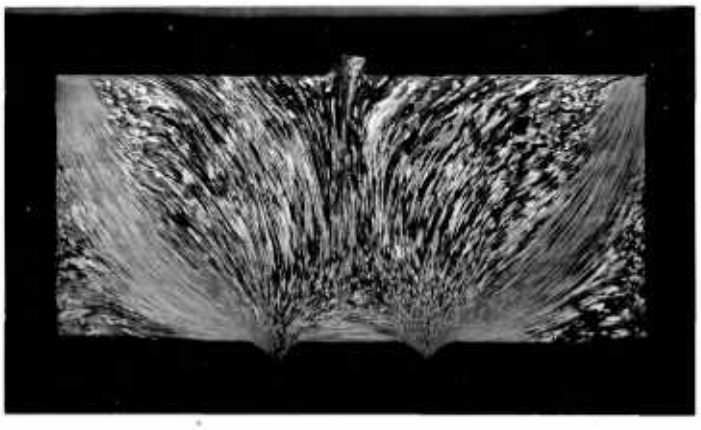
In figure 18a , the plane strain patterns from the minimised upperbound solutions compare reasonably well with the experimental patterns, allowing for the simplicity of the solution, a more complex flow pattern of the type used for the single hole flow patterns will give a better correlation but the solution will involve extensive computation.



50:1



60:1



100:1

Fig 5.19 Flow patterns developed during multihole extrusion

5.14 The Structures Observed During Extrusion.

Up to now little mention has been made of the range of structures observed in the extrusions. The initial homogenized structures have been discussed in section 5.2 , and are depicted in figure 5.1 .

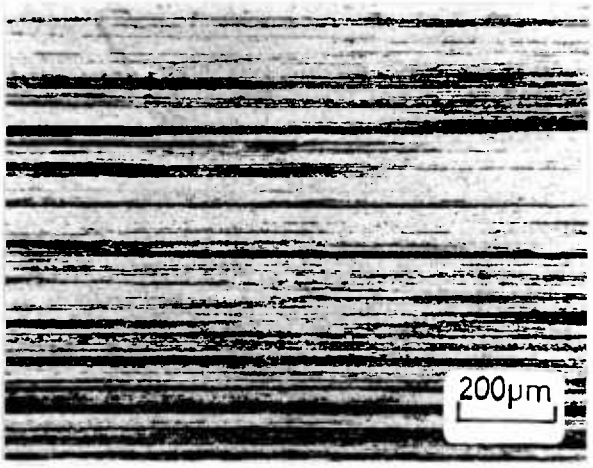
The structures observed may be classified into three main types typically as shown in figures 5.20a&b , frequently the structure was a combination of one or more of these types.

Micrograph (a) is of a typical fibrous structure with very long grains aligned in the extrusion direction. The similarity between this structure, formed at high temperatures, and that produced by a large reduction at low temperatures, prompted much of the current interest in hot working and dynamic recovery. The classical theory of hot working suggested that a recrystallized structure was obtained by working above a critical recrystallization temperature, the fibrous structure shows that this is not the case.

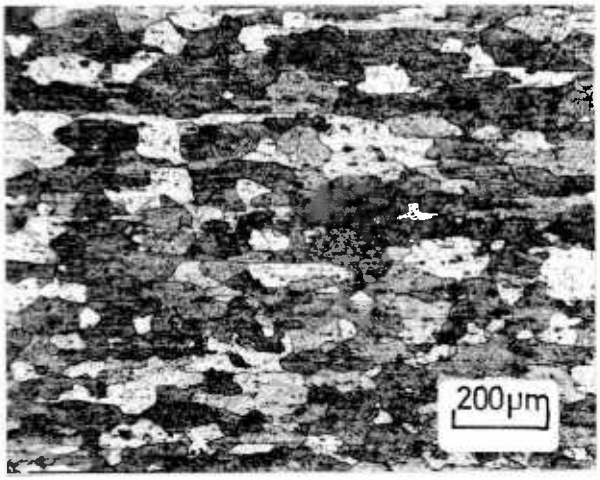
In (b) an elongated structure can still be detected but recrystallization has occurred. Some of the recrystallized grains have their largest axis in the extrusion direction. The extent of the elongation is exaggerated by the aligned precipitates, they tend to make the grains appear longer than they are in reality.

In (c) a fully recrystallized structure is seen. The only indication of the extensive deformation that has been used is the preferential orientation of the precipitates, which lie in the direction of extrusion. These precipitates appear to be much larger than those observed under the electron microscope. Two reasons for this may be given. One is the exaggeration of the size caused by the etchant. The other is that such large precipitates would be unlikely to thin down with the bulk matrix during the preparation of the thin foils.

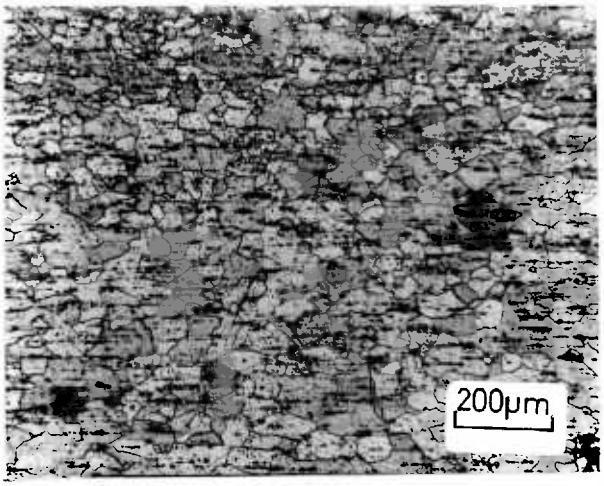
Some of the variations of these basic structures are shown in (d), (e) and (f). Very fine recrystallized grains are seen at the edge in (d) but further in the grain size increases and a slightly elongated structure is found. This change from a fine to a relative coarse grain size occurs over a very small distance. It is also known that the coarse grain perpheral region found after heat treatment has a definite width, independent of the time of heat treatment. It may be that this region is associated with the observed band of fine



a) Alloy B, 30:1 single, 338°C, 5 mm sec^{-1}

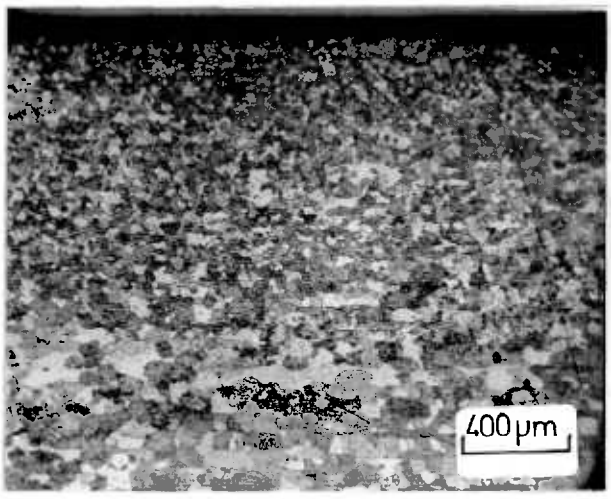


b) Alloy CE, 60:1 three hole, 353°C, 5 mm sec^{-1}

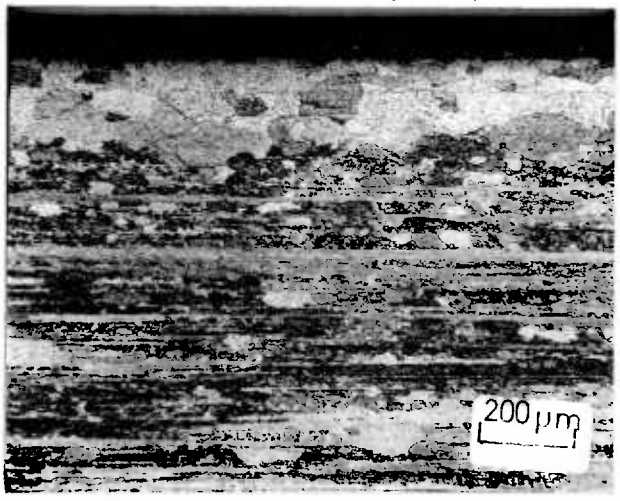


c) Alloy DF, 60:1 three hole, 468°C, 5 mm sec^{-1}

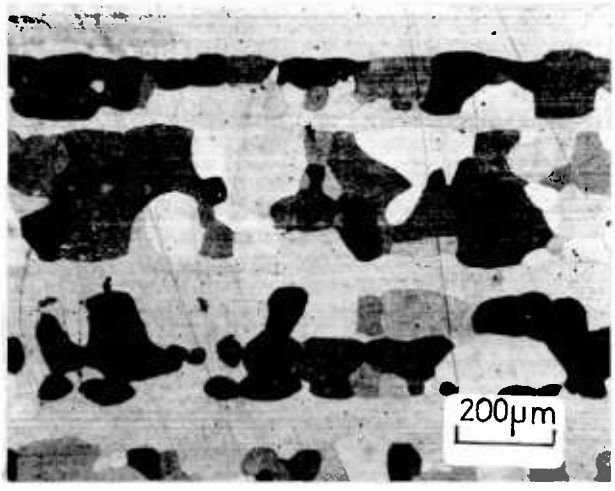
Fig 5.20(a) Optical micrographs of typical structures found in the as extruded rod



d) Alloy A, 50:1 single, 378°C, 12.7 mm sec^{-1}



e) AlloyA , 30:1 single, 378°C, 14 mm sec^{-1}



f) Alloy A, 50:1 three hole, 500°C, 11.6 mm sec^{-1}

Fig 5.20(b) Optical micrographs of typical structures found in the as extruded rod

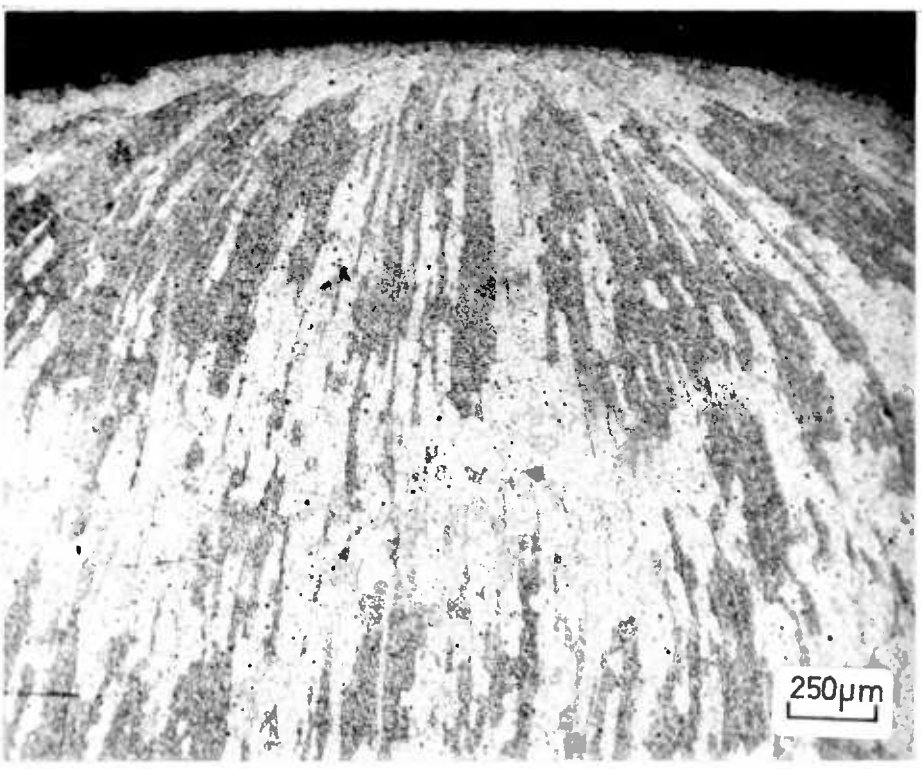
grains near the surface. This region is also where the heaviest working would have occurred.

An almost fibrous structure is depicted in (e) with some elongated recrystallized grains within the fibrous structure. The surface of the extrude consists of large equiaxed recrystallized grains and can be compared with the previous micrographs where very fine grains can be seen at the edge. The difference between the two is related to the different degrees of working undergone by these extrudes.

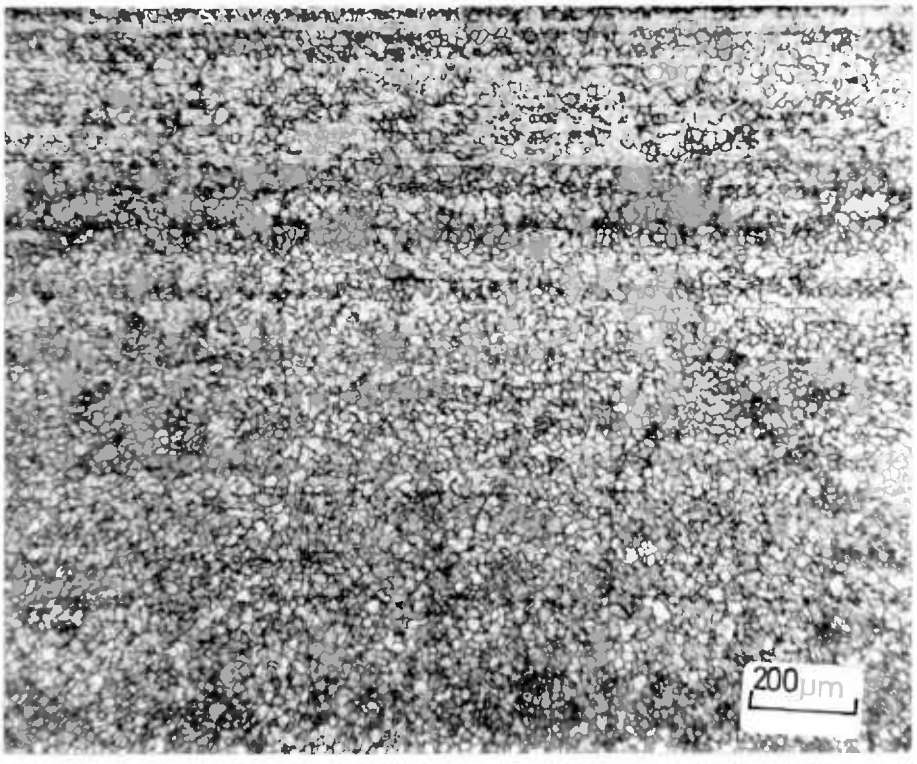
Occasionally the structure in (f) was seen. Here bands of recrystallized grains lie in the extrusion direction and are surrounded by areas that have not been attacked by the etchant, which was Kellars solution. Akin to this structure was a similar one, where the bands of recyrstallized grain consisted of grains whose length was several times their width. The unetched region is probably a fibrous structure.

In figure 5.21 (a), the cross section of a multihole extrude is seen. The main structure is fibrous but the lines radiate from one point on the edge. In the two hole extrusion, and the outer rods of the three hole extrusion, only one of these regions of radiating lines was seen. Two were found in the centre rod of the three hole extrusion. This non uniform flow is a direct result of the flow occurring in multihole extrusion. In these extrusions the longitudiral section observed under the optical microscope were not symmetrical about the centre axis, where recrystallization had occurred no such radiating lines or non symmetrical structures were seen. Comparing the optical structures with the flow patterns, it can be seen that the displaced structure can be related to the differing flow found. In the two hole case a large volume of metal has to flow from the edge of the billet to the extrude, a smaller volume flows from the central region. To accomodate these differing flow rates the line of symmetry, where the flow rates are equal, will be displaced towards the centre. The three hole extrusions will be similar but more complex.

The last micrograph, figure 5.21 (b), is representative of an overheated structure, and is the product of a combination of the accumulator drive, a high initial billet temperature, and a high reuction ratio, 100:1 three hole. The temperature rise was high enough to cause localized melting and the structure consists of very fine grains surrounded by a continuous intergranular network. The mechanical properties of this structure were very poor. It was



a) Transverse section of a multihole extrude, alloy B, 30:1 three hole, 420°C, 11.1 mm sec^{-1}



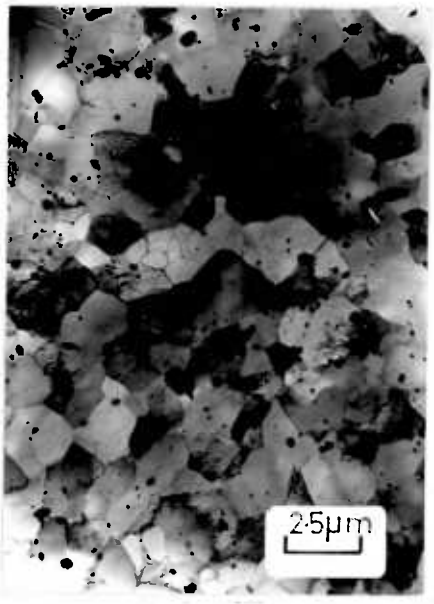
b) Overheated structure. Alloy CE, 60:1 threehole, 497°C, accumulator

Fig 5.21 Optical micrographs of the as extruded rod, multihole transverse section, and overheated structure

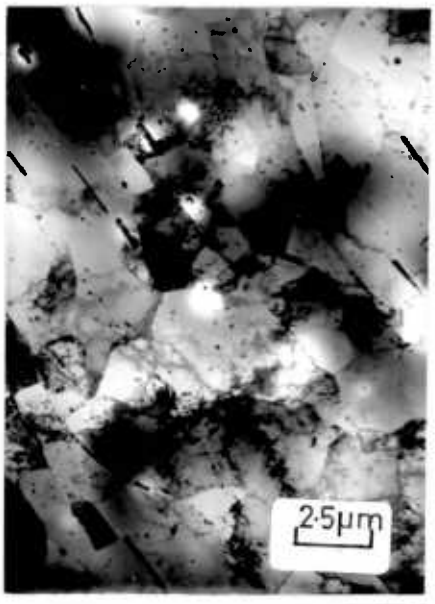
extremely brittle and could be snapped with little effort. A cracking noise was clearly audible before fracture. A structure of this kind, with its associated mechanical properties is characteristic of alloys that have been heated to a temperature above the melting point of one or more of its constituents. The molten phase forms an intergranular network, and rapid quenching freezes this structure. The phase forming the network is usually very brittle and as it is a continuous film the properties are extremely poor.

The range of structures observed in the transmission electron microscope, associated with the optical micrographs are depicted in figure 5.22 .

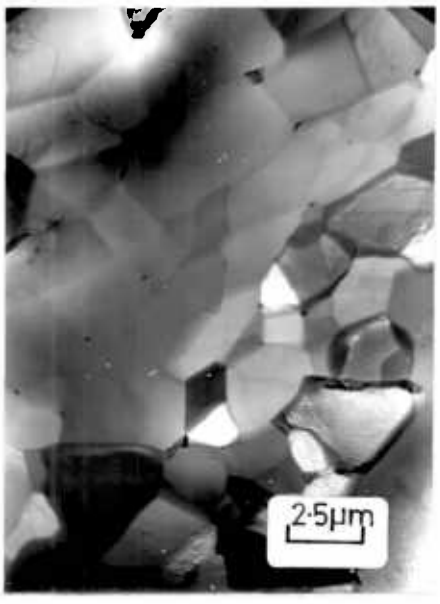
In every case the fibrous structure consisted entirely of subgrains, such as those in (a). The lack of contrast between the subgrains is an indication of the low misorientation between them. Networks of dislocations can also be seen. This structure is direct evidence of dynamic recovery during the deformation. The rate of dislocation multiplication is balanced by the rate of annihilation and the dislocations form into well defined walls to form the subgrains. Comparison with the fibrous structure has shown the fibres to be composed of these low angle grains. In between each fibre there must be a band of higher misorientation to account for the action of the etch in depicting the fibres. These high angle boundaries can be associated with the original grains of the material that have been elongated by a factor equal to that of the extrusion ratio. When examining these electron micrographs it must be remembered that the observed structure depends on the orientation of the foil in the microscope, consequently all of the dislocations present cannot be observed at the same time, or retained on the same micrograph. Some of the subgrain boundaries are pinned by the precipitates present but there are as many precipitates that are not associated with any boundary. This micrograph is from a transverse section. In (b) a typical longitudiral section is given. Comparing the two, the larger precipitates seen are in the form of rods that have been orientated during the deformation into the extrusion direction. It is not possible to determine the direction of extrusion from any alignment of the subgrain. This agrees with the work of Wong and Jonas on commercial purity aluminium, who only found aligned subgrains at the lower temperature range of the hot working region. This led to the idea of repolyganisation during hot working, where the subgrains have to be constantly reforming, otherwise some elongation would be found.



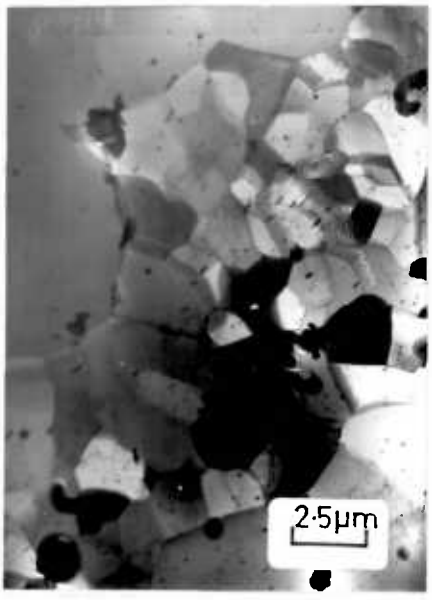
a) Alloy B, 30:1 threehole
420°C, 11.1 mm sec^{-1}



b) Alloy CE, 100:1 single,
486°C, 12.6 mm sec^{-1}

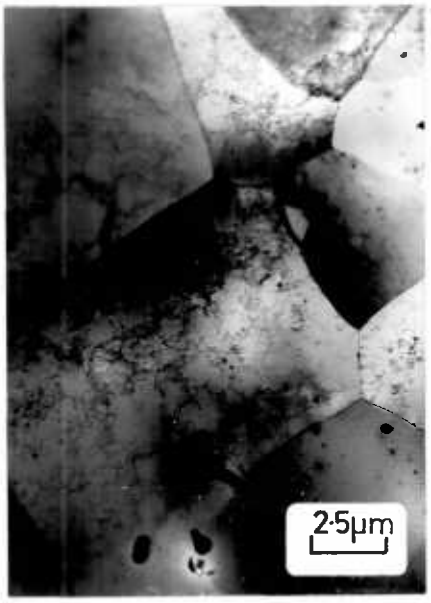


c) Alloy CE, 60:1 single
373°C, 5.3 mm sec^{-1}

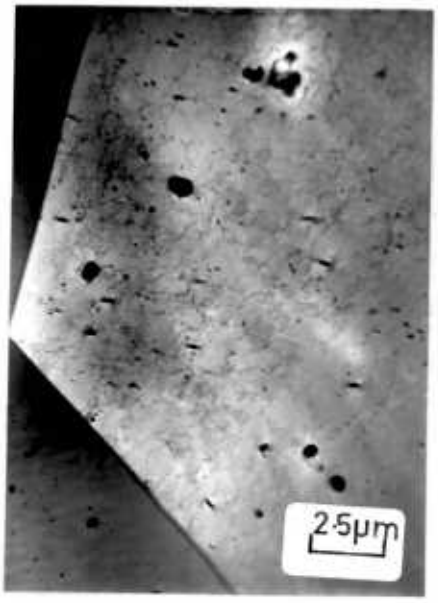


d) Alloy DF, 60:1 two hole
440 C, accumulator

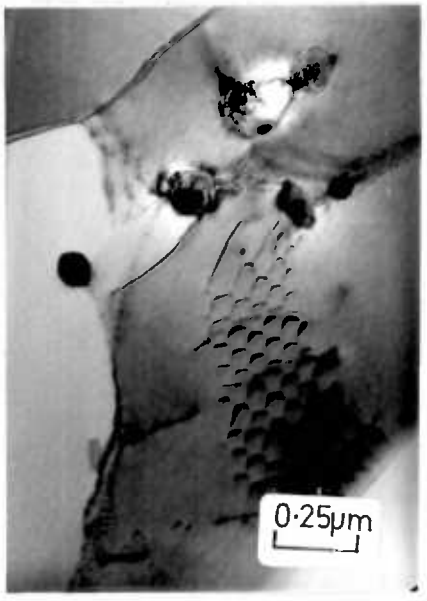
Fig 5.22(a) Transmission electron micrographs of the typical structures found in the as extruded rod



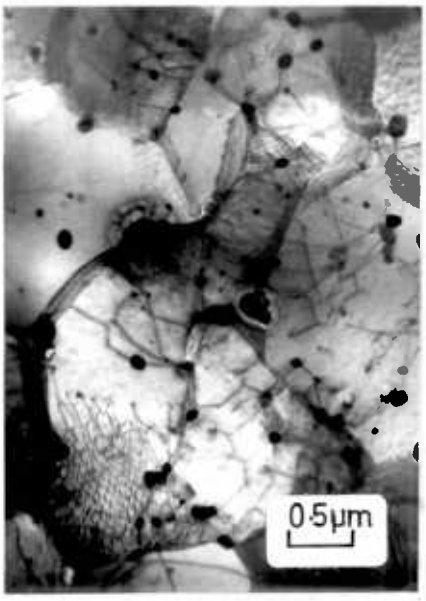
e) Alloy 266D, 60:1 single
330°C, 13.6 mm sec^{-1}



f) Alloy CE, 60:1 single
433°C, accumulator



g) Alloy B, 30:1 single
338°C, 5mm sec^{-1}



h) Alloy B, 30:1 single
378°C, 14 mm sec^{-1}

Fig 5.22(b) Transmission electron micrographs of the typical structures found in the as extruded rod

The micrograph in (d) is of another transverse section of a fibrous structure but this time the volume fraction of precipitate is much lower. Otherwise the basic features are similar to (a) with well defined subgrain walls and no dislocation within the subgrain. The diameter of the cells is larger than that in (a) and this illustrates the role of the precipitates on the cell size.

When the elongated recrystallized structures were studied the observations were similar to those given in (d) and (e). In the former, a region composed entirely of subgrains is surrounded by a subgrain free region. Tilting the foil in the microscope did not produce any trace of subgrains in these regions and the dislocation density was low. The second micrograph shows no subgrains but instead large grains are seen with dislocation cells within them. Compared with the previous micrographs the size of these microcells is similar to the subgrain size.

In the extrudes with a fully recrystallized optical structure the electron microscope showed large grains with high angle boundaries (f). No subgrains or cells could be seen within them but dislocations were usually present, but not always. The observed dislocations did not have any definite configuration, such as network formation or cells. When dislocations interact with each other the tendency is for them to lower their energy by forming equilibrium networks. The boundaries of the subgrains are made up of such networks and typical examples are seen in figure 5.22, (g) and (h). The first shows a typical subgrain boundary and how precipitates can act as pinning points. In the second the role of the precipitates in pinning dislocations is revealed more clearly. Although the precipitates are not uniquely associated with the subgrain walls they still act as barriers to the dislocations and the dislocations between these precipitates tend to lower their energy by linking up with each other. This is the nearest approach that was found to the continuous dislocation networks within the subgrains mentioned by McLean. It is not possible to deduce from mircographs of this nature whether the dislocations within the grains are the hot worked structure, or a stage in a static restoration process. The definite networks seen are the two dimensional subgrain boundaries.

5.15 The Relationship Between the Flow Stress and the As Extruded Structure.

Figures 4.41 to 4.49 indicate that the structure can be related to the theoretical mean flow stress and therefore presumably to Z. In general the lower the flow stress the greater the tendency for a recrystallized structure. As a lower flow stress is associated with a higher working temperature this is not surprising. The change from the completely fibrous structure to the fully recrystallized structure is a gradual one and it is not possible to say that recrystallization occurs below a certain value of Z without qualifying the percentage of recrystallization.

The structures in the two alloys A and B were studied in the most detail. These alloys were based on super purity aluminium and effects due to complex alloying will not be present. Alloy A did not have any manganese present and an elongated recrystallized structure started to appear at a flow stress of approximately $75 N/mm^2$ and was fully recrystallized by $60/Nmm^2$. A completely fibrous structure was only seen at the very high flow stresses associated with a high value of Z, i.e. a low deformation temperature and a high strain rate. When a mixed structure was seen, e.g. elongated recrystallized and fibrous, the recrystallized structure was always found nearer the edge of the extrude. Alloy B, with manganese was similar but the fibrous structure extended to below $70/Nmm^2$ and no trace of a fully recrystallized structure could be found above $56/Nmm^2$. Alloys CE and DF, which were not studied in such detail, exhibited the same correlation. The fibrous structure occurring over a wider range of flow stresses in the manganese bearing alloy DF.

This correlation between the structure and the flow stress was found to apply to both single and multihole extrusion. This proves that the flow stresses calculated from the simple upperbound solution for the more complex flow are correct, relative to each other. It also vindicates the application of a correction factor to log Z rather than to $\bar{\sigma}$ in figures 4.14 -17.

5. 16 The Occurrence of a Recrystallized Structure in Extrusion.

The press used was fitted with a water quench situated as close to the die as possible, 340mm. This distance was limited by the design of the press. The extrude would therefore have a very short time between leaving the die and entering the quench. If any static recrystallization had occurred it must have been in this time interval. For an extrusion ratio of 30:1 and a ram speed of 5mm/sec the exit velocity is 150mm/sec. The time between leaving the die and quenching is then 2.37 seconds. The work by Evans and Dunstan[83] found that the delay time for static recrystallization in hot compressed commercial purity aluminium was less than one second. The effect of alloying would effect this delay time, the presence of precipitates can aid or hinder nucleation depending on their size and dispersion. If the time for recrystallization to occur is of the same order as that found for commercial purity aluminium then the possibility of a static restoration process operating cannot be excluded. Recrystallization structures were also observed at the high ram speeds achieved with the accumulators. At these exit speeds the time before quenching is less than 0.2 seconds. However, this high velocity will also reduce the time in the most effective part of the quench. Also the high ram speeds will result in the heat losses being minimal and virtually adiabatic conditions can be assumed. The exit temperature will be very high, hot shortness was a common feature of these extrudes, and coupled with the high strain rate, the nucleation time will accordingly be low.

If dynamic recrystallization had occurred the structure should show deformed recrystallizated grains and possibly some region of subgrain being consumed by a migrating high angle boundary. Dislocations were seen in the recrystallized structure shown in figure 5.22b, and subgrains surrounded by recrystallized grains in figure 5.22a(d). In the latter the curvature of the high angle grain boundaries indicates the movement of these boundaries into the subgrain region. Also an elongated recrystallizaed structure was found in the optical longitudiral structures, figure 5.20a(b) These structures cannot be considered to be conclusive evidence of dynamic recrystallization. The dislocation in the recrystallized grains were not always seen, none were visible in figure 5.22a(d) and those seen did not have any resemblance to the cell structure that forms during these high deformations. Any recrystallized grains formed in

the deformation zone will be elongated in the extrusion direction, the extent of this elongation will depend on the deformation suffered after recrystallization. This explanation can be applied to the observed elongated structure and if any recrystallization did occurr it would be nucleated in the most heavily worked regions, close to the surface, as observed. Another possibility is that static recrystallization of the fibrous structure starts immediately the extrude emerges from the die, or even in the die land region, and that these recrystallized grains follow the preferred orientation found in extrusion. If the stored energy is high enough then normal recrystallization occurs with no preferred orientation. The presence of any precipitates will hinder the migration of any grain boundary and recrystallization will be retarded. The precipitates formed by the Mn in alloys B and DF will therefore retard recrystallization.

The possibility of dynamic recrystallization cannot be ignored but no conclusive evidence to its existance was found. The possibility of static recrystallization in the short time prior to quemching is more likely. The high conductivity of aluminium will lead to a complex heat balance in this region between the quench and the die. At one end the extrude has been quenched to virtually room temperature, at the other is a heat source pumping heat into the extrude because of the thermal gradients.

The fibrous structure found at the high flow stress is indicative of the dynamic recovery that takes place during deformation. This recovery will tend to lower the energy of the system and on leaving the die, there is not enough thermal energy to initiate the nucleation of recrystallized grains. The microcells observed in some of the elongated optical structures is an indication of the method of nucleation. This structure is associated with a lower value of Z and the thermal energy is just sufficient to cause some of the subgrains to reduce their misorientation byrotation. The remaining subgrain walls then commence to coalesce. This is the stage at which the extrude from which micrograph figure5.22e was quenched. If the stored energy is high enough the internal dislocations will all migrate to the walls, where they will either be annihilated or combined into the networks present. This will leave a dislocation free grain with a relatively high angle boundary between it and its neighbours which may still contain subgrains. Similar to that depicted in522(d).

The remaining subgrains have not been able to rotate with respect to each other, to lower their misorientation, and therefore no nucleation of a recrystallized grain has taken place. This evidence of the nucleation of recrystallization by subgrain coalesence agrees with that given by Hu[85].

The possibility of dynamic recrystallization cannot be ignored but no conclusive evidence to its existence was found. The possibility of static recrystallization in the short time at temperature prior to quenching is more likely. If dynamic recrystallization had occurred then the use of a constant activation energy of 160,000 joules/mole would be incorrect, some evidence of this would be expected in the analyses of the data. No such evidence was seen.

5. 17 The Relationship of the Mechanical Properties with the Structure and the Flow Stress.

The mechanical properties of alloys A,B,CE, and DF were studied by tensile tests. All four had higher properties for the recyrstallized structure than for the fibrous structure, figures 4·41,4·44 This is the opposite of what was expected. In commercial purity aluminium the fibrous structure has the higher properties and the use of manganese or zirconium to retain the fibrous structure usually gives superior mechanical properties. Electron microscope studies of the as-extruded structures revealed a common feature between the alloys. The number of small precipitates present decreased as the macro structure changed from fibrous to recrystallized. In alloys A and CE, which started off as an almost complete solid solution, some small precipitates were still seen. The higher mechanical properties can therefore be realted to the percentage of solute in solid solution. Two reasons for this change in solubility may be given. The first is in the temperature of extrusion. At high temperatures the equilibrium solid solubility is increased, and any precipitates present at room temperature willtend to dissolve. At lower temperatures this tendency will be reduced. The heating cycle prior to extrusion will be important in this aspect. Discussion with other workers in this field raised another possibility. These alloys are very sensitive to the rate of quenching, and when the structure consists of subgrains, precipitates tend for form along these subgrain boundaries, during quenching. The retention of a high vacency concentration will aid this precipitation. The boundaries are preferential sites for nucleation

and, if the solid solution is super saturated, precipitates will occur. It should be possible to control the extent of precipitation by controlling the quenching rate. The temperature prior to quenching will be a controlling factor in the extent of super saturation.

The observed change from low to high mechanical properties in the elongated recrystallized structure is an indication of the ease of precipitation in the fibrous structure. As the volume percentage of this fibrous structure is reduced the subgrain density is lowered, reducing the nucleation sites for precipitates.

The observed relation between the mechanical properties and the recrystalized grain size may also be explained by the presence, or absence of precipitates. As the flow stress decreases i.e. the temperature rises, the grain size increases and normally this would lead to lower mechanical properties, as give by the Hall-Petch relationship. If the amount of solute in the solid solution is also increasing, this grain size will be masked by the accompanying increase in strength. The observed dependence will be a function of the hardening caused by an increase in solid solubility and softening due to an increased grain size.

5.18 The Variation in Mechanical Properties Across the Extrude.

Figure 4.51 shows the variation found in the hardness across a single hole extude and a multi hole extrude, both with a fibrous structure. The deformation in single hole extrusion is symmetrical, as can be seen in the flow patterns figure 5.18, therefore a symmetrical variation in the hardness is expected and this is found. The hardness at the very edges is slightly lower than that of the matrix but away from the surface there is almost a constant hardness with a slight maximum at the centre. The low hardness at the surface may be attributed to an unidentified change in the microstructure brought about by the higher degree of working and higher temperature developed.

The variation across the outer rods of the multihole extrudes do not have the same symmetrical variation. There is no region of constant hardness and a maximum occurs towards one side. The micrograph of a cross section of a multihole extrude figure 5.21 depicts non uniform flow, the flow patterns also show this figure 5.19. The variation in hardness may be related to this observed flow. The hardness measurements were taken across the diameter, from the point where the flow lines

radiated from in the cross section. Along this diameter the maximum variation in the flow will have occurred. At the very edge a relatively low hardness was found. This increased along the diameter to a maximum away from the centre axis, and then fell as the opposite surface was reached. The measured mechanical properties will represent an average of this variation in hardness.

The central rod in the three hole extrusions showed two points of radiating flow lines and the hardness variation followed the same trend, with a minimum at these two points and a maximum at the very centre. Each minimum corresponds to those found in the outer rods and is a direct result of the differing rates of flow needed to maintain uniform rate of deformation.

5.19 The Variation in Mechanical Properties in the Multihole Extrude.

Over the range of flow stresses studied no clear variation in mechanical properties within experimental error, between the multi hole extrudes was found. None was expected in the two hole extrusions but it was felt that there would be a noticeable difference between the central rod and the outside rods in the multihole products, because the higher degree of deformation undergone by the two outer rods. The diameters of the extrudes were relatively small, reduction ratios of 30:1 to 100:1 being considered, and the eccentricity was limited to low values by the size of the die backer. As a result the difference in the degree of working received by the different rods could not have been high enough to cause any noticeable difference in the properties.

If the eccentricity and the diameter of the rods had been larger the same significant difference would have been expected. As stated in the previous section the mechanical properties average the variation found across the section, as indicated by the hardness. In larger sections produced by the multihole method this variation in hardness suggests that significant variations in the mechanical properties would be found, and for this reason care must be taken in positioning the holes to achieve the most uniform flow.

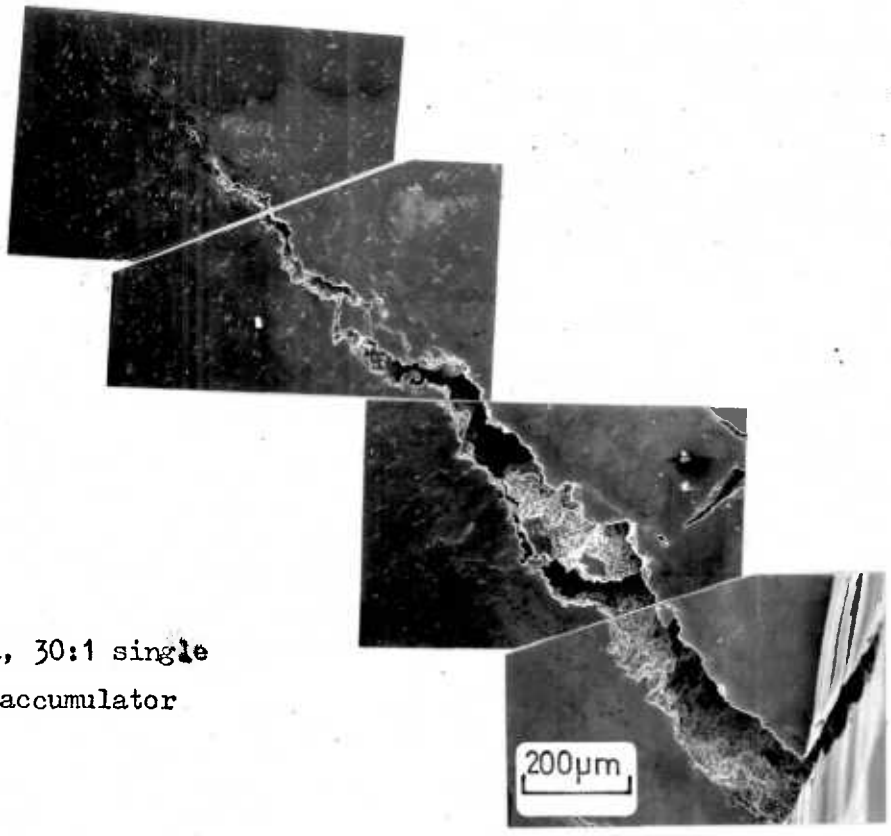
Any variation in hardness is a reflection of a variation in structure and as well as a variation in mechanical properties, some variation in other properties is to be expected e.g. the susceptibility to corrosion and stress corrosion. This variation instructure could not be examined under transmission electron microscope because of the method

used in preparing thin foils. In larger sections especially shapes, the variation across the extrude as well as along its length must be examined.

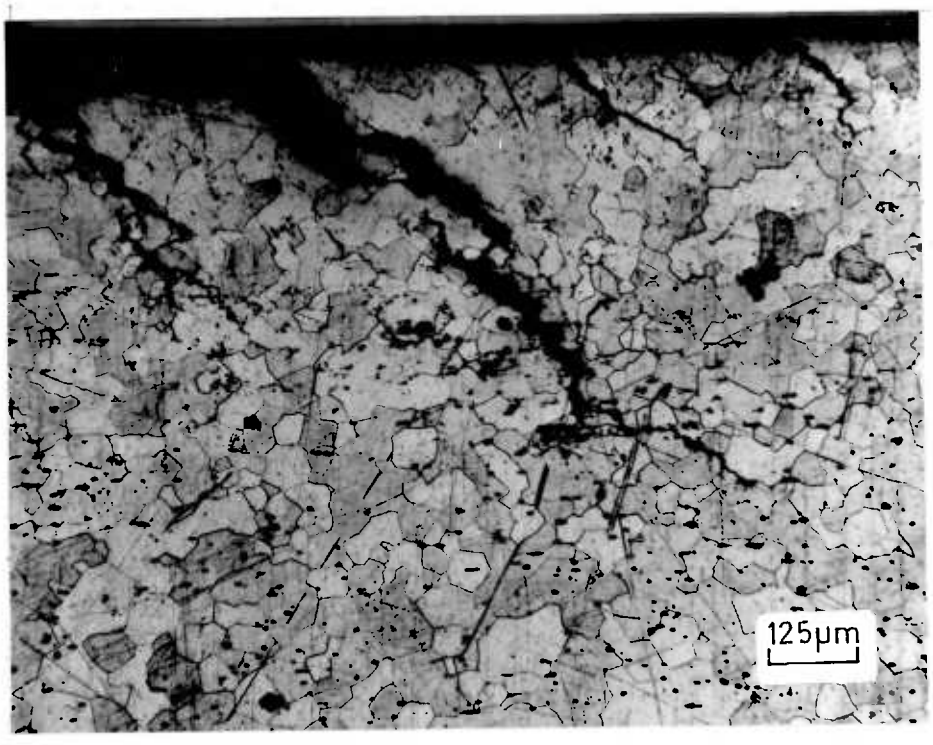
5.20 Surface Defects in Aluminium Alloy Extrusion.

Only visual defects were studied and no anodizing treatments were examined. Many of the problems in aluminium extrusion is in the variation in surface finish obtained after extrusion, this is related to structural defects in the surface layer. Two types of defect were seen, hot shortness and pickup. At high temperatures the product often had small cracks perpendicular to the direction of extrusion and running around the entire circumference. The cracks are usually attributed to localized melting. Figure 523a shows a crack examined in the scanning electron microscope and below it is an optical micrograph of a similar defect. The cracks are intergranular in nature and run towards the back end of the extrusion. The evidence of the localized melting is found in the precipitates. There are fewer precipitates aligned in the extrusion direction, compared with figure 5.20 , and, in the region close to the cracks, intergranular networks are seen. The occurrence of these cracks was noted only when the calculated emergent temperature was above 540°C in alloy CE and 560°C in alloy DF. These temperatures agree approximately with the solidus lines on the appropriate phase diagrams. Williams also found this defect to occur only above a certain temperature, which he estimated by using a contact thermocouple on the extrude. He also demonstrated the importance of the temperature cycle of the container during a batch of extrusions. This increases during the extrusion and falls in the dead cycle time, as the press is prepared for the next extrusion. Over a period of time the mean of these oscillations in the temperature approached a steady state value, and, if the temperature was above the solidus, hot shortness occurred. The use of water cooled tooling can play an important role in controlling this temperature.

If the defect was caused by fracture, due to internal stresses, the surfaces seen in the scanning electron microscope would have the more definite structure associated with fracture. The observed nature of the surface coupled with the temperature dependence of the defect verifies localized melting as the cause. Figure 5.24 shows other views of this defect. In (b) the view is along the surface, which

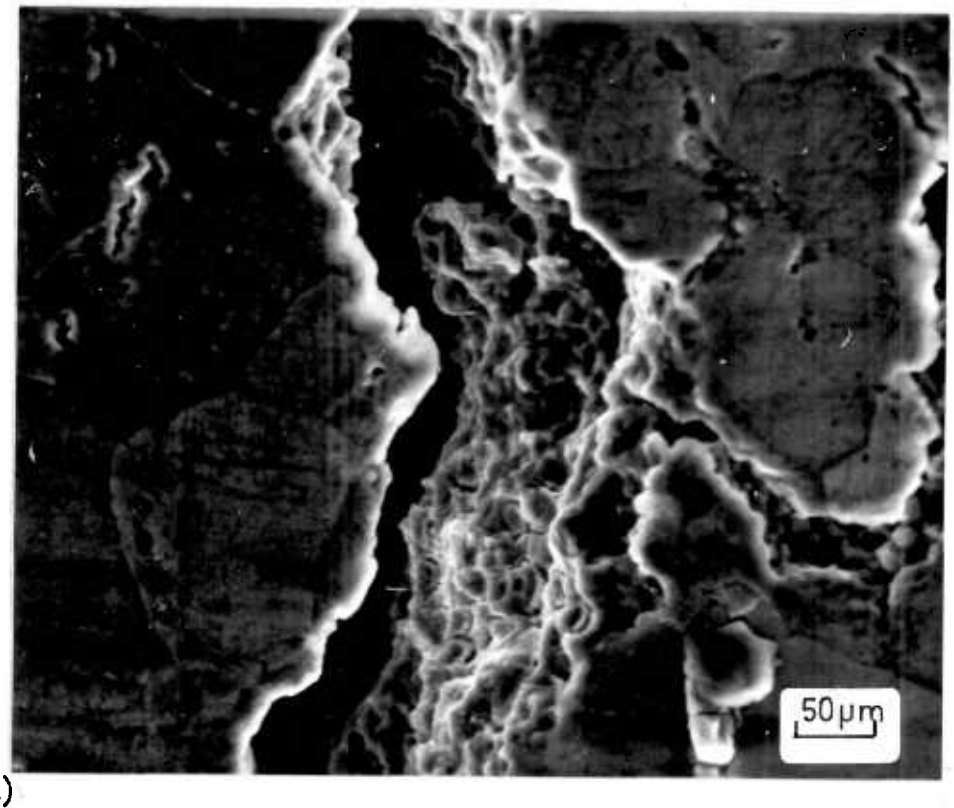


a) Alloy A, 30:1 single
420° C, accumulator

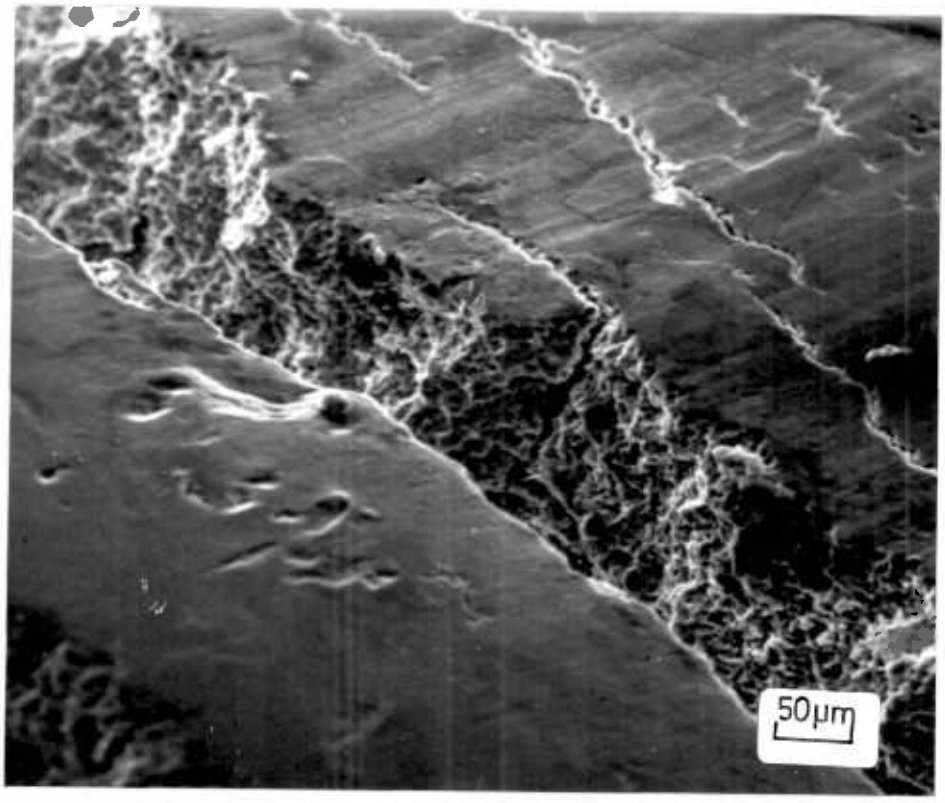


b) Alloy A, 30:1 single, 378°C, accumulator

Fig 5.23 Scanning electron and optical micrographs of hot shortness

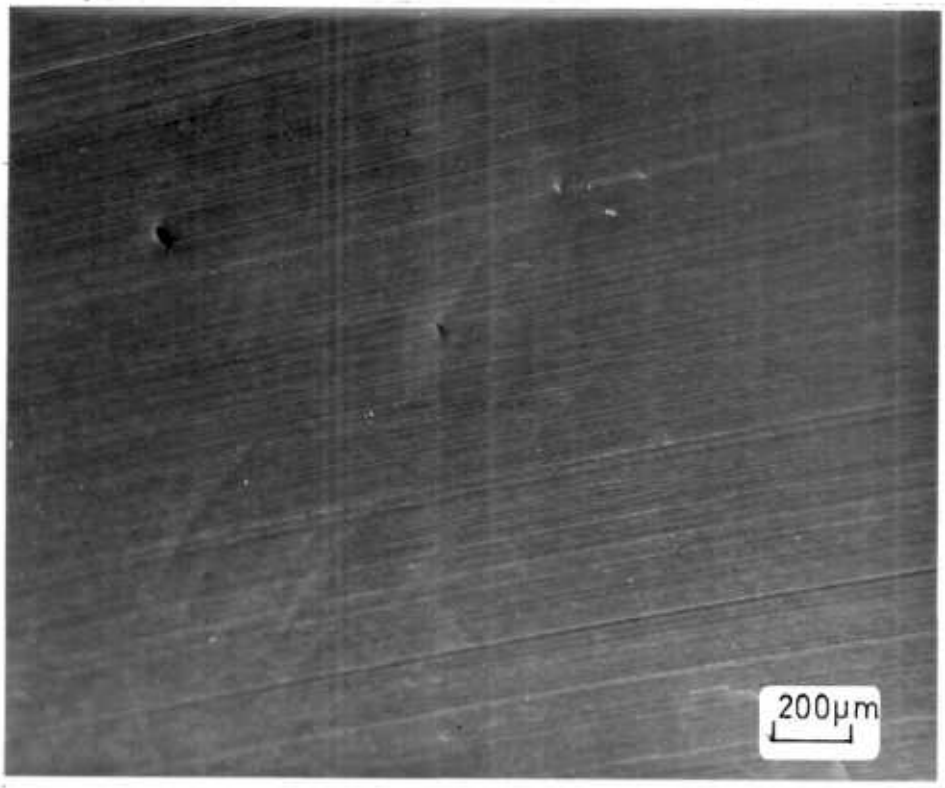


a)

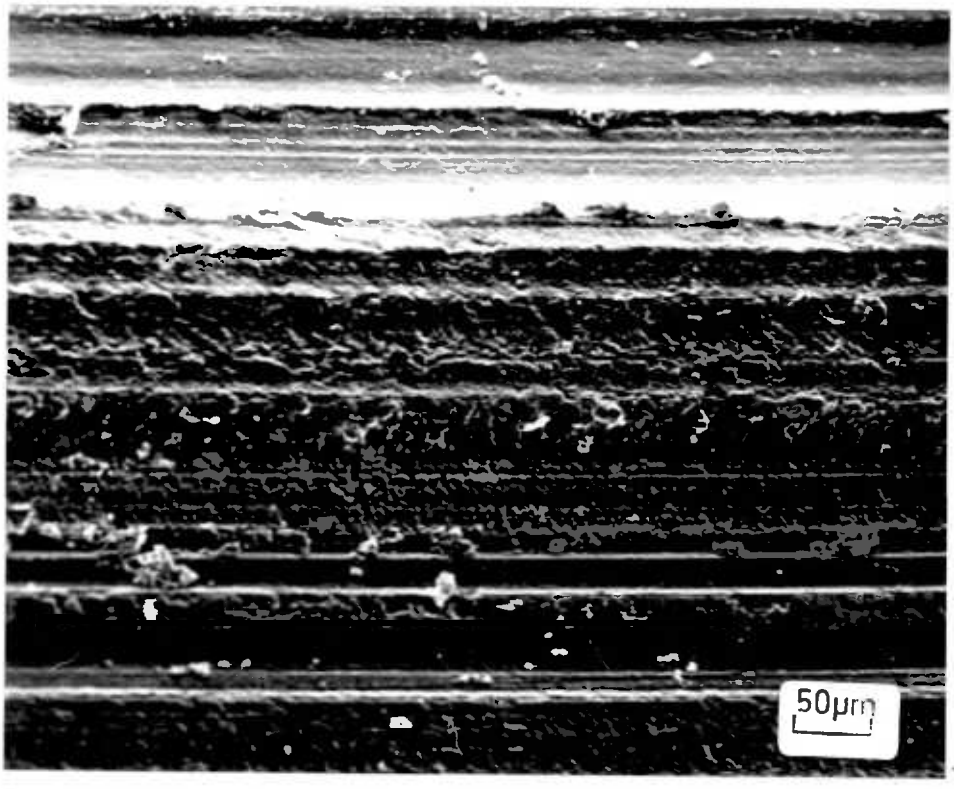


b)

Fig 5.24 Scanning electron micrographs of the surface appearance of hot shortness cracks. Alloy A, 30:1 single ,420°C, accumulator



a) Alloy CE, 60:1 single hole, 390°C, accumulator



b) Alloy CE, 60:1 three hole, 497°C, accumulator

Fig 5.25 scanning electron micrographs of the different surface finishes seen

is very smooth with no evidence of pick up or scoring. The inside of this crack does not have the appearance of a fracture face. In the second micrograph (c) the surface had been deep etched in Tuckers reagent. The recrystallized grains forming the surface and the intergranular nature of the crack are clearly visible.

Hot shortness can be avoided by limiting the initial billet temperature and the extusion speed, which lowers the production rate. It was a very common defect in the extrusion produced with the accumulator drive, where adiabatic conditions are in operation. The extent of this defect never extended more than a short distance into the billet. The mechanical properties of the material bearing this defect were comparable to the defect free structure. The depth of penetration is a measure of the temperature rise associated with the heavier working undergone by the outer surface. The order of magnitude of this depth agrees with that found for the fine grain structures shown in figure 520d and the two may be related.

The quality of the surface finish is also important, from a sales point of view. The appearance of a high quality surface in the scanning electron microscope is shown in figure 5.25. The visual appearance of the surface was very smooth, but fine lines along the length of the extrude are still visible at high magnifications. These lines are caused by small pieces of aluminium or large precipitates adhering to the die surface, known as pick up. One theory is that the die deflects under the high pressure and only the entrance to the die is in contact with the extrude. This is clearly shown in figure 5.26. In the small gap between the extrude and the die lands some aluminium tends to collect. Williams found that this pick up was not severe below 520°C, for an Al-Mg-Si alloy, and this suggests that there is some temperature dependent interaction between aluminium and the tool steel. If the load is removed the material accumulated under the bearing entrance adheres to the billet and forms the stop mark when extrusion is continued. If this is the cause of pick up then a modification of the die entrance and angle of the die lands will minimize its occurrence. This was verified by Williams. The presence of the pick up lines emphasizes the need for die cleaning, but there is a limitation to the amount of cleaning possible, some scoring was found midway through an extrusion even when a new die was being used. At very high temperatures a surface similar to that shown in (b) was found.

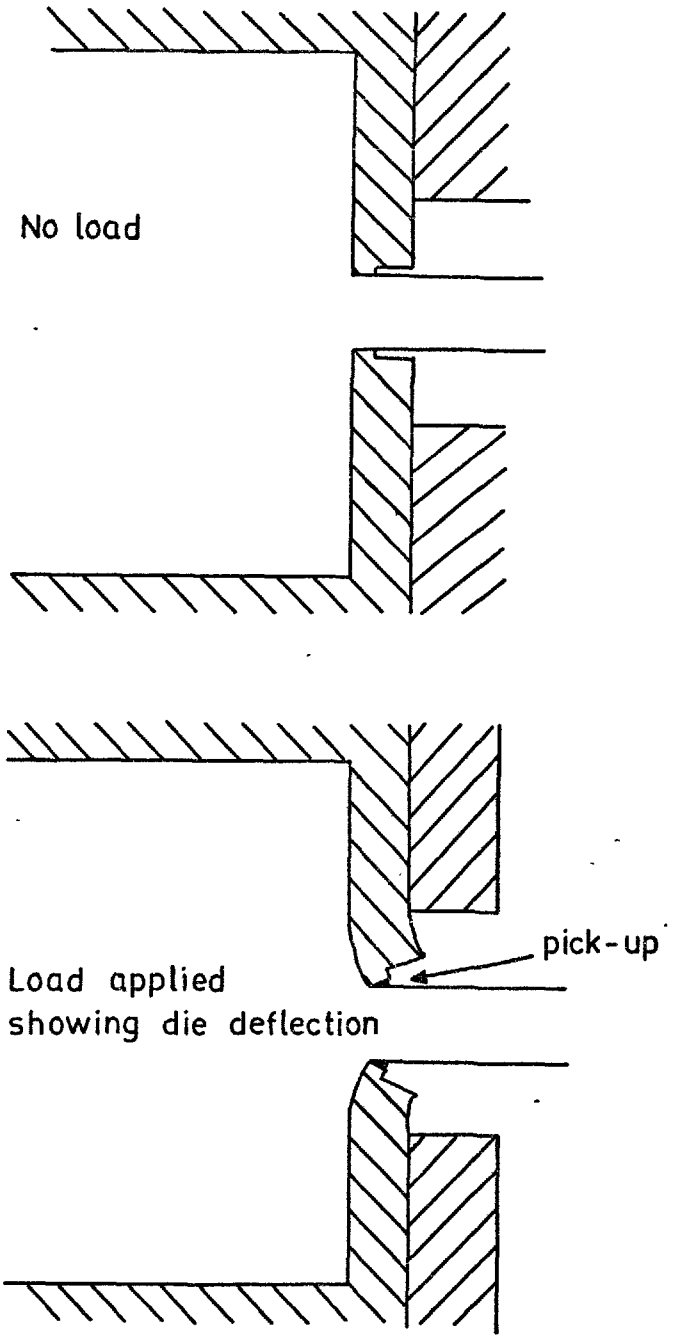


Fig.5·26 Die deflection model for die pick-up.

This is the surface of the extrude with the overheated structure given in figure5.21 . As well as having poor mechanical properties the surface is totally unacceptable. Very heavy scoring can be seen but there are no hot shortness cracks. Hot shortness occurs when localized intergranular melting occurs. If the temperature is high enough the extent of this melting will increase throughout the extrude width and, the extrusion will consist of pushing an almost pasty material through the die, pieces of the alloy will adhere to the die and score the surface producing the observed finish. The size of the extrude will play a significant role, as this will govern the temperature variation. In extrusions with a very small diameter the temperature at the surface will be the same as that in the interior. A small diameter implies a high reduction leading to a higher temperature rise. A rapid quench will then freeze the overheated structure with its intergranular network of the low melting constituent, to leave a microstructure similar to that shown in figure 5.21(b).

Providing that the exit temperature did not exceed the critical value for hot shortness the quality of the surface was more dependent on the condition of the die than on the extrusion speed. At very low speeds an unusual defect in the form of a continuous spiral running the length of the extrude was often observed, especially in the softer alloys 266D and 265D. No explanation of this could be given.

5.21 The Load Displacement Curves.

Four different curves were found during the cause of the experiments, figures 4.40 . The first three may be related to the different temperature conditions in operation. At low temperatures the billet and the container are initially the same temperature. After the peak load the almost linear reduction in load is due to the changing length of the frictional interface between the billet and the container. If the flow stress remains constant the linear relationship would be obeyed exactly, but at these low temperatures the high load leads to a high temperature rise and consequently the flow stress decreases throughout the ram stroke. Raybould's experimental results proved that the temperature rose very rapidly at the start of extrusion, but then only a slight rise was found. This slight rise throughout the extrusion indicates that the decrease in flow stress is slight and this

accounts for the observed almost linear relationship. At much higher temperatures the billet is continually losing heat to the container which, coupled with the low temperature rise because of the lower extrusion load, will lead to an increase in the flow stress. The net effect is an increase in the load, as depicted in T_3. The curve for T_2 is an intermediate case. The occurrence of precipitates or dissolution will alter the curves still more as both the temperature rise and the flow stress will be affected.

No peak or noticeable minimum was noticed during extrusion with accumulator drive. The continual fall in the ram speed was a direct effect of the nature of operation of the accumulators and this, coupled with the difficulty in measuring the load, precluded the quantitative analyses of these results.

5.22 The Effect of Section Shape on the Extrusion Load.

In figure 4.39 , the load displacement curves for several different shapes and hole configurations are given. Both the initial and final load depend on the section being extruded, with the load to extrude through a three hole die being highest and that for a square the lowest. This is a direct reflection of the effect of the complexity of deformation on the extrusion load.

One method of correlating data for different shapes is to compare the peripheral ratios.* These are given below along with the ratio of the peak loads. All the ratios are given relative to that for the square hole.

	Peripheral ratio	Initial load
Three hole	1.54	1.12
Two hole	1.25	1.07
Square	1.00	1.00
Strip	1.51	1.02

It is clear that the peripheral ratio is not a suitable means of comparing the loads for even these simple shapes. It is unlikely to apply for the more complex shapes encountered in industrial practise. The reason for its failure is that it cannot include any term to account for the differing deformation that must be taking place.

A more successful method maybe to adapt the method used to correlate the data with the hot working equations and to experimentally measure the correction factor, relative to a given datum line, that must.

* the ratio of the circumference to that of a bar of equal area

be applied. The flow stress can be obtained from the plane strain upperbound for an equivalent single hole reduction.

The loads at the end of extrusion showed different relations to those found at the start of the extrusion. The two hole extrusion load is higher than that found for three hole and that for the strip is the lowest. This difference would be due to a combination of the differing deformations and the associated temperature rise. The shape of the extrude also seems to have a significant effect on the peak height, which again may be a direct result of the complex shape of the deformation zone.

5.23 Limit Diagram

The Original limit diagrams by Hirst and Ursell and others, were based on either simple theory or a laborious experimental technique. Raybould used hot working theory and an upperbound solution to predict the limiting load lines and the limiting temperature line. His load line was calculated from the load at the deformation zone plus a frictional term. This predicted the dependence of the load on the strain rate. The present work has shown that this load is independent of the strain rate and is only dependent on the alloy, temperature and reduction ratio. The temperature line is limited by the occurrence of hot shortness and the temperature rise must not take the billet temperature over this limiting value. For a given ram speed and reduction ratio the flow stress can be found, from the experimental results figure 4.20 . Working back from this the flow stress can be used to predict the deformation load and hence the temperature rise can be calculated for a known billet length. The position of the minimum load has to be assumed but this will only lead to a small error. Subtracting the temperature rise from the maximum temperature gives the initial billet temperature for that particular set of conditions. Repeating this the limiting lines can be drawn for different strain rates. Figures 4.53 and 4.54 give the limit diagrams for alloys CE and DF respectively. The heat losses to the container at high temperatures mean that an initial billet temperature higher than the limiting temperature is predicted, at low strain rates. Obviously it is not possible to heat the billet above the melting point of any of its constituents, although the time at the temperature will be important. Therfore the limiting line at these low strain rates is indantical to the critical temperature for hot shortness.

The diagrams are drawn with three limiting temperature lines, each corresponding to a different strain rate. The diagram could therfore be drawn in a three dimensional form with the axes log R, initial billet temperature, and strain rate. The two surfaces obtained would be the limiting boundaries for the press capacity and hot shortness but other surfaces could be added for the limiting condition of complex shape extrusion, tube extrusion, or even other defects. At the present stage these other boundary surfaces would have to be found by experimental means, but the result would be a useful method of selecting the optimum production conditions. The use of video display units connected to a computer would be a possible means of examining and storing these diagrams.

5. 24 A Criticism of the Present Work.

No discussion is complete unless a criticism of the whole work is included. There are several criticisms that can be made.

1. The temperature model used was not verified experimentally. Although the integral profile method has been shown to give a reasonable estimate of the temperature rise, the suggested method of allowing for temperature losses to the container has to be tested.
2. A mean flow stress and mean strain rate was used to correlate the results from extrusion. No analysis was made of the variations in these parameters throughout the deformation.
3. No account was made of the temperature rise in the hot working and tensile tests and it was shown that these will effect the constants calcualted for the hot working equations.
4. Only one billet size was studied, except for a few experiments at different lengths. Although the dimensions of the billet were larger than those usually used in experiments of this kind. It remains to be seen whether results obtained can be applied to the size of billets used in industry.
5. Alloys similar to the ones studied are heat treated before use. The relationship between the properties after heat treatment to the extrusion parameters was not studied.
6. For ease of experimentation only one homogenization treatment was used. The heat treatment before extrusion will have some influence on the behaviour during extrusion.

7. The structure of the alloys before and after extrusion was not studied in great detail. It should be possible to determine the true nature of the precipitates, their original orientation, and their orientation after extrusion by using standard techniques.
8. The variation in structure and mechanical properties across the extrude and throughout its length was not studied in great detail.

5.25 The Industrial Relevance of the Present Work.

Extrusion is one the major methods of metal fabrication in use to-day and consequently experimental work of this nature should have some industrial relevance.

The scale of the experiments was more akin to industrial practice than is the usual case, although there is still a big difference between the experimental 5IMN press and the 50MN presses common in industry.

It has been shown that the empirical hot working equations can be applied to extrusions on this scale, and that the presence of the impurities usually found in aluminium alloys can have a significant effect on the hot working behaviour. It is not possible to gain more than a qualitative idea of the relative extrusion properties of the two alloys by the usual laboratory testing techniques. A useful idea is the application of correction factors to log Z when correlating data for different shapes and reduction ratios.

The capacity of a press limits the initial load that can be applied to a billet. The dependence of this peak load on the extrusion parameters and the structural changes was studied in more detail, and more important, the height of the peak seen at the start of extrusion was shown to depend on the alloy and the structural changes taking place at the start of extrusion. The peak load, as well as being linearly related to the logarithm of the reduction ratio, is practically independent of the ram speed and is related to the temperature through an Arrhenius type expression. By knowing the peak load at a given temperature the maximum reduction ratio or billet length for a given press can be calculated. A knowledge of the latter can increase the output during each run and this will lead to a reduction in the volume of discard during a production run.

The defect known as hot shortness was only found above a critical temperature and, using this as the limiting temperature, limit diagrams were drawn for alloys CE and DF. From these diagrams the optimum conditions forextrusion can be found. A suggestion was also made to increase the usefulness of this diagram be extending them to three dimension and plotting the limiting lines for other shapes and defects.

CONCLUSIONS

Within the accuracy of the experimental results the following conclusions can be drawn;

1. The results from hot torsion and hot tensile tests have been correlated over a wide range of the temperature compensated strain rate by the general hot working equation

$$Z = A(\sinh \alpha\sigma)^n$$

2. The constants in the above equation depend on the alloy. The presence of manganese has a significant effect on the hot workability of an Al- 4% Cu alloy.

3. The use of an activation energy of 160000 joules/mole is justified by a comparison of previous work and by the correlation found in the present results.

4. The mean flow stresses for single and multihole extrusion calculated from a simple minimized plane strain upper bound solution gave a qualitative agreement with those measured in torsion and tensile tests.

5 Using the mean flow stress, a mean strain rate and the calculated mean deformation temperature a graph of logZ against the flow stress gave a series of parallel straight lines, each corresponding to a different hole profile. The gradient of the lines was alloy dependent.

6. By applying a correction factor to logZ the results gave a linear correlation. The correction factor was only dependent on the die profile and not on the alloy. It is suggested that this approach may be utilised in the analysis of the extrusion of complex shapes

7. There was a considerable difference between the results from extrusion and those from the torsion and tensile tests. Although the general hot working equation could be applied to both sets of data the value of n was almost three times in the case of extrusion, although the ratios between the alloys were the same. This difference was not a result of neglecting the temperature rise in the torsion tests. It is due to the assumptions made in the extrusion theory.

8. It is therefore not possible to correlate the results from the different methods of testing.

9. The peak load is practically independent of the ram speed but is linearly related to logR. Its dependence on the temperature

is given by an Arrhenius type expression.

11 The height of the peak at the start of extrusion has a similar dependence on the ram speed and temperature as the peak load. There is almost a linear relationship between the peak height and the load necessary to cause extrusion. This line did not pass through the origin. The exact nature of the relationship depended on the alloy.

12. The peak load may be associated with the formation of a steady state flow pattern, which is related to the microstructural changes occurring at the start of extrusion.

13. The observed flow patterns for single hole extrusion agreed with those predicted by a minimized plane strain upper bound solution.

14 Removing and reapplying the load midway through an extrusion had two effects. If the load was completely removed a peak higher than the initial one was seen. Partial removal of the load led to a lower peak. these differences are related to the static structural changes occurring when extrusion stops

15. The structures in the as-extruded rod could be classified into three types, occurring at different levels of the flow stress.

1. fibrous
2. elongated recrystallized
3. fully recrystallized

More than one structure may be present in any extrude. The range over which each was found depended on the alloy content. The presence of manganese reduced the tendency for a recrystalliz ed structure to form.

16. Dynamic recrystallization does not occur in the extrusion of aluminium alloys.

17 The recrystallized structure had the highest mechanical properties. This can be attributed to precipitation in the fibrous structure.

18. There was no significant variation in the mechanical properties of the extrudes from the multihole extrusions.

19. The loads measured in the extrusion of simple shapes could not be correlated by the use of the peripheral ratio.

20 Hot shortness is due to incipient melting and is found above a critical temperature. At much higher temperatures an overheated structure is found.

21 the pressure lines on the limit diagrams are independent of the strain rate. The temperature lines are very dependent.

Appendix I

The computer programs used are given below.

1. The Conversion of the Torque Time Curves to Stress Strain Curves

The torque was measured by a load cell with a millivolt output. The reading obtained from the U.V. recorder was related to the torque by

$$T = U.V / TANPHI + CONSTANT$$

where U.V is the reading on the U.V chart

TANPHI and CONSTANT depend on the amplification used in the recorder

The data required is;

1. The radius of the specimen
2. The gauge length
3. The speed in R.P.M.
4. The constants TANPHI and CONSTANT
5. The time at which the torque was initially applied.This enables the time for each point on the curve to be conveniently measured from a chosen reference line.
6. The initial temperature.
7. The alloy identification code used.
8. The millivolt reading U.V at a time T.
9. The output is obtained by reading in U.V = 999.999

2. The Minimized Plane Strain Upper Bound Solution for Single Hole Extrusion.

This is a simple iteration program using the theory given in chapter two. The data needed is ;

1. The billet diameter
2. The extrusion ratio
3. The assumed values of the angles ω and ψ

The program calculates the optimum values of x, ω , and ψ , the latter being taken to an accuracy of 0.1 . Using these values the extrusion load and pressure are calculated.

3 The Minimized Multihole Plane Strain Solution

The theory used is given in chapter two and the program is a mod modified version of that given in section two. The program shown is that for the two hole solution.

The required data is ;

1. The billet diameter
2. The extrusion ratio
3. The estimated values of and

The results are given for the range of eccentricities 0.1 to 0.9 The three hole program is identical except for the following modifications;

line 00160 B=D/3.0 x ER

00165 A=(d- 3.0 x B) - ETA x (D- 3.0 x B)

00166 Z=(ETA/ 2.0) x (D - 3.0 x B)

00538 TOTLD = ALOAD + 2.0 x A2LOAD

4. The Simple Axisymmetric Solution

Up to line 00600 the program is identical to that for the plane strain solution, i.e. it calculates the optimum values of x, w, and ψ. Using these values the surface areas of the velocity discontinuities and the squares of the velocities are calculated. the load is then found from the theory given in chapter two.

5. The Complex Plane Strain Solution Used to Predict the Flow Patterns

This program calculates the load for the complete range of the variables for a given billet length, radius, and extrusion ratio. It then selects the minimum. The data that must be supplied is

1. The billet length
2. The billet radius
3. The extrusion ratio

The output lists the values of the angles and the length x that gives the minimum load.

6. A General Least Squares Program

This calculates the best fit straight line thr ugh a set of data by the standard least squares formula. The variables X and Y are fed in as the data. At lines 00171 and 00172 it is possible to insert the functions of X and Y that have to be correlated. In the example shown lines 00164 and 00166 calculate the value of sinh9 o). The best fit straight line between logX and logsinh(o) is then found. The output lists X,Y,f(X),f(Y), the mean values of f(X)and f(Y), the equation of the line, and the regression coefficient.

PROGRAM 1

```
ØØ1ØØ PROGRAM TORQUE(INPUT,OUTPUT)
ØØ11Ø DIMENSIONUV(5ØØ),T(5ØØ)
ØØ12ØC READ IN R,LENGTH AL,R*P*M S,TANPHI,CONSTANT,TIME AT
ØØ13ØCZERO,TEMP,ALLOY,C =1,D =2
ØØ14Ø PRINT 1
ØØ141 1 FORMAT(*ENTER R,AL,S,TPHI*)
ØØ142 READ 5,R,AL,S,TPHI
ØØ143 5 FORMAT(F1Ø·5,F1Ø·5,F1Ø·5,F1Ø·5)
ØØ15Ø PRINT 2
ØØ151 2 FORMAT(*ENTER C,TO,TEMP,ALLOY*)
ØØ152 READ 4,C,TO,TEMP,J
ØØ153 4 FORMAT(F1Ø·5,F1Ø·5,F1Ø·5,I1)
ØØ17ØCCALCALUATE OMEGA
ØØ18Ø OM = 2·Ø*3·142*S/6Ø·Ø
ØØ19ØC CALCULATE SHEAR STRAIN RATE,TRUE STRAIN RATE
ØØ2ØØ STR = R*OM/AL
ØØ21Ø TSTR =STR/SQRT(3·Ø)
ØØ22Ø PRINT 6,TEMP,J,STR,TSTR
ØØ23Ø 6 FORMAT(5HTEMP=,F1Ø·5,2X,6HALLOY ,I1,2X,4HSTR=,F12·6
ØØ24Ø+,2X,5HTSTR=,F12·6)
ØØ28Ø+TRUE STRESS*)
ØØ29ØC CALCULATE TORQUE
ØØ3ØØ DO 1ØØ I=1,5ØØ
ØØ31Ø READ 8,UV(I),T(I)
ØØ32Ø 8 FORMAT(F1Ø·5,X,F1Ø·5)
ØØ33Ø IF(UV(I)·EQ·999·999) GO TO 1Ø
ØØ34Ø GO TO 1ØØ
ØØ35Ø 1Ø N=(I-1)
ØØ36Ø GO TO 11
ØØ37Ø 1ØØ CONTINUE
ØØ375 11 PRINT 7
ØØ376 7 FORMAT(*   S·STRAIN          S·STRESS          TSTRAIN       TSTRESS
                                                                    )
ØØ377+*)
ØØ38Ø DO 1Ø1 I=1,N
ØØ39Ø AM=(UV(I)/TPHI)+C
ØØ4ØØ THETA =(2·Ø*3·142*S/6Ø·Ø)*(T(I)-TO)
ØØ41Ø GAM =R*THETA/AL
ØØ421 TOR =3·Ø*AM/(2·Ø*3·142*(R**3)*(1Ø·Ø**6))
ØØ43Ø SIGMA =SQRT(3·Ø)*TOR
ØØ44Ø ETA =GAM/(SQRT(3·Ø))
ØØ45Ø PRINT 9, GAM,TOR,ETA,SIGMA
ØØ46Ø 9 FORMAT(F12·4,3X,F12·4,3X,F12·4,3X,F12·5)
ØØ47Ø 1Ø1 CONTINUE
ØØ48Ø STOP
ØØ49Ø END
```

PROGRAM 2

```
      PROGRAM UPPERB(INPUT,OUTPUT)
    1 PRINT 4
    4 FORMAT(*READ IN DIAMETERD,ER,OM,PHI*)
      READ 5,D,ER,OM,PHI
    5 FORMAT(4F10.4)
      IF(J.EQ.9)GO TO 105
      A= D-(D/ER)
      B=D-A
C CONVERT OMEGA AND PHI TO RADIANS
      R1OM =OM/57.29578
      R1PHI =PHI/57.29578
C CALCULATE DEPTH OF WORKING
   10 A1=A**2/(1.0+((A/B)*(SIN(R1OM))**2))
      B1=B*A/(1.0+((A/B)*SIN(R1PHI))**2))
      PRINT 6,A1,B1
    6 FORMAT(5X,3HA1=,F10.4,5X,3HB1=,F10.4)
      X=SQRT(A1+B1)
      N=N+1
C CALCULATE AND WRITE OUT NEW ANGLES
      EOM=(4.0*A)/(3.0*X)
      EPHI=(4.0*B)/(3.0*X)
      R2OM=ATAN(EOM)
      R2PHI=ATAN(EPHI)
      PRINT 7,R2OM,R2PHI
    7 FORMAT(5X,6HOMEGA=,F10.4,5X,4HPHI=,F10.4)
      DIF1=SQRT((57.29578*(R1OM-R2OM))**2)
      DIF2=SQRT((57.29578*(R1PHI-R2PHI))**2)
      PRINT 8,DIF1,DIF2,X
    8 FORMAT(5X,5HDIF1=,F10.4,5X,6HDIF2=,F10.4,5X,2HX=,F10.4)
      IF(DIF1.LT.0.1.AND.DIF2.LT.0.1) GO TO 9
      IF (N.EQ.50) GO TO 101
      R1OM =R2OM
      R1PHI=R2PHI
      GO TO 100
C CALCULATE LOAD USING VALUES OF X,OM PHI
    9 C1=(2.0*(A**2))/(X*(SIN(R2OM))**2)
      C2=(2.0*A*B)/(X*(SIN(R2PHI))**2
      C3=(3.0*A)/TAN(R2OM)
      C4=(3.0*A)/TAN(R2PHI)
      PRINT 15 ,C1,C2,C3,C4
   15 FORMAT(3HC1=,F10.4,2X,3HC2=,F10.4,2X,3HC3=,F10.4,2
     10+X,3HC4=,F10.4)
      ALOAD=(2.0*X)+(2.0*X*A)/B+C1+C2-C3-C4
      PRESS=ALOAD/D
      OM=R2OM*57.29578
      PHI=R2PHI*57.29578
      PRINT 10,A,B,D,ER,X,OM,PHI,ALOAD,PRESS
   10 FORMAT(2HA=,F10.4,2X,2HB=,F10.4,2X,2HD=,F10.4//16
     20HEXTRUSION RATIO=,F10.4/2HX=,F10.4,2X,3HOM=,F10.
     3+4,2X,4HPHI=,F10.4//5HALOAD=2K,F10.4//12HPRE
     4SSURE = K,F10.4)
      GO TO 1
  101 PRINT 102
  102 FORMAT(*N=50*)
  105 STOP
      END.
```

PROGRAM 3

```
      PROGRAM UPPERB(INPUT,OUTPUT)
    1 PRINT 4
    4 FORMAT(*READ IN DIAMETER,D,ER,OM,PHI*)
      READ 5,D,ER,OM,PHI
    5 FORMAT(4F10.4)
      IF(J.EQ.9)GO TO 105
      DO 150 IETA=1,9
      STOREL=0.0
      B=D/(2.0*ER)
      ETA=FLOAT(IETA)/10.0
      A=(D-2.0*B)-(ETA*(D-2.0*B))
      Z=ETA*(D-2.0*B)
      PRINT 25 A,Z,ETA
   25 FORMAT(2HA=,F10.4,2X,2HZ=,F10.4,2X,4HETA=,F10.4)
      B=D-A
C CONVERT OMEGA AND PHI TO RADIANS
      R1OM =OM/57.29578
      R1PHI =PHI/57.29578
C CALCULATE DEPTH OF WORKING
      A1=A**2/((1.0+((A/B)*(SIN(R1OM))**2))
      B1=B*A/((1.0+((A/B)*SIN(RIPHI))**2))
      PRINT 6,A1,B1
    6 FORMAT(5X,3HA1=,F10.4,5X,3HB1=,F10.4)
      X=SQRT(A1+B1)
      N=N+1
C CALCULATE AND WRITE OUT NEW ANGLES
      EOM=(4.0*A)/(3.0*X)
      EPHI=(4.0*B)/(3.0*A)
      R2OM=ATAN(EOM)
      R2PHI=ATAN(EPHI)
      PRINT 7,R2OM,R2PHI
    7 FORMAT(5X,6HOMEGA=,F10.4,5X,4HPHI=,F10.4)
      DIF1=SQRT((57.29578*(R1OM-R2OM))**2)
      DIF2=SQRT((57.29578*(R1PHI-R2PHI)**2)
      IF(DIF1.LT.0.1.AND.DIF2.LT.0.1) GO TO 9
      IF (N.EQ.50) GO TO 101
      R1OM =R2OM
      R1PHI=R2PHI
      GO TO 100
C CALCULATE LOAD USING VALUES OF X,OM PHI
    9 C1=(2.0*(A**2))/(X*(SIN(R2OM))**2)
      C2=(2.0*B*A*B)/(X*(SIN(R2PHI))**2
      C3=(3.0*B*A)/TAN(R2OM)
      C4=(3.0*B*A)/TAN(R2PHI)
      ALOAD=(2.0*X)+(2.0*X*A)/6+C1+C2-C3-C4
      DO LOM2=2,89,2
      OM2=LOM2
      ROM2=OM2/57.29578
      C21=(2.0*(Z**2))/(X*(SIN(ROM2))*2)
      C22=(2.0*B*Z*B)/(X*(SIN(R2PHI))*2)
      C23=(3.0*B*Z)/TAN(ROM2)
      C24=(3.0*B*Z)/TAN(R2PHI)
      A2LOAD=(2.0*X)+2.0*Z*X/B)+C21+C22-C23-C24
      TOTLO=ALOAD+A2LOAD
      OM=R2OM*57.29578
      PHI=R2PHI*57.29578
      IF(STOREL.LE.0.0)GO TO 200
      GO TO 201
  201 IF (STOREL.GE.TOTLO) GO TO 200
      GO TO 140
  200 STOREL=TOTLO
      STOM=OM
      STPHI=PHI
      STOM2=OM2
  140 CONTINUE
      PRESS=STOREL/D
      PRINT 10,ETA,ER,D,B,A,X,Z,STOM,STPHI,STOM2,STOREL,PRESS
   10 FORMAT(4HETA=,F10.4,2X,3HER=,F10.4,2HD=,F10.4
     +,2HB=,F10.4//2HA=,F10.4,2X,2HX=,F10.4,2X,2HZ=,F10.4
     +//3HOM=,2X,4HPHI=,F10.4,2X,4HOM2=,F10.4//14HTOT
     +AL LOAD = K,F10.4,2X,12HPRESSURE = K,F10.4)
     +4,2X,4HPHI=,F10.4//8HALOAD=2K,F10.4//12HPRE
  150 CONTINUE
      GO TO 1
  101 PRINT 102
  102 FORMAT(*N=50*)
  105 STOP
      END
```

Program 4

```
ØØ1ØØ PROGRAM UPPERØ(INPUT,OUTPUT)
ØØ11Ø 1 PRINT 4
ØØ12Ø 4 FORMAT(*HEAD IN DIAMETERS,LH,UM,PHI*)
ØØ13Ø READ U,D,EH,UM,PHI
ØØ14Ø 5 FORMAT(4F1Ø.4)
ØØ15Ø IF(U.EQ.Ø)GO TO 1Ø5
ØØ16Ø A= D-(D/EH)
ØØ17Ø B=D-A
ØØ18ØC CONVERT OMEGA AND PHI TO RADIANS
ØØ19Ø R1UM =UM/57.2957Ø
ØØ2ØØ R1PHI =PHI/57.2957Ø
ØØ21ØC CALCULATE DEPTH OF WORKING
ØØ22Ø 1ØØ A1=A**2/(1.Ø+((A/B)*(SIN(R1UM))**2))
ØØ23Ø B1=B*A/(1.Ø+((A/B)*SIN(R1PHI))**2))
ØØ24Ø PRINT 6,A1,B1
ØØ25Ø 6 FORMAT(5X,3HA1=,F1Ø.4,5X,3HB1=,F1Ø.4)
ØØ26Ø X=SQRT(A1+B1)
ØØ27Ø N=N+1
ØØ28ØC CALCULATE AND WRITE OUT NEW ANGLES
ØØ29Ø EUM=(4.Ø*A)/(3.Ø*X)
ØØ3ØØ EPHI=(4.Ø*B)/(3.Ø*X)
ØØ31Ø R2UM=ATAN(EUM)
ØØ32Ø R2PHI=ATAN(EPHI)
ØØ33Ø PRINT 7,R2UM,R2PHI
ØØ34Ø 7 FORMAT(5X,6HOMEGA=,F1Ø.4,5X,4HPHI=,F1Ø.4)
ØØ35Ø DIF1=SQRT((57.2957Ø*(R1UM-R2UM))**2)
ØØ36Ø DIF2=SQRT((57.2957Ø*(R1PHI-R2PHI))**2)
ØØ37Ø PRINT 8,DIF1,DIF2,X
ØØ38Ø 8 FORMAT(5X,5HDIF1=,F1Ø.4,5X,6HDIF2=,F1Ø.4,5X,2HX=,F1Ø.4)
ØØ39Ø IF(DIF1.LT.Ø.1.AND.DIF2.LT.Ø.1) GO TO 9
ØØ4ØØ IF (N.EQ.5Ø) GO TO 1Ø1
ØØ41Ø R1UM =R2UM
ØØ42Ø R1PHI=R2PHI
ØØ43Ø GO TO 1ØØ
ØØ44ØC CALCULATE LOAD USING VALUES OF X,UM PHI
ØØ45Ø 9 C1=(2.Ø*(A**2))/(X*(SIN(R2UM))**2)
ØØ46Ø C2=(2.Ø*A*B)/(X*(SIN(R2PHI))**2
ØØ47Ø C3=(3.Ø*A)/TAN(R2UM)
ØØ48Ø C4=(3.Ø*A)/TAN(R2PHI)
ØØ49Ø PRINT 15 ,C1,C2,C3,C4
ØØ5ØØ 15 FORMAT(3HC1=,F1Ø.4,2X,3HC2=,F1Ø.4,2X,3HC3=,F1Ø.4,2
ØØ51Ø+X,3HC4=,F1Ø.4)
ØØ52Ø ALOAD=(2.Ø*X)+(2.Ø*X*A)/B+C1+C2-C3-C4
ØØ53Ø PRESS=ALOAD/D
ØØ54Ø UM=R2UM*57.2957Ø
ØØ55Ø PHI=R2PHI*57.2957Ø
ØØ56Ø PRINT 1Ø,A,B,D,EH,X,UM,PHI,ALOAD,PRESS
ØØ57Ø 1Ø FORMAT(2HA=,F1Ø.4,2X,2HB=,F1Ø.4,2X,2HD=,F1Ø.4//16
ØØ58Ø+HEXTRUSION RATIO=,F1Ø.4/2HX=,F1Ø.4,2X,3HUM=,F1Ø.
ØØ59Ø+4,2X,4HPHI=,F1Ø.4//8HALOAD=2K,F1Ø.4//12HPRE
ØØ6ØØ+SSURE = K,F1Ø.4)
ØØ6Ø5 AØ=SIN(R2UM)
ØØ61Ø BC=B/SIN(R2PHI)
ØØ62Ø BØ=X
ØØ63Ø AØ=SQRT(((A**2)/(SIN(R2UM))**2)+(X**2)-(2.Ø*A*X*COS
ØØ64Ø+(R2UM)/SIN(R2UM)
ØØ65Ø BC=SQRT(((B**2)/(SIN(R2PHI))**2)+(X**2)-(2.Ø*A*B*X*
ØØ66Ø+COS(R2PHI),SIN(R2PHI)))
ØØ67Ø A13=A/(X*SIN(R2UM))
ØØ68Ø A54=A/(X*SIN(R2PHI))
ØØ69Ø A23=(1.Ø/X)*AØ
ØØ7ØØ A24=(A/(X*B))*BC
ØØ71Ø A34=1.Ø+(A/B)-(A/X)*((COS(R2UM)/SIN(R2UM))+(COS
ØØ72Ø+(R2PHI)/SIN(R2PHI)))
ØØ73ØC CALCULATE AXISYMMETRIC LOAD AND PRESSURE
ØØ74Ø AXØ=AØ*3.1416*(D+B)
ØØ75Ø BXP=2.Ø*3.1416*BØ*B
ØØ76Ø UXC=BC*3.1416*B
ØØ77Ø AXB=AB*3.1416*(D+B)
ØØ78Ø BXC=BC*3.1416*B
ØØ79Ø X13=(A13)**2
ØØ8ØØ X54=A54**2
ØØ81Ø X23=A23**2
ØØ82Ø X24=A24**2
ØØ83Ø X34=A34**2
ØØ84Ø AXLOAD=(AXØ*X13)+(BXØ*X34)+(UXC*X54)+(AXB*X23)+(BXC*
ØØ85Ø+X24)
ØØ86Ø EXH=(D**2)/(B**2)
ØØ87Ø PRESSX=AXLOAD/(3.1416*(D**2))
ØØ88Ø PRINT 4Ø,EXH,AXLOAD,PRESSX
ØØ89Ø 4Ø FORMAT(19HAXIEXTRUSION RATIO=,F1Ø.4//
ØØ9Ø+3HAXLOAD=K,F1Ø.4//14HAXIPRESSURE =K,F1Ø.4)
ØØ91Ø GO TO 1
ØØ92Ø 1Ø1 PRINT 1Ø2
ØØ93Ø 1Ø2 FORMAT(*N=5Ø*)
ØØ94Ø 1Ø5 STOP
ØØ95Ø END


CP        Ø.ØØ7 SECS.
READY.
```

PROGRAM 5

```
      PROGRAM UBM2(INPUT,OUTPUT,TAPE5=INPUT,TAPE6=OUTPUT)
  200 READ(5,2)L,RB,ER
    2 FORMAT(I5,F10.7,F13.7)
      IF(L.EQ.0) GO TO 201
      D=SQRT((RB**2)/ER)
      A=RB-D
      WRITE(6,4)L,A,D
    4 FORMAT(3HL= ,I5,3X,3HA= ,F10.4,3X,3HD= ,F10.4)
      ALOAD= 0.0
      DO 100 NX=1,L,1
      X=FLOAT(NX)
C CONVERT L TO REAL VARIABLE
      AL=FLOAT(L)
      IF(AL.LE.X) GO TO 11
      AOMAX=ATAN(A/X)
      AOMIN = ATAN(A/AL)
      IOMAX = AOMAX*180.0/3.1425
      IOMIN = AOMIN*180.0/3.1415
      DO 101 IOM= IOMIN,IOMAX,2
C CONVERT IOM TO REAL VARIABLE
      AO = FLOAT(IOM)*3.1415/180.0
      GAM=(ATAN((A-(X*TAN(AO)))/(AL-X)))
      IF(GAM.GE.AO.OR.GAM.LE.0.0) GO TO 101
C CALCULATE ALPHA
      ALF =((ATAN(A/(AL-X)))-GAM)
      B=ATAN((A/X)/(((A+D)/D)-1.0))
      C =ALF+GAM
      IF(C.LT.B) GO TO 101
      JB = B*180.0/3.1415
      JC = C*180.0/3.1415
      DO 102 JBT =JB,JC,2
      BETA = FLOAT(JBT)*3.1415/180.0
      XT=X-(D/TAN(BETA))
      IF(XT.LT.0.0)GO TO 102
      DXT=D/XT
      IF(DXT.LT.0.0.OR.DXT.GT.1.0) GO  TO 102
      RO =AO
      RT= ARSIN(DXT)
C CALCULATE EXPRESSION FOR LOAD
      BO=D/SIN(RT)
      AC=X/TAN(RO)
      DC=(AL-X)/COS(GAM)
      DA=A/(SIN(ALF+GAM))
      CO=X/COS(RO)
      AB=SQRT((D**2)+((X-D/TAN(RT))**2))
      A50=A/(X*SIN(RT))
      A25=(((A+D)/D)-(A/(X*TAN(RO)))-(A/(X*TAN(RT)))
      IF(A25.LT.0.0) GO TO 102
      A23=(A/X)-(SIN(GAM)/SIN(ALF))*(SIN(GAM+ALF))
      IF(A23.LT.0.0) GO TO 102
      A43=SIN(GAM)/SIN(ALF)
      A13=SIN(180.0-(ALF+GAM))/SIN(ALF)
      IF(A13.LT.0.0) GO TO 102
       B45=((((A+D)/D)-1.0)**2)+((A/(X*SIN(RT)))**2)-2.0*(((A+D)/D)-1.0
     1)*(A/(X*SIN(RT)))*COS(RT))
      IF(B45.LT.0.0) GO TO 102
      A45=SQRT(B45)
      A12=A/(X*(SIN(RO)))
      BLOAD=(BO*A50)+(X*A25)+(AC*A23)+(DA*A43)+(DC*A13)+(AB*A45)+(CO*A12
```

```
      1)
        IF(ALOAD.EQ.0.0) GO TO 10
       IF(BLOAD.LT.ALOAD) GO TO 10
       GO TO 102
C STORE VALUES OF L,OMEGA,THETA,X,GAMMA,ALPAH,LOAD
   10 ALOAD=BLOAD
      ARO=RO
      ART=RT
      AX=X
      AGAM=GAM
      AALF=ALF
      XA50=A50
      XA25=A25
      XA23=A23
      XA43=A43
      XA13=A13
      XA45=A45
      XA12=A12
      XRO=RO
      XAC=AC
      XDC=DC
      XDA=DA
      XCO=CO
      XAB=AB
  102 CONTINUE
  101 CONTINUE
  100 CONTINUE
C CONVERT ANGLES TO DEGREES
   11 ARO=ARO*180.0/3.1415
      ART=ART*180.0/3.1415
      AGAM=AGAM*180.0/3.1415
       AALF=AALF*180.0/3.1415
      WRITE(6,3)ER,ALOAD,AX,ARO,ART,AGAM,AALF
    3 FORMAT(3X,18HEXTRUSION RATIO = ,F10.4,8HALOAD = ,F10.4,5X,4HX = ,F
     110.4//3X,8HOMEGA = ,F10.4,3X,8HTHETA = ,F10.4,3X,8HGAMMA = ,F10.4,
     28HALPHA = ,F10.4)
      PRESS=ALOAD/(A+D)
      WRITE(6,25)PRESS
   25 FORMAT(10HPRESSURE =,F10.4)
      XALOAD=(3.1416*XRO*D*(XA50**2))+(AX*3.1416*2.0*D*(XA25**2))+((((XA
     1O+D)**2)-(D**2)*3.1416)*(XA23**2))+((XDA*(RB+D)*3.1416)*(XA43**2))
     2+((XDC*(RB+XAC+D)*3.1416)*(XA13**2))+((XAB*3.1416*D)*(XA45**2))+((
     3XCO*(XAC+D+D)*3.1416)*(XA12**2))
      XPRESS=XALOAD/(3.1416*(RB**2))
      WRITE(6,5)XRO,XAC,XDC,XDA,XCO,XAB,AX,XA50,XA25,XA23,XA43,XA13,XA45
     U,XA12,XALOAD,XPRESS
    5 FORMAT(7F10.4//7F10.4//7HXALOAD=,F10.4,2X,7HXPRESS=,F10.4)
      GO TO 200
  201 STOP
      END
```

PROGRAM 6

```
ØØ1ØØ PROGRAM FUDGE(INPUT,OUTPUT)
ØØ1Ø5 DIMENSION X(2ØØ),Y(2ØØ),AX(2ØØ),AY(2ØØ)
ØØ11Ø DO 1Ø1I=1,1ØØ
ØØ12Ø READ 5,X(I),Y(I)
ØØ13Ø 5 FORMAT(F1Ø.7,F1Ø.5)
ØØ14Ø IF(X(I).EQ.999.999)GO TO 1Ø
ØØ15Ø 1Ø1 CONTINUE
ØØ16Ø 1Ø N=I-1
ØØ161 PRINT 2Ø
ØØ162 2Ø FORMAT(*X = LOG(ETAD) Y= SINH(A*SIGMA)*)
ØØ163 DO 1Ø2 I=1,N
ØØ164 SA =Ø.324*(Y(I))
ØØ166 SINSA =(EXP(SA)-EXP(-SA))/2.Ø
ØØ171 AX(I)=ALOG(X(I))
ØØ172 AY(I)=ALOG(SINSA)
ØØ173 PRINT 21,X(I),AX(I),Y(I),AY(I)
ØØ174 21 FORMAT(F1Ø.4,1X,F1Ø.4,1X,F1Ø.4,1X,F1Ø.4)
ØØ175 X(I) =AX(I)
ØØ176 Y(I) =AY(I)
ØØ18Ø AN=N
ØØ19Ø SX=SX+X(I)
ØØ2ØØ SY=SY+Y(I)
ØØ22Ø AVX=SX/AN
ØØ23Ø AVY=SY/AN
ØØ24Ø SUMXY=SUMXY +(X(I)*Y(I))
ØØ25Ø SUMX2=SUMX2 +X(I)**2
ØØ255 SUMY2 =SUMY2+Y(I)**2
ØØ26Ø 1Ø2 CONTINUE
ØØ27Ø A1 =(SUMXY-(AN*AVX*AVY))/(SUMX2-(AN*AVX**2))
ØØ28Ø AØ =AVY-(A1*AVX)
ØØ282 R1=(SUMXY-(SX*SY/AN))
ØØ284 R2=(SUMX2-((SX**2)/AN))*(SUMY2-((SY**2)/AN))
ØØ286 R=R1/SQRT(R2)
ØØ29Ø PRINT 6,AVX,AVY,AØ,A1,R
ØØ3ØØ 6 FORMAT(4HAVX=,F1Ø.4,3X,4HAVY=,F1Ø.4/2HY=,F1Ø.4,1H+,
ØØ31Ø+ F1Ø.4,1HX,4X,7HCORREL=,F1Ø.6)
ØØ32Ø STOP
ØØ33Ø END
745.Ø      Ø.12

CP       Ø.ØØ1 SECS.
READY.
```

APPENDIX II

The Constants Used in the Analysis of the Extrusion Results

1. Strain Rates

R	$\dot{\varepsilon}$ sec^{-1}
10:1	0.64V
30:1	1.59V
50:1	2.40V
60:1	2.77V
70:1	3.14V
80:1	3.48V
90:1	3.80V
100:1	4.16V

2. The Load Constants

Single Hole

R	C
10:1	4.70
30:1	8.44
50:1	10.97
60:1	12.04
70:1	13.02
80:1	13.93
90:1	14.79
100:1	15.59

Two Hole

R		C
30:1	0.156	10.18
50:1	0.189	12.70
60:1	0.195	13.33
70:1	0.200	14.8
80:1	0.204	15.85
90:1	0.207	16.8
100:1	0.210	17.74

Three Hole

R		C
30:1	0.183	9.78
50:1	0.228	12.24
60:1	0.239	13.35
70:1	0.248	14.25
80:1	0.255	15.24
90:1	0.260	16.05
100;1	0.265	16.98

3. Temperature Rise

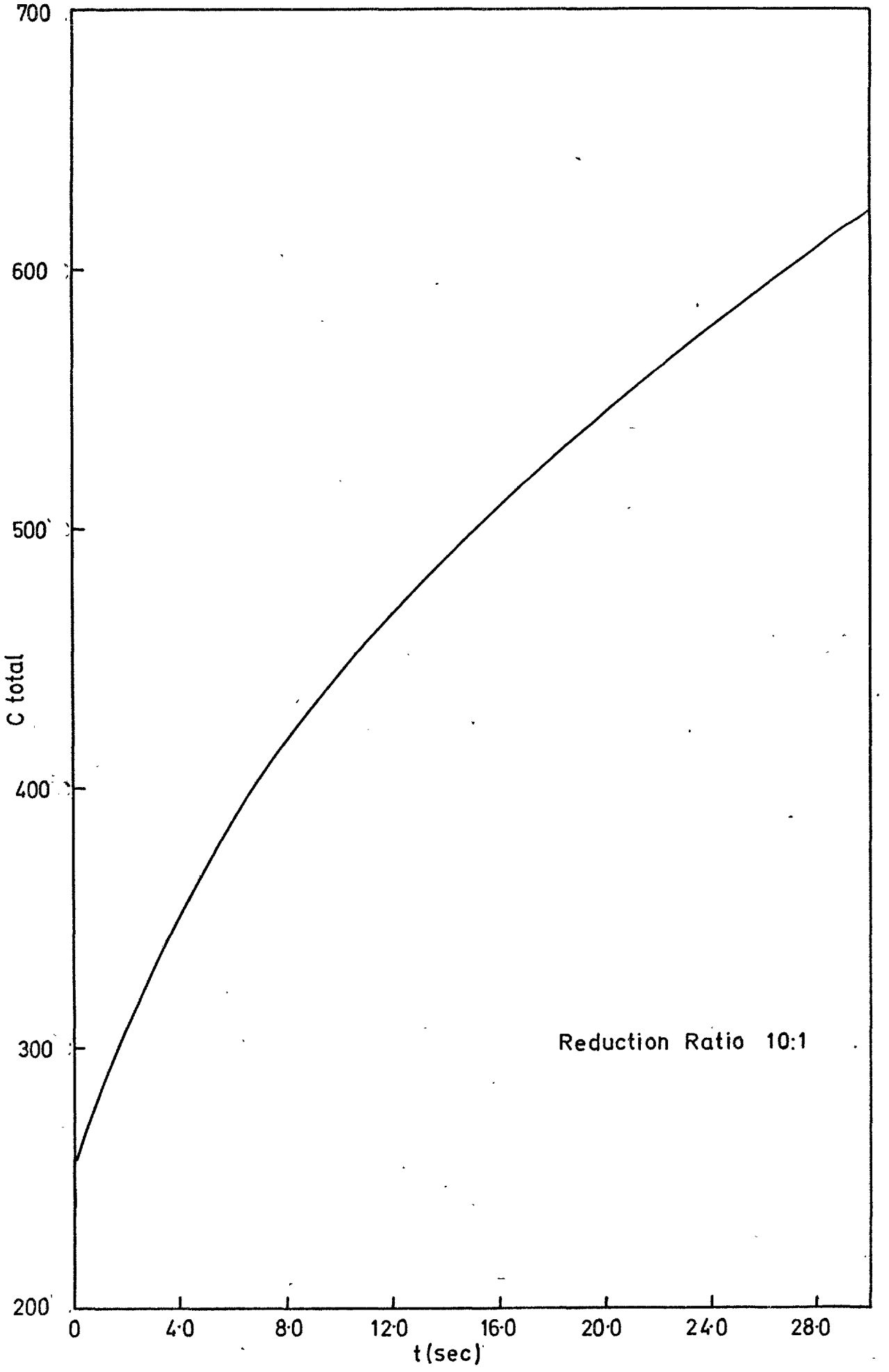
Graphs of C_{tot} against time are given for the different extrusion ratios used.

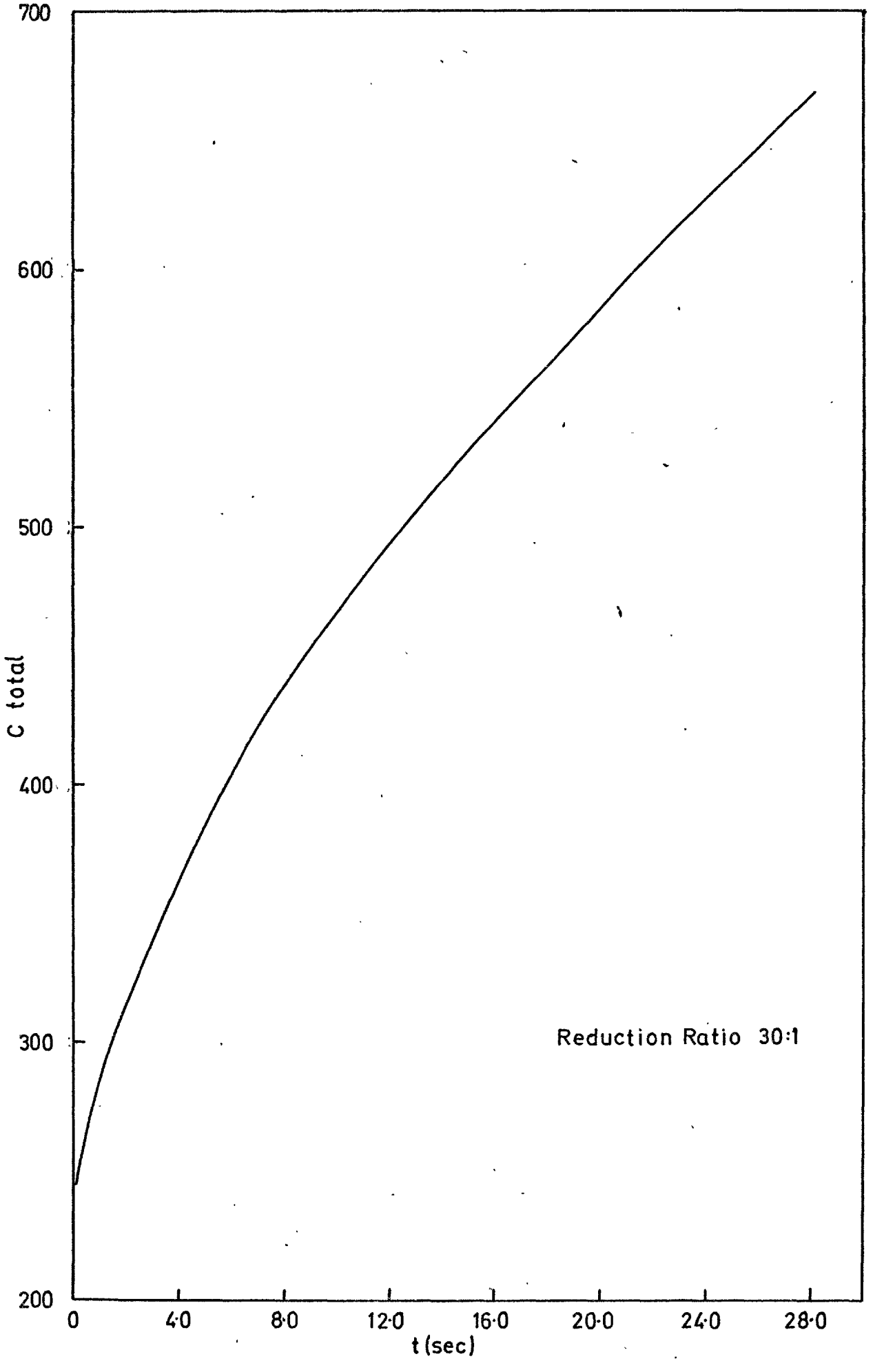
These curves were calculated using the specific heats and thermal conductivities for the container steel given below.

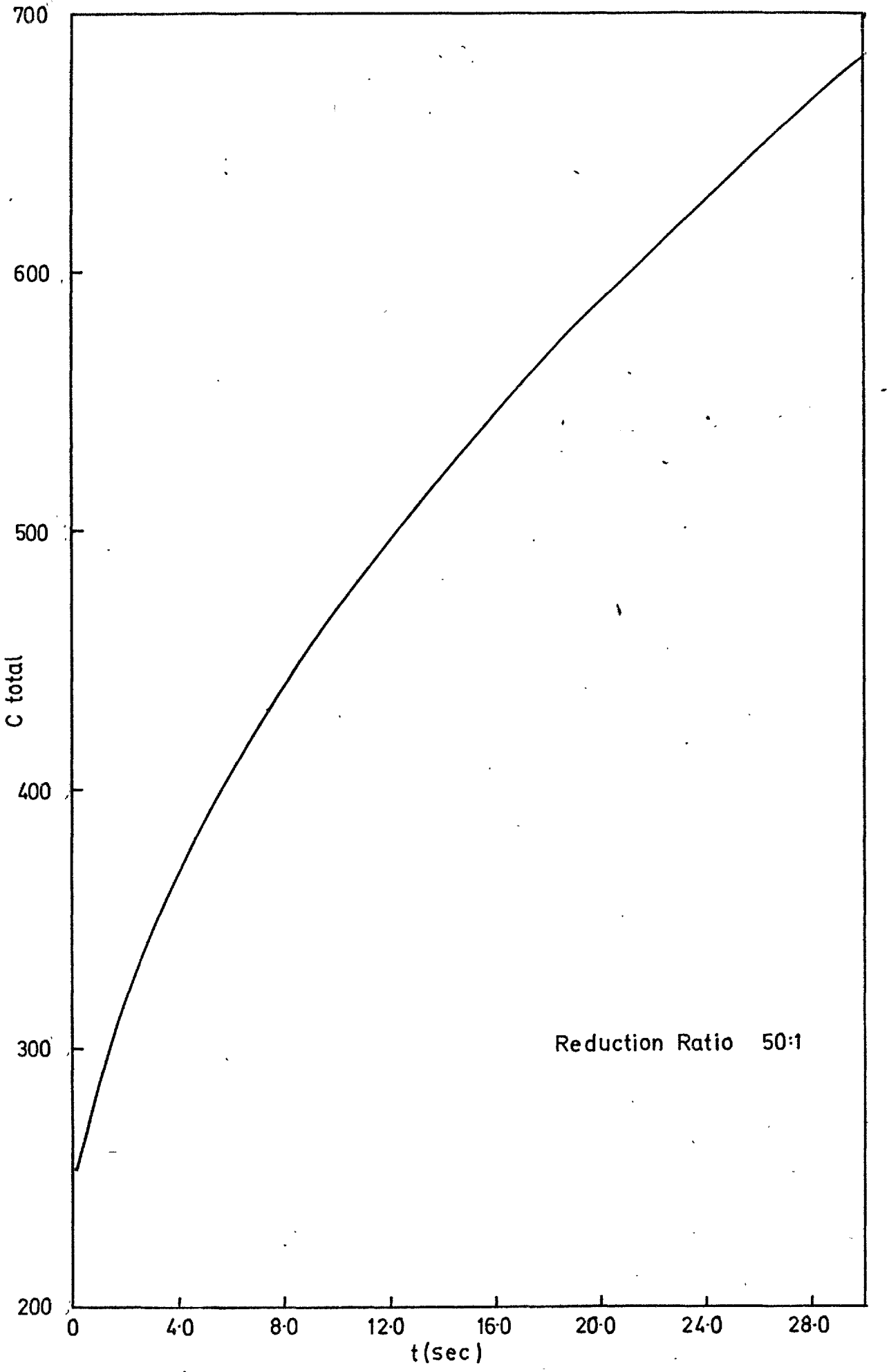
Specific Heat = 0.117 cal/gm/ C

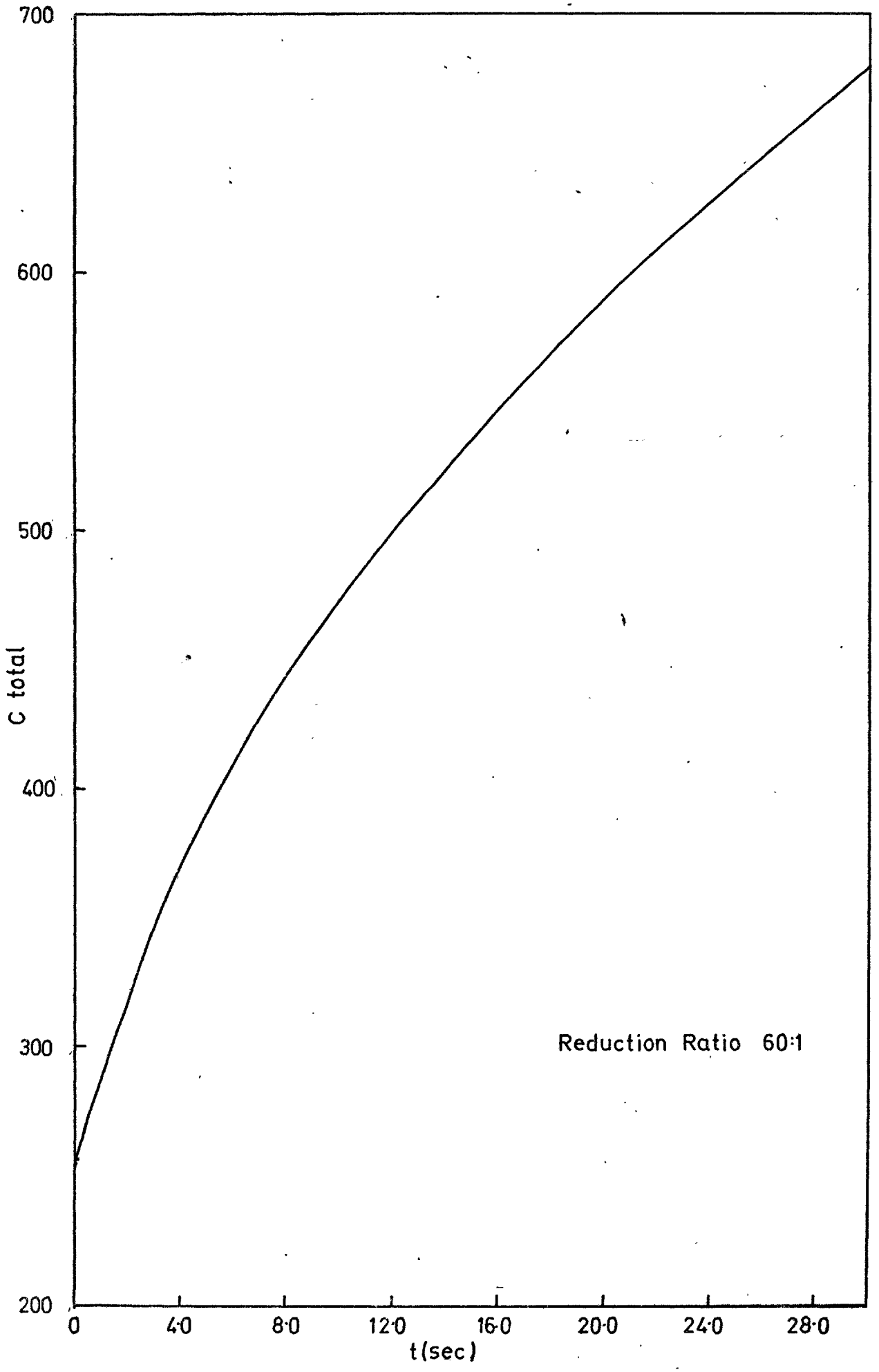
Thermal conductivity K

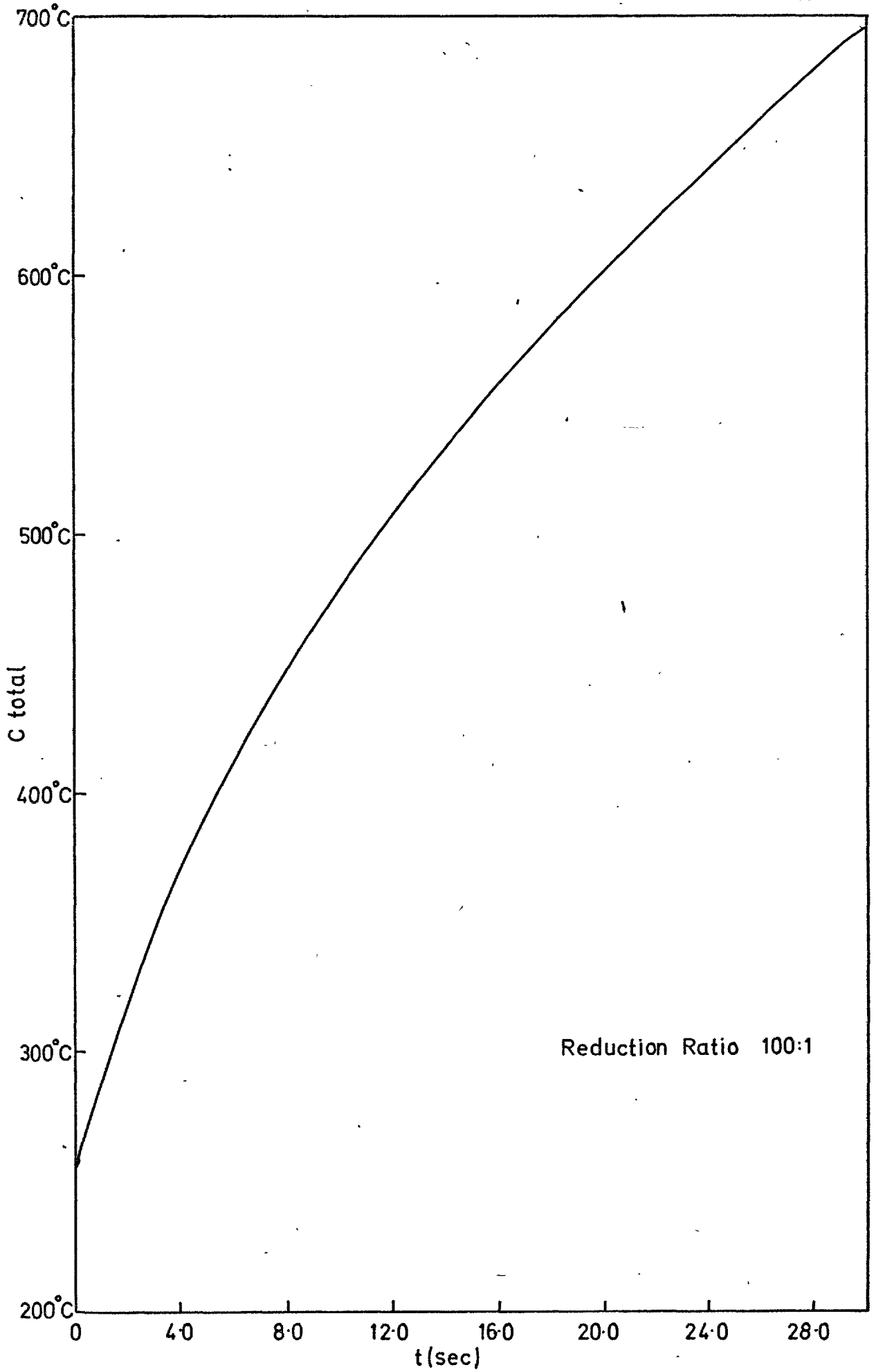
T C	K
200	0.077
250	0.078
300	0.078
350	0.079
400	0.077
450	0.076
500	0.075
550	0.073
600	0.072


700
600
500
400
300
200
C total
0
4·0
8·0
12·0
16·0
20·0
24·0
28·0
t (sec)
Reduction Ratio 10:1


700
600
500
400
300
200
C total
0
4·0
8·0
12·0
16·0
20·0
24·0
28·0
t (sec)
Reduction Ratio 30:1


700
600
500
400
300
200
C total
0
4·0
8·0
12·0
16·0
20·0
24·0
28·0
t (sec)
Reduction Ratio 50:1


700
600
500
400
300
200
C total
0
4·0
8·0
12·0
16·0
20·0
24·0
28·0
t(sec)
Reduction Ratio 60:1

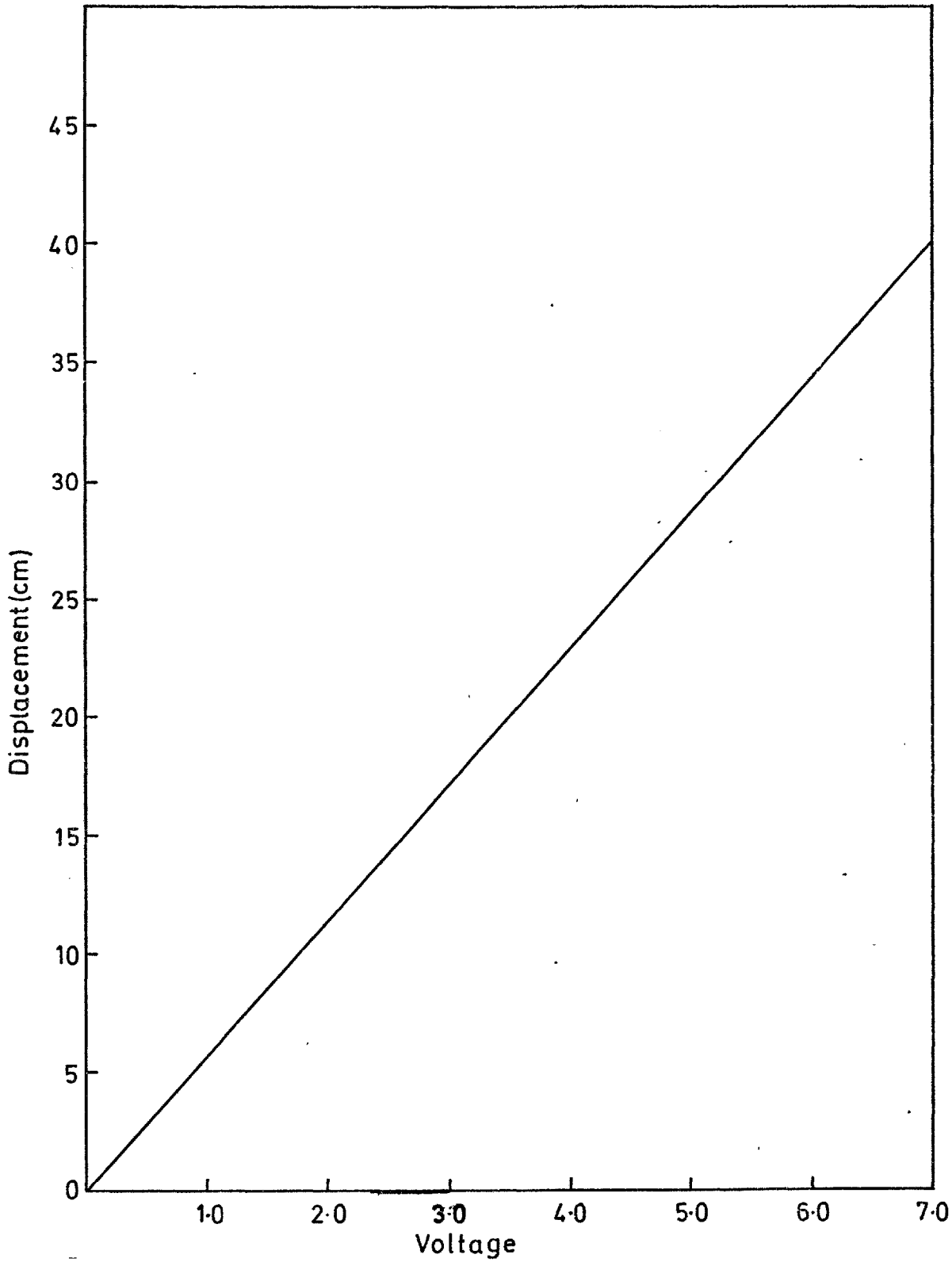

700°C
600°C
500°C
400°C
300°C
200°C
C total
0
4·0
8·0
12·0
16·0
20·0
24·0
28·0
t (sec)
Reduction Ratio 100:1

APPENDIX III

Calibration curves

The following calibration curves are given in graphical form;

1. The voltage output from the linear potentiometer used to measure the ram displacement and speed
2. The millivolt output from the load cell
3. The cooling curve for the billet in the container
4. The cooling curve for the billet in the induction heater



A III.1. The calibration curve for the ram displacement.

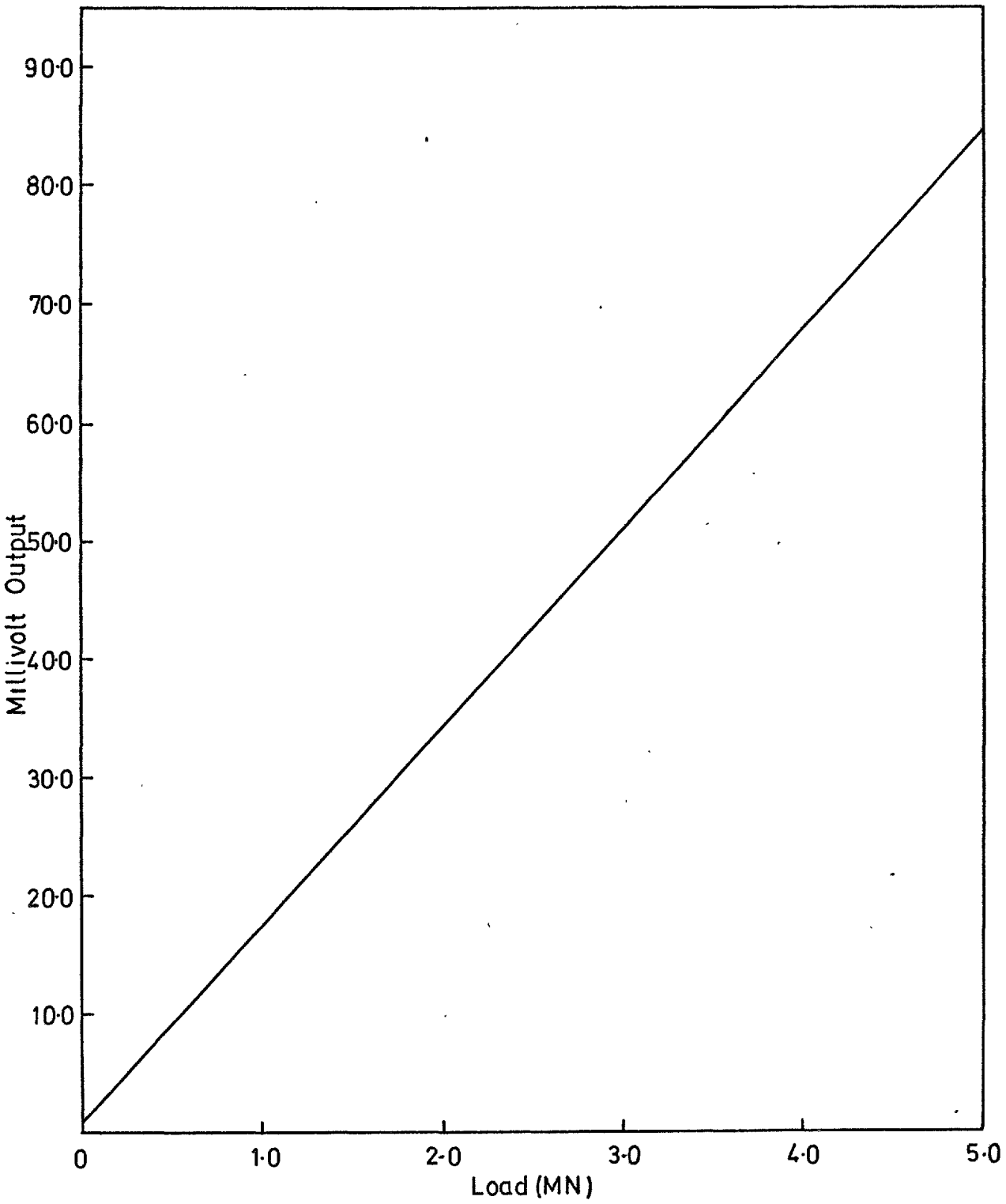
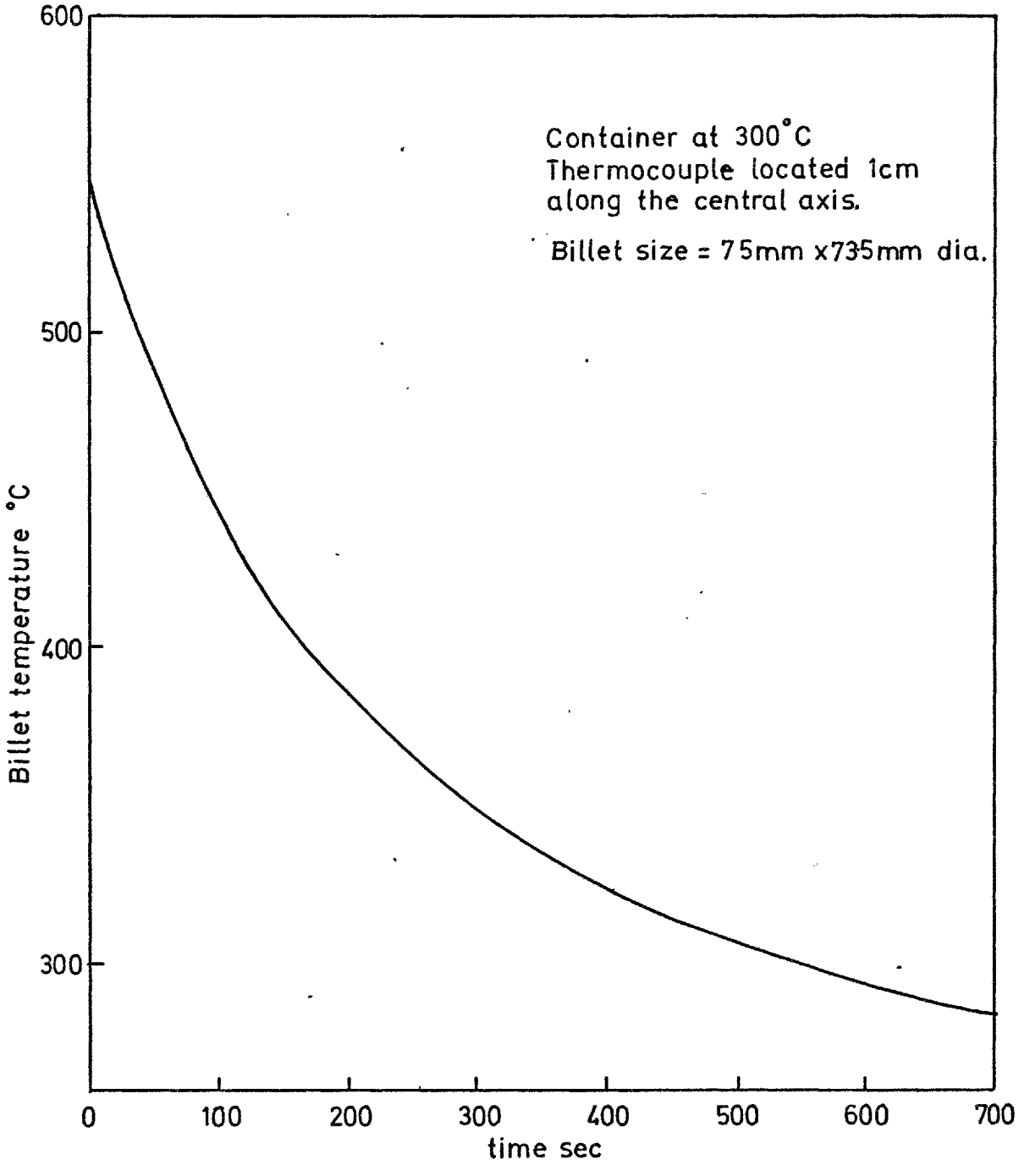
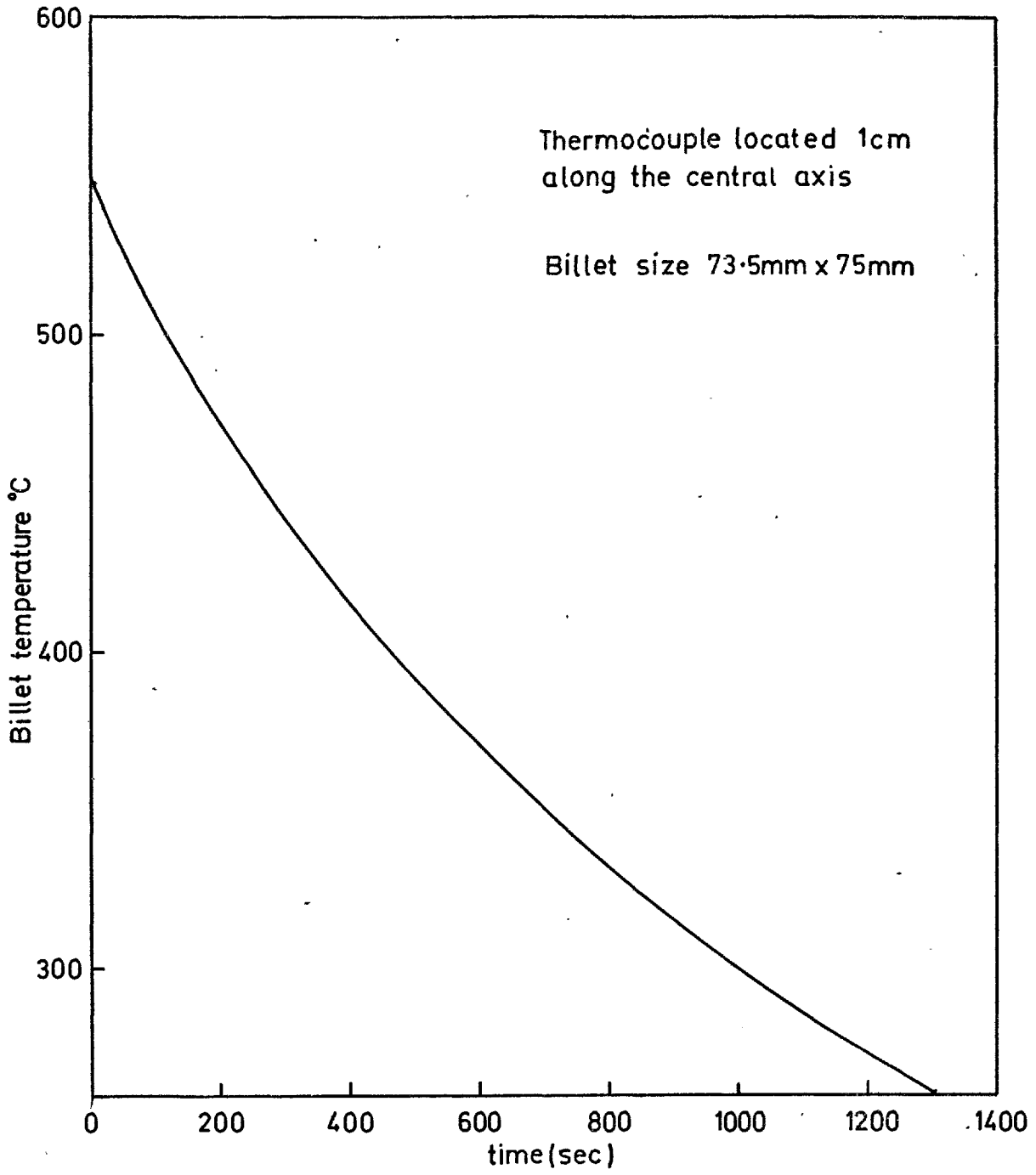


Fig.III.2 The load cell calibration.



A III.3. Cooling curve for the billet in the container.



A II4 Cooling curve for the billet in the induction heater.

APPENDIX IV

Die Dimensions

1 Single Hole Dies

With reference to figure 3.2

R	a (mm)	b (mm
10:1	23.72	27.0
30:1	13.69	17.78
50:1	10.62	12.70
60:1	9.68	12.70
70:1	8.97	12.70
80:1	8.38	12.70
90:1	7.90	10.16
100:1	7.49	10.16

2. Two Hole Dies

With reference to figure 3.3

R	ε	a (mm)	b(mm)
30:1	0.381	9.68	12.70
50:1	0.296	7.52	10.16
60:1	0.270	6.86	10.16
70;1	0.250	6.35	10.16
80:1	0.233	5.92	7.62
90:1	0.220	5.59	7.62
100:1	0.209	5.31	7.62

3. Three Hole Dies

With reference to figure 3.3

R	ε	a (mm)	b (mm)
30:1	0.311	7.90	10.16
50:1	0.241	6.12	7.62
60:1	0.220	5.59	7.62
70:1	0.204	5.18	7.62
80:1	0.190	4.83	7.62
90;1	0.180	4.57	7.62
100:1	0.170	4.32	7.62

Alloy A

R	mm/s	T_i °K	T °K	L_p MN	L_m MN	ΔL MN	$\dot{\varepsilon}$ sec^{-1}	σ N/mm^2	log Z	0.2 % P kg/mm^2	U.T.S kg/mm^2	Rxd g. s µm
30:1 (s)	12.4	693	781	2.96	2.36	0.30	19.7	63.4	12.00	11.8	25.7	
	12.4	651	765	3.50	2.96	0.40	19.7	79.4	12.23	14.0	28.5	
	12.4	611	721	4.31	3.05	0.60	19.7	81.8	12.89	10.5	24.8	
	5.6	611	700	4.49	3.22	0.50	8.9	86.4	12.03	13.8	27.0	
	5.0	651	720	3.76	2.76	0.36	7.9	74.1	12.51	12.3	25.5	
	4.7	693	751	3.08	2.82	0.10	7.5	75.7	11.13			
	12.2	773	851	1.55	2.22	0.00	19.4	59.6	11.11	19.5	31.6	
30:1 (2)	12.4	651	750	3.54	2.57	0.42	19.7	57.1	12.44	14.3	27.1	62
										14.0	27.0	54
	13.9	611	731	4.44	2.99	0.64	22.1	66.5	12.52	10.8	24.9	29
										11.9	25.4	24
	12.5	733	866	1.95	2.61	0.01	19.9	58.0	10.95	18.3	32.2	
	12.5	693	796	3.00	2.75	0.20	19.9	61.2	11.80	13.7	26.3	
										12.3	28.2	
	13.6	651	780	3.30						14.0	26.0	
										17.8	28.3	
30:1 (3)	12.0	693	797	3.16	2.86	0.18	19.1	66.2	11.77	13.9	26.5	
										15.4	26.7	63
										13.4	26.4	68
	12.4	773	863	2.29	2.53	0.09	19.7	58.6	10.98	17.6	31.3	111
										18.2	30.4	125
										18.0	31.1	81
	12.4	611	733	4.21	3.09	0.50	19.7	71.5	12.70	13.1	26.4	64
										13.5	26.9	69
										12.7	25.5	69
50:1 (s)	12.4	693	808	3.32	3.02	0.40	29.8	62.3	11.82			
	12.5	693	806	3.76	3.05	0.20	30.0	62.9	11.85	14.1	27.9	44
	12.7	651	762	3.98	3.32	0.40	30.5	68.5	12.45	14.8	28.5	90
	11.9	773	867	1.83	2.68	0.01	28.6	46.7	11.14	20;5	32.7	73
50:1 (3)	12.9	773	866	1.88	2.62	0.00	31.0	46.7	11.14	17.3	29.6	94
												65
	11.9	693	812	3.41	3.21	0.20	28.6	57.2	11.75	11.2	24.8	66
										10.9	24.8	66
	12.2	611	738	4.48	3.3	0.58	29.3	58.9	12.79	11.6	25.1	47
												47

R	V mm/s	T_i °K	$\bar{T}$ °K	Lp MN	Lm MN	ΔL MN	$\dot{\varepsilon}$ sec^{-1}	σ N/mm^2	logZ	0.2% P.S kg/mm^2	U.T.S kg/mm^2	Rxd g.s μm
50:1 (3)	11.6	611	738	4.58	3.32	0.55	27.9	61.4	12.77			150
												256
												259
	12.2	693	806	3.23	3.06	0.24	29.3	56.6	11.84	13.6	27.7	81
												59
												81
	12.0	773	865	2.10	2.58	0.08	29.8	47.7	11.14			189
												299
												381
				ALLOY B								
30:1 (s)	13.9	693	800	3.04	2.77	0.12	22.1	74.3	11.79	13.7	27.6	
	14.5	651	763	3.75	3.04	0.42	23.1	81.6	12.32	14.5	28.3	
	14.6	611	743	4.55	3.21	0.52	22.3	86.1	12.60	14.3	27.6	
	4.3	693	740	4.26	2.58	0.21	6.8	69.2	12.13	13.4	26.9	
	4.3	651	714	4.27	2.96	0.27	6.8	79.4	12.54	12.9	26.5	
	5.0	611	691	4.5	3.05	0.54	8.0	81.8	13.00	14.5	28.6	
30:1 (2)	14.0	651	739	4.29	3.21	0.50	22.3	71.4	12.66	13.9	28.3	
										13.0	27.6	
	12.7	773	861	2.29	2.50	0.03	20.3	55.6	11.01	14.9	30.1	42
										14.5	30.1	41
	12.7	693	792	2.85	2.68	0.15	20.2	59.6	11.86	8.9	23.9	
										10.2	24.7	
30:1 (3)	11.1	693	759	3.13	2.92	0.14	17.7	67.6	12.26	12.6	23.7	
										13.7	27.6	
										12.9	26.2	
	12.7	773	868	2.32	2.73	0.06	19.1	63.2	10.9	15.7	30.4	71
										15.5	30.4	90
										15.6	30.4	124
	14.0	651	740	4.26	3.22	0.5	23.3	74.5	12.70	11.0	26.3	
										12.7	28,2	
										13.3	28.2	
	12.1	773	857	1.91	2.43	0.00	19.2	52.3	11.04	11.5	30.9	

R	V mm/s	T_i °K	T °K	L_p MN	L_m MN	ΔL MN	$\dot{\varepsilon}$ sec^{-1}	σ N/mm^2	logZ	0.2% P.S kg/mm^2	U.T.S kg/mm^2	Rxd g.s μm
50:1	12.0	773	865	2.24	2.66	0.00	28.7	54.8	11.12	13.9	28.6	
50:1	12.0	773	865	2.21	2.64	0.03	28.7	48.0	11.12	13.7	29.1	59
(s)										14.1	29.7	87
	11.7	693	811	3.55	3.26	0. 0	28.1	58.1	1176	18.2	23.8	
	11.8	611	743	4.28	3.40	0.54	28.4	60.7	12.70	18.8	24.1	65
										7.1	23.1	58
50:1												
(s)	11.8	693	801	3.24	3.02	0.18	28.4	55.8	11.89			
	11.0	773	861	2.19	2.71	0.00	26.4	50.1	11.13			
	12.1	651	735	4.23	3.15	0.54	29.0	58.2	12.83			

R	V mm/s	T_i °K	$\bar{T}$ °K	Lp MN	Lm MN	ΔL MN	$\dot{\varepsilon}$ sec^{-1}	σ N/mm^2	log Z	log sinh	0.2% P.S kg/mm^2	U.T.S kg/mm^2	Rxd g.s µm
	12.8	747	849	2.63	2.95	0.05	35.5	50.0	11.39	0.385			
	12.0	705	802	3.27	2.80	0.36	40.0	47.5	12.02	0.347			
	12.5	633	751	4.30	3.28	0.6	34.5	55.6	12.67	0.469			
	4.82	755	801	2.30	2.67	0.04	13.4	45.3	11.56	0.312	15.2	28.9	76
											14.3	27,9	83
	4.9	706	765	3.05	2.89	0.18	13.5	49.0	12.06	0.370	12.7	28.7	
											12.9	28.3	
	13.2	767	858	2.15	2.64	0.08	36.7	44.8	11.31	0.305	14.3	28.8	43
											11.6	28.8	40
	12.5	637	751	3.95	3.19	0.48	34.6	54.1	12.70	0.447	11.2	26.4	
											13.0	27.3	
60:1													
(3)	5.0	626	700	4.47	3.19	0.55	13.9	54.1	13.08	0.447			
	4.9	693	752	3.38	2.98	0.29	13.5	50.5	12.24	0.386			41
													57
													99
	12.2	756	848	2.77	2.72	0.06	33.8	46.1	11.38	0.325			55
													47
													49
	5.0	754	802	2.37	2.70	0.07	13.8	45.8	11.56	0.321	12.5	30.4	
80:1													
(s)	6.5	664	749	3.66	2.89	0.27	22.5	47.0	12.52	0.339			
90:1													
(s)	7.8	663	766	3.61	3.25	0.21	29.5	49.8	12.40	0.382			
100:1													
(s)	12.7	751	861	2.81	3.17	0.08	52.6	46.0	11.43	0.324	12.7	27.8	
	12.5	719	825	3.13	3.01	0.14	51.8	43.7	11.85				52
	10.3	665	771	3.79	3.19	0.04	42.8	46.3	12.48	0.328			
	2.8	732	756	.97	3.20	0.00	11.6	46.5	12.12	0.331			
	2.6	661	697	3.82	3.21	0.26	10.8	46.6	13.03	0.332			
	2.5	661	697	4.47	3.29	0.40	10.5	47.8	13.02	0.			

ALLOY CE

R	V mm/s	T_i °K	T °K	L_p MN	L_m MN	ΔL MN	$\dot{\varepsilon}$ sec^{-1}	σ N/mm^2	LogZ	log sinh	0.2% P.S kg/mm^2	U.T.S kg/mm^2	Rxd g.s /μm
10:1	8.5	663	726	2.01	1.91	0.00	5.5	92.0	12.25	0.992			
(s)	5.0	583	651	4.38	2.43	0.35	3.2	117.0	13.35	1.35			
30:1													
(s)	12.4	663	751	2.94	2.65	0.13	19.7	71.1	12.42	0.695			
30:1													
(2)	12.5	663	764	3.17	2.76	0.29	19.9	61.4	12.24	0.555			
	12.9	659	761	2.21	2.75	0.24	20.6	61.1	12.30	0.559			
30:1													
(3)	7.8	664	743	3.30	2.67	0.30	12.4	61.8	12.34	0.561			
	12.3	663	761	3.35	2.67	0.33	19.6	61.8	12.27	0.561			
	5.1	659	730	3.30	2.73	0.23	8.1	63.9	12.36	0.591	11.8	23.4	
											14.3	23.0	
30:1													
(sq)	13.1	663	759	3.13	2.80	0.15	20.8	75.1	12.31	0.753			
30:1													
strip	13.2	663	755	3.05	2.43	0.25	21.0	65.2	12.39	0.610			
50:1													
(s)	7.5	665	745	3.41	2.70	0.27	17.9	55.7	11.92	0.471			
50:1													
(2)	8.9	661	751	3.66	3.03	0.27	21.4	56.0	12.46	0.475			
60:1													
(s)	4.5	745	794	2.81	2.81	0.12	12.5	52.8	11.62	0.428	14.2	30.1	65
	4.9	690	752	2.92	2.91	0.03	13.6	54.7	12.24	0.456	14.9	30.5	
	14.5	558	686	4.61	3.24	0.60	40.1	60.9	13.79	0.547	9.0	24.9	
	11.9	763	854	2.14	2.74	0.01	33.0	51.5	11.31	0.408	13.6	28.5	71
	13.7	706	788	3.28	3.29	0.02	37.9	44.9	12.19	0.306	12.3	28.5	
	2.6	736	750	2.72	2.85	0.06	7.2	53.6	12.00	0.439			
	2.8	737	750	2.36	2.78	0.00	7.9	52.7	12.04	0.426			
	2.7	664	697	3.08	2.79	0.06	7.6	52.5	12.87	0.423			
	12.3	664	761	3.43	2.73	0.20	34.0	51.3	12.51	0.405			
	11.4	573	695	4.22	3.27	0.60	31.7	61.5	13.53	0.556			
60:1													
(2)	5.0	706	769	3.05	2.66	0.07	13.8	45.1	12.61	0.310	12.7	27.1	43
	5.3	619	699	4.40	3.10	0.64	14.6	52.6	13.12	0.424			

ALLOY DF

R	V mm/s	T_i °K	T °K	L_p MN	L_m MN	ΔL MN	$\dot{\epsilon}$ sec^{-1}	σ N/mm^2	logZ	log sinh	0.2% P.S kg/mm^2	U.T.S kg/mm^2	Rxd g.s μm
	3.5	664	729	1.96	1.93	0.05	5.5	92.9	12.21	0.216			
(s)	5.0	481	567	4.59	2.58	0.60	3.2	124.2	15.26	0.423			
	5.5	483	566	4.29	1.29	0.55	3.6	93.1	15.32	0.416			
30:1													
(s)	13.0	665	759	2.76	2.42	0.11	20.7	64.9	12.33	0.005			
30:1													
(2)	12.3	665	763	3.03	2.60	0.18	19.5	57.8	12.25	-.057			
30:1													
(3)	8.4	663	746	3.08	2.58	0.25	13.4	59.7	12.33	-.040			
50:1													
s)	7.9	745	820	3.12	2.64	0.21	19.0	54.5	11.47	-.087			
50:1													
(2)	8.6	659	758	3.63	3.07	0.36	20.7	54.7	12.35	-.085			
60:1													
(s)	3.0	733	760	2.49	2.63	0.06	8.2	49.5	11.92	-.139			
	2.6	662	702	3.09	2.99	0.06	7.2	56.2	12.55	-.072			
	12.6	763	881	2.43	2.34	0.06	35.0	44.0	11.03	-.194			
	9.8	665	730	3.17	2.80	0.14	27.0	52.6	12.88	-.105	14.6	28.9	38
	4.9	703	762	3.15	2.88	0.09	13.5	54.1	12.15	-.091	13.9	29.9	
	14.8	573	687	4.61	2.93	0.60	41.1	55.5	13.78	-.078	12.4	28.6	27
	13.1	751	836	2.46	2.74	0.03	36.2	51.5	11.56	-.116	12.1	27.9	40
	12.6	720	824	2.94	3.00	0.08	34.9	56.4	11.69	-.069			
	12.6	635	751	3.68	3.18	0.36	34.9	56.4	11.69	-.069	12.1	29.2	
60:1													
(2)	4.9	706	761	3.19	2.80	0.24	13.6	47.5	12.12	-.156			
	12.4	720	827	3.21	3.10	0.18	34.4	52.6	11.64	-.105			
	12.6	629	749	4.20	3.37	0.42	34.8	57.2	12.70	-.062			
	4.9	754	805	2.45	2.92	0.06	13.4	49.6	11.51	-.135	13.4	29.2	71
											14.0	30.1	50
	4.9	703	761	2.93	2.88	0.14	13.5	48.9	12.11	-.142	14.4	28.8	
											12.3	27,7	
	12.9	755	866	2.21	2.91	0.05	35.6	49.4	10.99	-.137	16.4	30.2	62
	12.4	720	827	2.89	3.00	0.13	34.3	50.9	11.60	-. 122	10.8	26.8	
											11.2	27.1	
	12.2	628	743	3.72	3.14	0.35	33.7	53.3	12.76	-.098			

R	V mm/s	T_i °K	$\bar{T}$ °K	L_p	L_m	ΔL	$\dot{\varepsilon}$ sec^{-1}	σ N/mm^2	logZ	log sinh	0.2% kg/mm^2	U.T.S kg/mm^2	Rxd G.s μm
60:1													
(3)	5.0	626	705	4.29	3.31	0.50	13.8	56.1	12.99	-.072			
	4.9	710	770	3.29	3.07	0.16	13.4	52.1	11.98	-.110			
	4.8	742	798	2.81	3.11	0.07	13.3	52.7	11.60	-.104			
	13.4	745	839	2.80	2.70	0.10	37.3	45.8	11.53	-.174			
	10.85	770	844	2.31	2.76	0.10	30.1	46.8	11.38	-.164			
80:1													
(s)	6.2	664	756	3.45	3.20	0.16	21.5	52.0	12.39	-.111			
90:1													
(s)	7.2	664	758	3.54	3.26	0.19	27.3	49.9	12.47	-.132			
100:1													
(s)	8.5	664	774	3.97	3.14	0.46	35.2	45.6	12.34	-.176			
	2.5	725	744	3.08	3.32	0.00	10.4	48.2	12.25	-.149			
	2.6	659	698	3.79	3.33	0.27	10.9	48,3	13.10	-.148			
	2.7	619	671	4.41	3.44	0.42	11.10	49.9	13.0	-.132			
	12.2	713	823	3.15	3.13	0.06	50.7	45.4	11.87	-.178	12.1	27.6	45

265D

R	V mm/sec	T_i °K	$\bar{T}$ °K	L_p MN	L_m MN	ΔL MN	$\dot{\varepsilon}$ sec^{-1}	σ N/mm^2	logZ
60:1									
(s)	12.7	665	759	2.48	2.75	0.48	35.1	51.8	12.56
	2.5	662	688	2.69	2.94	0.00	7.0	55.2	12.99
	4.8	664	710	2.51	2.71	0.00	13.3	50.8	12.89
	13.9	624	738	2.90	2.96	0.11	38.5	55.6	12.91
	4.8	623	680	2.10	2.81	0.05	13.5	52.8	13.39
	2.5	624	657	2.66	2.94	0.00	6.8	55.3	13.56
	9.6	624	723	2.91	2.76	0.00	28.6	51.7	13.02
	10.5	665	748	2.46	2.88	0.00	28.9	54.1	12.64
	7.0	622	704	2.76	2.74	0.01	19.4	51.5	13.17
			266D						
60:1	13.7	664	765	2.60	2.54	0.07	37.9	47.7	12.51
(s)	4.8	667	724	2.64	2,72	0.11	13.2	51.2	12.67
	4.0	662	713	2.66	2.79	0.07	11.1	52.5	12.77
	13.6	624	768	2.94	3.00	0.13	37.8	56.4	12.46
	4.9	624	697	2.96	2.60	0.14	13.6	48.9	13.3
	2.7	620	666	2.98	2.72	0.14	7,5	51.1	13,43
	10.1	623	721	2.89	2.82	0.07	28.1	53.0	13.05
	10.2	669	763	2.48	2.78	0.09	28.3	52.2	12.41
	7,1	622	690	2.77	2.48	0.16	19.7	46.6	13.41
			272D						
60:1	13.3	667	814	3.77	3.47	0.24	38.9	65.2	11.86
(s)	4.7	663	763	3.70	3.45	0.23	13.0	64.9	12.07
	3.9	656	758	4.00	3.51	0.26	10.8	66.0	12.06
	13.6	623	766	4.43	3.77	0.49	37.8	70.9	12.49
	4.8	623	714	4.42	3.65	0.45	13.3	68.6	12.81
	2.5	617	669	4.40	3.53	0.46	6.9	66.4	13.33
	10.6	623	748	4.24	3.47	0.44	28.5	65.2	12.63
	10.2	669	756	3.79	3.42	0.25	28.4	65.2	12.51
	7.3	623	726	4.46	3.41	0.45	20.2	64.1	12.82

ACCUMULATOR RESULTS

Alloy	R	T_i K	L_p MN	0.2%p P.S kg/mm^2	U.T.S kg/mm^2	Rxd g.s
A	30:1 (s)	693	2.60	15.8	28.4	44
		611	4.02			
		651	3.20	15.5	29.4	99
B	30:1 (s)	611	3.45			74
		651	3.01	6.51	22.9	37
	30:1 (s)	651	3.13	7.2	23.3	50
				7.3	23.4	59
CE	60:1 (3)	739	2.72			
		625	4.09			
		770	2.12			
	100:1 (s)	665	3.79			
		729	3.04			
		669	2.74			
		613	4.54			
	60;1 (s)	663	3.04			
		678	5.08			
		729	2.58			
	10:1 (s)	581	4.88			
DF	10:1 (s)	483	4.89			
	60:1 (s)	662	3.39			
		628	2.84			
	60:1 (2)	713	3.00			
	60:1 (3)	745	2.58			
		769	2.57			
		632	4.06			
	100:1 (s)	664	3.13			
		619	4.41			

The Effect of Different Billet Lengths

AlloyCE, extrusion ratio 60:1 , ram speed 8.0 mm/sec

length mm	T_i K	L_p MN	L_m MN	L MN
30	693	2.89	3.16	0.00
60	703	2.70		0.12
90	706	2.84	2.93	0.03
120	700	3.18	2.75	0.20

Hot Torsion and Tensile Results

Alloy CE

T K	sec^{-1}	N/mm^2
673	0.0589	32.5
	5.89	63.0
	0.0589	41.0
	8.84	67.0
	29.5	54.5
653	5.19×10^{-3}	26.0
663	5.19×10^{-4}	18.1
573	0.0589	98.0
	5.89	105.5
	0.0589	82.0
	5.19×10^{-4}	67.2
	5.19×10^{-2}	90.2
773	5.89	44.5
	0.0589	35.5
793	5.89	41.0
473	5.89	182.5
	1.04×10^{-3}	151.0
	5.19×10^{-3}	155.0
	0.311	172.0

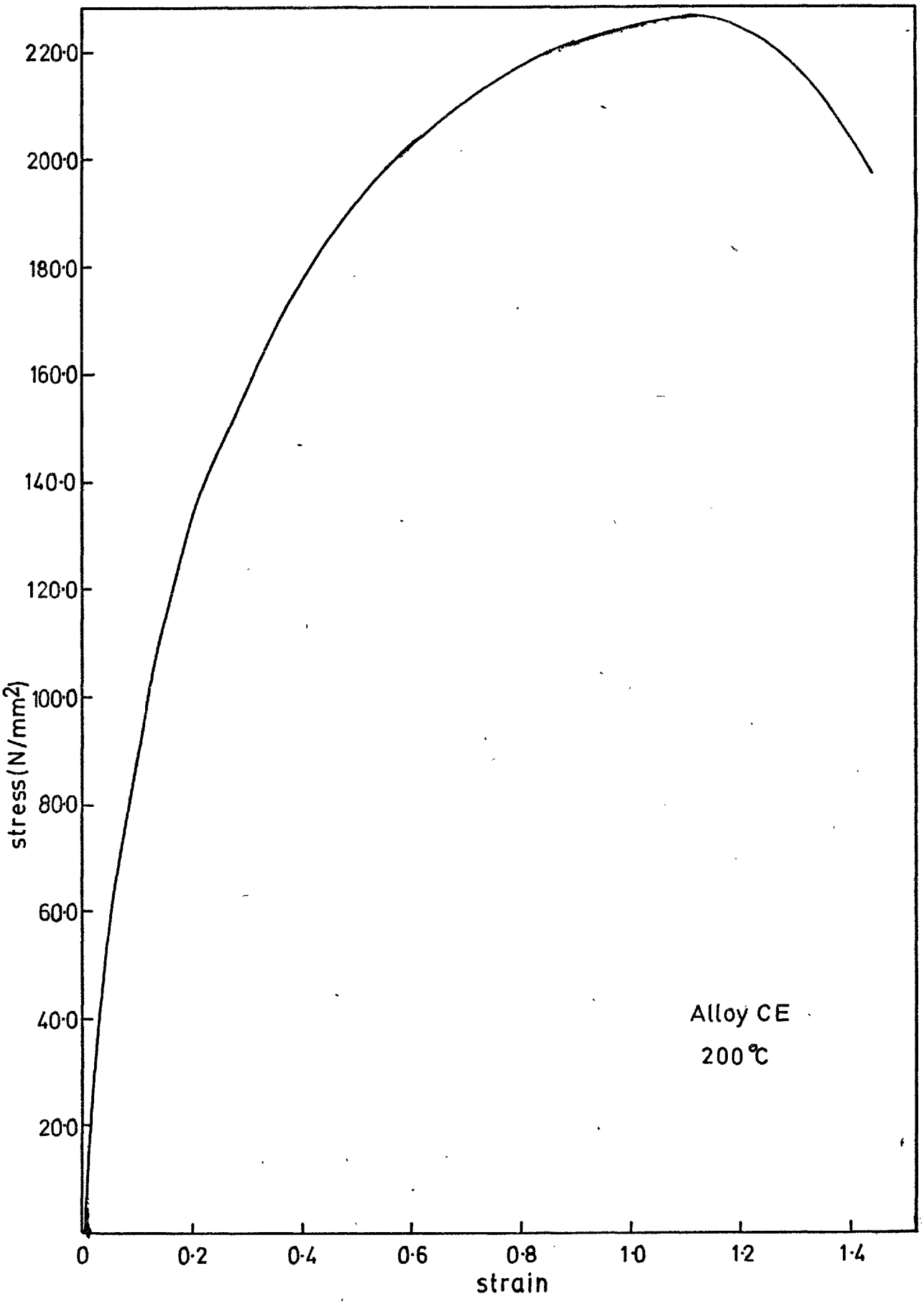
Alloy DF

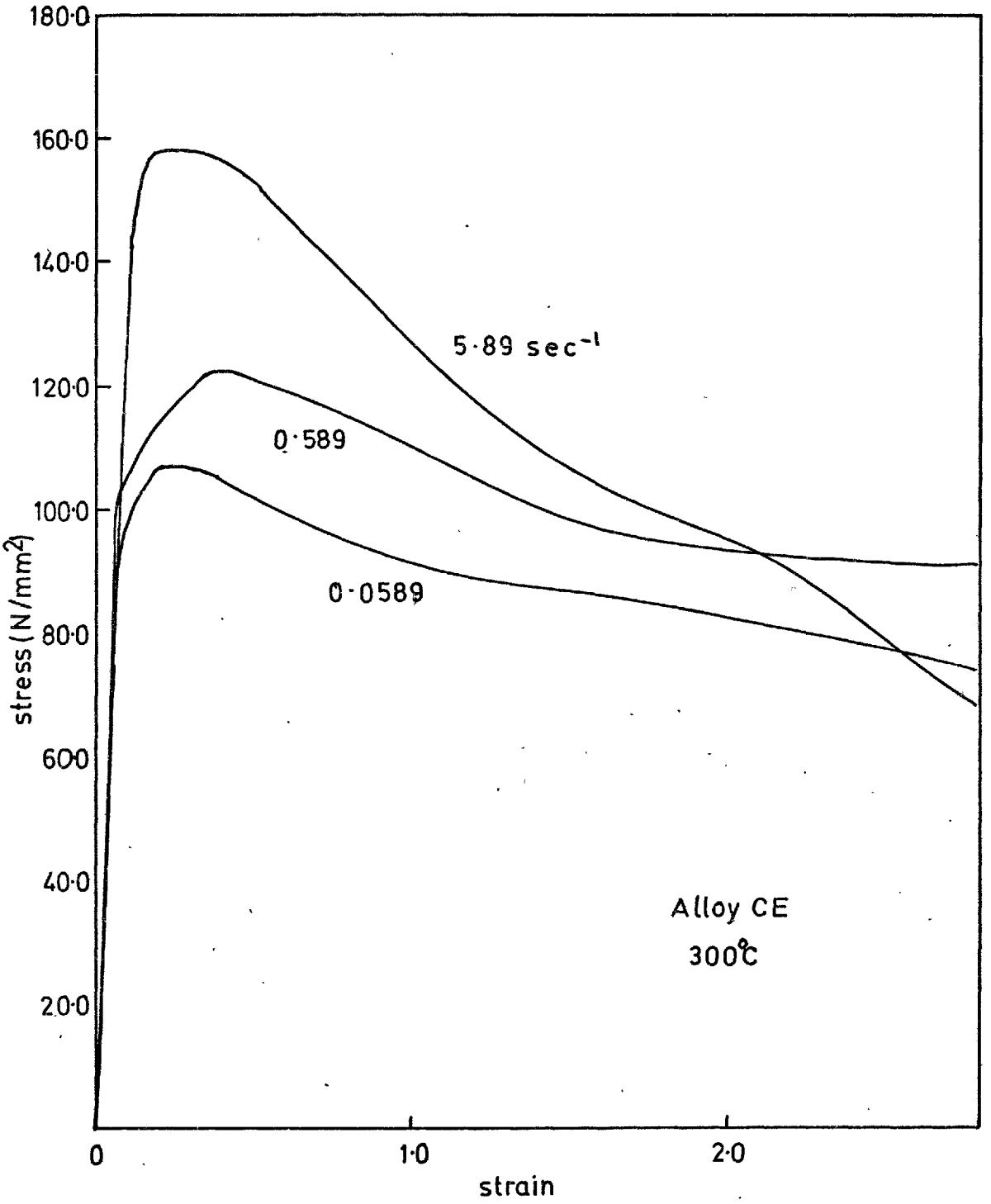
T K	$\dot{\varepsilon}$ sec^{-1}	σ N/mm^2
573	0.0589	93.0
	0.589	102.0
	5.89	119.5
	5.19×10^{-4}	69.0
	5.19×10^{-3}	64.6
	5.19×10^{-2}	92.9
673	5.89	58.0
	0.0589	37.0
	0.589	45.5
	2.95	58.0
	8.84	66.0
663	5.19×10^{-4}	25.3
653	5.19×10^{-5}	37.8
773	5.89	55.5
	0.0589	37.8
	0.589	39.5
793	5.89	50.5
473	5.19×10^{-3}	161.5
	0.311	174.0

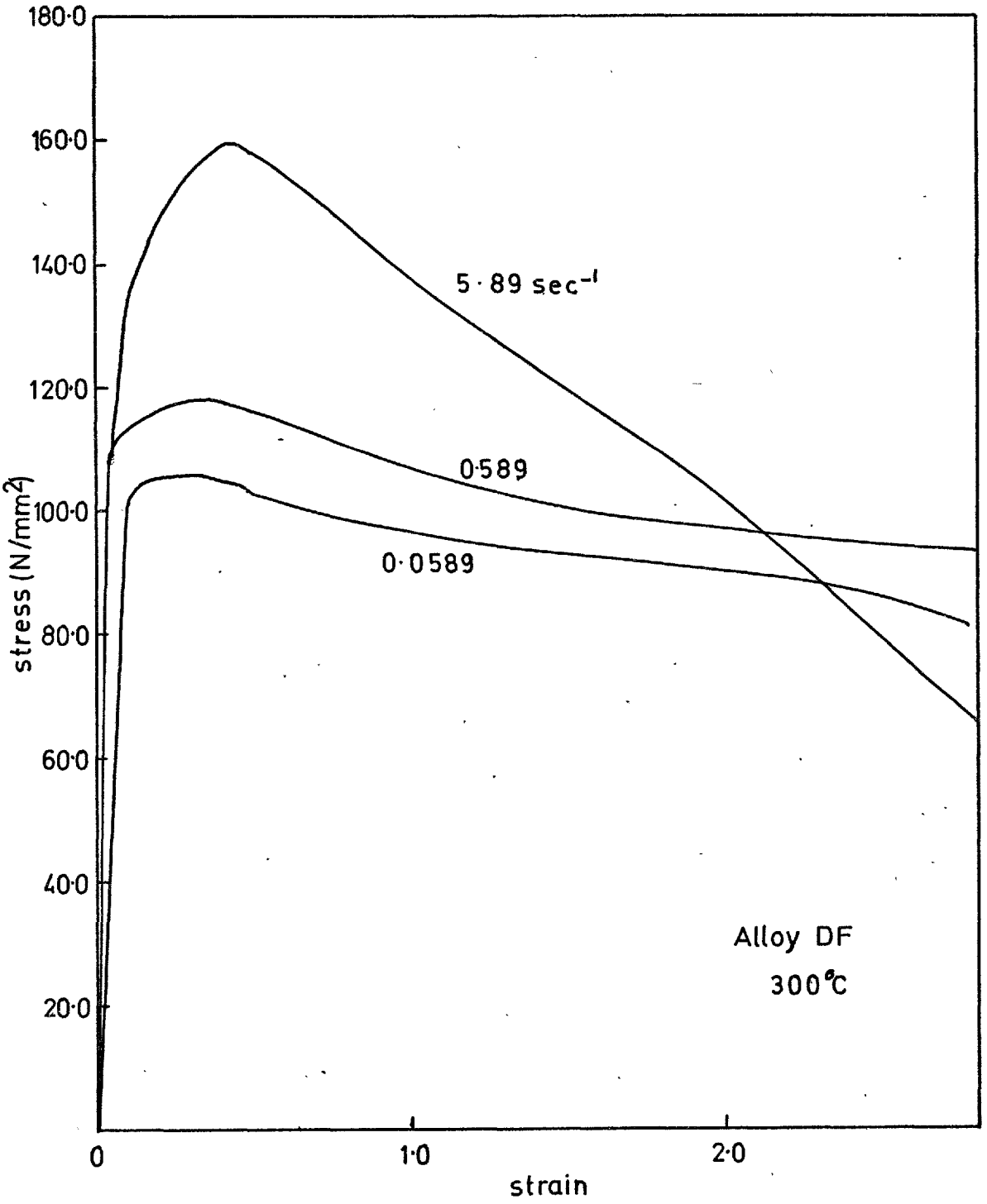
Appendix VI

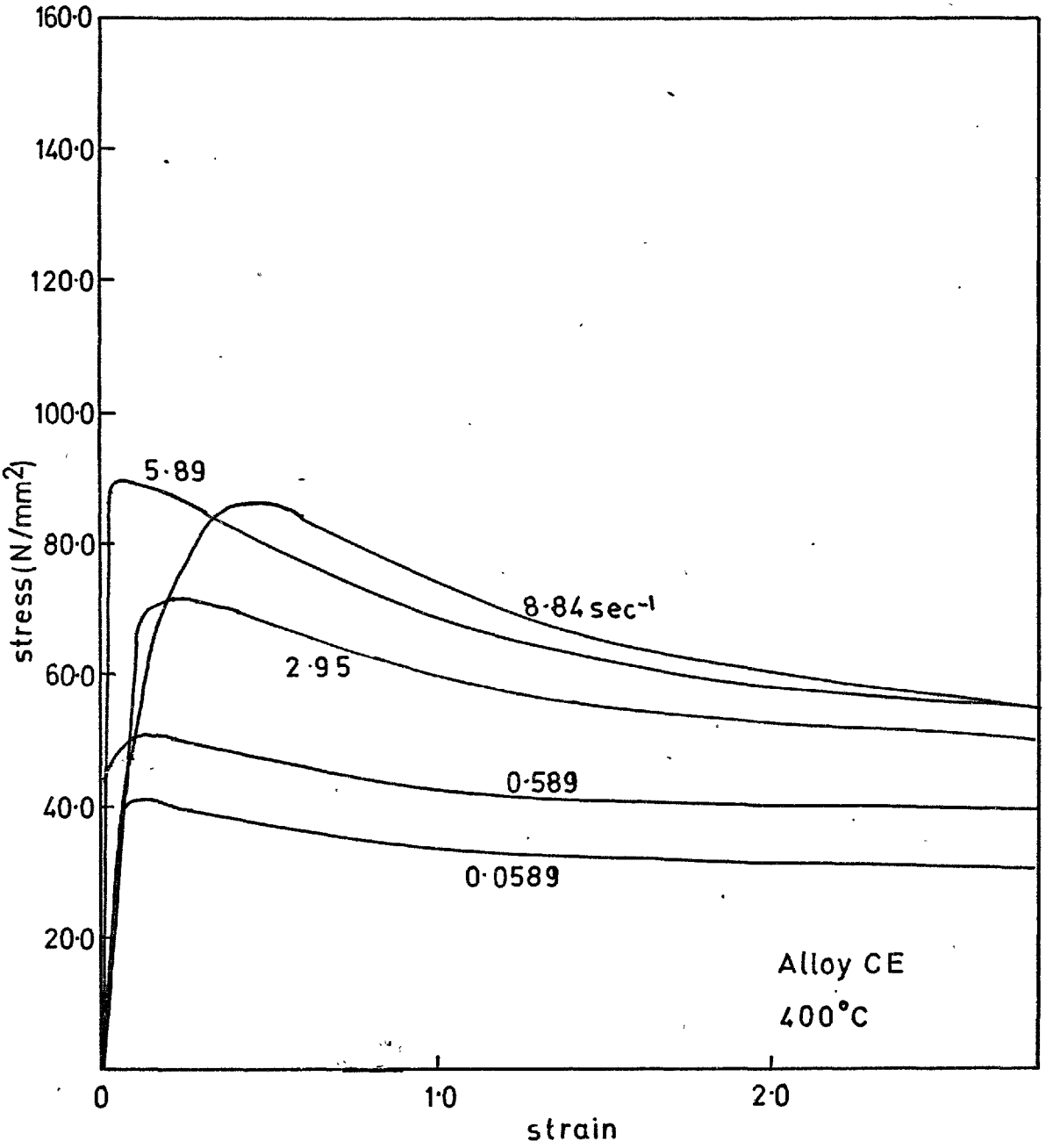
The Stress Strain Curves For Alloys CE and DF derived from the Torsion Tests.

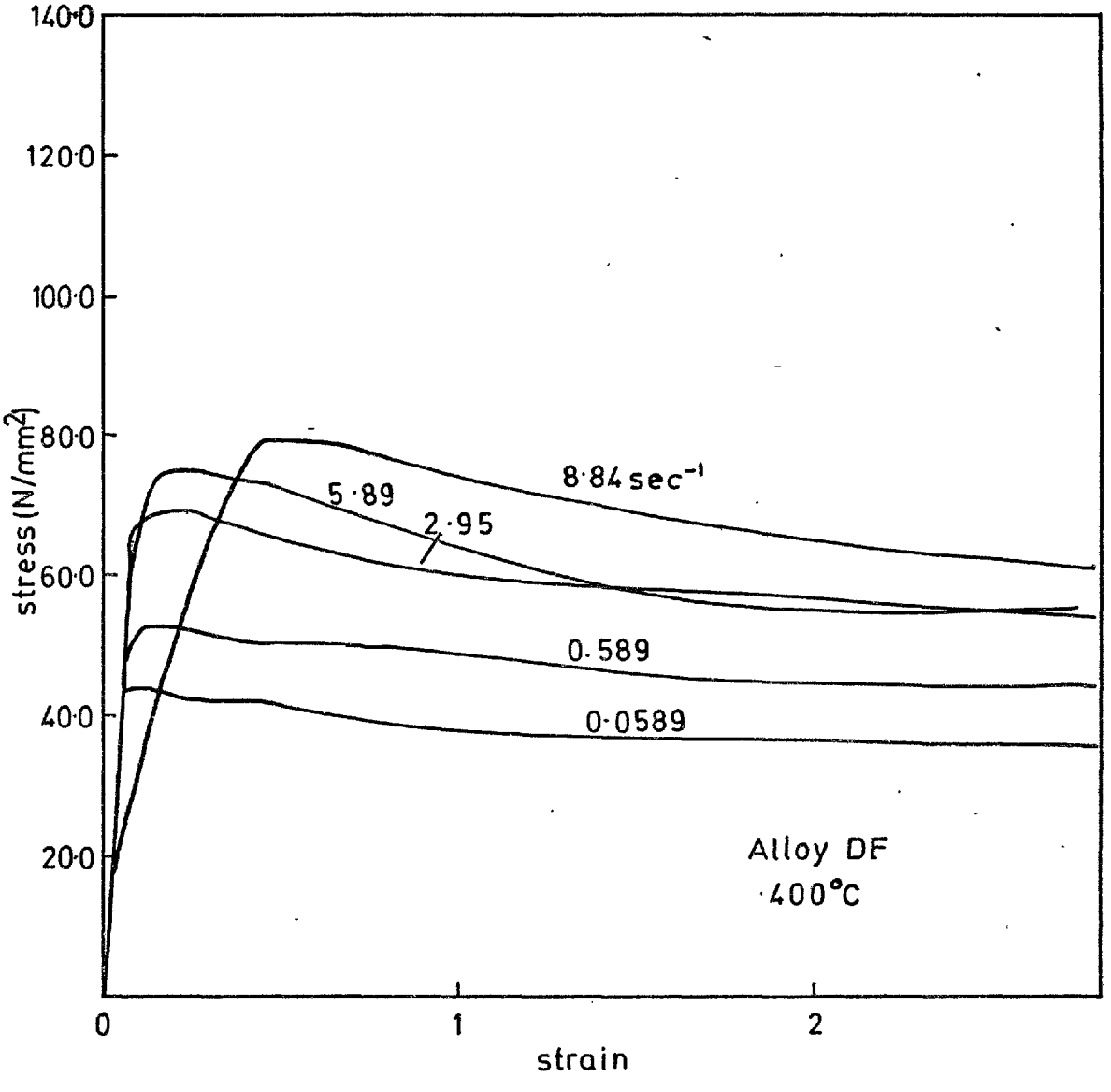
The curves were calculated using the theory given in chapter two. For clarity the strain is only given to approximately 2.0.

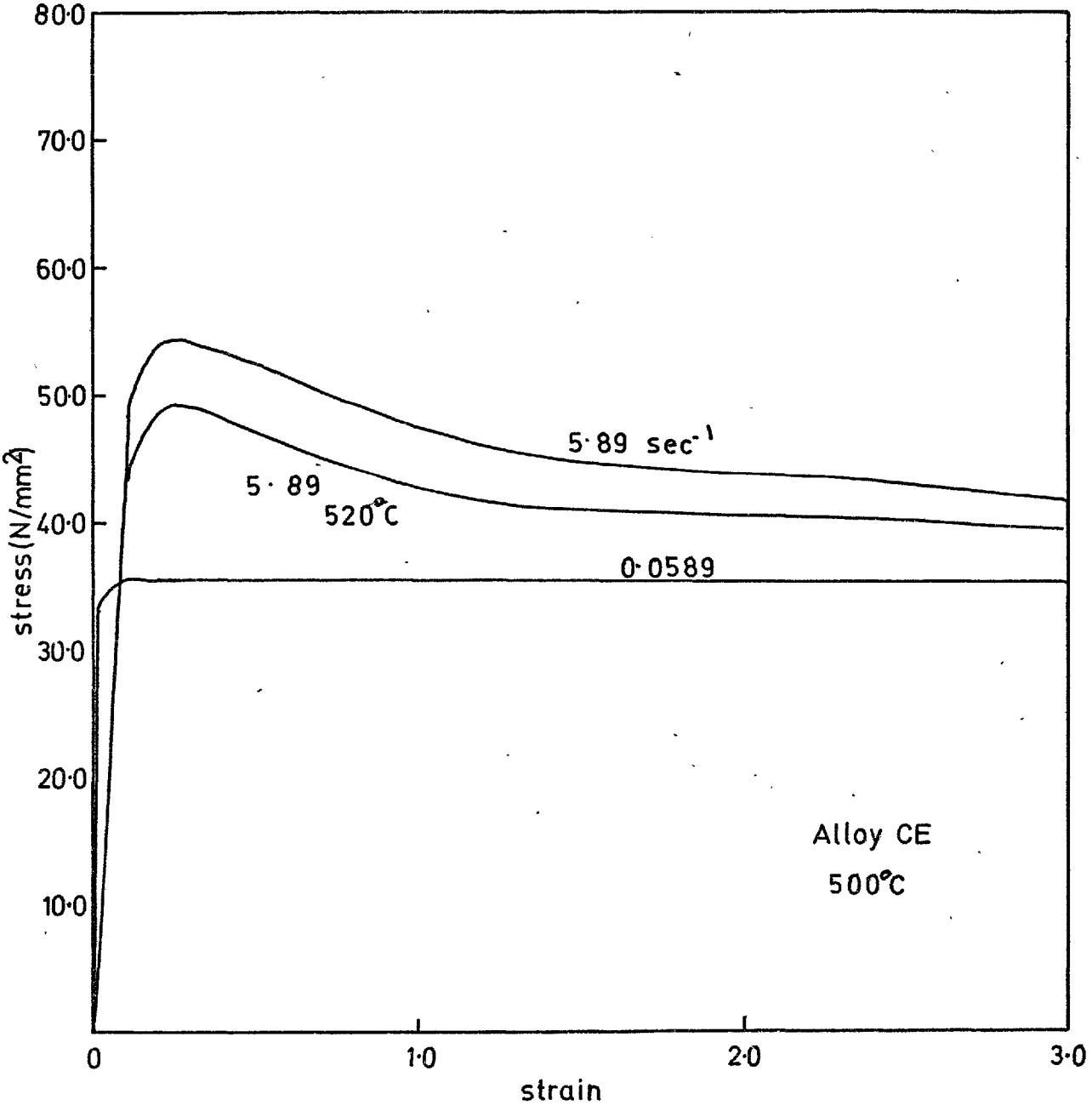

220·0
200·0
180·0
160·0
140·0
120·0
100·0
80·0
60·0
40·0
20·0
stress (N/mm2)
0
0·2
0·4
0·6
0·8
1·0
1·2
1·4
strain
Alloy CE
200 °C

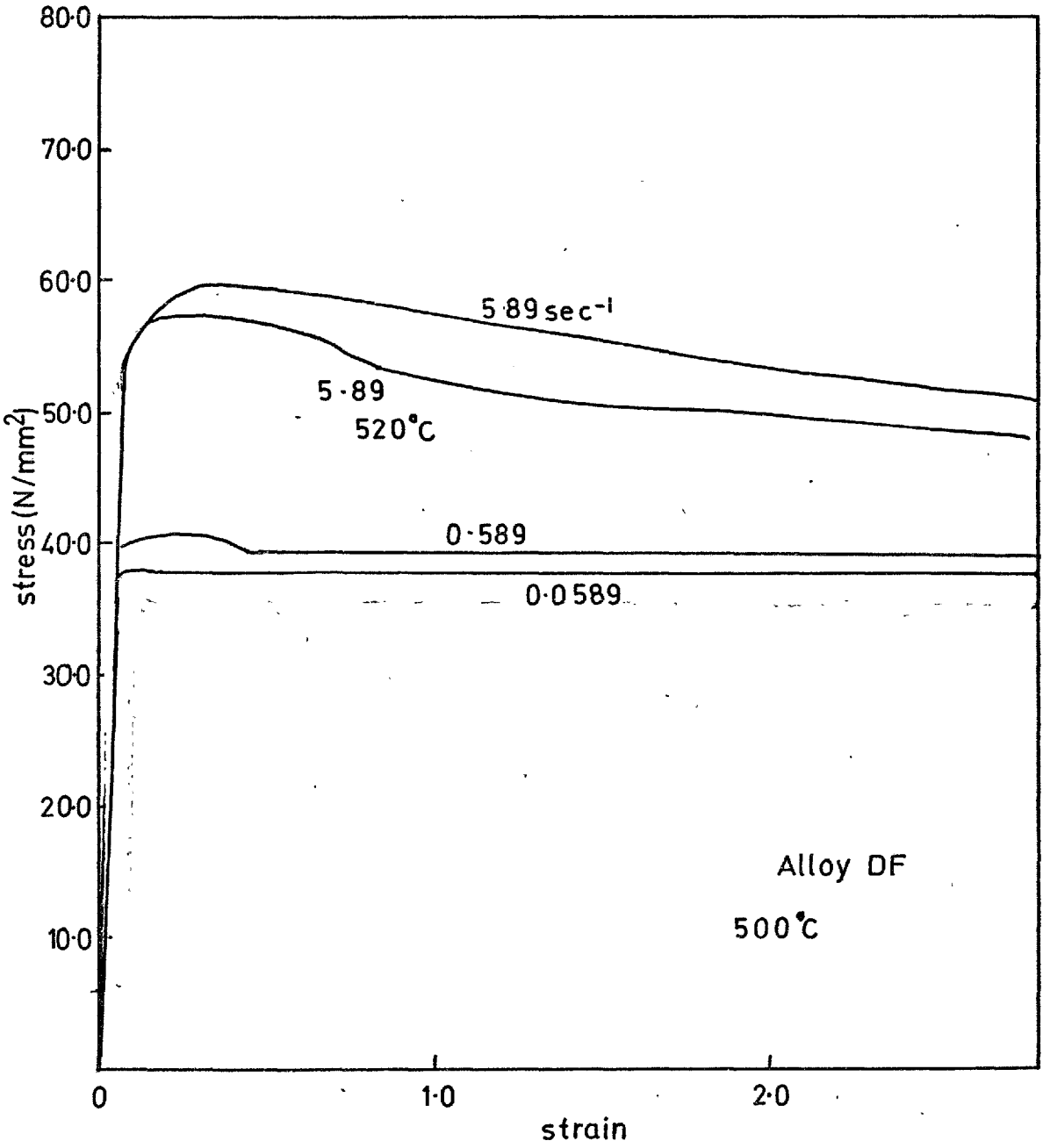

180·0
160·0
140·0
120·0
100·0
80·0
60·0
40·0
20·0
stress (N/mm²)
5·89 sec⁻¹
0·589
0·0589
Alloy CE
300°C
0
1·0
2·0
strain


180·0
160·0
140·0
120·0
100·0
80·0
60·0
40·0
20·0
stress (N/mm²)
5·89 sec⁻¹
0·589
0·0589
Alloy DF
300°C
0
1·0
2·0
strain


160·0
140·0
120·0
100·0
80·0
60·0
40·0
20·0
stress (N/mm²)
5·89
8·84 sec⁻¹
2·95
0·589
0·0589
Alloy CE
400°C
0
1·0
2·0
strain


140·0
120·0
100·0
80·0
60·0
40·0
20·0
stress (N/mm²)
8·84 sec⁻¹
5·89
2·95
0·589
0·0589
Alloy DF
400°C
0
1
2
strain


80·0
70·0
60·0
50·0
40·0
30·0
20·0
10·0
stress (N/mm²)
5·89 sec⁻¹
5·89
520°C
0·0589
Alloy CE
500°C
0
1·0
2·0
3·0
strain


80·0
70·0
60·0
50·0
40·0
30·0
20·0
10·0
stress (N/mm²)
5·89 sec⁻¹
5·89
520°C
0·589
0·0589
Alloy DF
500°C
0
1·0
2·0
strain

NOMENCLATURE

A, A_1, A_2, A_3, A_4	hot working constants
$A_1, A_0,$	billet and extrude area
A'	constant
a	constant; radius of torsion specimen
b	constant; burgers vector
B	efficiency factor
B'	constant
C_1, C_2, C_3, C_4	heat losses from the billet
c, c_{AL}, c_{ST}	specific heat(Al, steel)
c_{ACC}	heat accumulated
c_{RAD}	radial heat flow
d	subgrain size
D_B	billet diameter
D_E	extrude "
D	diameter of the deformation zone
D'	diffusion coefficient
dp	displacement to peak load
ΔH	activation energy
h	jog height
J	polar moment of inertia
l_j	jog spacing
L_B	billet length
L_m	load at the end of extrusion
L_p	peak load
ΔL	peak height
k', k_1, k_2	constants
k	shear yield stress
$\bar{k}$	mean " "
K	thermal conductivity
m	constant
M_T	torque
n, n_1	hot working exponents
p	constant
P	extrusion pressure
P_t	total " "
P_h	extrusion pressure for homogenous deformation
P_r	pressure expended in redundant work
P_f	pressure to overcome friction
Q, Q_{HW}, Q_{CR}	activation energies(hot working, creep)

q	constant
R_B	billet radius
R_E	extrude"
R	gas constant
Rxd g.s	recrystallized grain size
r_1, r_2	inner and outer radii of the container
S	depth of penetration of the heatfront
ΔS	activation entropy
T_1, T_2	inner and outer temperatures of the container
T_i, T_0	initial temperature
T_f	final temperature
ΔT	temperature rise
$\bar{T}$	mean deformation temperature
T_m	melting point
V	ram speed
V_B	volume of the billet
x	depth of the deformation zone
x_f	axial distance from the die
Y	yield stress
$\bar{Y}$	mean "
Z	temperature compensated strain rate
α	hot working constant; angle in upper bound
β	hot working constant
$\dot{\varepsilon}$	strain rate
$\bar{\dot{\varepsilon}}$	mean " "
$\dot{\varepsilon}_{RMP}$	root mean power strain rate
λ	constant
μ	coefficient of friction
ρ	dislocation density ; material
σ	flow stress
σ_B	back stress
σ_o	constant
$\sigma_{P.S.}$	proof stress
τ	shear stress
ν	attempt frequency
ψ	angle in upper bound solution
ω	" " " ";angular velocity
ϕ, ϕ_f	structure factor
ϕ'	angle of twist
γ	shear strain - ;angle in upper bound
$\dot{\gamma}$	shear strain rate

REFERENCES

1. C.E. Pearson and R.N. Parkins, " The Extrusion of Metals", 1961 Chapman and Hall Ltd, London
2 R. Hill, "The Mathematical Theory of Plasticity
3. W. Johnson and H. Kudo, "The Mechanics of Metal Extrusion",1962 Manchester University Press
4. L.E. Farmer and P.L.B. Oxley, J. Mech. Phys. Solids, 1971,19,p369
5. P.L.B. Oxley, Proceedings Conf; Mech. Props. of Materials at High Rates of Straon. Inst. of Physics 1973
6. J.F.W. Bishop, Quart. J. Mech Appl. Math., 1956, 9, p236
7 R.I. Tanner and W. Johnson, Inter. J. Mech. Sci., 1960, 1, p28
8 M.T. Watkins, K. Ashcroft and J. McKenzie, Mech. Eng. Research Lab. (Plasticity Division) Rep. 1954 (102), 1956 (111)
9. K. Ashcroft and G.S. Lawson, ibid,1958,(146)
10. A.R.E. Singer and S.H.K. Al-Samarrai, J.I.M.,1960, 89, p225
11. A.R.E. Singer and J.W. Coakham, ibid ,1960 ,89, p177
12. R.Akeret, ibid, 1967, 95, p204
13. T. Sheppard and D. Raybould, ibid, 1973,101,p33
14. W.A. Wong ,Ph.D Thesis, McGill University
15. C. Gagnon and J.J. Jonas, Trans.Met., Soc. A.I.M.E.,1969, 245, p2581
16. D.Raybould and T.D. Sheppard, J.I.M., 1973 ,101, p 65
17. M.M. Farag and C.M. sellars, ibid, 1973, 101,p137
18. C. Smith, ibid, 1949 - 50, 76, p435
19. H.K. Hardy, Metallurgia, 1944,30,p240
20. K.L. Dreyer and M. Hanson ,Z für Metal.,1941,33, 193
21. J. Althoff, Aluminium,1973, 49,p799
22. M.Van Lanker, Metallurgy of Aluminium Alloys, Chapman and Hall Ltd London, 1967
23. A.J. Bryant and A.T. Thomas, J.I.M., 1972,100, p40
24. A.J. Bryant, Z, für Metal., 1971,62,p705
25. M. Bauser and G. Fees, ibid, 1971 , 62, p705
26. J. Willis and A.J. Bryant, ibid, 1970, 61,p683
27. T. Sheppard private communication
28. R Chadwick, Met. Reviews, 1959, 4, p15
29. P. Allais and P. Mercher, Proceedings of Int. Conf. on "The Effective and Economic Use of the Special Characteristics of Aluminium and its Alloys", Zurich 1972,(I.M. 35)

30. A.J. Bryant, ibid,p89
31. L. Northcott, D. McLean, and O.R.Lee, J.I.M., 1948, 74,p81
32. S. Hirst and D.H. Ursell, Metal Treatment, 1958,25, p409
33. B. Meadows and M.J. Cutler, J.I.M., 1969, 97, p321
34. T. Sheppard and D. Raybould, J.I.M., 1973, 101, p73
35. J.J. Jonas, C.M. Sellars and W.J. McG. Tegart, MET. Rev.,1969,14,p1
36. C. Rossard and P. Blain, Rev. Met., 1958, 55, p573
37. H. Ormerod and W.J. McG. Tegart, J.I.M.,1960-61,89,p94
38. J.A. Bailey and A.R.E. Singer, ibid,1963-64, 92, p404
39. J.A. Bailey, Int. J. Mech. Sci., 1972,14,p375
40. R.R. Arnold and B.J. Parker, J.I.M.,1959-60, 88, p255
41. J.F.Alder and V.A. Phillips,ibib, 1954-55,83, p80
42. J.J. Jonas, Trans. A.S.M., 1969, 62, p300
43. D.Raybould and T. Sheppard, J.I.M.,1973, 101,p45
44. H.J. McQueen, Materials Technology an American Approach, A.S.M.E. 1968,p379
45. C.M. Sellars and W.J. McG. Tegart, Inst. Met. Rev.,1972, 17,p1
46. A. Nicholson, Iron and Steel, 1964, 37, p290 and 363
47 Reference 5
48. A.I. Kemppin,"Deformation Under Hot Working Conditions", I.S.I. publication 108, 1968,p117
49. S.K. Samanta, Int, J. Mech. Sci, 1968 ,10,p614
50. J.E. Hockett , Trans. Met. Soc. A.I.M.E., 1967, 239, p969
51. C.A. Redfern and C.M. Sellars, ref 48,p29
52. M.M. Farag and C.M. Sellars,ibid, p60
53. Y. Ohtakara et al, Trans I.S.I.J,1972, 12, p36
54. Y. Ohtakara et al, ibid, 1972, 12, p207
55. Robins et al, Journal of Materials, 19
56. D. Hardwick and W.J. McG. Teagrt, Mem. Sci. Rev. Met, 1961, 58,p869
57. J.D. Campbell, Mat, Sci. Eng.,1973,12,p3
58. F, Garafalo, Trans. Met. Soc. A.I.M.E., 1963, 227, p351
59. C.M. Sellars and W.J. McG. Tegart, Mem. Sci. Rev. Met.,1966,63, p731
60. C. Zener and J. Holloman, J. Appl. Phys.,1944, 15, p22
61. W.A. Wong and J.J. Jonas, Trans. Met. Soc. A.I.M.E. ,1968, 242,p227
62. R.C. Gagnon, Ph.D thesis, McGill University,1968
63. J.J. Jonas and J.P. Immarigeon, Z. für Metal., 1969,60 ,p227
64 S.K. Samanta, Int. J. Mech. Sci.,1969,11, p433
65. S.K. Samanta, J. Mech. Phys. Solids, 1971, 19, p117

66 P.R.Swann, Electron Microscopy and the Strength of Metals, Inter science New York, 1963

67. D. Raybould, Ph.D thesis, London University 1971

68. P.R. London et al, Trans. A.S.M., 1959, 51, p94

69. D. Walton et al, Trans. Met. Soc. A.I.M.E., 1961, 221, 454

70. J.J. Jonas, H.J. McQueen and W.A. Wong, re 48, p49

71. J. Cotner and W.J. McG. Tegart, J.I.M., 1969, 97, p73

72. D. Hardwick and W.J. McG. Tegart, ibid, 1961, 90, p17

73. H,J, McQueen and J.E. Hockett, Met. Trans., 1970, 1, p2997

74. R.A. Reynolds and W.J. McG. Tegart, J.I.S.I., 1962, 200,p1044

75. C. Rossard and P. Blain, Mem. Sci. Rev. Met., 1960, 57,p173

76. R. Bromley, Ph.D thesis, Sheffield,1969

77. B. Drübe and H.P. Stüwe, Z für Metal., 1967, 58, p799

78. J. Byrne ,"Recovery Recrystallization and Grain Growth," Collier MacMillon Ltd, New York, 1965

79. J.E. Bailey , ref 66, p535

80. H. Hu,ibid, p564

81. R,D, Doherty and R.W. Cahn, J. Less Common Metals, 1972, 28, p279

82. A.T. English and W.A. Backofen, Trans. Met. Soc. A.I.M.E.,1964,230,p279

83. R.W. Evans and G,R. Dunstan, J.I.M., 1971, 99, p4

84. H. Ormerod and W.J. McG. Tegart, ibid,1963, 92, p297

85. H. Hu, Trams. Met, Soc. A.I.M.E., 1964, 230,p572

86, J.L. Uvira and J.J. Jonas,ibid, 1968, 242,p1619

87. F. Garafalo,"Fundamentals of Creep and Creep Rupture in Metals", MacMillan, New York,1965

88. H.J. McQueen, W.A. Wong and J.J. Jonas, Can. J. Physics,1967,45 ,p1225

89. D. Mclean ,"Mechanical Properties of Metals", 1962

90. H.P. Stüwe, ref 48, p1

92. H.P. Stüwe , Acta Met., 1965, 13, p1337

93. H.J. McQueen, J. Metals, 1968, 20(4), p31

94. R.W.K. Honeycombe and R.W. Perthen, J. Less Comm. Metals,1972,28,p201

95. N.J. Greenwood and K.H. Warner, J.I.M., 1939, 64, p135

96. E.N. da C. Andrade, J.I.S.I., 1952, 171, p217

97. R.C. Griffins, J.I.M., 1958, 87, p255

98. M.J. Luton and C.m. Sellars, Acta Met, 1969, 17, p1033

99. H.P. Stüwe and B. Ortner, Metal Science, 1974, 8, p161

100. G. B. Gibbs, Phys. Stat. Solidi, 1964,5,p693; 1965,10, p507

101. P.B. Hirsch and D.H. Warrington, Phil. Mag., 1961, 6, p735

102. C.R. Barrett and W.D. Nix, Acta Met., 1965, 13 p1247

103. J.J. Jonas, Acta Met., 1969, 17, p397
104. A. Seeger, Phil. Mag., 1955, 46, p1194
105. J. Weertman, J. Appl. Physics, 1955,26, p1213
106. R.W. Christy, ibid, 1959, 30 p760
107. D. McLean, Rep. Proc. Phys., 1967, 29 ,p1
108. D. McLean, Can. J. Physics, 1967, 45, p973
109. J.J. Jonas and J.P. Immarigeon, Z. für Metal., 1969, 60, p227
110. J.J. Jonas, H.J. McQueen, andD.W. Demianczuk, ref 48, p97
111. D.J. Abson and J.J. Jonas, Metal Science Journal, 1970,23
112. J.F.W. Bishop, Met. Reviews, 1957, 2, No8, p361
113. J.M. Alexander, J.I.M., 1961-62, 90, p361
114. J.M. Alexander, Metal Industry, 100, 268 and 311
115. K.E. Hughes, Metallurgist, 1973, , p572
116. R. Hill, J.I.S.I., 1948, p177
117. W. Johnson., Proc. Inst. Mech. Eng.,1959, 173, p61
118. W. Johnson, J. Mech. Phys Solids, 1955, 3, 218
119. W. Johnson, ibid, 1956, 4, p191
120. L.C. Dodeja and W.Johnson, ibid, 1957, 5, p267 and 281
121. L. Kronsjö and P.B. Mellor, Int. J. Mech Sci.,1966,8,p516
122 . R. Sowerby ,W.Johnson and S.K. Samanta, ibid, 1958 , 10,p231
123M M.J. Hillier and W. Johnson, Int. J. Mech. Sci.,1963,5,p191
124, W. Pragwr, Proc. Inst. Mech. Engrs. , London, 1955, 196, p41
125 J. F.W. Bishop, Met. Review, 1957, 2, p361
126. H. Kudo, Int. J. Mech. Sci., 1960, 1, p229
127. H. Kudo, ibid, 1960, 2, p102
128. H. Kudo, ibid, 1961, 3, p91
129. S. Kobyashi, Prod. Eng. Conf. A.S.M.E.(Cincinnati), May 1963
30. B, Avitzur," Metal Forming Processes and Analysis", McGraw Hill,1968
131. J. Halling and L.A.Mitchell, Int. J. Prod. Research, 1965,4 , 141
132. J. Halling and L.A. Mitchell, Int. J.Mech. Sci., 1965, 7, p277
133. W. Johnson, J. Mech. Phys. Solids, 1956, 4, p269
134, W. Johnson, J.I.M, 1957,85 , p403
135. N.W. Purchase and S,J,Tupper, J. Mech. Phys. Solids, 1953,1, p277
136. R.J. Wilcox and P.W. Whitton, J.I.M., 1958-59, 87, p289
137. S. Hirst and D.H. Ursell, Metal Treatment, 1958, 25, p409
138. W. Johnson, B.I.S.R.A. Report MW/E/55/54
139. E.G. Thomsen, C.T. Yang and S. kobayashi,"Plastic Deformation in Metal Processing", MacMillan Co., 1965
140. K. Ashcroft and G.S. Lawson, J.I.M., 1960-61, 89, p369
141. T.M. Watkind, K. Ashcroft and J. McKenzie,1954, D.S.I.R.M.E.R.O. report MF/MS102

142. M Vater and H. P. Heil, Aluminium, 1969,3, p141
143. W. Johnson , J. Mech. Phys. Solids, 1958,7 p37
144. T.M. Watkins, K Ashcroft and J. McKenzie,1958, Proc. Conf on Tech. Of Eng. Manuf. , London, p155
145. K Laue, Z. für Metal, 1963, 54, p667
146. K. Laue and H. Hornauer, ibid, 1956, 47, p117
147, H. Hornauer, Alumimium, 1956, 32, p350
148. A.J. Bryant private communication
149. H. Walbert, Aluminium, 1938, p379
150. E.G. Thomsen and T. Jordan, J. Mech. Phys. Solids,1956,4,p189
151. C.P. Hinesley and H. Conrad, Mat. Sci. Eng, 1973,12,p47
152. W.S. Farren and G.I. Taylor, Proc. Roy. Soc. 1925(a), 107, p422
153. R.I. Tanner and W, Johnson, Int. J. Mech. Sci. , 1960,1,p28
154. W. Johnson and H. Kudo, ibid, 1960, 1, p175
155. M.T. Watkins, K. Ashcroft and J. McKenzie, Mech. Eng. Research Lab (plasticity division), Rep 1954(102), 1956(111)
156. K. Ashcroft, G.S.Laws n, ibid, 1958(146
157. T. ALtan and S. Kobayashi,"Trans A.I.M.E. Conf on Progress in Eng," 1967, p67
158. G.A. WOolvet and J.M. Alexander, J.I.M., 1964, 92, p430
159 P.M. Reynolds, ibid, 1966,94, p379
160. A.M. Rytikov etal, Tsuetnaya Metallurgiya, 1967,8,p42
161 P. Feltham, Metal Treatment, 1956, 23, p440
162. T. Chandra and J.J Jonas ,Met. Trans, 1970,1, p2079
163. T. Chandra and J.J. Jonas, ibid, 1971, 2, p877
164. J.J. Jonas and . Chandra, "Metal Forming: Interralation Between Theory and Practise", p115 , Plenum Press, New York
165. K. Hughes, M. Met Thesis, Sheffield, 1971
166. W. Ziegler and K. Siegert, Z. für Metal, 1973, 64, p224
167. D.M. Kearne, C.M. Sellars and W.J. McG. Tegart, ref 48, p 21
168. A. Greasley, private communication
169. T.R.G. Williams, M.Sc. thesis, Cardiff, 1954
170 G. Dieter Mechanical Metallurgy